AN INVESTIGATION OF NAPHTHALENEDIIMIDES AS CENTRAL BUILDING BLOCKS IN MODEL COMPOUNDS FOR SCANNING TUNNELING MICROSCOPE INDUCED LIGHT EMISSION EXPERIMENTS AND FÖRSTER RESONANCE ENERGY TRANSFER STUDIES

Inauguraldissertation

zur

Erlangung der Würde eines Doktors der Philosophie

vorgelegt der

Philosophisch-Naturwissenschaftlichen Fakultät

der Universität Basel

von

Sandro Gabutti

aus

Basel, Schweiz

Basel 2010

Genehmigt von der Philosophisch-Naturwissenschaftlichen Fakultät der Universität Basel auf Antrag von:

Prof. Dr. Marcel Mayor

Prof. Dr. W.-D. Woggon

Basel, den 8.12.2009

Prof. Dr. Eberhard Parlow (Dekan)

AN INVESTIGATION OF NAPHTHALENEDIIMIDES AS CENTRAL BUILDING BLOCKS IN MODEL COMPOUNDS FOR SCANNING TUNNELING MICROSCOPE INDUCED LIGHT EMISSION EXPERIMENTS AND FÖRSTER RESONANCE ENERGY TRANSFER STUDIES

Abstract

Scanning tunnelling microscopy (STM) is a powerful technique to observe surfaces at the atomic level. The resolution of this STM technique is good enough to study the electronic properties of single molecules adsorbed onto metallic substrates. An important step towards controllable single molecular technologies is the determination of how the molecule-substrate interaction changes the local molecular electronic structure. Since this electronic structure of molecules is strongly perturbed by the electrons of the underlying metallic substrate, an electronic decoupling of the molecules from the metal surface is required to isolate the electronic properties of an individual molecule.

Förster resonance energy transfer (FRET) has found many applications in different fields of science, because it allows the determination of the distance between two chromophores in the 1-10 nm range. In addition to other factors, this energy transfer is also dependent on the relative orientation of donor and acceptor chromophores to each other.

This thesis describes the design, synthesis and investigations of model compounds for:
1). STM induced light emission experiments from single molecules and
2). for FRET studies.

Chapter 1 provides an introduction to cyclophanes, energy transfer and scanning tunnelling microscopy.

Chapter 2 gives a description of the aims of this work, which is split into the synthesis of cyclophanes for STM induced luminescence investigations and FRET studies. The later is complemented by the synthesis of a linear NDI system.

Chapter 3 describes the design, synthesis and characterisation of all model compounds. In the first half STM investigations are presented and the electronic structure of two cyclophanes and complexation studies of the crown ether model compound are discussed. In the second half a modular synthetic route to asymmetric *N,N'*-naphthalenediimides is presented for FRET studies.

Chapter 4 gives a summary of this thesis and presents a short outlook.

Chapter 5 provides the synthesis and characterisation of all the compounds listed in this thesis and experimental details for STM investigations.

Acknowledgements and Thanks

Sandro Gabutti
Basel, 2009

Table of Contents

Theoretical Part

Experimental Part

Appendix

Theoretical Part

1. Introduction

The following introduction is divided into three parts, namely cyclophanes, energy transfer and scanning tunnelling microscopy (STM).

[2.2] Paracyclophane celebrated its 60th birthday this year. So in fact cyclophane-chemistry is an old and well-established field. However, the unabated interest in cyclophanes remains, not only because of the discovery of new cyclophanes and new synthetic strategies but principally due to the increasing field of supramolecular chemistry and that cyclophanes can be incorporated into devices and therefore find more and more applications in material science.[1,2]

Presented in this work new cyclophanes and linear model compounds have been synthesized, where the energy transfer between two conjugated systems is discussed according to a Förster resonance energy transfer mechanism (FRET).

The behaviour of several organic molecules upon adsorption onto metallic and semiconducting surfaces has been investigated by scanning tunnelling microscopy in recent years. Thus, not only the observed self-assembly of molecules on surfaces but also the electronic properties of the molecules has been analyzed. Scanning tunnelling spectroscopy (STS) not only reveals the electronic structure of the molecules but also offers the possibility to design, probe and modify properties of individual molecules.[3]

Since the electronic structure of the molecules is strongly perturbed by the electrons of the underlying metallic substrate, an electronic decoupling of the molecules from the metal surface is required to separate the electronic properties of an individual molecule and reduce the complexity to facilitate the comprehension of the system.

1.1. Cyclophanes

According to Cram,[4] Schubert[5] and Smith[6] a cyclophane consist in principle of an aromatic core (arene ring) and an aliphatic chain that forms a bridge between two non-adjacent positions of the aromatic unit (*figure 1*).

aromatic core

aliphatic bridge
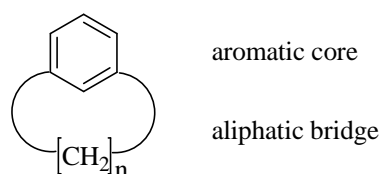
Figure 1: Definition of a cyclophane according to Cram,[4] Schubert[5] and Smith.[6]

In 1899 Pellegrin[7] synthesized the first cyclophane ([2.2] metacyclophane; *figure 2*) by a Wurtz coupling, but the field we now know of as cyclophane chemistry probably started in 1949 with the synthesis of [2.2] paracyclophane by Brown and Farthing[8] by simple pyrolysis of *p*-xylene. In order to study the electronic interactions between "face to face" arranged aromatic systems, Cram and Steinberg[4] synthesized the same cyclophane two years later by a designed synthetic strategy.

Nowadays [2.2] paracyclophane (*figure 2*) is commercially available (Fluka 5 g cost 94.90 SFr) and can be further functionalized at the aromatic core. A more recent example in this series of bridged benzene systems is the [2_6] cyclophane (superphane), which is completely bridged and was isolated by Boekelheide[9] in 1979 (*figure 2*).

[2.2] Metacyclophane   [2.2] Paracyclophane   Superphane
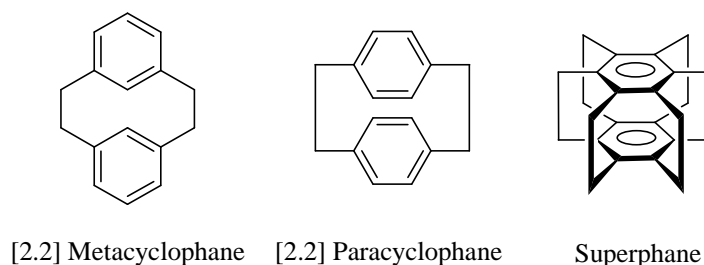
Figure 2: Schematic presentations of [2.2] metacyclophane,[7] [2.2] paracyclophane[4,8] and superphane.[9]

Following this initial synthesis of [2.2] paracyclophane, the aromatic systems in cyclophanes were further expanded with the synthesis of [2.2] (2,6) naphthalenophane[10] and [2.2] (2,7) pyrenophane[11-13] as model compounds for excimer fluorescence studies (*figure 3*).
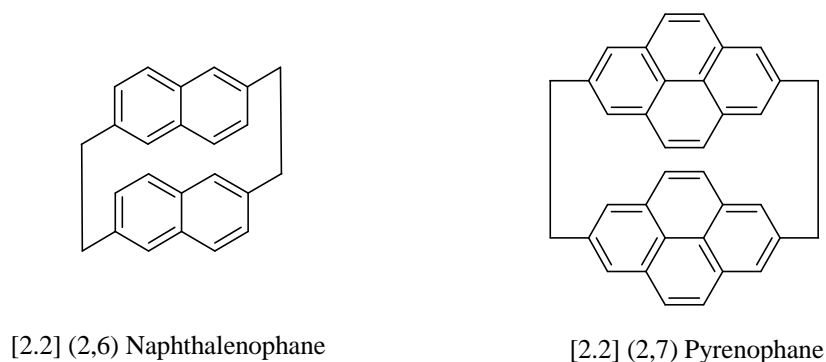
[2.2] (2,6) Naphthalenophane   [2.2] (2,7) Pyrenophane

Figure 3: [2.2] (2,6) Naphthalenophane[10] and [2.2] (2,7) pyrenophane[11-13] as model compounds for excimer fluorescence studies.

The interaction between "face to face" arranged chromophores, with respect to the distance and orientation to each other, has been studied in [m,n] paracyclophanes, [n,n] pyrenophanes and donor-acceptor cyclophanes.[1,2] Recently, Hopf and coworkers[14,15] reported an efficient route to the preparation of [m,n] paracyclophanes and their electrophilic aromatic substitution reactions. In addition, they suggest a stereocontrolling effect for a second electrophilic substitution on the neighbouring chromophore if the distance between the two benzene rings is less than 4 Å.

The initial driving force for cyclophane chemistry was its synthetic challenge, the investigation of the extent of aromaticity of strained cyclic compounds and the electronic interactions of interlinked aromatic systems. More recently, their supramolecular host properties have been investigated. Lehn and coworkers[16] synthesized a naphthalenediimide (NDI) cyclophane as a receptor for complexation of flat substrates and could isolate a corresponding crystal with an intercalated nitrobenzene (*figure 4*).
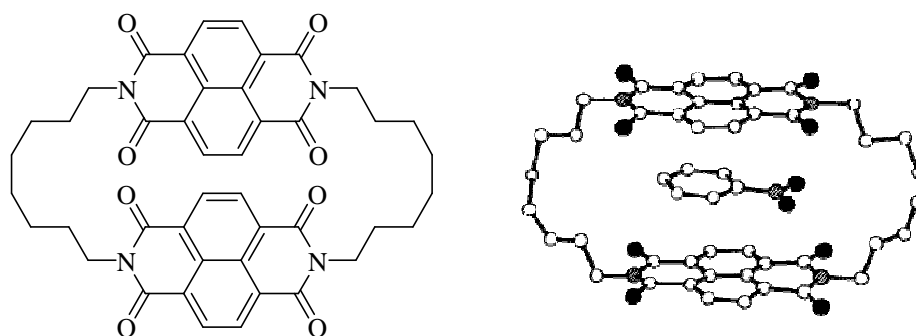
Figure 4: Crystal structure of Lehn's naphthalenediimide cyclophane, incorporating a nitrobenzene.[16]

3

The considerable stability of the resulting supramolecular complexes even made mechanically interlinked supermolecules, like catenanes and rotaxanes, synthetically accessible (*figure 5*). Catenanes and rotaxanes can undergo movements upon external stimuli and have therefore attracted much attention in the areas of material science and nanotechnology.

For example, a controllable donor-acceptor neutral [2]rotaxane (*figure 5* top) was synthesized by Stoddart and coworkers[17] on the way to switches in future molecular electronic devices.

Alternatively, Langford and coworkers[18] demonstrated a nice concept for the synthesis of an NDI cyclophane as a subunit of a catenane by using a template directed approach around a preformed macrocycle to first yield a [2]catenane, which could subsequently be hydrolyzed to the desired NDI cyclophane structure (*figure 5* bottom).
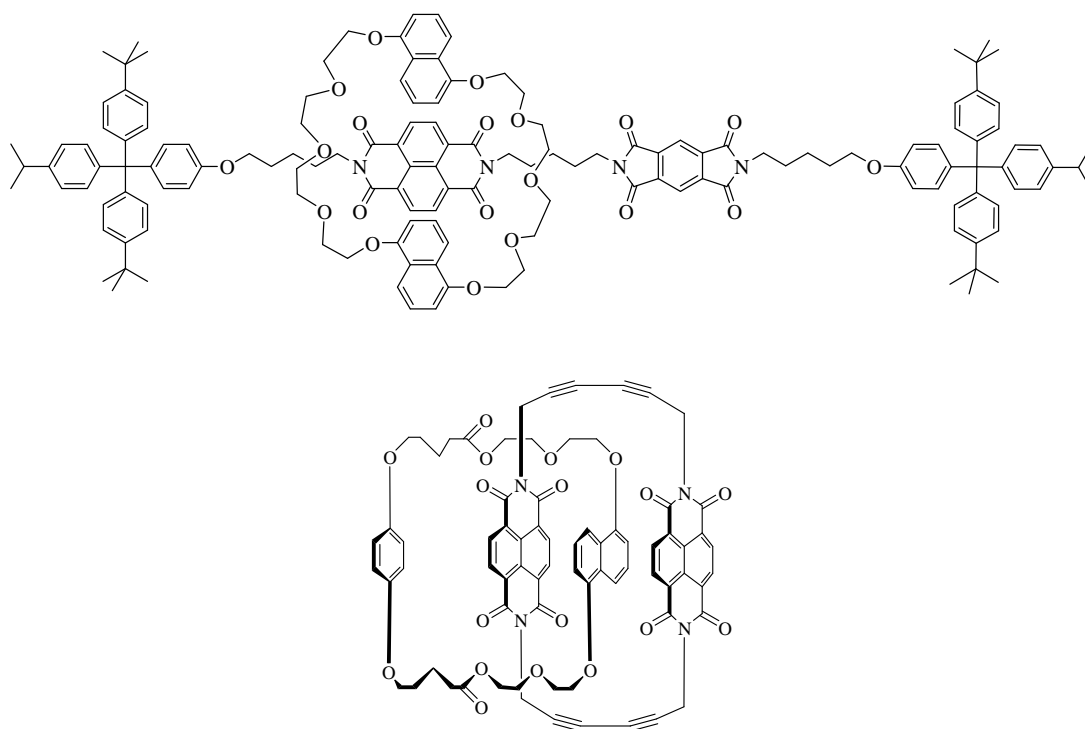
Figure 5: Top: A rotaxane consisting of a 1,5-dinaphto[38]crown-10 as ring and a naphthalenediimide and a pyromelliticdiimide unit in the rod as docking stations[17]; Bottom: A catenane with a naphthalenediimide cyclophane.[18]

4

1.2. Cyclophane Nomenclature

The nomenclature of cyclophanes developed by Cram, Schubert and Smith was further expanded by Vögtle and Neumann.[1] Consequently a "phane" has become a genuine term to describe bridged aromatic structures including condensed aromatic systems and hetero aromatic structures. Phanes are divided into three classes, the cyclophanes (more precise would be benzenophanes), the heterophanes and the heteraphanes. Heterophanes contain a heteroatom in the aromatic ring, whereas for the heteraphanes it is located in the aliphatic chain (*figure 6*).

Cyclophanes   Heterophanes   Heteraphanes
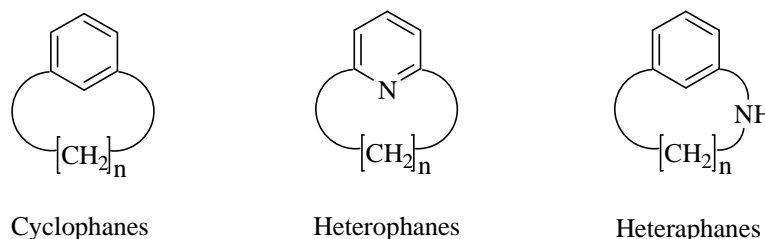
Figure 6: The three classes of phanes: cyclophanes, heterophanes and heteraphanes.

The length of the bridge (number of atoms between two aromatic centers) is put in front of the name in brackets and the suffix "phane" is added. Following this the position of the bridging atoms signed by *ortho*, *meta*, *para* or numbers in round brackets. So therefore [2.2] paracyclophane is also known as [2.2] (1,4) cyclophane. For multiple bridged cyclophanes, where all bridges have the same length, a subscript is used as simplification (see e.g. superphane *figure 2*).

An alternative nomenclature system for cyclophanes different from the IUPAC-nomenclature system can be used for complicated phanes, known as the Nodal-nomenclature.[1,19,20]

Under the Nodal-nomenclature all aromatic units are first "collapsed" to simple dots and the resulting simplified framework is named. In the case of [2.2] metacyclophane a simple cyclohexane skeleton would result (*figure 7*). Secondly, the "collapsed" aromatic cores are named again and the suffix -nodan is added. So in the case of [2.2] metacyclophane one obtains the name 1,4-di(1,3-benzena)cyclohexa-nodan.

[2.2] Metacyclophane or
1,4-Di(1,3-benzena)cyclohexa-nodan
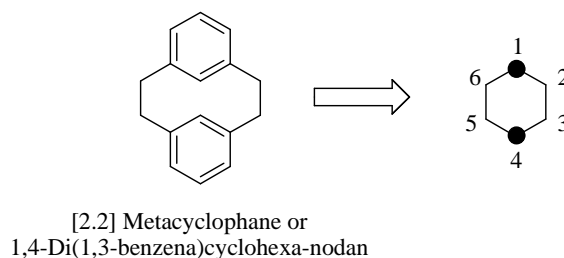
Figure 7: Applying the Nodal-nomenclature for [2.2] Metacyclophane.

The advantage of the Nodal-nomenclature is that the name of the aromatic ring is used e.g. naphthalene. As a further example for more complex cyclophanes, an asymmetric naphthalenediimide cyclophane structure, which was part of this work, is named after the Nodal-nomenclature system (*figure 8*).
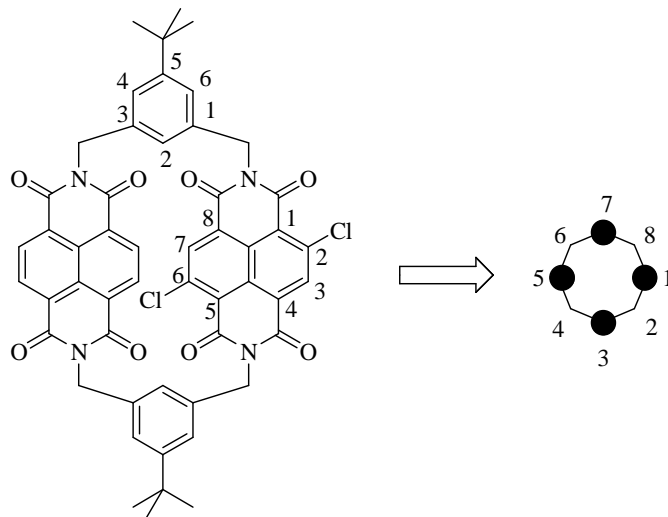
Figure 8: The name of an asymmetric naphthalenediimide cyclophane was derived from the Nodal-nomenclature: 1(1,4,5,8)-2,6-Dichloronaphthalenetetracarboxylic acid diimide-5(1,4,5,8)-naphthalene-tetracarboxylic acid diimide-3,7-di(1,3)-5-*tert*-butyl-benzenacycloocta-nodan.

Within this thesis several cyclophanes based on the structural motive displayed in *figure 8* were synthesised, fully characterised and their optical and surface decoration features were investigated. All cyclophane structures were named by using the Nodal-nomenclature.

1.3. Energy transfer

Absorption of a photon by a molecule results in an electronically excited state. This absorbed energy after a short time is released by the emission of a photon, so called luminescence. Depending on the nature of the excited and the ground state, luminescence is separated into fluorescence and phosphorescence. Fluorescence is observed if the emission occurs from an excited singlet state ($S_1 \rightarrow S_0$), whereas phosphorescence results from a transition of an excited triplet state to the singlet ground state ($T_1 \rightarrow S_0$). Molecules in an excited state may undergo alternative photochemical processes such as internal conversion, intersystem crossing and vibrational relaxation.

In *figure 9* the absorption and emission of light is illustrated by a Jablonski diagram. S_0, S_1 and S_2 represent the ground, first and second electronically excited states respectively. Each of these electronic states show a complete range of vibrationally excited levels indicated by 0, 1 and 2.
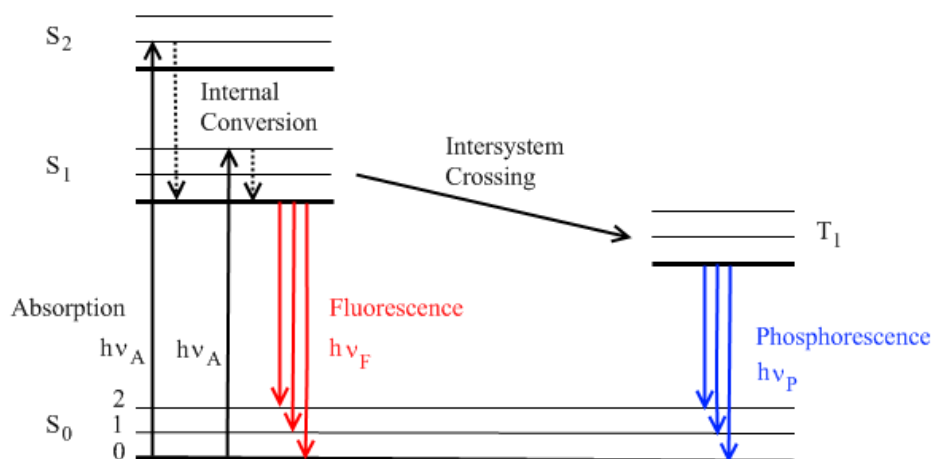
Figure 9: Jablonski diagram.

Following light absorption and subsequent excitation, a rapid relaxation to the lowest vibrational level of S_1 occurs within 10^{-12} s. Since the lifetime of fluorescence is near 10^{-8} s, internal conversion is usually completed before luminescence occurs. Thus, fluorescence emission principally results from the lowest energy vibrational state of S_1 and therefore the energy of emission is typically less than that of absorption, a so called Stoke shift. Return to the ground state usually populates higher excited vibrational ground state levels, which is the reason that the emission spectra appears typically as a mirror image of the absorption spectrum of $S_0 \rightarrow S_1$ as can be seen for perylene in *figure 10*. Born-Oppenheimer approximation states that electronic excitation does not greatly affect the nuclear geometry and therefore the spacing of the vibrational energy levels of the excited and the ground state are similar. Consequently, we observe comparable vibrational structures in the absorption and emission spectra.

Alternatively molecules from the S_1 state can undergo a spin conversion to the first triplet state T_1 (intersystem crossing, *figure 9*), which is a radiationless transition. Phosphorescence is the spin

forbidden transition from $T_1 \rightarrow S_0$ and requires population of the triplet state prior to emission and thus has an increased lifetime over fluorescence of $> 10^{-4}$ s.
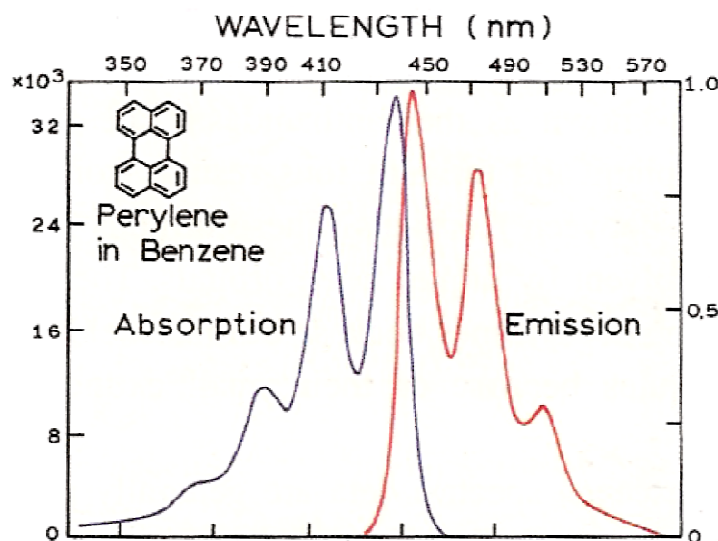
Figure 10: Absorption (purple line) and emission (red line) spectra of perylene.[21]

Further, if the lifetime of an excited molecule is reduced by another molecule, we speak from quenching. Usual bimolecular quenching processes are: collision, electron transfer or energy transfer (D = donor and A = acceptor):

Collision: $\qquad$ $D^* + A \rightarrow D + A + energy$

Electron transfer: $\qquad$ $D^* + A \rightarrow D^+ + A^-$ or $D^- + A^+$

Energy transfer: $\qquad$ $D^* + A \rightarrow D + A^*$

According to a simplified picture of molecular orbitals, electron and energy transfer can be described by occupied and unoccupied orbitals of donor and acceptor levels.[22] An electron transfer quenching mechanism involves only one electron which is transferred from an occupied orbital of a donor to an unoccupied orbital of an acceptor, resulting in a radical ion pair, also known as charge-transfer complex (*figure 11*).
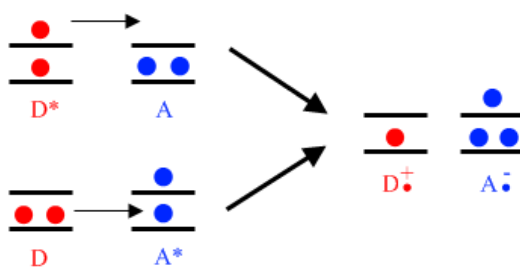
Figure 11: Quenching by electron transfer leads to charge-transfer complex formation (orbital overlap is required).[22]

In 1946 Theodor Förster discovered the physical process which now bears his name, where the energy of an excited chromophore (donor) was transfered to an acceptor molecule at a distance of 1.5 to 10 nm.[23,24] Actually this energy transfer is the result of a long range dipole-dipole interaction between donor and acceptor ("transmitter-antenna mechanism" *figure 12*) and occurs without the appearance of a photon. Therefore the F in a resonance energy transfer mechanism (FRET) should stand for "Förster" in acknowledgement of its discoverer and not for "Fluorescence", which is misleading.[25] Another possible pathway for an energy transfer mechanism is a double electron exchange as proposed by Dexter (*figure 12*). For electron transfer as well as energy transfer by electron exchange (Dexter mechanism) to occur, an orbital overlap is required and therefore their distances are generally limited to less than 10 Å. In contrast, no such orbital overlap is involved in a dipole-dipole energy transfer mechanism and therefore this energy transfer can still be effective over larger distances and has been used to probe the structure of biological macromolecules.

Förster mechanism   **Dexter mechanism**

- long distances (r = 10-100 Å).
- spectral overlap of the emission spectra from the donor with the absorption spectra from the acceptor is necessary.
- coulombic dipole-dipole interaction.

- short distances (r = 5-10 Å).
- overlap of orbitals necessary.
- electron exchange and usually collision of the molecules is needed.

Figure 12: Energy transfer mechanism according to Förster and Dexter.[22]

The explenation for Förster resonance energy transfer is best understood if the donor is separated by a certain distance (r) from the acceptor. Then the rate of energy transfer (k_T) is described by the following equation (**1**) or by the simplified equation (**2**):

$$k_T(r) = \frac{Q_D \kappa^2}{\tau_D r^6} \left(\frac{9000(\ln 10)}{128\pi^5 N n^4} \right) \int_0^\infty F_D(\lambda)\, \varepsilon_A(\lambda) \lambda^4 d\lambda \qquad (1)$$

$$k_T(r) = \frac{1}{\tau_D} \left(\frac{R_0}{r} \right)^6 \qquad (2)$$

Q_D = quantum yield of the donor without acceptor molecules

κ^2 = orientation factor, usually assumed to be 2/3

τ_D = lifetime of the donor

r = distance between donor and acceptor

N = Avogadro's constant

n = refractive index

$F_D(\lambda)$ = corrected fluorescence intensity of the donor (area under the curve)

$\varepsilon_A(\lambda)$ = excitation coefficient of the acceptor at λ

R_0 = Förster radius, at this distance half of the donor molecules decay by energy transfer and half decay by radiative and non-radiative pathways.

By comparing (**1**) and (**2**) the Förster radius is given by:

$$R_0^6 = \frac{9000(\ln 10)\kappa^2 Q_D}{128\pi^5 N n^4} \int_0^\infty F_D(\lambda)\varepsilon_A(\lambda)\lambda^4 d\lambda \qquad (3)$$

This critical quenching radius or Förster radius (R_0) is defined as the distance between donor and acceptor at which k_T and $1/\tau_D$ are equal, such that energy transfer and spontaneous decay of the excited donor are equally probable. Furthermore the efficiency of energy transfer (*E*) is given by the fraction of absorbed photons by the donor which are transferred to the acceptor (equation **4**). Rearrangement of equation **4** by the use of (**2**) provides equation **5**.

$$E = \frac{k_T(r)}{\tau_D^{-1} + k_T(r)} \qquad (4)$$

$$E = \frac{R_0^6}{R_0^6 + r^6} \qquad (5)$$

Assuming that r = R_0 the transfer efficiency is 50%. The transfer efficiency can be calculated from the relative intensity of the donor, in the absence (F_D) and presence (F_{DA}) of the acceptor:

$$E = 1 - \frac{F_{DA}}{F_D} \qquad (6)$$

Finally, using *E* and R_0 in a simple rearrangement of equation **5**, the distance (r) between the donor and the acceptor can be determined.

The term κ^2 describes the relative orientation in space of the transition dipoles of the donor and the acceptor. This orientation factor κ^2 is given by equation (**7**):

$$\kappa^2 = (\cos\theta_T - 3\cos\theta_D\cos\theta_A)^2 \qquad (7)$$

In this equation θ_T is the angle between the emission transition dipole of the donor (μ^D) and the absorption transition dipole of the acceptor (μ^A), where θ_D and θ_A are the angles between μ^D respectively μ^A and the vector connecting the donor and acceptor (r) as presented in *figure 13*.
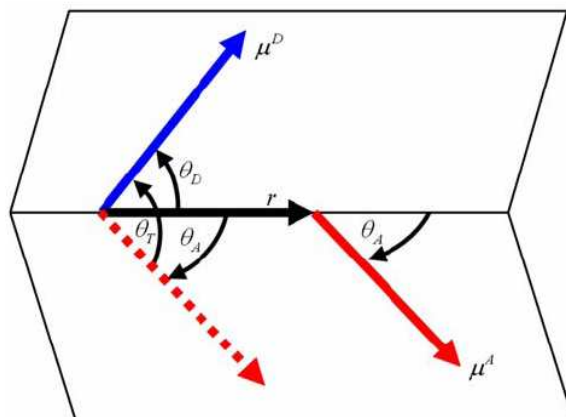
Figure 13: Orientation factor κ^2 depending from the direction of the emission dipole (μ^D) of the donor and the absorption dipole (μ^A) of the acceptor.[21]

Depending on the relative orientation of donor and acceptor to each other this factor can range from 0 to 4. For parallel transition dipoles in a head to tail arrangement the maximum $\kappa^2 = 4$ is reached, for parallel dipoles $\kappa^2 = 1$ and if the dipoles are perpendicularly oriented to each other $\kappa^2 = 0$ (*figure 14*).
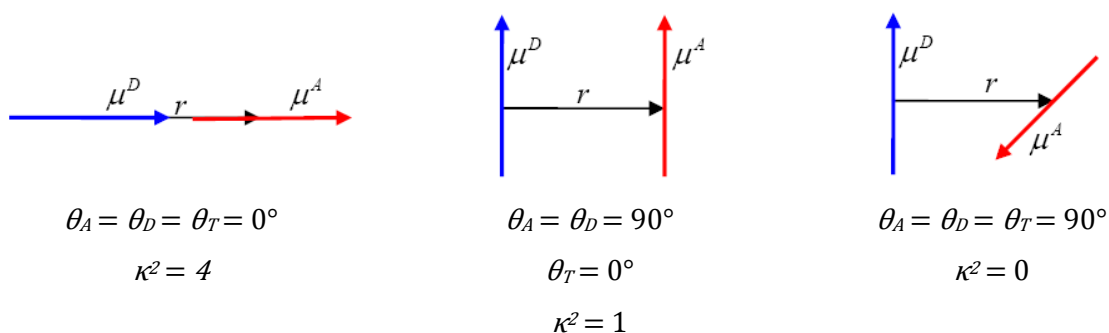
Figure 14: Three special cases are presented resulting in κ values equals 0, 1 or 4.[21]

For highly flexible biological systems, it is assumed that the average of many relative orientations of κ^2 is 2/3. As only the 6th root of κ^2 appears in the equation of the Förster distance between a suitable pair of chromophores, the inaccuracy emerging from the assumption of κ^2 can be neglected.

In this thesis cyclophanes were synthesized for STM induced luminescence experiments (see following section). For such experiments the energy transfer between the two chromophores in the cyclophane structure should be minimised in order to decouple the optical properties of the mounted chromophore. To inform the structural selection for these STM measurements, Förster resonance energy transfer was studied in asymmetric NDI cyclophanes with respect to the spectral overlap of donor and acceptor moieties. Energy transfer by Dexter mechanism was neglected due to the increased spacing arising from the presence of rigid spacers between the two chromophores in these cyclophanes, minimizing the orbital overlap.

The second half of this thesis deals with the synthesis of a model compound with a variable spacer between two NDI dyes. In such FRET systems the orientation factor κ^2 can be studied by variation of the central spacer unit (see chapter 2).

1.4. Scanning tunnelling microscopy (STM)

A scanning tunnelling microscope was developed by Gerd Binning and Heinrich Rohrer as an instrument to observe atomic structures on surfaces.[26-28] In principle there is a metallic tip held a few angstroms above the surface, separated by a vacuum gap. Due to the wave-particle phenomena in quantum mechanics the electrons can pass the vacuum barrier, which is referred to as quantum tunnelling. Since electrons can tunnel, an electrical current is obtained if one applies a sufficiently large bias voltage between the tip and the sample (*figure 15*).
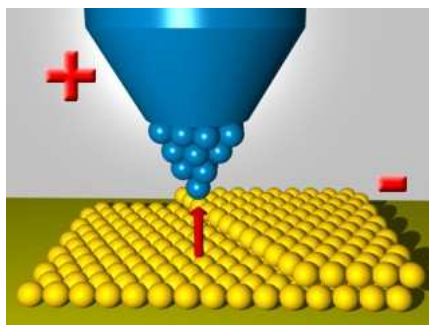
Figure 15: A schematic representation for a current flow from the negative sample to the positive charged metallic tip.[29]

The surface can be scanned by controlling the sample tip distance by maintaining a constant current flow or a constant height (*figure 16*). Consequently, by recording the vertical movement of the tip a height profile map of the analyzed sample can be made.

Figure 16: Schematic representation of a metallic tip scanning the surface.[29]

The resolution of this STM technique is great enough to study the electronic properties of single molecules adsorbed on the metal surface. In scanning tunnelling spectroscopy measurements (STS) the derivative of the tunnelling current (*I*) with respect to the applied bias voltage (*V*) is recorded in order to provide information of the sample surfaces' electronic states. If a new tunnelling channel opens, an increased slope in the *I*(*V*) curve is obtained, while for the *dI/dV* signal a step (e.g. for metal surface states) or different peaks (e.g. for molecular orbitals) are monitored as shown in *figure 17*.[30-32]
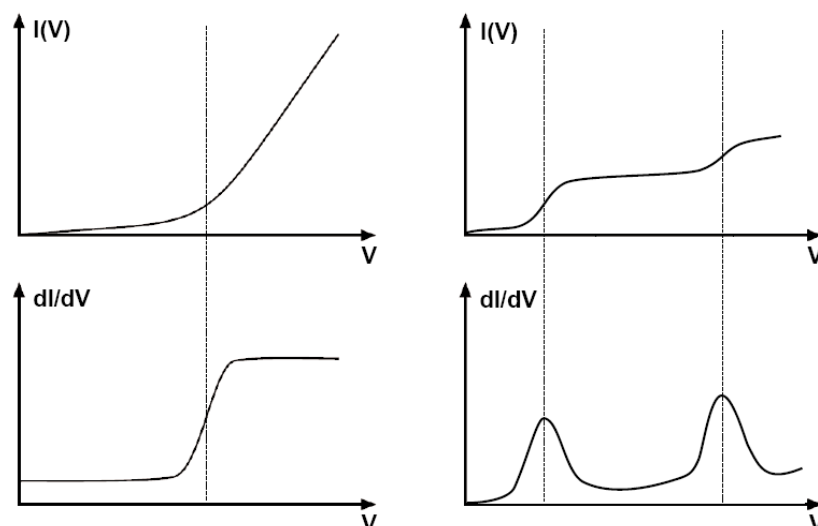
Figure 17: Constant height STS: The tip-sample distance is held constant. The bias voltage *V* is ramped and *I(V)* and *dI/dV* are recorded. Left: A new tunnel channel opens, resulting in an increased *I(V)* curve and a step in the *dI/dV* signal as can be seen e.g. for metal surfaces. Right: A new tunnel channel opens, resulting in a stepwise observation in the *I(V)* curve and corresponding peaks in the *dI/dV* signal as can be seen e.g. for molecular orbitals.[30]

The STM can also be used to investigate the intramolecular photon emission by locally exciting the molecule with tunnelling electrons. Therefore electrons from the metallic tip are transferred to the lowest unoccupied molecular orbital (LUMO). Extraction of an electron from the highest occupied molecular orbital (HOMO) followed by an intramolecular transition gives then rise to light emission as shown in *figure 18*.
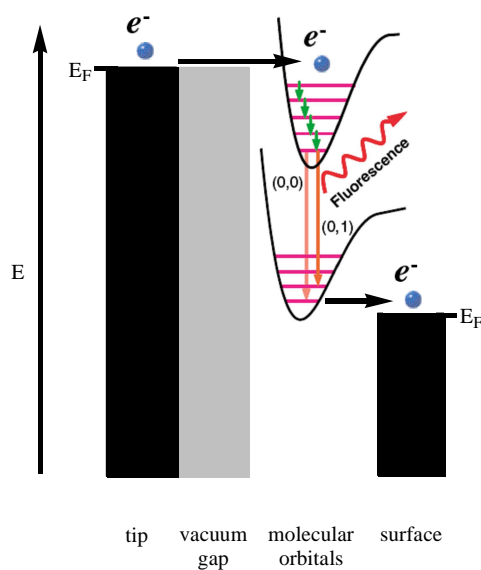
Figure 18: Energy diagram of a STM junction (E_F = Fermi Level).

The optical properties of chromophores are strongly affected by the underlying substrate and therefore luminescence is hardly observed due to quenching of the excited state by the metal surface.[31,33-40] For this reason it is necessary to spatially decouple the chromophore from the metallic substrate.[31,36-39]

In this thesis a new strategy for decoupling a chromophore from the surface within one molecule is presented by the use of rigid and compact cyclophanes as model compounds for STM induced light emission experiments.

An alternative approach to decouple a chromophore from the metallic substrate consists of a small insulating salt layer on the surface. Therefore the synthesis, characterisation and complexation studies of a naphthalenediimide (NDI) chromophore unit comprising peripheral 15-crown-5 ethers as "binding" sites for K^+ cations of the salt layer is also presented in this thesis (see chapter 2).

2. Description of the aims of this work

This work is split into two parts according to two projects. One concerns the development of model compounds for scanning tunnelling microscope and induced light emission experiments from single molecules. A second investigation was made of the orientation factor according to Förster resonance energy transfer (FRET).

2.1. Development of model compounds for STM induced light emission experiments

Luminescence from chromophores bound to metallic substrates is hardly observable due to quenching of the excited state by the metal surface. Therefore the synthesis and characterisation of a cyclophane model compound with two chromophores as shown in *figure 19* was envisaged in order to decouple one chromophore from the surface.

The first chromophore is hypothesised to adsorb onto the metal surface for self-assembly, which is supposed to arrange the molecules in a regular packing motif required for high resolution STM investigations. Consequently, the second chromophore should be spatially separated and therefore decoupled from the metallic surface, remaining its luminescence properties for STM induced light emission experiments.
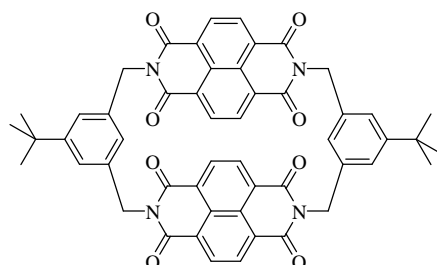
Figure 19: Symmetric NDI cyclophane structure as model compound for STM induced light emission experiments.

It has been observed that a thin salt layer can act as an insulator between the substrate and the metallic surface[38] and therefore the synthesis and characterisation of a naphthalenediimide (NDI) chromophore unit with two 15-crown-5 ethers attached was envisaged (*figure 20*).

Using this approach for STM induced light emission experiments via decoupled chromophores by a small salt insulator, we expect that the attached 15-crown-5 ether units at the NDI show a higher binding affinity to the salt layer compared to the bare metallic surface. Moreover, 15-crown-5 ethers are known to form sandwich-like complexes with barium and potassium cations and therefore they are ideally suited for the envisaged experiments, because each one only occupies the half hemisphere of a cation. Thus, the 15-crown-5 ethers are expected to be located at well defined positions on the salt layer and therefore responsible for a regular packing motif.
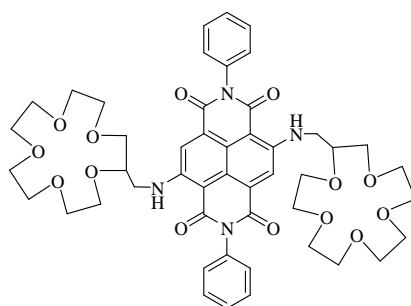
Figure 20: NDI derivative with two 15-crown-5 ethers attached at the core as model compound for better binding to the salt layer.

2.2. Development of a linear model compound for FRET studies

The second project presented in this work focuses on the synthesis and characterisation of a model compound for studying the orientation factor (κ^2) in a FRET system. The general concept was to connect two different dyes by a short spacer, in order to induce FRET (*figure 21*).

A stepwise synthetic strategy should allow varying the central, connecting spacer between the two different dyes (highlighted in blue; *figure 21*).
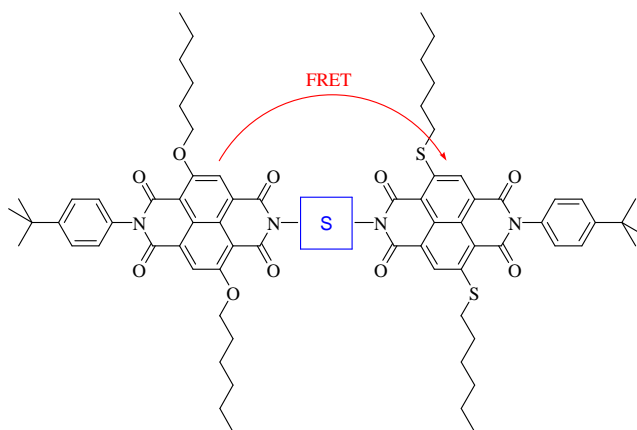
Figure 21: Linear bichromophoric NDI system for studying the orientation factor according to a FRET mechanism; S = spacer.

3. Results and Discussion

3.1. Concept and design of model compounds for STM induced light emission from single molecules

In scanning tunnelling microscope induced light emission experiments the STM is not only used to study the molecules by topographic imaging and tunnelling spectroscopy but also to investigate the intramolecular photon emission by locally exciting the molecule with tunnelling electrons. As displayed by ultrahigh vacuum scanning tunnelling microscopy (UHV-STM) investigations, delocalized planar π-systems form well ordered surface patterns on flat substrates if they have long alkyl substituents attached or functional groups for hydrogen bonds as stabilizing effect between different molecules or if they have a strong interaction with the substrate.[41] However, optical properties of these arranged chromophores are strongly affected by the underlying substrate. Subsequently luminescence is hardly observed due to the quenching effect of the excited state by the metal surface (*figure 22*).[31,33-40]
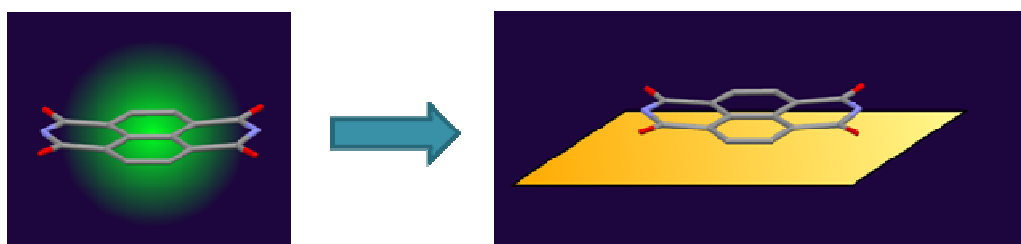
Figure 22: Schematic of a fluorescent molecule and its luminescence quenching upon absorption on a metallic surface.

For this reason several strategies to decouple the chromophore from the metallic substrate were pursued. Insulating salt-[38] or oxide-layers[31,36] or the deposition of double[39] or multilayers[37] of the chromophore under investigation were considered (*figure 23*).

Figure 23: Strategies for decoupling the chromophore from the surface, either by an insulating salt layer (left) or by multilayers (right).

A new concept to address this problem is to use a cyclophane consisting of two chromophores as model compound for such STM induced luminescence experiments. While one chromophore is expected to lie flat on the surface enhancing the self-assembling of molecules,[41,42] which is desired to

arrange the molecules in a regular packing motive required for high resolution STM investigations, the second should be spatially separated and therefore decoupled from the metallic surface by two rigid spacers whilst maintaining its luminescence properties (*figure 24*).
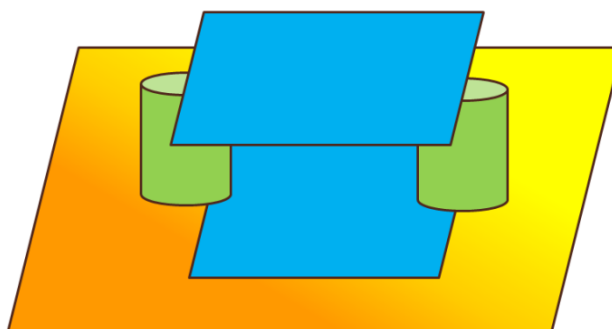
Figure 24: Schematic representation for the decoupling of a chromophore from the metallic surface in a rigid cyclophane structure (blue planes represent the chromophores and the green columns the rigid spacers).

Cyclophanes have already been investigated by STM, either at the solid/liquid interface[43,44] or after deposition from solution.[45] High resolution UHV investigations have not been conducted thus far due to the poor sublimability of the macromolecular cyclophanes that have previously been investigated. Naphthalenediimides (NDIs) have already been successfully used as building blocks for cyclophanes with interesting host/guest properties[16] and in donor-acceptor systems.[46] Moreover, NDIs as well as the 2,6-core substituted derivatives have gained attention in various field's including building blocks for rotaxanes and catenanes,[47-62] hydrogen-bonded organic nanotubes,[63,64] supramolecular metal complexes,[65-70] dyes with unique properties,[71-78] thin film transistors[79,80] and anion-π-slides.[81-83] Furthermore, NDIs display physical features ideally suited for the envisaged experiments such as the tuneability of the electronic properties by its core substituent and a comparably low molecular weight, increasing the chance for the sublimability of NDI derivatives required for UHV surface experiments. Therefore our desired cyclophane structure should comprise two NDI chromophores, which are tightly fixed by two rigid *meta*-methylenebenzene spacers in order to decouple one chromophore from the metallic substrate (*figure 25*). Furthermore, to maintain both the requirements of solubility for chemical processing and sublimability for UHV investigations, the spacer will be functionalized with an additional bulky *tert*-butyl group, keeping the molecule compact in shape (red circles in *figure 25*).
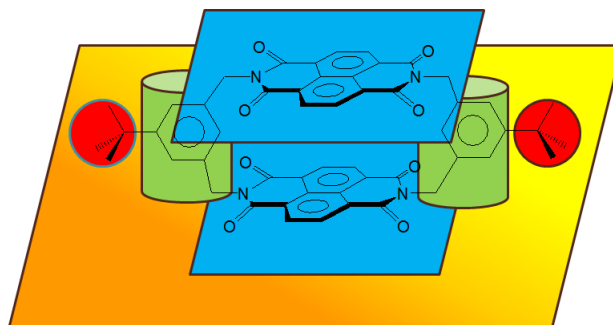
Figure 25: Design of a rigid NDI cyclophane structure for STM induced luminescence experiments.[84]

On the other hand, as previously mentioned, another strategy to decouple a chromophore from the metallic surface can be achieved by deposing first an insulating small salt layer on the surface (see *figure 23* left).

Cyclic polyethers are known in organic chemistry to form complexes with cations.[85] Depending on the size of the cyclic polyethers, Ba^{2+} and K^+ ions (ion radii: 149 pm and 152 pm)[86] can form sandwich-like complexes, which were even isolated as single crystals (*figure 26*).[87-91]
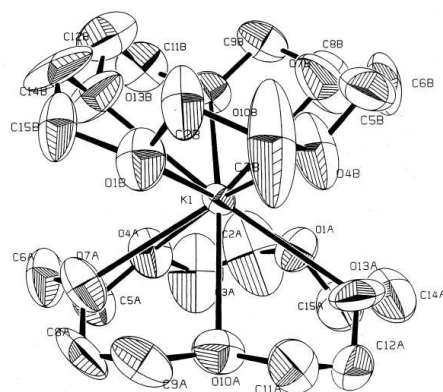
Figure 26: Solid state structure of two 15-crown-5 ethers complexing one potassium cation.[91]

For our purpose to deposit molecules onto an insulating salt layer, 15-crown-5 ethers seemed to be the ideal choice because they occupy only the half hemisphere of a potassium cation. However, we want to adjust it such that the favourable optical properties of the NDI are maintained and therefore we considered the attachment of the crown ether moieties to the NDI core through an amine functional group (*figure 27*). Furthermore, phenyl units without additional *tert*-butyl groups were attached at the imide parts to minimise the molecule-substrate distance.
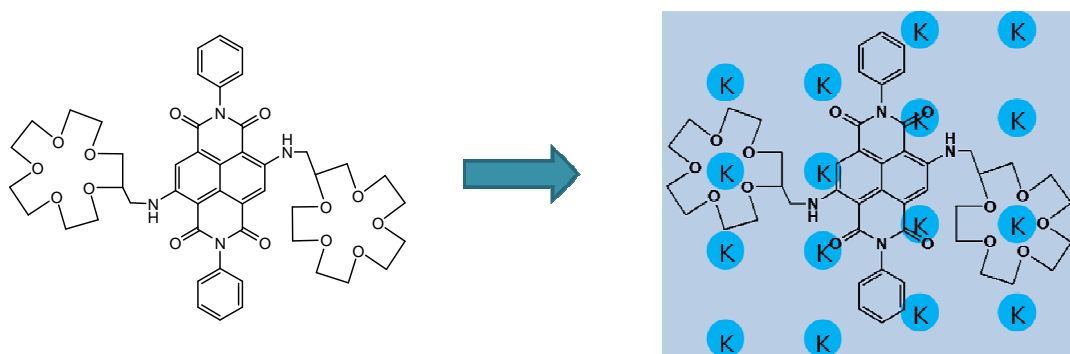
Figure 27: Design and supposed absorption mechanism of an NDI crown ether derivative for STM induced luminescence experiments on a small insulating salt layer.

3.2. Synthesis of model compounds

The following four sections present the synthetic routes towards asymmetric and symmetric NDI cyclophanes, together with the synthesis of crown ether NDIs.

3.2.1. The symmetric NDI cyclophane

A symmetric NDI cyclophane **1** was designed for STM induced light emission experiments as previously described. It is specially thought to be suitable for such investigations because the NDI chromophores are spatially separated from each other by two rigid spacers, meaning that one NDI unit is, after absorption onto a gold surface, decoupled from the metallic substrate. Moreover, the delocalized planar NDI system is believed to form well ordered surface patterns on flat substrates by self-assembly. Finally, the low molecular weight and the compact shape, compared t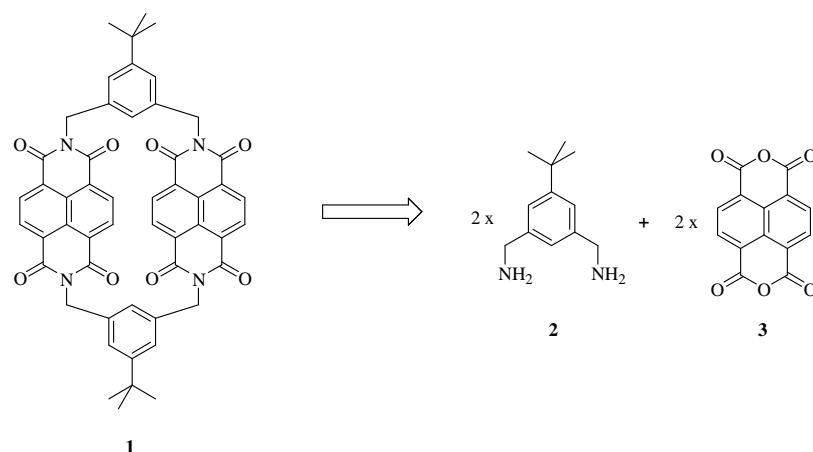o other cyclophane structures, were considered for the sublimability properties for sample preparation. Thus, retrosynthetic analysis of the symmetric NDI cyclophane **1** (*scheme 1*) implied a straightforward condensation of 1,4,5,8-naphthalenetetracarboxylic acid dianhydride **3** with the appropriate diamine **2**.

Scheme 1: Retrosynthetic analysis of NDI cyclophane.

The assembly of the cyclophane **1** is displayed in *scheme 2*. Starting from commercially available 1-*tert*-butyl-3,5-dimethylbenzene (**4**), bromination followed by a *Gabriel* synthesis afforded the rather labile diamine **2** after cleavage with hydrazine. A variety of reaction conditions, including microwave irradiation, was investigated to eventually obtain the cyclophane **1** in a single reaction step by condensing **2** and **3**. However, the isolated yields of **1** did not exceed 4 %.

The synthesis of such macrocycles is usually achieved under high dilution conditions, where both reactants are simultaneously added in a 1:1 ratio, in order to minimize polymerisation (see Lehn's macrocycle in *figure 4* with 10% yield).[16] Due to the fact that **3** was found to be poorly soluble at room temperature in both polar and nonpolar solvents, simultaneous addition of both reactant was not pursued.

Consequently in a typical 1:1 reaction, a 36 mM solution of both, **2** and **3** in *iso*-propanol, containing triethylamine as a base, was refluxed for 3 days. After column chromatography, the desired cyclophane **1** was isolated as white solid in only 1.2 % yield. The decreased yield by using a rigid diamine **2** is possibly due to the higher ring tension for the formation of the desired macrocycle, resulting in more oligomer formation compared to the more flexible octane-1,8-diamine linker used by Lehn.[16]

Interestingly, the best isolated yield of 3.4 % for the cyclophane assembly in a single step has been obtained from a reaction mixture comprising a large excess of the dianhydride **3** (36 mM) in a mixture of dimethylformamide and acetic acid at 120 °C to which the dissolved diamine **2** in dimethylformamide had been added over a period of 1 hour. This observation implies that not only polymerisation and ring tension are responsible for the low yields obtained, but also a possible cyclophane opening process at the imide positions by free amines in solution leading to randomisation of the imide substituents.

$R_1 = R_2 = H$: **4**
$R_1 = R_2 = Br$: **5**   a)
$R_1 = R_2 = N(CO)_2C_6H_4$: **6**   b)
$R_1 = R_2 = NH_2$: **2**   c)
$R_1 = NH_2, R_2 = NHCOO\textit{t}Bu$: **7**   d)

3

3 + **7** $\xrightarrow{\text{e)}}$

$R_3 = NHCOO\textit{t}Bu$: **8**
$R_3 = NH_3^+CF_3COO^-$: **9**   f)

2 + **3** $\xrightarrow{\text{g)}}$

9 + **3** $\xrightarrow{\text{h)}}$

1
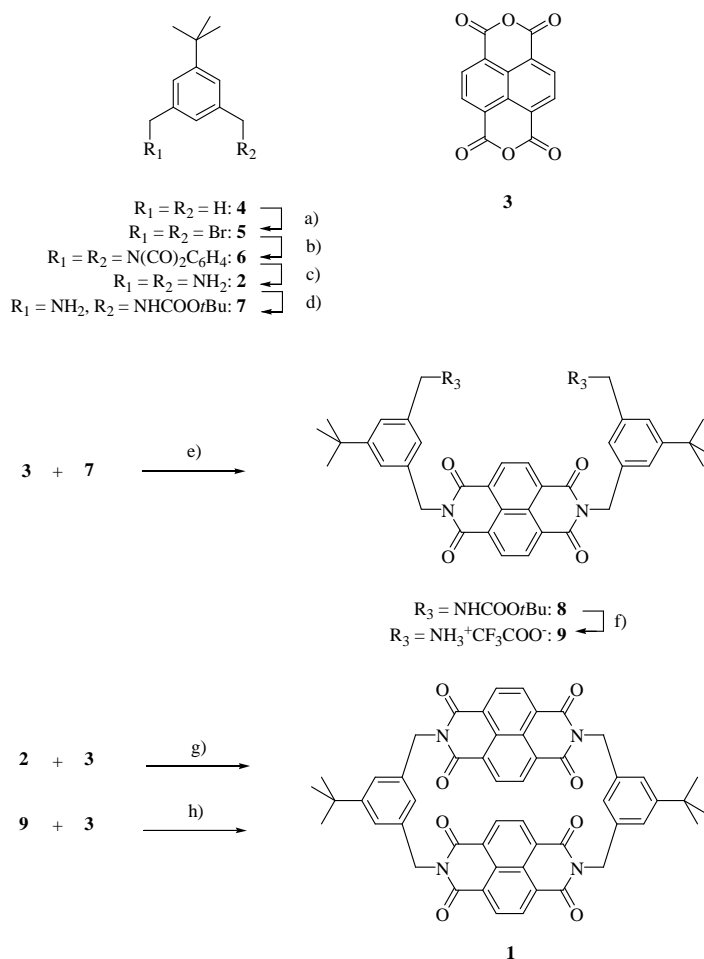
Scheme 2: Synthesis of NDI cyclophane applying a) NBS, AIBN, CHOOCH$_3$, $h\nu$, 4.5 h, 48 %; b) C$_6$H$_4$(CO)$_2$NK, K$_2$CO$_3$, CH$_3$CN, reflux, 5 h, 86 %; c) N$_2$H$_4$, MeOH, reflux, 2 h, 82 %; d) BOC$_2$O, CHCl$_3$, 0 °C, 5 h, 47 %; e) Et$_3$N, *i*-PrOH, reflux, 3 d, 44 %; f) CF$_3$COOH, CH$_2$Cl$_2$, rt, 2 h, quant.; g) Et$_3$N, *i*-PrOH, reflux, 3 d, 1.2 % or DMF, CH$_3$COOH, reflux, 4 d, 3.4 %; h) Et$_3$N, *i*-PrOH, reflux, 3 d, 40 %.

To further improve the yield of the desired cyclophane, a stepwise approach was investigated in order to increase the probability of macrocyclisation against polymerisation (*scheme 2*). Thus, one of the two amine functions of **2** was protected with a *tert*-butoxycarbonyl group (BOC) to provide the amine **7**. Condensation of 2 equivalents of **7** with the dianhydride **3** gave the doubly BOC protected naphthalenediimide **8** in a yield of 44 %, which was deprotected to the diamine **9** quantitatively. Subsequent condensation of the diamine salt **9** with the dianhydride **3** provided the desired cyclophane **1** in 40 % yield after column chromatography.

Whereas the overall yield for this sequence, starting from **2**, was only 8 %, it clearly demonstrated the higher efficiency for the stepwise macrocyclisation and opens an additionally route to asymmetric NDI cyclophanes.

3.2.2. Asymmetric NDI cyclophanes

The optical properties of naphthalenediimides can easily be changed by different substituents at the 2- and 6-positions, resulting in additional intense long wavelength bands, whereas only little influence on the optical properties is notable upon diverse substituents on the imide-nitrogen atoms. These additional absorption bands of 2-, 6-core substituted NDIs is separated by an absorption free region, which gives these dyes their bright colours. Moreover, the fluorescence properties of the chromophore can be dictated by the chemical nature of the substituents. Whereas heteroaryl-substituted derivatives are nonfluorescent, heteroalkyl-substituted NDIs exhibit intense fluorescence.[71-78]

Thus, to core substitute one of both decks of the cyclophane structure is particular appealing due to these additional intense long wavelength absorption bands of core substituted NDIs. Bulky substituents at the 2- and 6-positions of only one NDI chromophore should force the two NDI decks into a less parallel arrangement (*figure 28*) for disfavouring a possible Förster resonance energy transfer,[21] which will be discussed in section 3.3.1.2.
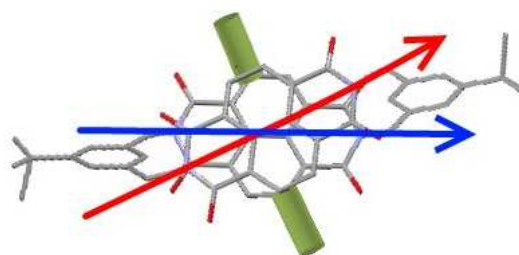
Figure 28: Schematic presentation for the introduction of bulky substituents on only one NDI chromophore which should force the asymmetric cyclophane into a twisted conformation, where the two main axes (red and blue arrows) are not anymore totally parallel to each other for disfavouring FRET.

Synthetically, the assembly of a cyclophane composed of two different NDIs should be straight forward from the stepwise macrocyclisation approach reported for cyclophane **1**. For having a huge diversity of different asymmetric NDI cyclophanes, the compound **10** comprising two chlorine atoms in 2- and 6-positions appeared to be the ideal building block because by simple nucleophilic aromatic substitution reactions various core substituents can be introduced. In order to maintain the fluorescent properties heteroalkyl substituents were considered and especially oxygen, sulphur and nitrogen nucleophiles were desired for achieving the broad diversity according to the absorption region, providing yellow, red and blue dyes.

Therefore, on one chromophore doubly chlorine substituted NDI cyclophane **11** was synthesized as a precursor of the heteroalkyl substituted target structures **12**-**18** as displayed in *scheme 3*.

$R_1 = R_2 = Cl$: **11**
$R_1 = R_2 = S(CH_2)_5CH_3$: **12**
$R_1 = R_2 = N(CH_2)_4CH_3$: **13**
$R_1 = R_2 = StBu$: **14**
$R_1 = R_2 = OMe$: **15**
$R_1 = Cl; R_2 = OMe$: **16**
$R_1 = R_2 = NHtBu$: **17**
$R_1 = R_2 = N(CH_2)_5$: **18**
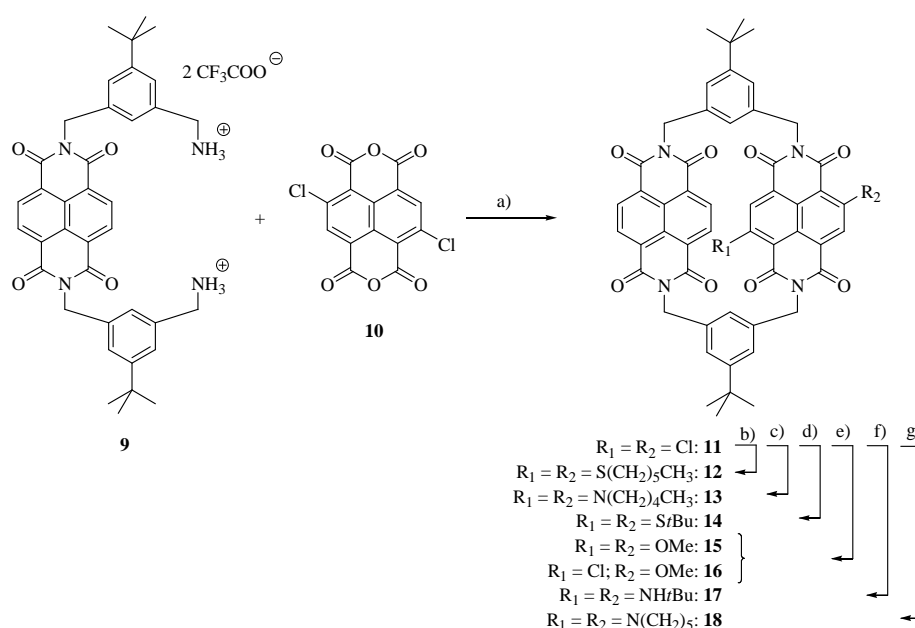
Scheme 3: Synthesis of asymmetric NDI cyclophanes applying a) CH_3COOH, microwave, 170 °C, 15 min, 27 %; b) hexane-1-thiol, K_2CO_3, *i*-PrOH, reflux, 2 h, 34 %; c) pentylamine, K_2CO_3, CH_3CN, 70 °C, 2 d, 45 %; d) 2-methyl-propane-2-thiol, K_2CO_3, CH_3CN, rt, 1 d, 96 %; e) NaOMe, MeOH, 50 °C, 20 h, 42 %; f) *tert*-butylamine, K_2CO_3, CH_3CN, 70 °C, 2 d, 5 %; g) piperidine, K_2CO_3, CH_3CN, 70 °C, 1 d, 71 %.

Various reaction conditions have been investigated for the condensation of the salt **9** with 2,6-dichloro-1,4,5,8-naphthalenetetracarboxylic acid dianhydride **10**. In a first attempt basic reaction conditions were applied by refluxing the diamonium salt **9** ($1.2 \cdot 10^{-2}$ mol/l) in a 10:1 mixture of iso-propanol and triethylamine together with 1.2 equivalents of the dianhydride **10** for 5 days. After purification by column chromatography the desired dichloro cyclophane **11** was isolated in 11 % yield as a white solid. High dilution reaction conditions were investigated for an acidic condensation. Thus, the diamonium salt **9** ($4.7 \cdot 10^{-4}$ mol/l) together with 1.6 equivalents of the dianhydride **10** were refluxed for 2 days in acetic acid. Isolation by column chromatography provided the desired dichloro cyclophane **11** in a slightly improved yield of 14 %. Interestingly, the best yield for this cyclisation reaction was obtained by irradiating with a microwave apparatus. Therefore the diamonium salt **9**

$(5.5 \cdot 10^{-3}$ mol/l) together with 0.97 equivalents of the dianhydride **10** in acetic acid were exposed in a sealed tube to a 400 Watt microvave set-up at 170 °C for 15 minutes. After purification by column chromatography the dichloro cyclophane **11** was obtained in 27 % yield. Assuming comparable chemical behaviour of the 2,6-dichloro-naphthalenediimide unit in a cyclophane structure as in a linear configuration, nucleophilic aromatic substitution reactions should allow replacement of both chlorine atoms by various heteroalkyl substituents.

In order to increase the solubility of NDI core substituted asymmetric cyclophanes a first attempt was made with hexane-1-thiol. After reluxing for 2 hours in *iso*-propanol **12** was isolated in a 34 % yield after column chromatography.

For the same reason pentylamine was chosen. Owing to the weaker nucleophilicity compared to hexane-1-thiol, an excess of pentylamine was added to a stirred suspension of asymmetric dichloro cyclophane **11** in anhydrous CH_3CN. After two days at 70 °C the nitrogen substituted asymmetric cyclophane **13** was isolated as a blue solid after column chromatography in a moderate 45 % yield.

Thus, the long chain heteroalkyl substituents nicely demonstrate the reactivity and addressability of the 2,6-dichloro-naphthalenediimide subunit of the asymmetric NDI cyclophane by nucleophilic aromatic substitution reactions. However, to combine solubility and processability with sublimability required for the envisaged UHV experiments, bulky and compact substituents seemed more promising. Bulky substituents were expected to sterically direct both NDI decks of the cyclophane into a less parallel arrangement (*figure 28*) and thus adding an additional component to the disfavouring of a possible Förster resonance energy transfer (FRET) mechanism (see section 3.3.1.2).[21]

Consequently **11** was exposed under mild reaction conditions to 2-methyl-propane-2-thiol to afford the doubly *tert*-butylsulfanyl substituted NDI cyclophane **14** in an almost quantitative yield of 96 % as a bright red solid after column chromatography. Initial attempts to obtain an oxygen analogue by exposing **11** to an excess of sodium *tert*-butoxide failed. However, a dialkyloxy substituted derivative was obtained by treating **11** with an excess of sodium methoxide in methanol at 50 °C for 20 hours. Besides unreacted **11** (66 %), the dimethoxy cyclophane **15** was isolated in 14 % yield after column chromatography as an intense yellow solid. Interestingly the mono methoxy substituted cyclophane **16** was also isolated in 12 % yield, indicating the lower reactivity of the second chlorine atom in these substitution reactions with alcoholates as nucleophiles. For bulky amine functionalisation a first attempt was made with *tert*-butylamine under the same reaction conditions as for the nitrogen substituted asymmetric cyclophane **13**. But in this case only 5 % of the desired doubly nitrogen functionalized cyclophane **17** was isolated. Mono *tert*-butylamine substituted cyclophane formation was observed by HPLC ESI-MS as for the oxygen derivative, indicating again the lower reactivity of the second chlorine atom for these nucleophilic aromatic substitution reactions.

As primary amines are less nucleophilic than secondary, diisopropylamine as a bulky secondary amine was investigated. After various reaction conditions were explored, the formation of the desired diisopropylamine functionalized cyclophane could not be observed. Probably diisopropylamine is too bulky a nucleophile. However, to maintain both, nucleophilicity and steric bulk, piperidine seemed ideally suited as bulky but compact secondary amine. This time, treatment of **11** with piperidine in anhydrous CH₃CN at 70 °C gave the doubly substituted piperidine cyclophane **18** as an intense blue solid after column chromatography in an unexpectedly high 71 % yield.

3.2.3. Cyclophanes with both NDIs substituted

Expecting that bulky substituent at the NDI core will force the two NDI decks into a less parallel arrangement, as previously shown in *figure 28* for asymmetric NDI cyclophane structures in order to avoid a possible energy transfer mechanism, the synthesis of a cyclophane with both NDIs substituted was envisaged. Once more a one pot synthetic strategy was realized for the both NDIs substituted cyclophane structure **19**, as for cyclophane **1**. The synthesis of NDI cyclophanes **19** and **20** is presented in *scheme 4*.
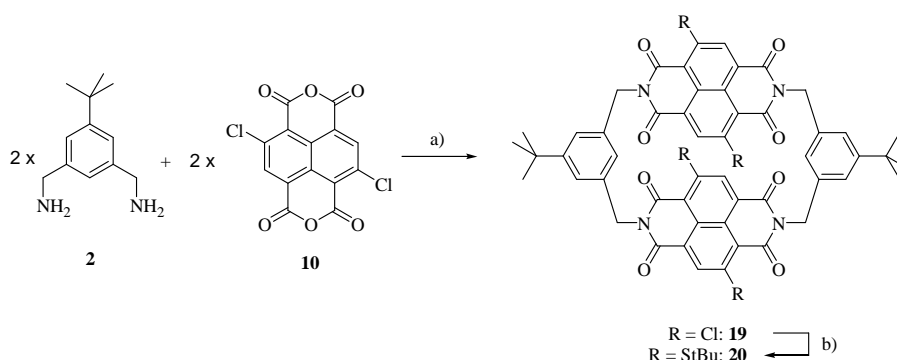

Scheme 4: Synthesis of NDI cyclophanes **19** and **20** applying a) acetic acid, 120 °C, 2 d, 2.7 %;
b) 2-methyl-propane-2-thiol, K₂CO₃, CH₃CN, rt, 2 d, 42 %.

To refluxing a solution of 2,6-dichloro-1,4,5,8-naphthalenetetracarboxylic acid dianhydride (**10**) in acetic acid (4.9 mM) diamine **2** was added dropwise over 1 hour. After stirring for two days, purification by column chromatography provided racemic cyclophane **19** as a white solid in 2.7 % yield. This is comparable to the yield for the one step cyclisation of the symmetric NDI cyclophane **1**. Subsequent nucleophilic aromatic substitution with 2-methyl-propane-2-thiol at room temperature for two days provided, after reversed phase column chromatography, cyclophane **20** as a red solid in moderate 42 % yield.

3.2.4. NDI with crown ethers attached

As previously mentioned in section 3.1, another strategy to decouple a chromophore from the metallic surface can be achieved by deposing first an insulating small salt layer onto the metallic surface (see *figure 23* left in section 3.1).

In order to place molecules onto an insulating salt layer to achieve this decoupling, 15-crown-5 ethers seem to be the ideal choice because they are able to form sandwich-like complexes with barium and potassium cations, meaning that they occupy only the half hemisphere of these cations (see *figure 26* in section 3.1). So, using e.g. a barium chloride or potassium chloride salt layer as an insulator, **22** is expected to be preferentially located on the salt than on the bare gold surface due to the higher affinity of the crown ethers to cations (*figure 29* and see also *figure 27* in section 3.1). Moreover, the nice optical properties of the NDI should be maintained and therefore the attachment of the crown ether moieties to the NDI core via an amine functional group was envisaged (*figure 29*). Finally, at the imide-nitrogen positions phenyl units without additional *tert*-butyl groups were considered to minimise the molecule-substrate distance.

22

⬤ = Ba^{2+} or K$^+$
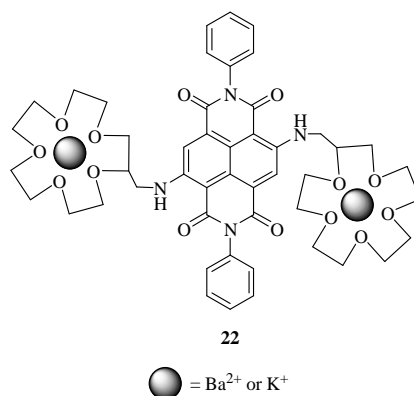
Figure 29: Design of a NDI with crown ethers attached for a better affinity to the salt layer.

The assembly of the NDI crown ether derivative **22** is displayed in *scheme 5* together with the triply substituted side product **23**.
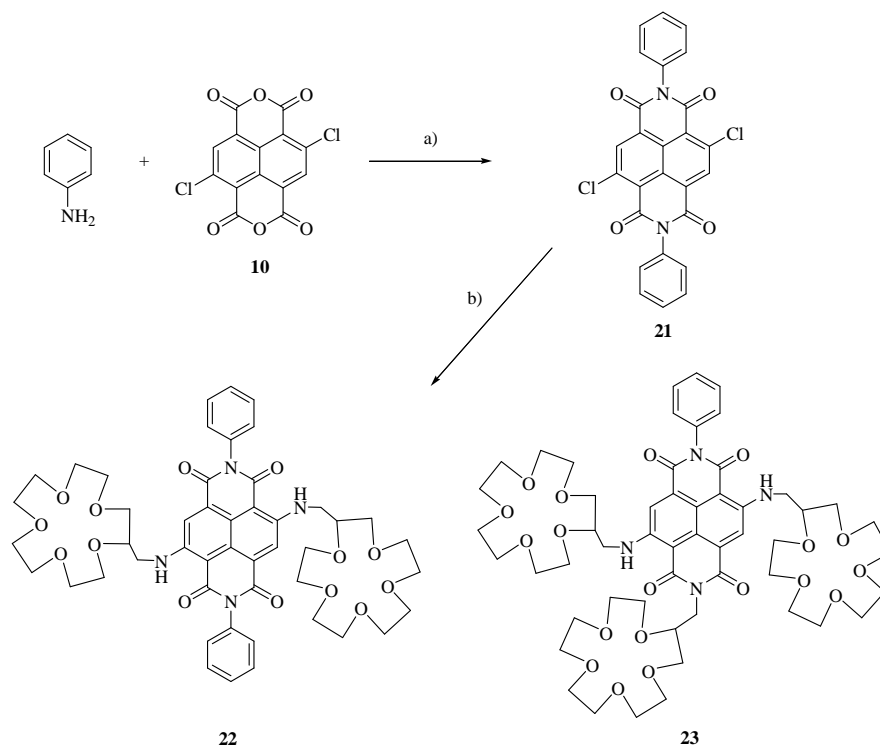

Scheme 5: Synthesis of a NDI crown ether derivative applying a) aniline, CH₃COOH, reflux, 20 min, 64 %; b). 2-aminomethyl-15-crown-5, toluene, Et₃N, reflux, 3 d, 21 % **22** and **23**, 7 %.

First 2,6-dichloro-1,4,5,8-naphthalenetetracarboxylic acid dianhydride (**10**) was condensed under acetic conditions with aniline to form NDI **21** in 64 % yield. Then poorly soluble **21** was further reacted with an excess of 2-aminomethyl-15-crown-5 in a mixture of toluene and Et₃N for 3 days. After column chromatography and washing with 1 M HCl and saturated NaHCO₃ solution the desired NDI crown ether derivative **22** could be isolated as a blue solid in 21 % yield. A side product bearing three crown ether moieties **23** was also isolated in 7 % yield. The formation of **23** proofs the previously hypothesized imide randomization reaction due to imide opening by an amine nucleophile under the applied reaction conditions. Two reddish bands were observed during purification by column chromatography. It is supposed, consistent their colour, that these bands correspond to mono core substituted NDIs, but because of the low quantities it was not possible to characterize them adequately.

3.3. Characterisation of the model compounds

3.3.1. The symmetric NDI cyclophane

The principle disadvantage of the one pot synthesis of the symmetric cyclophane **1** was the required assembly of four units to the desired macrocycle in one shot. Beside the desired ring formation, a multitude of polymer side products were formed and some were identified by HPLC-ESI-MS (*figure 30*).
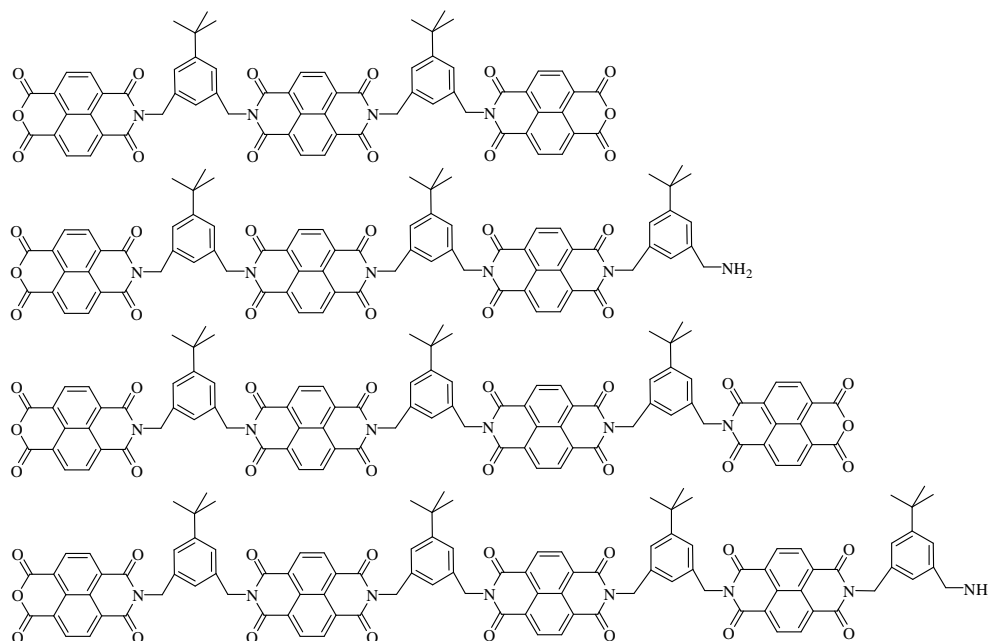

Figure 30: Four polymeric structures, which were formed by the one pot synthetic approach to the symmetric NDI cyclophane **1**.

The trouble in proving the right formation of the target cyclophane structure arose in the observation of three different masses by ESI-MS (see experimental part: 871 ([M+Na]$^+$), 1719 ([2xM+Na]$^+$), 2568 ([3xM+Na]$^+$). There are several plausible structures which could lead to such a detection of different masses (*figure 31*):

1) Larger macrocycles were formed during the reaction. But it seemed strange that the macrocycles consisting of an odd number of subunits were not detected. Disfavour formation of such cyclophanes could have been the reason for the detection of only macrocycles with an even number of subunits.

2) The desired cyclophanes are interlinked to catenanes. This would also explain why there are no macrocycles observed consisting of an odd number of subunits. On the other hand, for the highest mass detected such an interlinked structure seemed unbelievable on steric grounds.

3) It is due to a stacking effect of the cyclophanes to a dimer or trimer arrangement under the applied conditions for ESI-MS.

4) An ion-molecule reaction in the ESI-MS could have occurred.

macrocycles consisting of an even number of subunits

macrocycles consisting of an odd number of subunits

catenanes

π-π stacking
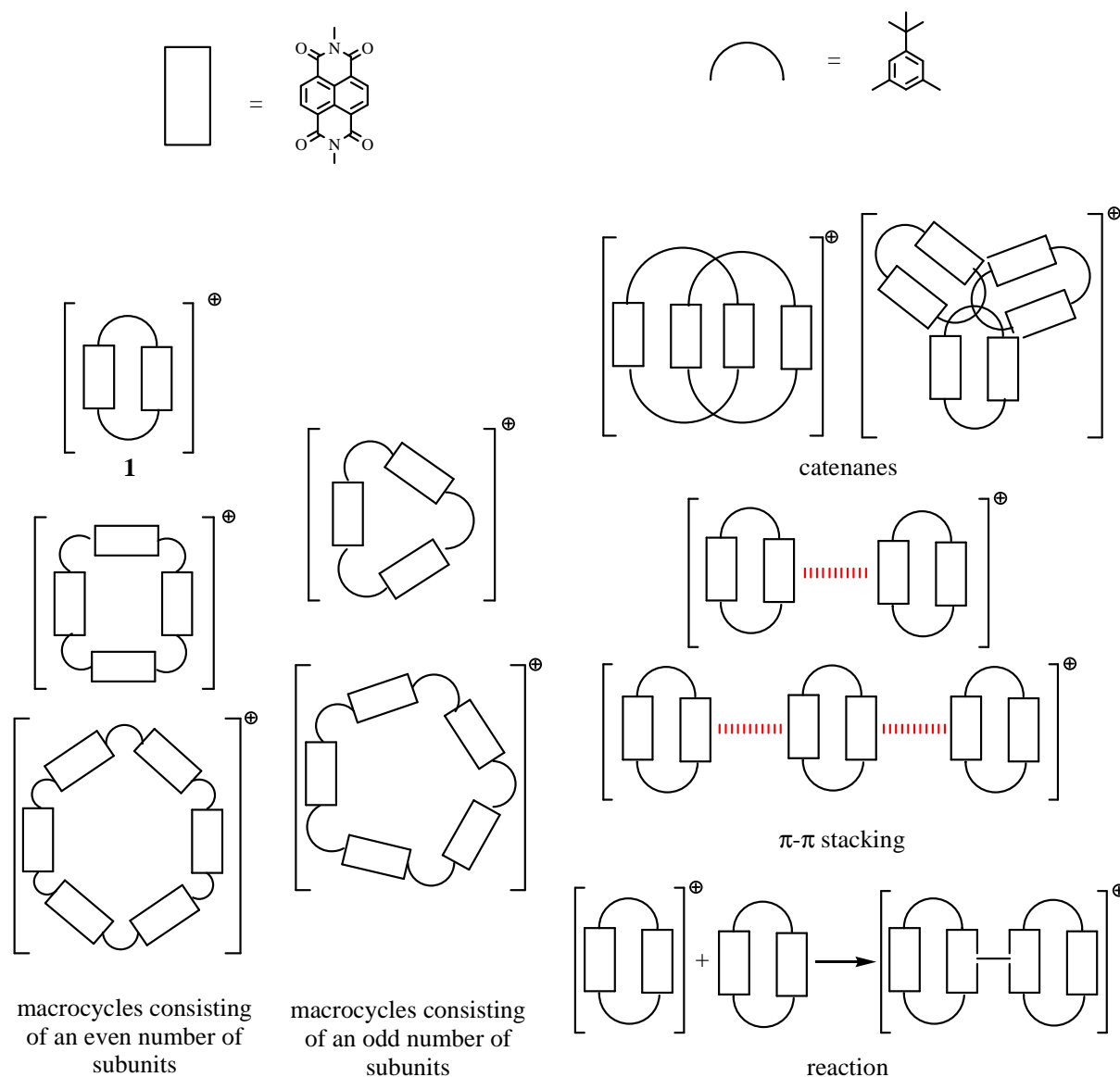
reaction

Figure 31: The different possibilities for the detected masses in ESI-MS: 1). Larger macrocycles, whereas no signal for odd macrocycles appeared; 2). Interlinking to catenanes; 3). π-π stacking; 4). An ion-molecule reaction taking place in the ESI-MS.

In fact the higher macrocycle structures (*figure 31* left) would not differ in ^{1}H-NMR, ^{13}C-NMR or elementary analysis from the desired cyclophane **1**. Therefore further analysis by gel permeation chromatography (GPC) was envisaged and revealed just one signal at 17.1 min, which is in the right range of mass for NDI cyclophane **1** according to polymer standards (see experimental part). From this observation it was possible to exclude the formation of larger macrocycles or catenanes and on the other hand to prove that the one pot synthesis strategy gave the desired NDI cyclophane **1**.

3.3.1.1. Solid state structure of the symmetric NDI cyclophane

Finally, after several attempts, single crystals suitable for X-ray analysis have been obtained by slow evaporation of a solution of **1** in CH_2Cl_2 and **1** in xylene. Despite the molecule's symmetry, the cyclophane **1** does not crystallize with an inversion centre, but opens a minute cavity by tilting both NDI planes with respect to each other (*figure 32*). The inter NDI C-C distances are 7.1 Å between C20 and C40 doubled at the front rim compared with the values of 3.6 Å observed in the back (C14-C46). Furthermore, the interlinking *tert*-butylphenyl spacers both point towards the open side with a distance between C1 and C33 of 15.9 Å.
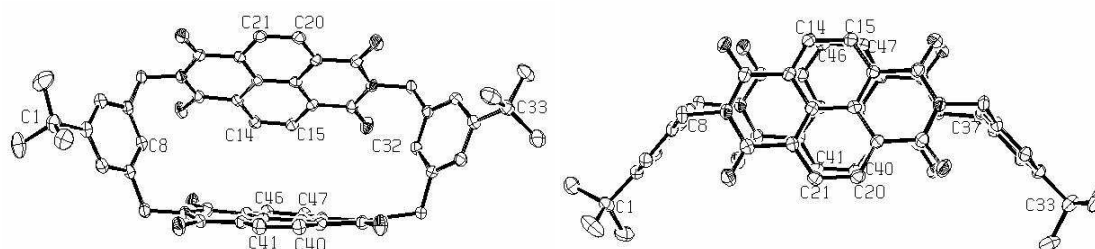
Figure 32: Solid state structure of the symmetric NDI cyclophane **1** obtained by evaporation of a CH_2Cl_2 solution. Front view (left) and top view (right). ORTEP representation; thermal ellipsoids are set at the 50 % probability level and H atoms as well as solvent molecules were omitted for clarity.

In the solid state structure, a CH_2Cl_2 solvent molecule is partially penetrating the cavity of the cyclophane **1**. A very comparable solid state structure has been obtained from technical xylene with a *para*-xylene molecule partially penetrating the cavity of **1** (*figure 33*).
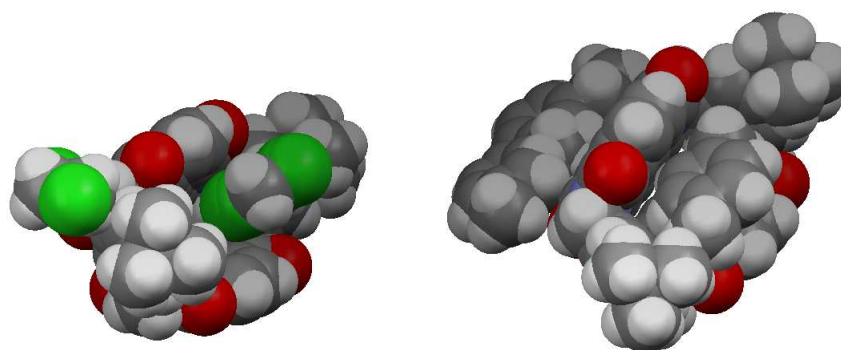
Figure 33: Left: Solid state structure of **1** with two CH_2Cl_2 solvent molecules, one partially penetrating the cavity. Right: Solid state structure of **1** with two *para*-xylene solvent molecules, also shown is one molecule of *para*-xylene partially penetrating the cavity.

Is it possible to form an inclusion complex between our cyclophane and a flat electron rich guest ?

To answer this question we studied the quenching effect of cyclophane **1** according to the fluorescence signal of 1,5-dimethoxynaphthalene **24** (*figure 34*). Assuming a 1:1 complex **1⊂24**, a moderate binding constant of 81 M^{-1} has been determined (see experimental part). As a control experiment, the model compound **25** displayed comparable quenching properties with an association constant of the same order (106 M^{-1}). Thus, we concluded that due to the short rigid spacers, the tiny cavity between the two NDIs does not allow complexation of electron rich aromatic systems, compared to Lehn's flexible hexyl bridged cyclophane (*figure 4*). The observed quenching effect is attributed to the association of **24** to the outer surface of cyclophane **1**, which is consistent with the control experiment.
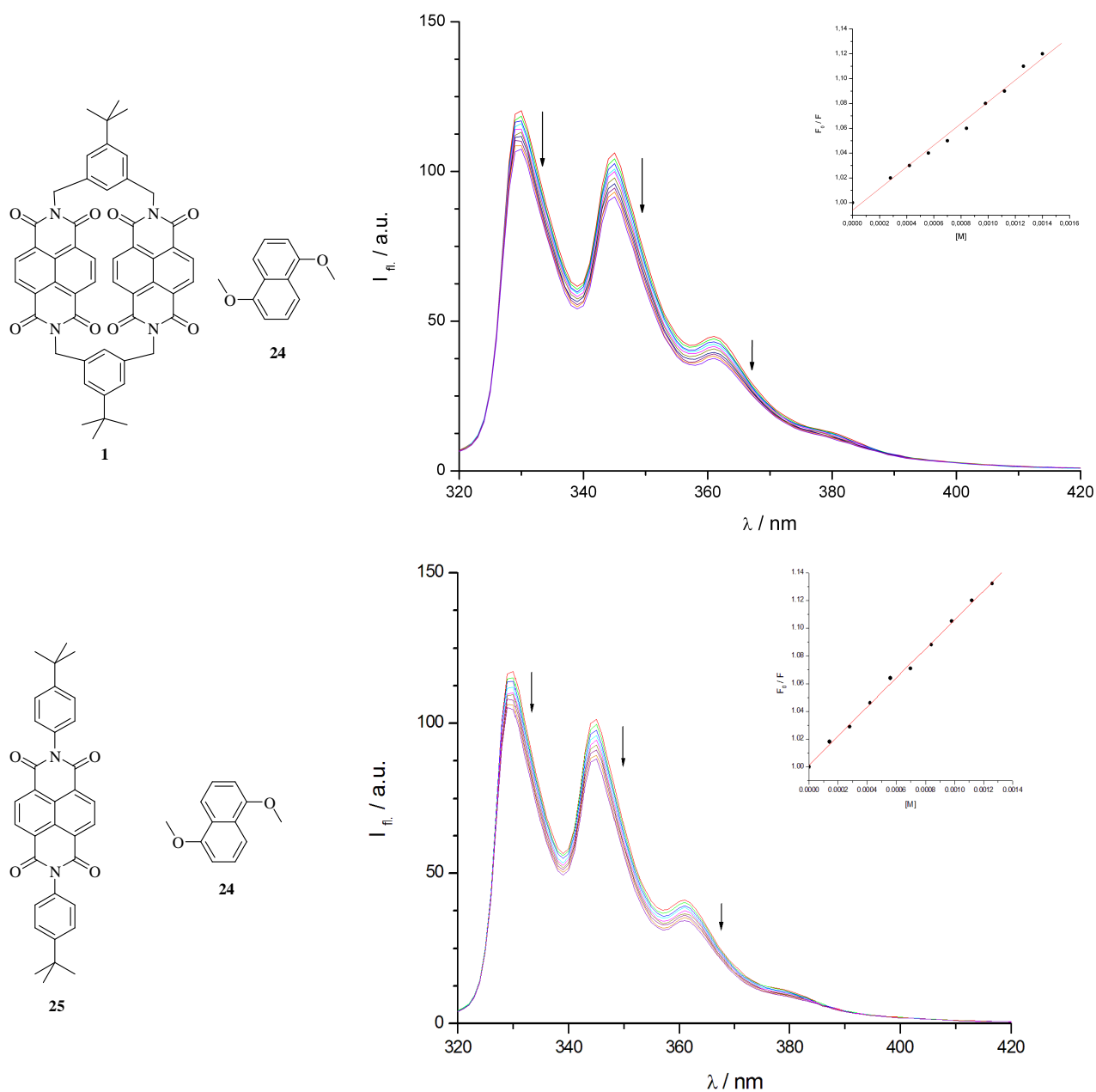

Figure 34: Top: Quenching of the fluorescence of 1,5-dimethoxynaphthalene (**24**) by adding cyclophane **1** (indicated by the arrows). Bottom: Quenching of the fluorescence of **24** by adding the linear model compound **25** (indicated by the arrows). Binding constants were determined assuming a 1:1 complex (see Stern-Volmer plots).

### 3.3.1.2. STM investigations of the symmetric NDI cyclophane

Of particular interest was the suitability of cyclophane **1** for UHV experiments and investigations of its self-assembly properties on metal surfaces. In order to become familiar with such NDIs for UHV experiments, concerning the possible decomposition of the molecules prior sublimation, the linear model compound **25** was investigated. **25** consist of similar building blocks, namely the NDI chromophore, a phenyl part and an additional *tert*-butyl unit, which increases the processability in solution. Therefore, we expect analogous molecule-molecule interactions on the metal surface for the NDI cyclophane **1** as for the model compound **25** upon self-assembling.

Thus, after deposition of **25** under UHV conditions onto an Au(111) surface, the STM image shows a large island of molecules (**25**) next to the bare gold surface (*figure 35*).
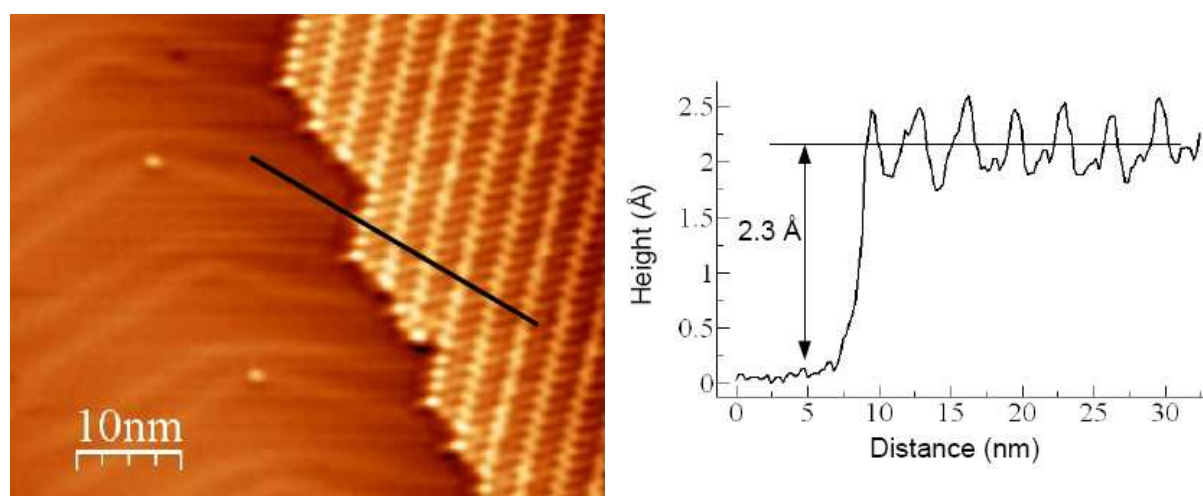

Figure 35: Large island of molecules (**25**) next to the bare gold surface. The height profile was measured along the black line in the STM image.

A height profile revealed an averaged distance of 2.3 Å from the surface. This indicates that the molecules of **25** are laying flat on the gold surface and not perpendicular as illustrated by *figure 36*.
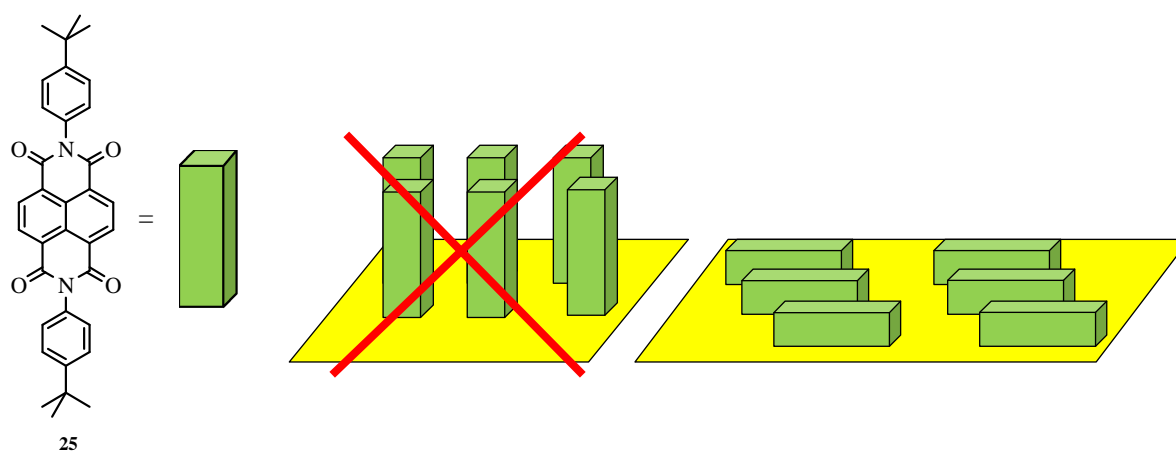

Figure 36: The molecules (**25**) are laying flat on the gold surface at a height of 2.3 Å.

25 self assembles in densely packed, regular parallel rows with a distance of about 1.5 nm as can be seen in *figure 37*. The *tert*-butyl units appear as bright spots, while the NDI chromophore lies flat on the surface between them in the darker region. The molecular structure of **25** is overlaid suggesting a pair of hydrogen bonds between neighbouring molecules stabilizing the arrangement in stripes.
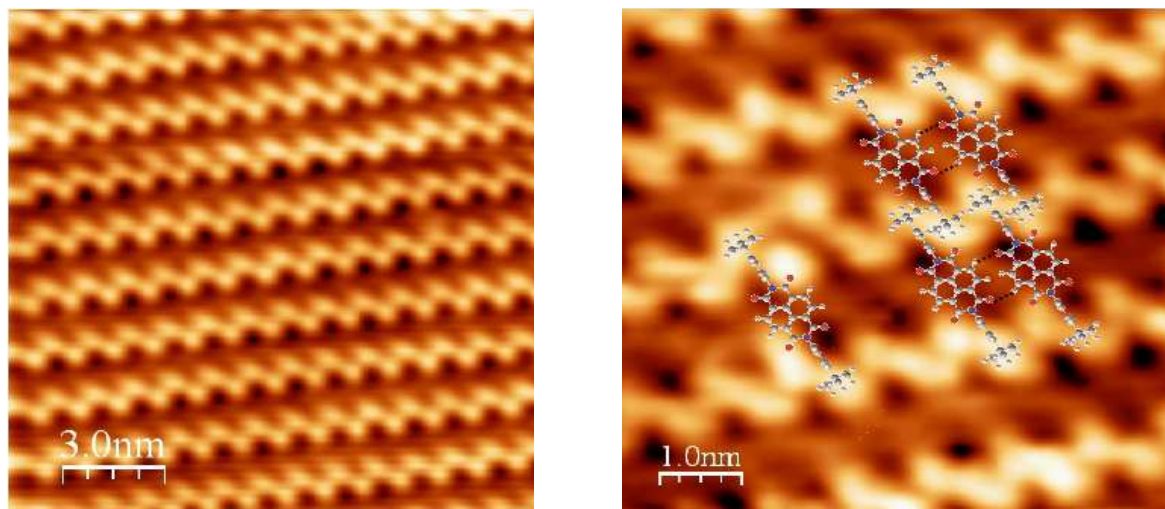

Figure 37: Self-assembled monolayers obtained by sublimation of the NDI model compound **25**; left: large area self-assembly in parallel stripes; right: high resolution image comprising overlaid molecules. Intermolecular hydrogen bonds are indicated by the dotted lines.

The spatial proximity (0.2 nm) of the carbonyl oxygen and the naphthalene hydrogen of the neighbouring NDI chromophore indicate the formation of two hydrogen bonds between two neighbours in a row (*figure 38*).
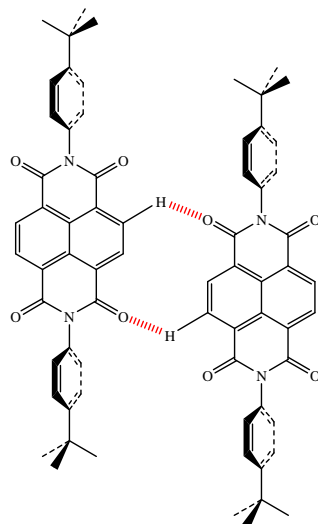

Figure 38: Formation of two hydrogen bonds between the carbonyl oxygen and the naphthalene hydrogen of the neighbouring NDI (red lines).

The cyclophane **1** was also deposited on Au(111) samples in a UHV chamber by sublimation. A low resolution STM picture showed the formation of a large island next to the bare gold surface as for the model compound (*figure 39*). The height profile revealed an average height of 5.7 Å, which is in good agreement with a mean value of both heights obtained from the crystal structure data (5.4 Å).
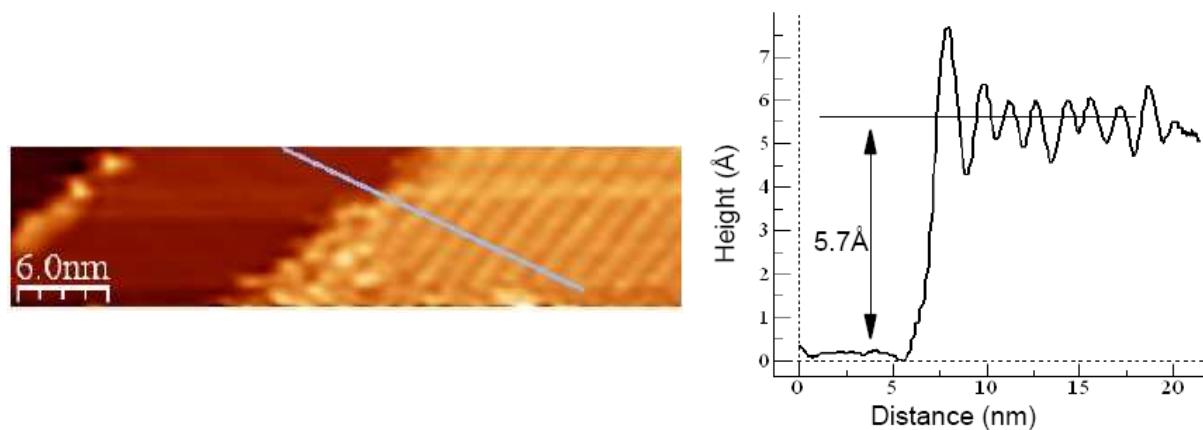
Figure 39: Large island of NDI cyclophane molecules **1** next to the bare gold surface. The height profile was measured along the grey line in the STM image.

Moreover, the height profile for symmetric NDI cyclophane **1** is more than the double of the linear model compound **25** (*figure 35*). Consequently, the cyclophane structure is not destroyed during the sublimation procedure onto the gold surface, because a possible breaking of the cyclophane structure e.g. at the benzylic positions would have led to a very similar height to that of the model compound **25** (*figure 40*).
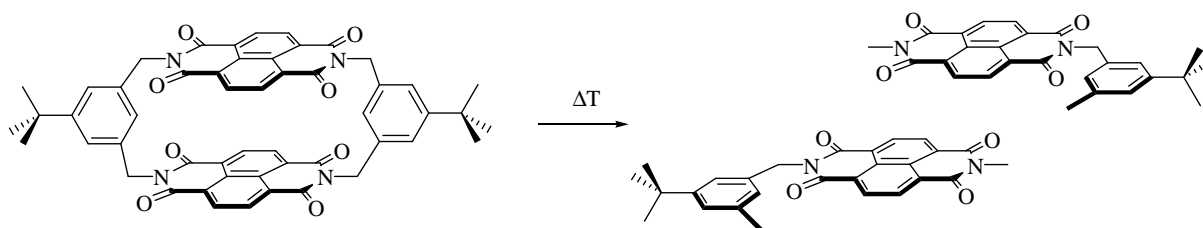
Figure 40: A possible decomposition of the cyclophane structure into smaller parts during the sublimation procedure was not observed in the subsequent STM images (~5Å vs ~2Å).

Further investigation of the sample surface by STM at 6 K revealed large islands consisting of parallel stripes with a regular periodicity of 2.7 ± 0.2 nm (*figure 41 a*). Comparison of the monolayers obtained from NDI model compound **25** with the high resolution STM pictures of the monolayers formed by **1** (*figure 37*), made it possible to identify individual cyclophanes as the building blocks of the stripes (*figure 41 b*) and further demonstrated the sublimation of cyclophane molecules without degradation. This time the chromophore units appear as bright spots in contrast to the previously obtained model compound images. The bent crescent-like shape of immobilized cyclophane **1** correlates nicely to its solid state structure. As illustrated by the added model, it is assumed that the stripes consist of two intercalated cyclophane molecules which are rotated by about 120° with respect to each other. Each row is stabilized by a pair of intermolecular hydrogen bonds (0.2 nm), formed between the carbonyl oxygens and the naphthalene hydrogens of the surface immobilized NDI chromophores as for the linear compound **25** (*figure 42*; green dotted lines).
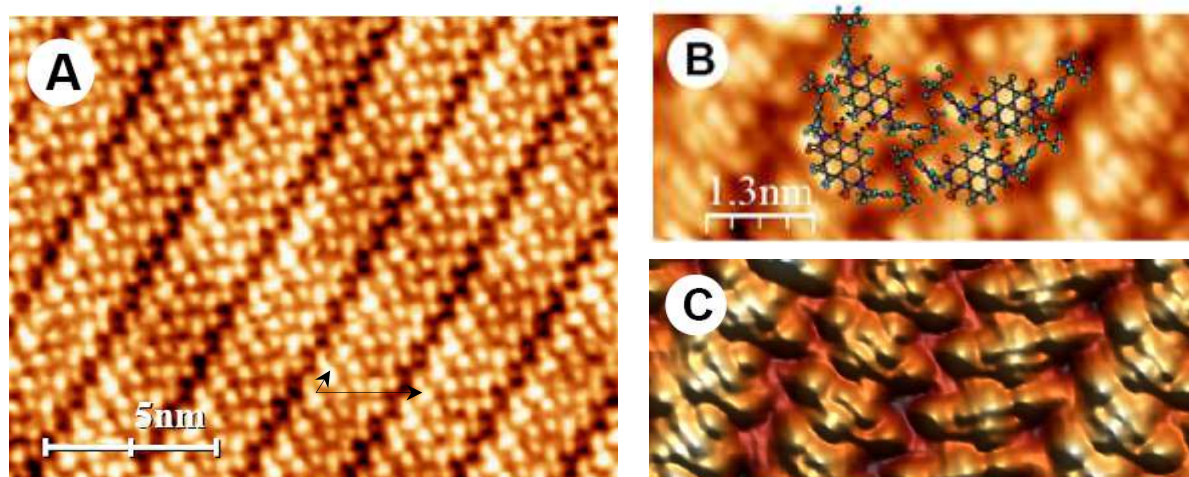
Figure 41: a) Large scale STM image of a cluster of self-assembled cyclophanes **1** on Au(111); b) enlarged stripe-region with the structure of **1** overlaid and c) high resolution image of the same area as displayed in b) Arrows in a) represent unit cell vectors of the 2D molecular organisation. Dotted lines in b) indicate stabilizing hydrogen bonds.
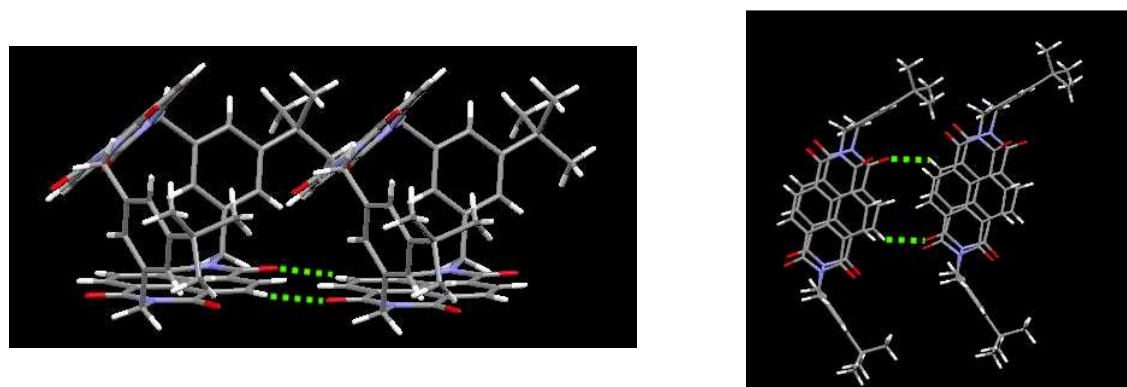
Figure 42: Model based upon crystallographic data showing hydrogen bonds (green dotted lines) between the carbonyl oxygens and the naphthalene hydrogens of the surface immobilized NDI chromophores; left: side view, right: top view.

Similar hydrogen bonds have been found to stabilize the formation of supramolecular nanotubes of amino acid functionalized NDIs.[63] The intercalation of both rows as well as the densely packed arrangement of the parallel stripes seems to be driven by maximisation of the surface coverage. The two vectors defining the 2D unit cell have lengths of 3.5 ± 0.2 and 0.9 ± 0.1 nm, respectively and open an angle of $50 \pm 3°$ (*figure 41 a*).

The Au(111) surface is known to undergo a long-range reconstruction with a typical herringbone pattern as e.g. observed in *figure 35*.[92,93] Moreover, the interaction between molecules and the surface leads to different observations of this reconstructed gold surface. For a weak molecule-substrate interaction the reconstructed surface can still be observed through the monolayer, whereas a strong interaction lifts the gold reconstruction and therefore it cannot be noticed anymore. *Figure 43* shows the reconstruction of the underlying gold surface, which can still be observed highlighted in yellow. This observation indicates that the interaction between the molecule and the substrate is weak, similar to the case of supramolecular polymers on Au(111).[92] A stronger interaction and charge transfer between the molecule and the Au(111) would lead to the lifting of the reconstruction as previously mentioned which can be observed in the case of C_{60} bound to Au(111).[93]
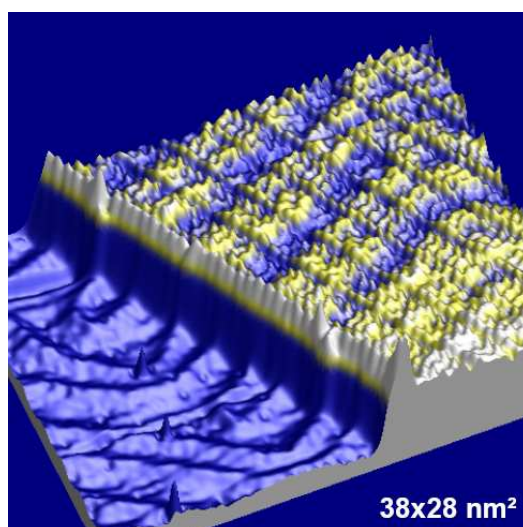
Figure 43: Topographical picture of the self-assembled monolayers obtained by sublimation of the cyclophane **1** displaying the reconstruction of the underlying Au(111) surface.

Thus, the self-assembly properties of symmetric NDI cyclophanes are driven by weak molecule-substrate interactions and additional molecule-molecule hydrogen bonds. Moreover, suggests the structural analogy of immobilized **1** with its solid state structure a comparable spacing of approximately 0.5 nm from the surface for the upper chromophore and therefore proofs the suitability of this concept. The conservation of the spatial separation of both chromophores in these surface immobilized cyclophanes and the predominant interaction of the metal surface with only one of the two π-systems are promising results on the way towards surface decoupled chromophores. Considering Förster resonance energy transfer (FRET) as a potential quenching mechanism for the decoupled chromophore, the parallel arrangement of both main axes of the NDI subunits may be less favourable as illustrated in *figure 44* by the red and blue arrows ($\kappa^2 = 1$).

Figure 44: From the crystallographic data the parallel arrangement of the main axes of both NDI subunits would enhance a possible FRET quenching mechanism (left: top view; right: side view).

Unfortunately, the first STM induced light emission experiments of these symmetric NDI cyclophane (**1**) coated gold surfaces failed.

Because of that reason the achievement of a less parallel arrangement of these main axes was envisaged by asymmetric NDI cyclophanes. As demonstrated in *figure 45* the introduction of bulky groups (green pillars) on just one NDI chromophore should lead to a twisted conformation, where both main axes are no longer totally parallel to each other. As a result, a possible FRET as quenching mechanism should be minimized ($\kappa^2 < 1$). In addition, the heteroalkyl 2-, 6-core substituted NDI chromophore has different optical properties compared to the unsubstituted one. In particular, heteroalkyl substituents at the 2- and 6-positions of NDIs have additional intense long wavelength bands responsible for the brilliant colours of these fluorescent dyes. Consequently, the spectral overlap of donor and acceptor moieties can be tuned according to different substituents, minimizing FRET.
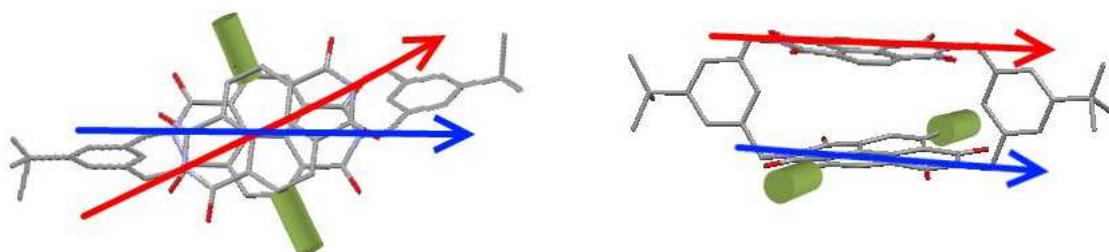
Figure 45: Schematic presentation for the introduction of bulky substituents on only one NDI chromophore which should force the asymmetric cyclophane into a twisted conformation, where the two main axes (red and blue arrows) are not anymore totally parallel to each other (left: top view; right: side view).
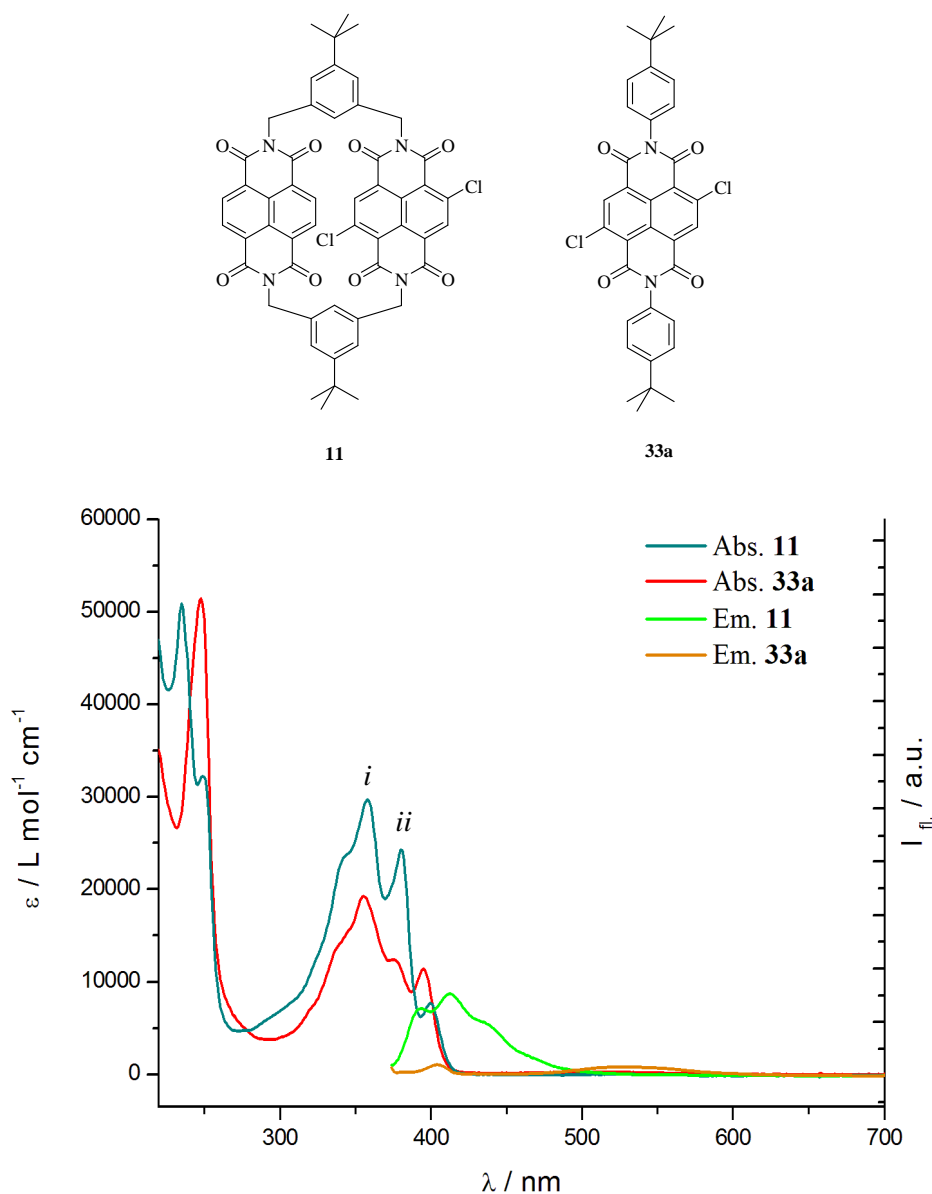
3.3.2. Asymmetric NDI cyclophanes

Measurement of the UV&Vis spectra of NDI cyclophane **1** in acetonitrile showed a minimum energy absorption band at 379 nm as shown in *figure 46*. In the fluorescence spectrum a weak emission band shift by about 16 nm to 395 nm was observed. As for cyclophane **1** the linear NDI model compound **25** showed the typical absorption bands between 300-400 nm.
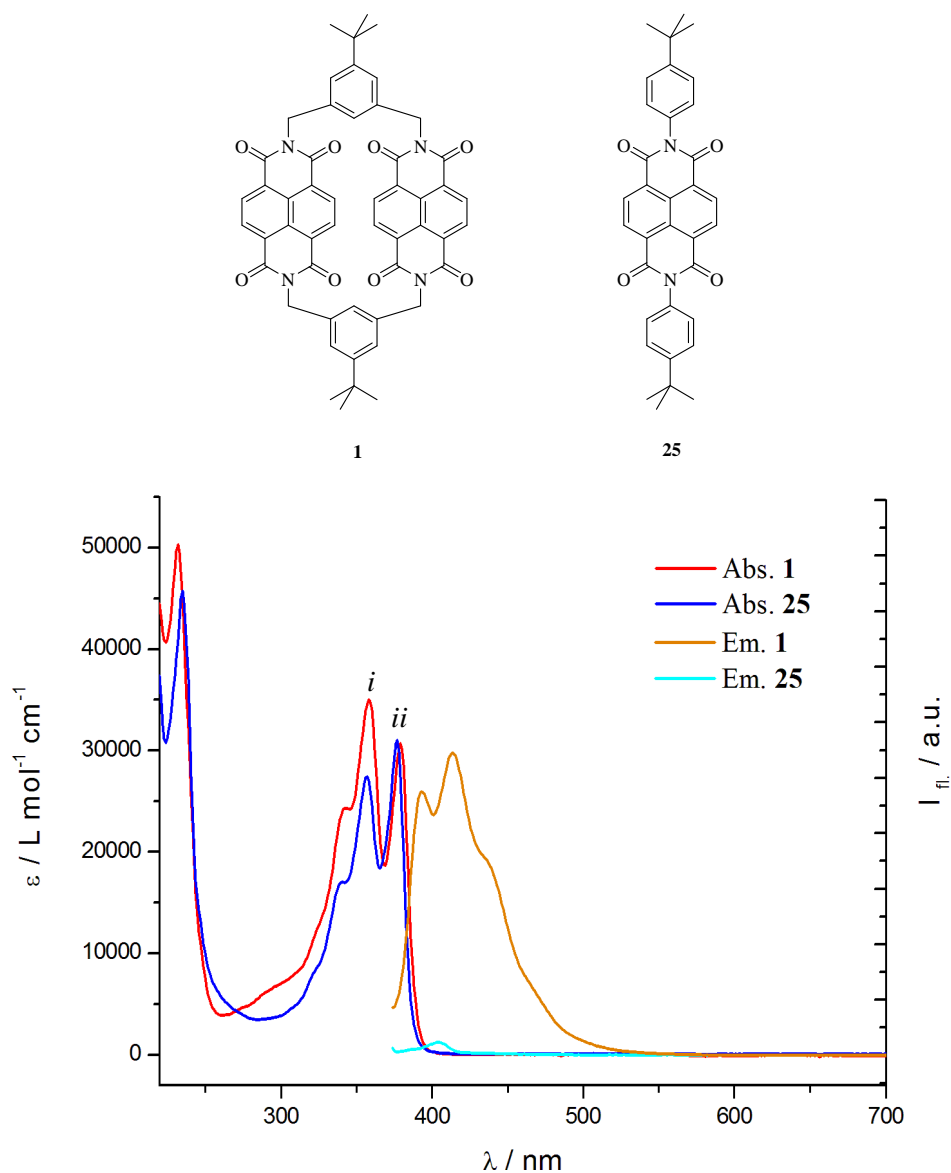
Figure 46: Absorption (straight lines; 10 µM solutions) and fluorescence (dashed lines) spectra of NDI cyclophane **1** (red lines) and linear NDI model compound **25** (blue lines) in CH$_3$CN; λ_{exc} = 358 nm.

Also the asymmetric Cl_2-NDI cyclophane **11** and the linear chlorine substituted **33a** showed absorption bands between 300-400 nm as displayed in *figure 47*. However **11** and **33a** showed an additional weak absorption band at 402 nm and 395 nm respectively. While both cyclophanes **1** and **11** showed the expected mirror image, no fluorescence signal was observable for the linear NDI **25** and **33a** (*figure 46* and *figure 47*).


Figure 47: Absorption (straight lines; 10 μM solutions) and fluorescence (dashed lines) spectra of asymmetric Cl_2-NDI cyclophane **11** (green lines), and linear Cl_2-NDI **33a** (orange lines) in CH_3CN; λ_{exc} = 358 nm.

The reduced fluorescence intensity of asymmetric NDI cyclophane **11**, compared to cyclophane **1**, is attributed to quenching by the heavy chlorine atoms attached at the NDI core. Flat chromophores e.g. naphthalene and perylene are known to form aggregates in solution depending on their concentrations. This "face to face" π-π stacking has been shown to be reflected in a change in the ratio of the bands in the absorption spectra.[77,94-96]

In our case a noticeable change of peak *i* and peak *ii* can be observed for the linear NDI model compound **25**, compared to the two cyclophane structures (**1,11**) and the linear Cl_2-NDI **33a** (*figure 46* and *figure 47*). Whereas for the linear NDI **25** peak *ii* appears more intense than *i* (*figure 46*), the absorption spectra of linear Cl_2-NDI **33a** is generally less intense, broadened and the ratio of peak *i* and *ii* is inverted (*figure 47*). This observation can be attributed to stacking of linear Cl_2-NDI molecules (**33a**) in acetonitrile due to the low solubility in contrast to the highly soluble linear NDI **25**. The same change of the absorption bands, peak *i* and *ii*, was seen for the NDI cyclophanes **1** and **11** as shown in *figure 46* and *figure 47*, a logical conclusion of two close chromophores, compared to the linear NDI model compound **25**.

Asymmetric NDI cyclophane **11** was further envisaged for STM investigations with the expectation of a less parallel arrangement of the two NDI main axes due to the bulkier chlorine atoms located on only one chromophore. Therefore the asymmetric Cl_2-NDI cyclophane **11** was placed onto the Au(111) surface by the same sublimation procedure as for linear NDI **25** and cyclophane **1**. *Figure 48* shows a low resolution STM image of Cl_2-NDI cyclophane **11**, acquired at 6 K together with the measured height profile. The height of 5.8 Å corresponds nicely with the previously obtained spacing for the symmetric NDI cyclophane **1** (5.7 Å) on the gold surface.
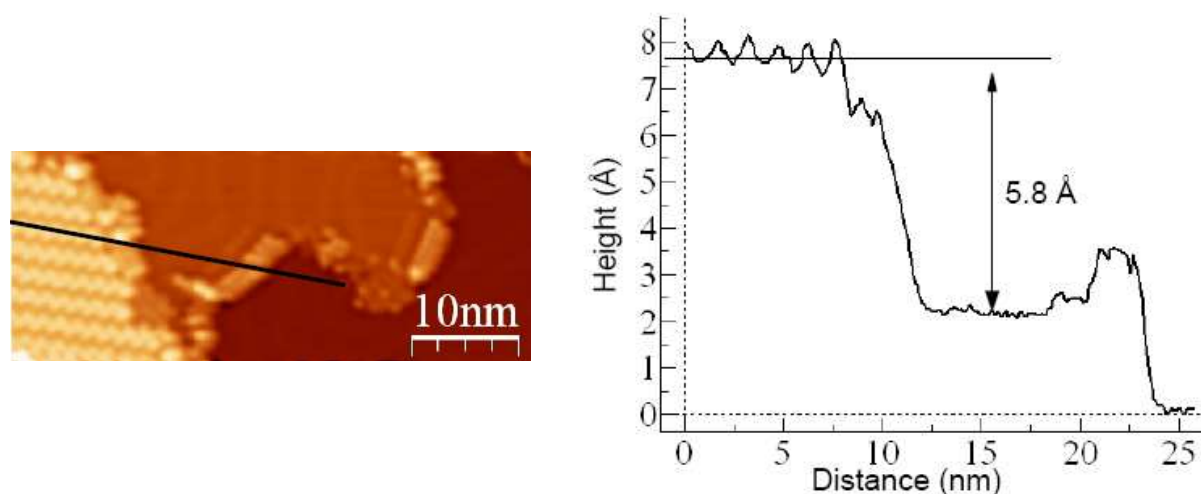
Figure 48: Island of asymmetric NDI cyclophane molecules **11** next to the bare gold surface. The height profile corresponds to the black line in the STM image.

Further investigation of the sample surface by STM revealed islands with alternating rows; forming an ordered zigzag pattern of asymmetric cyclophanes **11** (*figure 49*). Such a molecular organization is totally different from the prior observed parallel stripe pattern of cyclophane **1**. As illustrated by the added model in *figure 49* we assume that each row is consisting of just one enantiomeric form (see later S_2-NDI cyclophane). In comparison to the croissant-like, "C-shape" conformation of the symmetric NDI cyclophane **1**, asymmetric NDI cyclophane **11** shows an "S-shape" conformation. Consequently, one chromophore should lay flat on the metallic surface, while the other is decoupled from the underlying gold surface as proposed for the symmetric NDI cyclophane **1**.
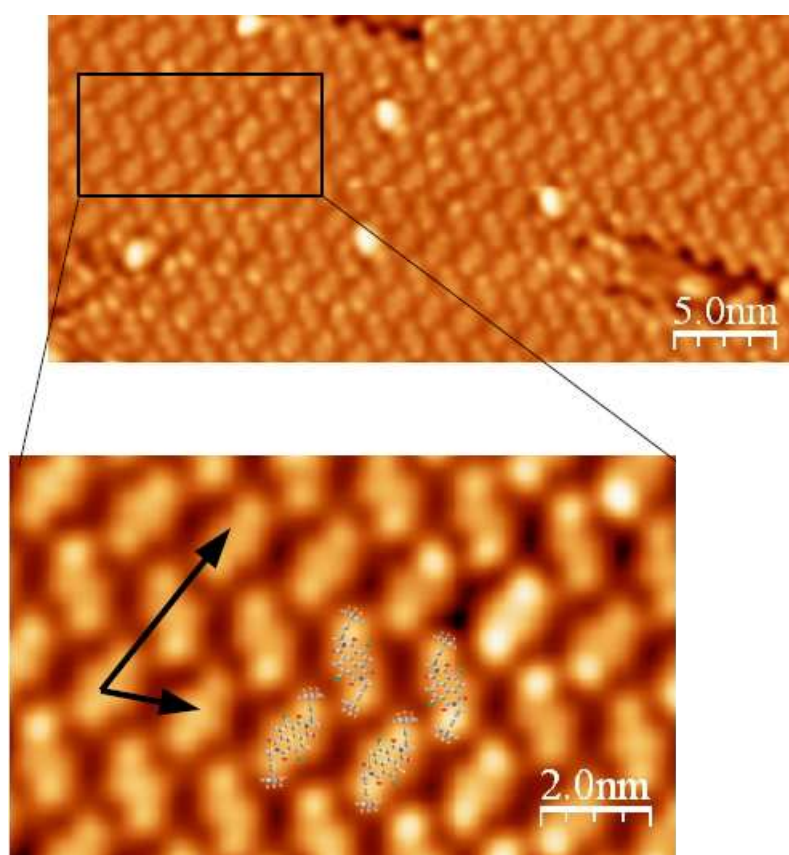
Figure 49: Large scale STM image of self-assembled Cl_2-NDI cyclophanes **11** on Au(111) with an enlarged region with the structure of **11** overlaid. The arrows represent unit cell vectors of the 2D molecular organisation.

The densely packed arrangement of the rows seems to be driven by maximisation of the surface coverage, while the increased distance between two adjacent molecules is unlikely to be attributed to the stabilizing effect of hydrogen bonding. Another possible hydrogen bond formation between the *tert*-butyl hydrogens and the chlorine atoms of the next "upper or lower" lying naphthalene core is not expected due to the large distance of about 0.3 nm. The two vectors defining the 2D unit cell have lengths of 3.4 ± 0.1 and 1.7 ± 0.1 nm respectively and open an angle of $63 \pm 1°$ (*figure 48*).

In fact, asymmetric NDI cyclophane **11** has two different plausible mechanisms for absorption onto the gold surface. Either the 2,6-chlorine core substituted NDI chromophore is lifted spatially from the gold surface, or it is directly attached to it. Due to the suspected higher Van der Waals interactions

between the chlorine substituted chromophore and the surface compared to the unsubstituted one, it is hypothesized that the Cl_2-NDI component lies on the gold in order to maximise the surface coverage. But, taking a closer look at the upper STM image of *figure 49* some randomly distributed bright spots are observable. This could be attributed either to defects in the self assembled monolayer or it could be that at these positions the unsubstituted NDI is attached to the gold surface, whereas the chlorine substituted one is lifted which leads to a different observation in the STM image.

Unfortunately, as was also the case for the asymmetric cyclophane **11**, no light emission from single molecules has been observed. However, the fascinating observation of different conformations of cyclophanes **1** and **11** on Au(111) led to the further design and synthesis of different substituted NDI cyclophanes **12**-**20**, as mentioned at the beginning of section 3.2.2., in order to insert larger bulky substituents in the 2- and 6-position of one naphthalene unit and to understand more about the interaction between the two chromophores.

It is particular appealing to core substitute one of both decks of the cyclophane **11** due to the additional intense long wavelength absorption bands of core substituted NDIs. These additional bands are separated by an absorption free region, which is the cause of the brilliance observed for core substituted NDI dyes. Furthermore, the spectral position of these additional bands depends on the substituent, allowing tailoring the spectral overlap between the emission of the unsubstituted NDI and the absorption of the core substituted NDI chromophore. Thus, in spite of the fact that the distance and the spatial arrangement of both chromophores is rather fixed in the framework of the rigid NDI cyclophane, the efficiency of the intramolecular interchromophore FRET can be tuned by these core substituents.

The proximity of both decks in these cyclophanes does not allow for rotation along the NDI main axis and therefore these structures comprising substituents in the 2- and 6-position of one NDI (**11**-**20**) are found to be planar chiral. The asymmetric cyclophanes **11**, **14**, **15** and **18** (*figure 50*) were fully characterized by ^{1}H- and ^{13}C-NMR spectroscopy, mass spectrometry and their purity was analysed by high performance liquid chromatography (HPLC).
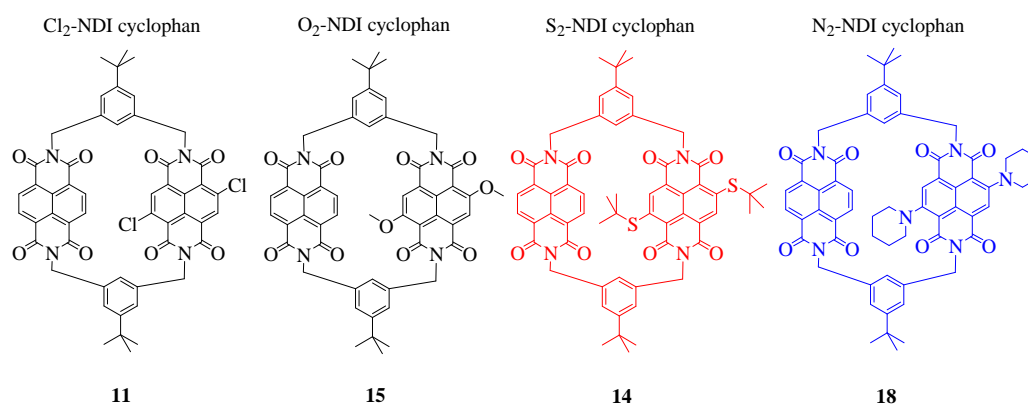
Figure 50: Structures of asymmetric cyclophanes **11**, **14**, **15** and **18**.

The UV/Vis spectra of the three asymmetric NDI cyclophanes **14**, **15** and **18** (sulphur, oxygen and nitrogen substituted) in dichloromethane are displayed in *figure 51*.
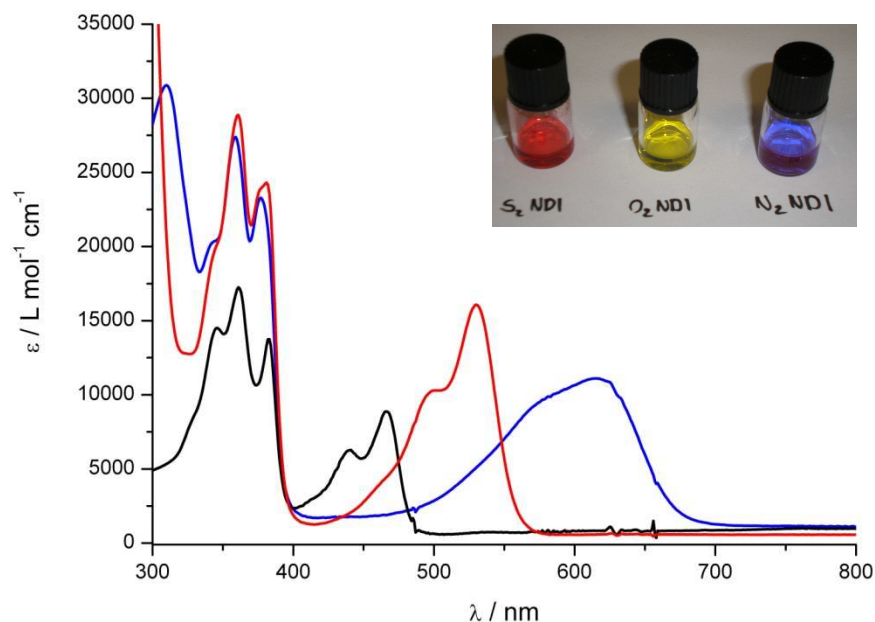
Figure 51: UV/Vis absorption spectra of asymmetric cyclophanes **14**, **15** and **18** (sulphur, oxygen and nitrogen substituted) in CH_2Cl_2 at room temperature (**14**: red line, 10.1 μM; **15**: black line, 6.1 μM; **18**: blue line, 9.5 μM); picture of the samples disolved in CH_2Cl_2 (top right corner).

The typical absorption bands between 300 and 400 nm of the unsubstituted NDI are present in all three spectra. These bands were mainly attributed to π-π* transitions along different directions of the NDI chromophore. Furthermore, all three spectra display additional bands at longer wavelength arising from the 2,6-disubstituted NDI chromophore. The strong effect of the core substituents on the position of these absorption bands is visible in the colour of these samples in *figure 51*.

The methoxy substituents of **15** gave two long wavelength absorption maxima at 438 and 466 nm, responsible for the intense yellow colour of the compound. The *tert*-butylsulfanyl substituents of **14** resulted in an absorption maximum at 530 nm with a pronounced shoulder at 500 nm, giving the compound an intense red colour. Finally, the piperidine substituents of **18** gave a less resolved broad absorption band with a maximum at 615 nm, resulting in the strong blue colour of this NDI cyclophane.

Due to this tuneability of the long wavelength absorption band of the core substituted deck these cyclophanes are particular appealing as model compounds to investigate intramolecular FRET mechanisms. Alternatively, intramolecular electron transfer mechanisms, which have been observed for [2,2]paracyclophane[97] and dithia[3,3]paracyclophane[98] derivatives, might also lead to an exchange of the excited state between both cyclophane decks. However, the increased spacing between both decks results in a decreased orbital overlap of their π-systems in the here reported NDI cyclophanes, compared to these more compact [2.2]paracyclophane and dithia[3,3]paracyclophane systems, which

rather favours a FRET mechanism.[21,22] Of particular interest were the emission spectra of the fluorescent cyclophanes **14**, **15** and **18** as a function of the excitation wavelength.

Figure 52 displays the absorption spectra of the dimethoxy substituted cyclophane **15** together with the emission spectra upon excitation at 361, 382, 440 and 466 nm. Upon excitation at 440 nm and 466 nm only the 2,6-dimethoxy substituted NDI was excited and provided the expected emission maximum at 490 nm with a band pattern resembling the mirrored long wavelength absorption bands. The small stoke shift of 25 nm was also expected for a rigid chromophore like the core substituted NDI. Interestingly, similar fluorescence spectra were recorded upon excitation at 361 nm and 382 nm where both chromophores of **15** were absorbing. These findings are attributed to an intramolecular FRET from the unsubstituted NDI to the 2,6-dimethoxy-NDI chromophore.
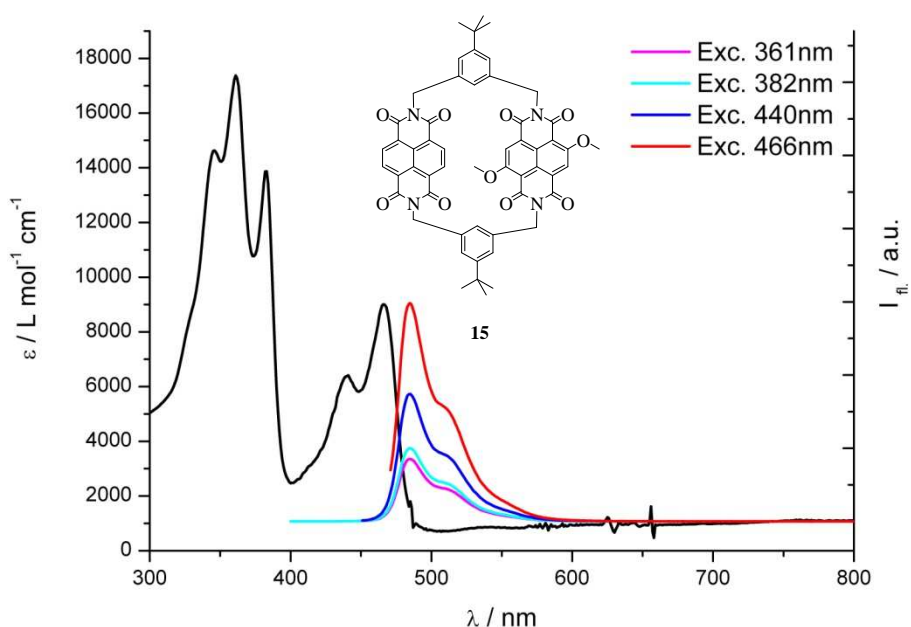
Figure 52: Absorption (black line) and fluorescence spectra (coloured lines: excitation at 361, 382, 440 and 466 nm) of O_2-NDI cyclophane **15** (6.1 μM in CH_2Cl_2 at room temperature).

For the *tert*-butylsulfanyl substituted cyclophane **14** a reduced intramolecular FRET was expected due to the further increased bathochromic shift of the long wavelength absorption bands of the core substituted deck with respect to **15**.

In *figure 53* the absorption spectra of the dialkylsulfanyl substituted cyclophane **14** together with the emission spectra upon excitation at 360, 380 and 531 nm are displayed.
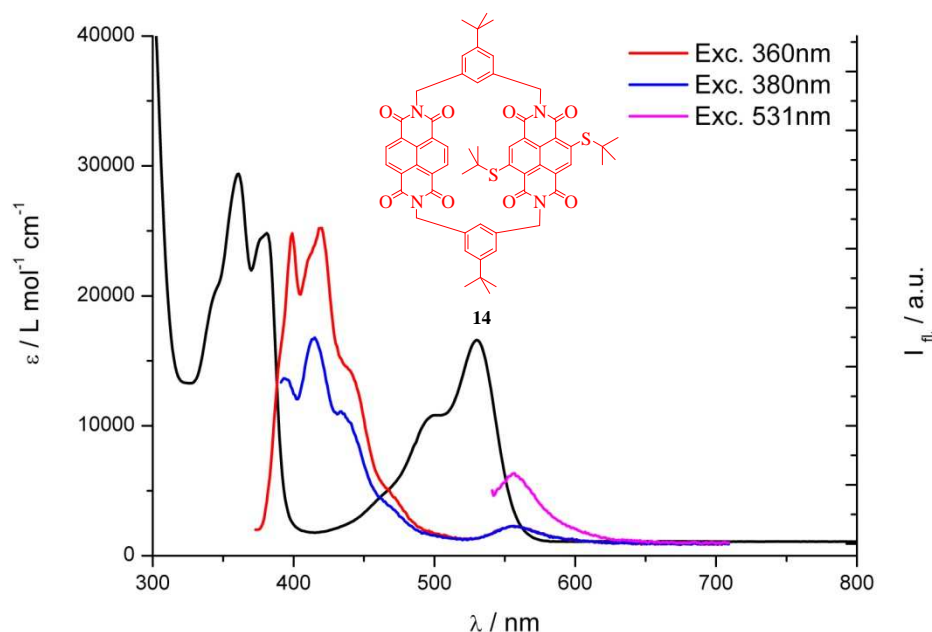
Figure 53: Absorption (black line) and emission spectra (coloured lines: excitation at 360, 380 and 531 nm) of S_2-NDI cyclophane **14** (17.9 μM in CH_2Cl_2 at room temperature).

Upon excitation at 360 and 380 nm, where both chromophores are excited, the typical fluorescence bands between 390 and 470 nm of the unsubstituted NDI were observed together with a weaker long wavelength emission at 560 nm, attributed to the dialkylsulfanyl NDI. The pattern of the bands between 390 and 470 nm resemble the mirrored absorption band pattern below 400 nm. Upon excitation at 531 nm the exclusive emission of the core substituted NDI at 560 nm was observed. Two different mechanisms may cause the emission at 560 nm upon excitation at 360 and 380 nm respectively. Either the emission originates from the excitation of the dialkylsulfanyl chromophore or the excited state is transferred by a FRET mechanism from the unsubstituted NDI to the substituted deck. The occurrence of such a FRET mechanism cannot be excluded due to the remaining small overlap between the emission of the unsubstituted NDI and the raising absorption of the coloured chromophore displayed in *figure 53*. However, as similar weak emissions have also been observed upon excitation at 360 and 380 nm of dialkylsulfanyl NDI model compounds lacking the second deck of the cyclophane, the excitation of the dialkylsulfanyl NDI chromophore of the cyclophane is supposed to be favoured as the origin of this emission.

Intramolecular FRET mechanisms should be further handicapped in the dipiperidinyl substituted cyclophane **18** with its further increased red shift of the long wavelength absorption band. As displayed in *figure 54*, emission of the dipiperidyl NDI subunit at 658 nm was only observed upon excitation at 616 nm, while excitation at 358 and 377 nm only gave rise to emission bands between 400 and 500 nm. Obviously, FRET is completely suppressed by the missing overlap between emission of the unsubstituted NDI and the absorption spectra of the doubly functionalized piperidine NDI in cyclophane **18**.
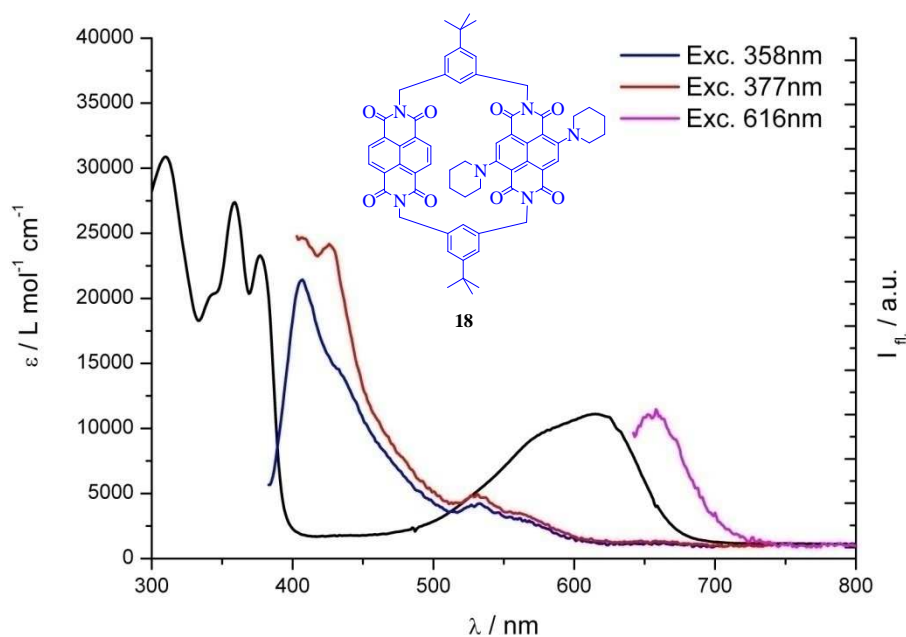
Figure 54: Absorption (black line) and emission spectra (coloured lines: excitation at 358, 377 and 616 nm) of N_2-NDI cyclophane **18** (9.5 μM in CH_2Cl_2 at room temperature).

These fluorescence investigations show that the energy transfer according to a FRET mechanism from the unsubstituted NDI to the core substituted can be controlled by varying the substitution pattern on the NDI subunit (*figure 55*).
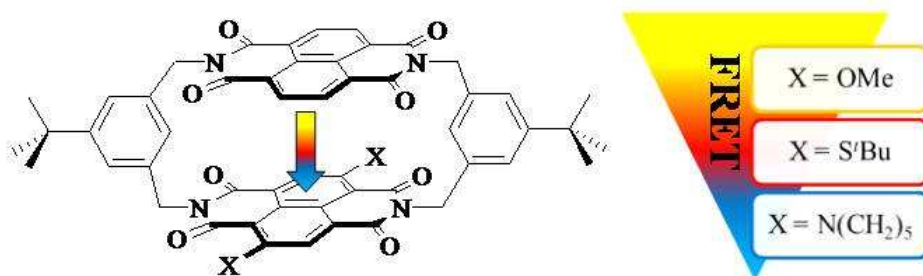
Figure 55: Schematic representation of the tunable FRET properties in asymmetric NDI cyclophanes.[99]

### 3.3.2.1. Solid state structures of asymmetric NDI cyclophanes 14 and 15

After numerous unsuccessful attempts to grow single crystals from the asymmetric planar chiral cyclophanes **11**-**18**, a diluted solution of the di-*tert*-butylsulfanyl cyclophane **14** in CH$_2$Cl$_2$ and EtOAc produced single crystals suitable for x-ray analysis upon slow evaporation. The racemic mixture of the asymmetric S$_2$-NDI cyclophane **14** crystallizes in the orthorhombic space group Pbca. Intermolecular π-π stacking between the electron poor unsubstituted NDI and the electron rich dialkylsulfanyl-NDI form pillars of more or less regular alternating *M* and *P* enantiomers of the cyclophanes **14** in the solid state structure (*figure 56*).
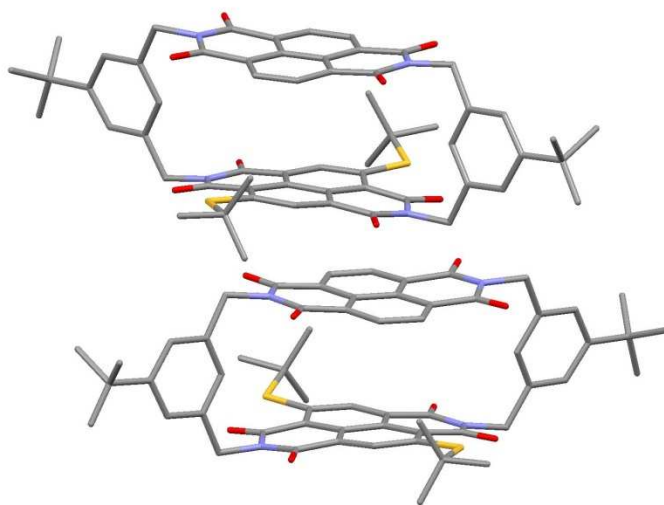
Figure 56: The two planar chiral enantiomers of **14** stacking above each other in the piles of the solid state structure. Top: (*P*)-**14**; Bottom: (*M*)-**14**.

While in *figure 57* an ORTEP picture of the *M* enantiomer of the S$_2$-NDI cyclophane **14** is displayed, *figure 56* shows the stacking of the *P* (top) and the *M* (bottom) enantiomer in the solid state. Interestingly, the spatial arrangement of both chromophores differs considerably from the one reported for the parent cyclophane **1**. While a tilted arrangement of both cyclophane decks with a penetrating solvent molecule was observed for the symmetric NDI cyclophane **1**, both chromophore planes of **14** are almost coplanar. Probably, the increased steric repulsion of both substituents no longer allows the tilting of the unsubstituted top chromophore.

The inter NDI C-C distances are in the centre with 4.3 Å slightly shorter than at the terminal nitrogen imide positions of 4.8 Å. Thus, the NDI planes are somewhat bent towards the middle.
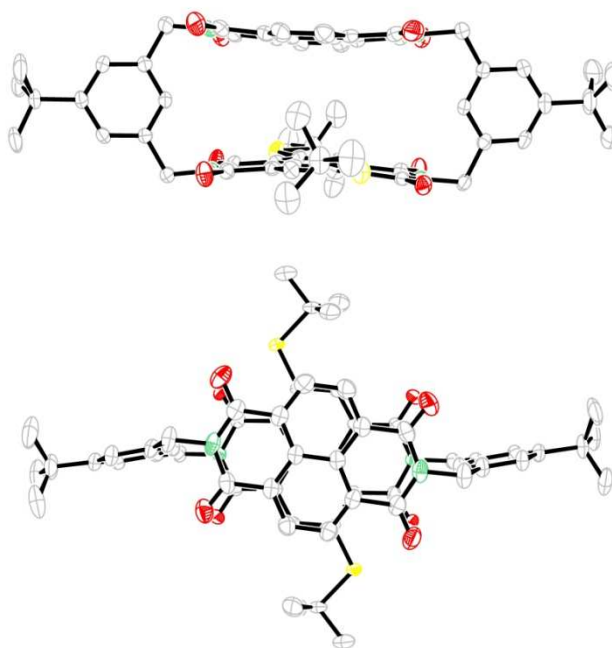

Figure 57: Top: side view; Bottom: top view of the solid state structure of the *M* enantiomer of the planar chiral S_2-NDI cyclophane **14**. Hydrogen atoms are omitted for clarity. Thermal ellipsoids are set at the 50 % probability level in the ORTEP representation.

In spite of the sterically directing substituents, the main axes of both NDI chromophores are almost parallel. This parallel arrangement of both NDI main axes might be further favoured by intermolecular packing effects within the piles. Due to the non-regular ordering in the piling of *M* and *P* enantiomers (*figure 56*) in the solid state, the structure is disordered at the sulphur substituted NDI core (see crystal structure in the experimental part). While the alteration between unsubstituted and substituted NDI within the pile is maintained, about 10 % of the substituted NDIs seem to be functionalized in the 3- and 7-position instead of the 2- and 6-position, indicating the presence of the other enantiomer in about 10 % of the cyclophane positions of each pile.

The enantiomeric compositions of the samples **11**, **14**, **15** and **18** were investigated by high performance liquid chromatography (HPLC) with a chiral column (Amylosetris (3,5-dimethyl-phenyl-carbamate)). All samples displayed the expected racemic 1:1 mixture of the *M* and *P* enantiomer. Preparative HPLC using the same chiral column packing enabled the enrichment of both enantiomers in small samples of the *tert*-butylsulfanyl substituted cyclophane **14**. While for the first isolated peak a ratio of 77/23 was recorded by analytical HPLC, a slightly smaller enrichment of 38/62 was observed for the second peak.

The circular dichroism (CD) spectra of both isolated fractions and of the racemic starting sample are displayed in *figure 58*.
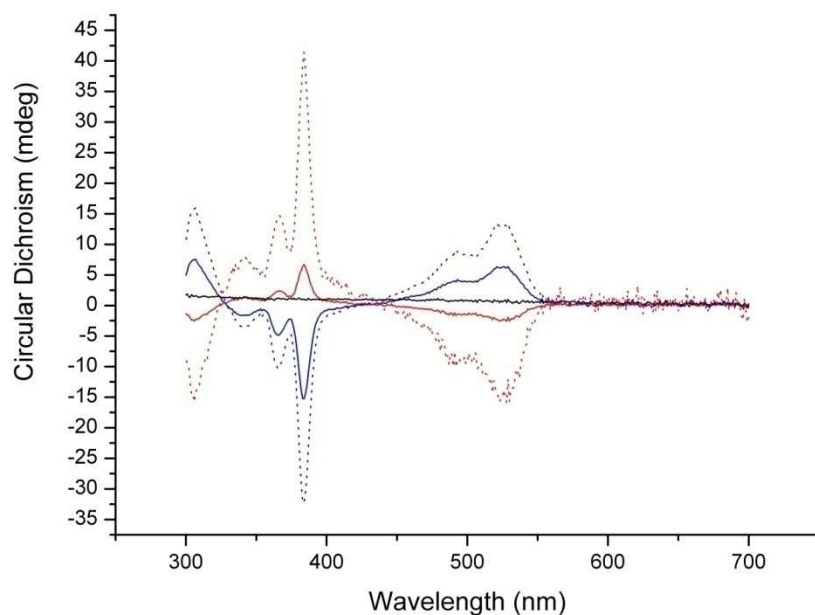

Figure 58: CD measurements of **14** in CH_2Cl_2 at room temperature. Starting mixture (black line) together with both enantiomerically enriched samples (1st peak enriched: blue lines, 8.1 μM; 2nd peak enriched: red lines, 7.0 μM). The dotted lines represent the spectra calculated for a pure enantiomer.

As expected, no signals were observed for the initial racemic mixture of **14**, while the two enantiomerically enriched samples displayed both mirrored features at the same spectral positions as absorption bands were observed by UV/Vis spectroscopy (*figure 51* or *figure 53*). The expected CD spectra of both pure enantiomers are displayed in *figure 56* as dashed lines. All attempts to crystallize the small samples of the enantiomerically enriched samples failed and thus, the assignment of the CD spectra to the corresponding enantiomers has not been possible.

From a diluted solution of O_2-NDI cyclophane **15** in CH_2Cl_2 it was possible, upon slow evaporation, to obtain single crystals for x-ray analysis. The crystal structure unfortunately could not be refined successfully and therefore no supplementary material is provided in the experimental part, but it clearly shows the desired O_2-NDI cyclophane structure (**15**) and its packing.

Intermolecular π-π stacking between the same NDI chromophores form pillars of alternating *M* and *P* enantiomers of the cyclophanes **15** in the solid state structure (*figure 59*).
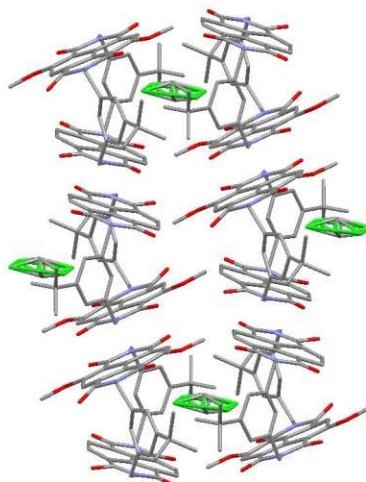
Figure 59: Crystallographic data of the two planar chiral enantiomers (*M* and *P*) of **15**, stacking over each other by intermolecular π-π interactions between the same NDI chromophores in the solid state structure.

Figure 60 shows the *P* (right) and the *M* (left) enantiomer opposite each other in the solid state structure including a distorted CH_2Cl_2 solvent molecule in the cavity formed between them. Interestingly, the O_2-NDI cyclophane displays the same tilted arrangement of both chromophores as observed for the symmetric NDI cyclophane **1**. The inter NDI C-C distances from the top to bottom chromophore are 6.7 Å on the side adjacent to the CH_2Cl_2 solvent molecule compared with the C-C value of 3.4 Å opposite to the CH_2Cl_2 (*figure 60*). In contrast to symmetric cyclophane **1**, where no intermolecular π-π interactions between different cyclophanes was observed, O_2-NDI cyclophane **15** forms columns by π-π stacking. Fascinatingly, it seems that because of the CH_2Cl_2 molecule in the formed cavity, the system is forced to organize the opposite enantiomer rotated by 180° due to steric reasons of the introduced methoxy groups.

Furthermore, in the pillars of the O_2-NDI cyclophane **15** the NDI chromophores of two different cyclophanes are lying perfectly over each other (*figure 59*), while for S_2-NDI cyclophane **14** they are rotated against each other by 60° (*figure 56*).
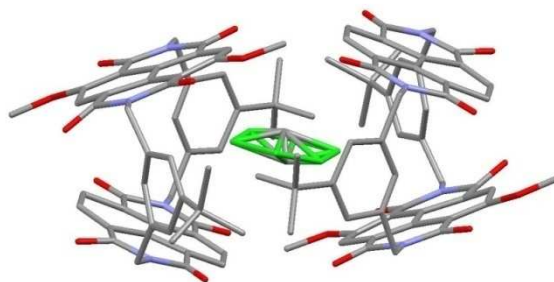

Figure 60: Crystallographic data of the two planar chiral enantiomers of **15** opposite each other in the solid state structure. Left: (*M*)-**15**; Right (*P*)-**15**.

3.3.2.2. STM investigations of the asymmetric NDI cyclophane 14

Due to the known FRET from the unsubstituted NDI to the methoxy substituted NDI, cyclophane **15** is not practical for STM induced luminescence experiments. In addition the piperidinyl substituted asymmetric NDI cyclophane **18** does not show any FRET between the two NDI chromophores, as was presented previously. However, because of its ease of synthesis and high isolatable yield compared to **15** and **18**, and the fact that FRET was predicted not to occur, S_2-NDI cyclophane **14** was envisaged for STM measurements.

Sublimation of S_2-NDI cyclophane **14** onto an Au(111) sample under UHV conditions and subsequent STM investigations revealed islands of self-assembled molecules (*figure 61*). An average height of 5.9 Å was obtained for the S_2-NDI cyclophane **14** monolayer, which is in good agreement to the previously measured heights of NDI cyclophane **1** (5.7 Å) and Cl_2-NDI cyclophane **11** (5.8 Å).
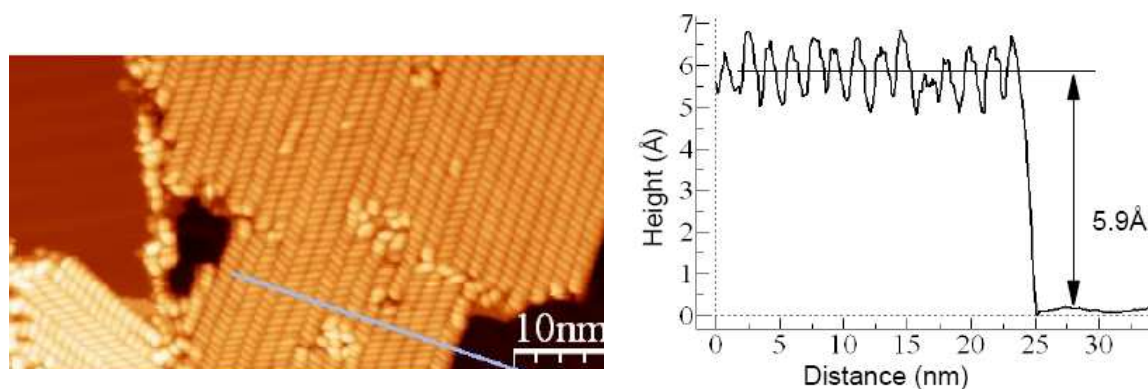

Figure 61: Large scale image with islands of self-assembled molecules **14** on Au(111) and the height profile along the grey line.

Additional investigation of the sample surface by STM revealed parallel rows (*figure 62*), which were not strictly alternating as previously observed for asymmetric NDI cyclophane **11** (*figure 49*). Interestingly, the distance between the individual molecules in a row is shorter compared to the STM image of Cl_2-NDI cyclophanes **11**.

As illustrated by the added model in *figure 62* we can deduce that each row is consisting of just one enantiomeric form. Where alternating rows are found, the molecules are rotated by 70° with respect to each other (*figure 62* on the right). From the overlaid model the distance between the hydrogen's of the sulphur *tert*-butyl substituent and the next carbonyl function of another cyclophane is about 0.3 nm. This distance is too great to expect hydrogen bonding between different molecules on the surface as was proposed for the asymmetric Cl_2-NDI cyclophane **11**.

Furthermore, the STM image of S_2-NDI cyclophanes **14** is very similar to the low temperature STM image obtained for symmetric cyclophane **1** (*figure 41 b* and *c*), implying that the di-*tert*-butylsulfanyl core substituted NDI chromophore of cyclophane **14** is preferentially attached to the surface, whereas the unsubstituted NDI chromophore is spatially decoupled from the metallic substrate.
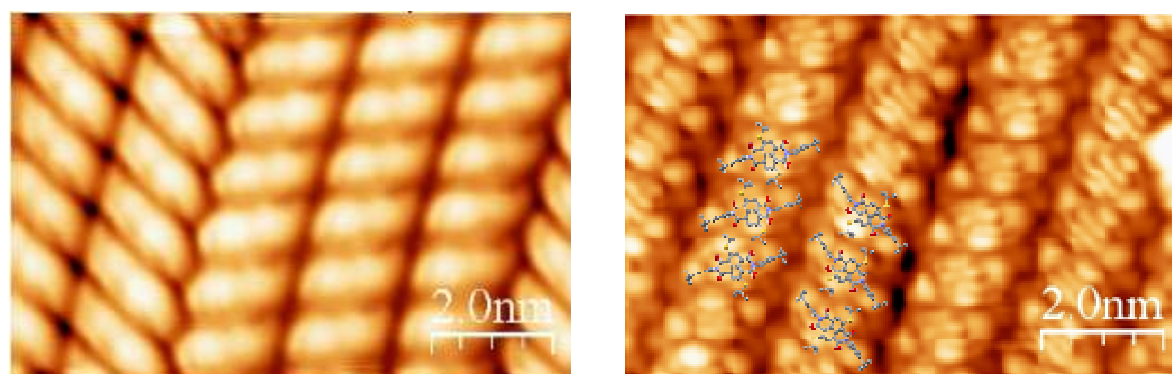
Figure 62: STM image of not alternating rows (left; 50 pA, 3 V) and an STM image with alternating rows (right; 50 pA, 1.7 V).

3.3.3. Electronic structures of 1, 11 and 25

In this section the electronic structures of the linear NDI **25** compared with the NDI cyclophanes **1** and **11** (*figure 63*) is presented using a variety of experimental techniques (UV/Vis experiments, theoretical calculations and STS measurements).
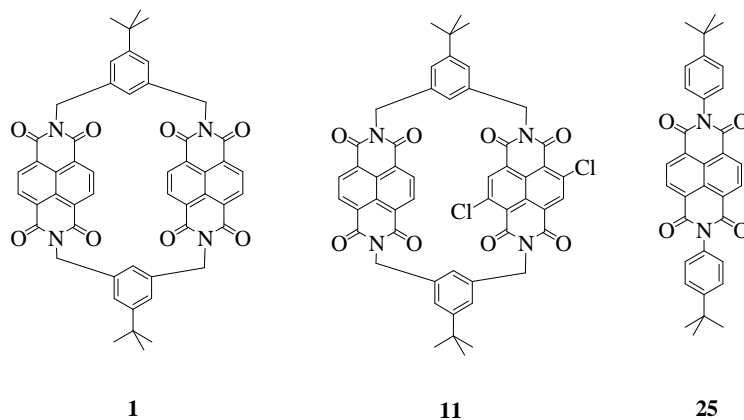
Figure 63: Structures of NDI cyclophanes **1**, **11** and the linear NDI model compound **25**.

From UV/Vis spectroscopy experiments in solution it is possible to determine the spacing between the highest occupied molecular orbital (HOMO) and the lowest unoccupied molecular orbital (LUMO). The electromagnetic radiation is characterised by a wavelength λ and a frequency ν, as related by equation **8**, where c is the velocity of light in vacuum (c $\approx$ 2.99$\cdot$10^8 m/s). The energy of a quantum of light is given by equation **9**, where h is the Planck's constant (h $\approx$ 6.63$\cdot$10^{-34} Js). Using equation **8** for the frequency and equating it with equation **9**, we deduce the relation between energy (E) and wavelength (λ) as given by equation **10** (1,602$\cdot$10^{-19}J = 1eV).

$$\lambda \nu = c \qquad\qquad \mathbf{8}$$

$$E = h\nu \qquad\qquad \mathbf{9}$$

$$E\,[eV] = \frac{1240{,}82\ nm}{\lambda} \qquad\qquad \mathbf{10}$$

The two peaks and shoulder from the absorption spectra of symmetric NDI cyclophane **1** in *figure 46* are assigned to π-π* transitions along the two axes accompanied by its vibronic progressions (380, 360 and 344 nm).[100] The absorption spectrum for the linear NDI **25** shows the same features, whereas the asymmetric Cl$_2$-NDI cyclophane **11** displays an additional peak at 402 nm (*figure 47*). Since the Cl$_2$-NDI cyclophane consists of two non-identical chromophores and no further peaks are observed above 402 nm, we can assume that this peak stems from a π-π* transition on the chlorine substituted chromophore. Theoretical calculations[30] revealed the same HOMO-LUMO spacing for the linear NDI **25** as for the symmetric NDI cyclophane **1** of 3.102 eV.

Results from a *GAUSSIAN* study showed that the LUMO for **25** is a single molecular orbital (MO), whilst for cyclophane **1** the LUMO consists of two degenerated MOs located on both chromophores. The LUMO for asymmetric Cl_2-NDI cylophane **11** appears as two distinct MOs close in energy, whereas the one on the chlorine core substituted NDI is 0.218 eV lower in energy, which is in good agreement with the difference of 0.172 eV observed in the UV/Vis data. The results obtained thus far from UV/Vis measurements and theoretical calculations are summerized in *table 1*.

	transition	UV/Vis	*GAUSSIAN*
NDI **25** and	π_0-π_2*	344 nm = 3.607 eV	-
NDI cyclophane **1**	π_0-π_1*	360 nm = 3.447 eV	-
	π_0-π_0*	381 nm = 3.257 eV	3.102 eV (HOMO-LUMO)
	π_0-π_2*	344 nm = 3.607 eV	-
	π_0-π_1*	360 nm = 3.447 eV	-
NDI cyclophane **11**	π_0-π_0*	381 nm = 3.257 eV	3.102 eV (HOMO-UMO)
	π_0-π_0*	402 nm = 3.085 eV	2.884 eV (HOMO$_{Cl}$-LUMO$_{Cl}$)

Table 1: π_0-π_0* denotes a transition from a ground state π_0 to the ground state of its excited electronic state π_0*, while π_ν* (ν = 1,2,3,…) represents the vibronic progressions of the excited state.

Previously, we described and compared the electronic structures of **1**, **11** and **25** in a vacuum (molecular modelling - GAUSSIAN) and in solution (UV/Vis spectroscopy). Additional results from STS experiments reveals information about the interaction between substrate and molecule. STS investigations show how the electronic structures are modified upon adsorption onto an Au(111) surface.

The constant height STS measurement for the linear NDI **25** showed two peaks at -0.823 ± 0.05 V and +1.325 ± 0.025 V with a shoulder towards +3 V, while in the range of -0.5 and +0.7 V or +1.9 and +2 V no additional features were observed (*figure 64*). The two peaks can be assigned to the HOMO and LUMO, while the shoulder represents the LUMO+1 level.
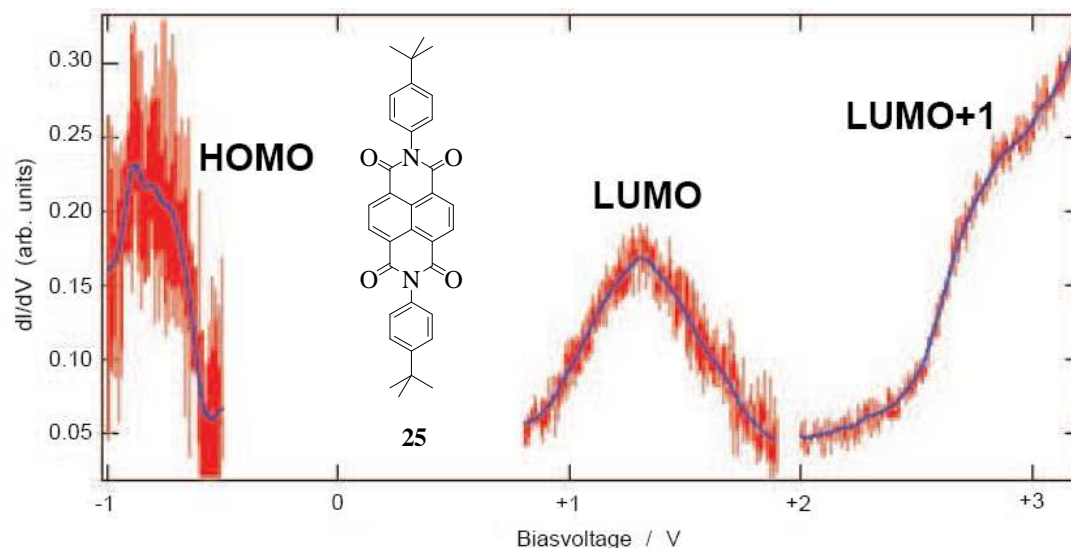
Figure 64: Constant height STS data for linear NDI **25** adsorbed on Au(111). The peaks at -0.823 V and +1.325 V were assigned to the HOMO and LUMO. The shoulder towards +3 V is assigned to represent the LUMO+1. AC voltage signal parameters: $V_0 = 28$ mV, $f = 2333$ Hz.

While the shoulder towards +3 V could not be resolved by constant height STS measurements, it was possible to obtain two distinct peaks at +1.355 ± 0.025 V and +2.708 ± 0.025 V with constant current STS investigations (*figure 65*). In fact, the position for the assigned LUMO was found to correlate well with the earlier constant height STS results, while the second peak is nicely resolved and assigned to the LUMO+1.
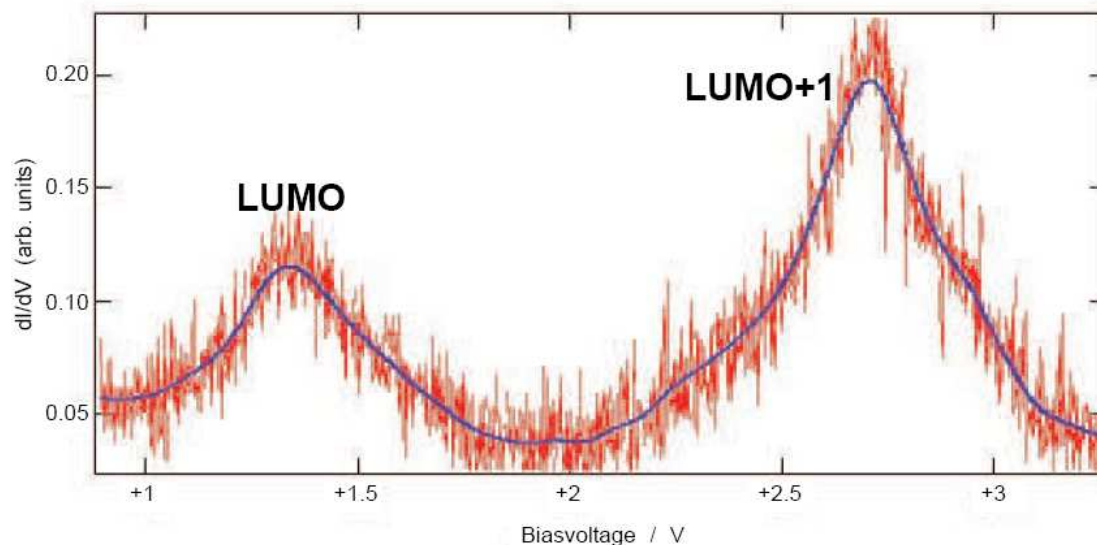
Figure 65: Constant current STS data for linear NDI **25** adsorbed on Au(111) in the range of +0.7 to +3.2 V. The peaks at +1.355 and +2.708 V were assigned to the LUMO and LUMO+1. AC voltage signal parameters: V_0 = 28 mV, f = 2333 Hz.

Thus, estimation of the relative HOMO-LUMO spacing from constant height STS measurements of the linear NDI **25** on an Au(111) surface gave 2.148 ± 0.075 V. Compared to the results of *GAUSSIAN* and UV/Vis spectroscopy the HOMO-LUMO gap was found to be considerably lower. This effect can be explained by a direct coupling of NDI **25** to the substrate, resulting in a broadening of the molecular orbitals. Indeed, this effect of a strong metal-substrate interaction can also be observed from the STM images in section 3.3.1.2, where the herringbone structure is no longer observable.

Figure 66 shows the constant height STS investigations of the NDI cyclophanes **1** and **11**. The range between –0.5 V and +2.0 V is omitted because in both cases only low conductance was found. For cyclophane **1** we find three peaks at -0.878 ± 0.025 V, +2.207 ± 0.025 V and +2.438 ± 0.025 V. While the HOMO seems not to be influenced compared to the linear NDI **25** (-0.823 V), the LUMO shows significant differences. In contrast to the LUMO of **25** (+1.325 V) we find two states close in energy at +2.207 V and +2.438 V assigned as LUMO* and LUMO.

On the other hand we observe three peaks at -0.922 ± 0.050 V, $+2.021 \pm 0.025$ V and $+2.441 \pm 0.025$ V for asymmetric NDI cyclophane **11** (*figure 66*).
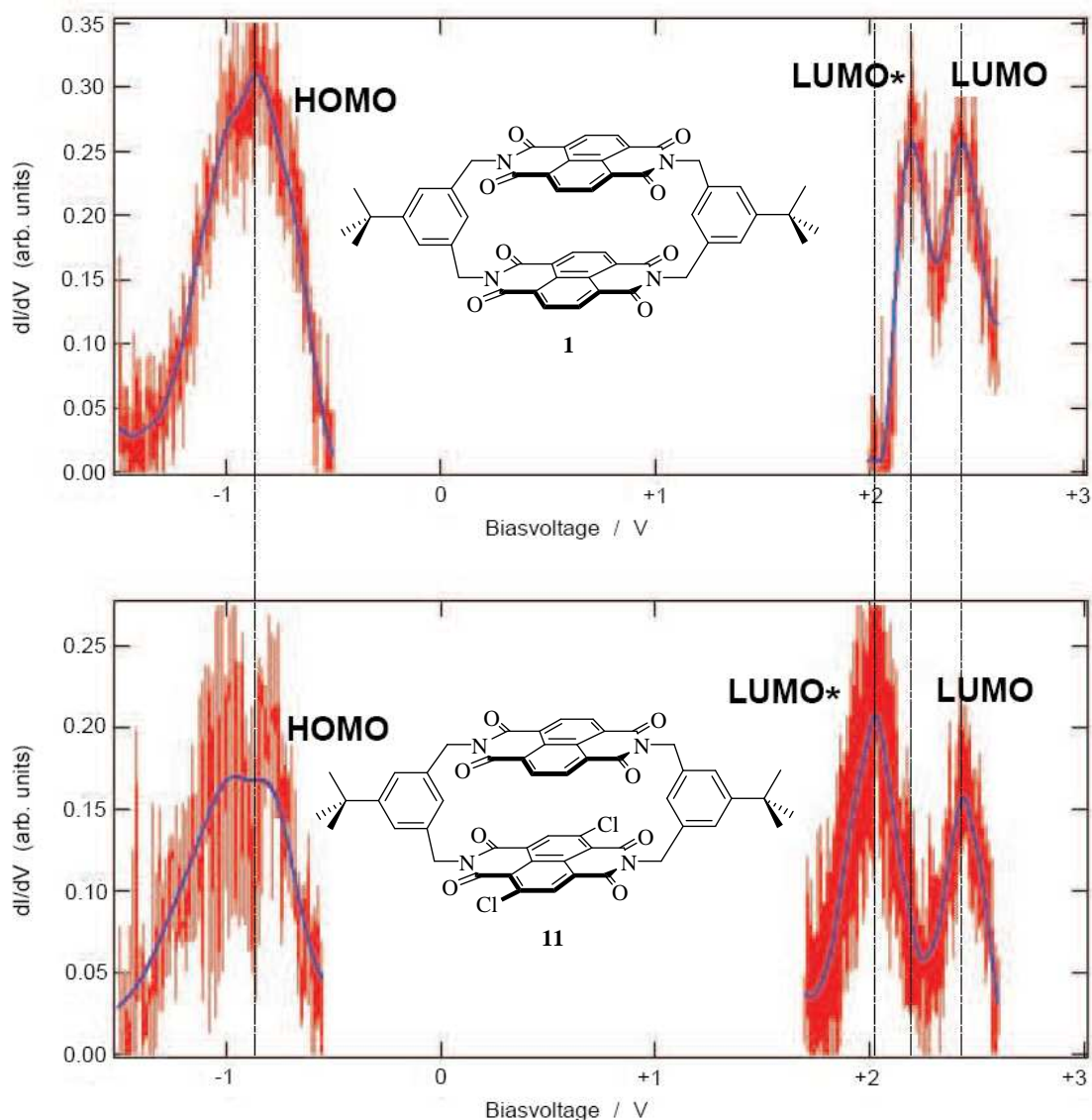

Figure 66: Top: Constant height STS data for symmetric NDI cyclophane **1** adsorbed on Au(111). The peaks at -0.878 V, +2.207 V and +2.438 V were assigned to HOMO, LUMO* and LUMO. AC voltage signal parameters: $V_0 = 11$ mV and 18 mV, $f = 2333$ Hz. Bottom: Constant height STS data for asymmetric NDI cyclophane **11** adsorbed on Au(111). The peaks at -0.922 V, +2.021 V and +2.441 V were assigned to HOMO, LUMO* and LUMO. AC voltage signal parameters: $V_0 = 17$ mV and 21 mV, $f = 2333$ Hz.

As discussed previously we found similar electronic structures for both cyclophanes except an additional splitting of the LUMO for Cl_2-NDI cyclophane, as it contains two different chromophores (*table 1*). As expected, STS measurements revealed no significant change of the HOMO positions, while the observed splitting between LUMO* and LUMO is larger for Cl_2-NDI cyclophane by about 0.2 eV.

In conclusion, we observed from STS investigations no splitting of the LUMO for the linear NDI **25**, but a general broadening of the peaks, which is attributed to strong molecule-substrate interactions. Furthermore, the energy difference between the HOMO and the LUMO is significantly decreased upon absorption compared to the relative HOMO-LUMO spacing as obtained from UV/Vis spectroscopy and molecular modelling (*figure 67*). For the symmetric NDI cyclophane **1** *GAUSSIAN* calculated the LUMO to be consisting of two degenerate MOs. STS data provided two states close in energy, assigned to LUMO* and LUMO. We assume that the adsorbed chromophore has a stronger interaction with the underlying Au(111) surface compared to the spatially separated chromophore and therefore the LUMO* - from the adsorbed NDI - is shifted in energy. It remains unclear as to the reason for the large observed shift of the LUMO for adsorbed NDI **25** compared to the symmetric NDI cyclophane **1** (*figure 67*).

Finally, for the asymmetric Cl_2-NDI cyclophane **11** we obtained from *GAUSSIAN* two MOs assigned as LUMO and $LUMO_{Cl}$, where the observed energy difference is in good agreement with the UV/Vis spectroscopy data. In addition STS measurements revealed two LUMO states close in energy. As for cyclophane **1**, we assumed that LUMO* is shifted in energy due to the interaction with the gold surface. This effect can be observed in the enhanced splitting of LUMO* and LUMO in the STS investigations. Furthermore we assume from previous STM measurements together with the reported STS investigations that the Cl_2-NDI chromophore is adsorbed on the Au(111) surface due to the fact that the relative HOMO-LUMO spacing remains unchanged compared to STS data of cyclophane **1** (*figure 67*).
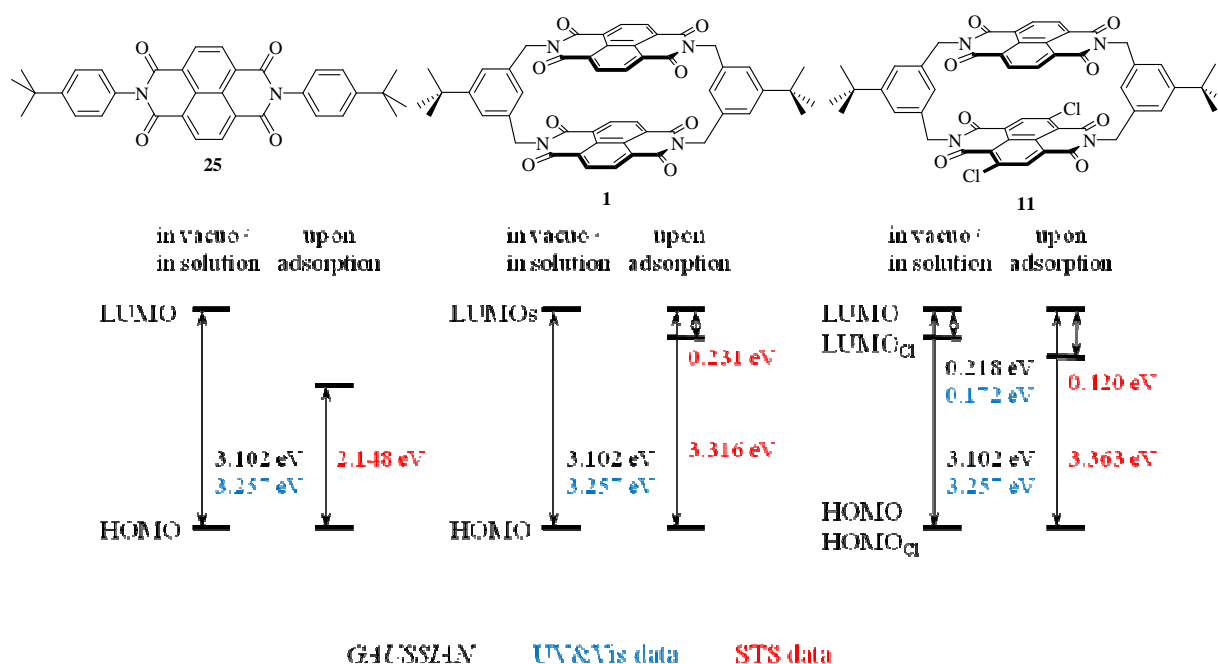
Figure 67: Summary of the results obtained from molecular modelling with *GAUSSIAN* (black), UV/Vis spectroscopy (blue) and STS investigations (red) for linear NDI **25** and NDI cyclophanes **1** and **11**.

3.3.4. Characterisation of both NDI substituted cyclophanes

Because of the difficulty in distinguishing which chromophore is lifted from the nobel metallic surface, as described for asymmetric Cl_2-NDI cyclophane **11**, tetrasubstituted NDI cyclophanes **19** and **20** were synthesized. Due to the introduction of bulky substituents at both chromophores an even more rotated arrangement of both main axes of the two NDI decks to each other is expected, minimizing a possible FRET mechanism.

Product formation of Cl_4-NDI cyclophane **19** was confirmed by ^{1}H-NMR spectrometry, mass spectrometry and the purity was analysed by HPLC. Interestingly, HPLC using a chiral column revealed only two peaks in a 2:1 ratio (*figure 68* top). It was postulated that from the statistical mixture formed by the synthetic approach the first peak comprises the two enantiomeric forms ((M)-**19**, (P)-**19**), whereas the second sharp peak arises from a meso form (($meso$)-**19**).

On the other hand, S_4-NDI cyclophane **20** revealed three peaks as expected by HPLC using a chiral column (*figure 68* bottom). The ratio is 1:1:0.2 implying that nucleophilic aromatic substitution for the meso form is less favoured due to steric repulsion.
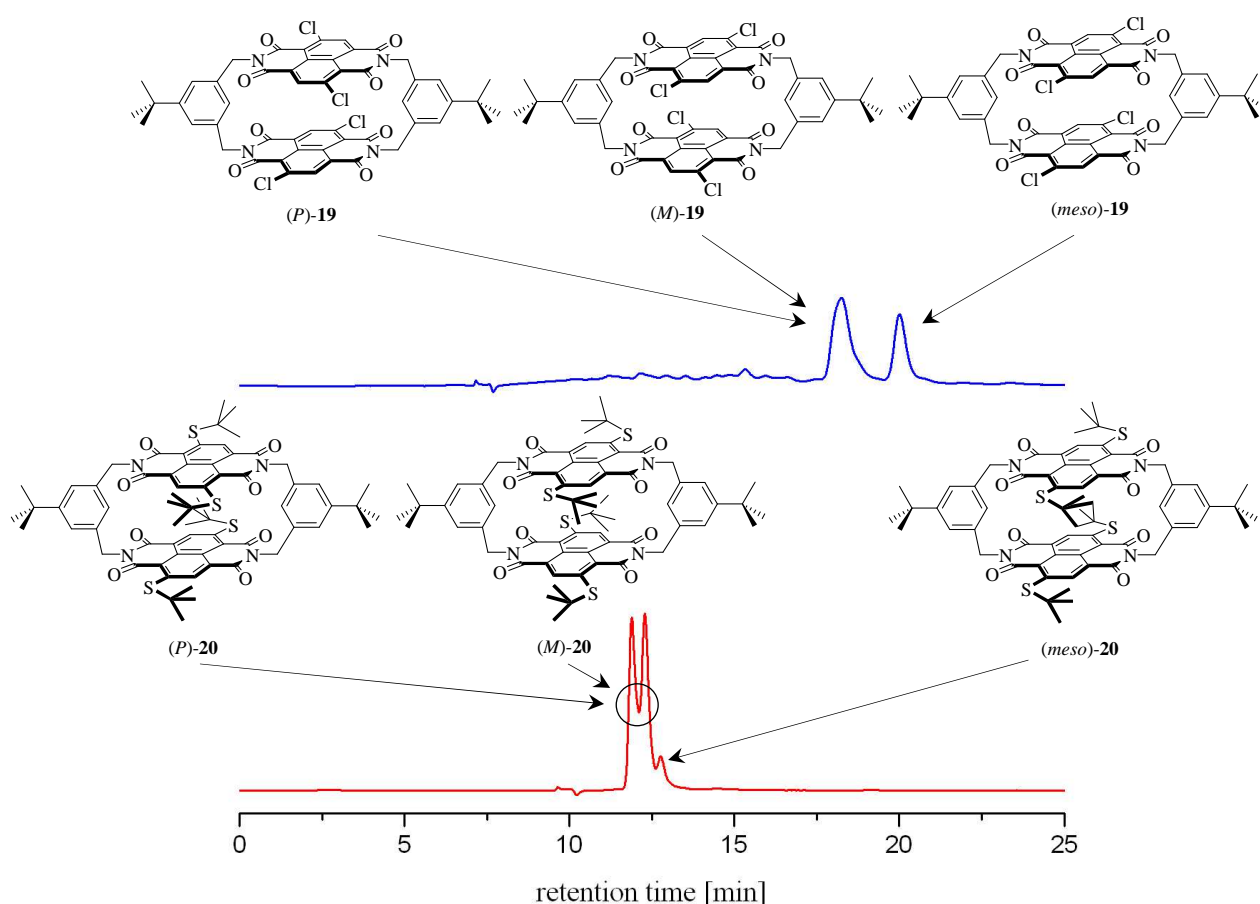
Figure 68: HPLC traces of Cl_4-NDI cyclophane **19** (blue line) and S_4-NDI cyclophane **20** (red line) using a chiral column.

The UV/Vis spectra were recorded from the HPLC runs for both tetrasubstituted NDI cyclophanes **19** and **20** using a reversed phase column, which afforded only one isolatable peak, meaning that all three isomers, (*M*), (*P*) and the *meso* isomers contributed to the UV/Vis spectra (*figure 69*). But in fact the UV/Vis spectra from the pure isomers recorded from the HPLC runs through the chiral column did not show any variation.

Thus, both compounds (**19** and **20**) displayed the expected absorption bands for NDIs in the range between 300-400 nm. In the case of Cl$_4$-NDI cyclophane **19** an additional absorption band at 400 nm was observed; S$_4$-NDI cyclophane **20** displayed a long wavelength shifted absorption band with two maxima at 491 nm and 520 nm giving rise to the red colour of sulphur core substituted NDIs.
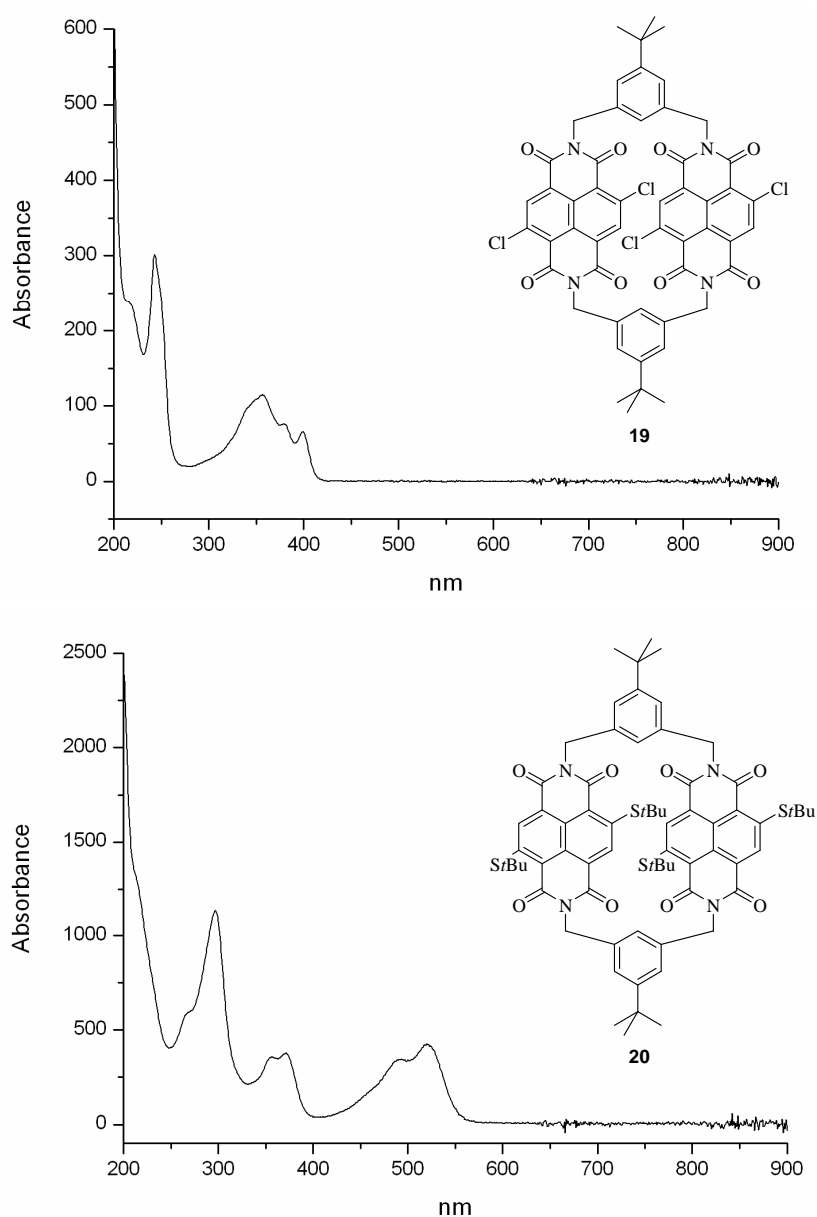
Figure 69: UV&Vis spectra of Cl$_4$-NDI cyclophane **19** and S$_4$-NDI cyclophane **20** recorded from the corresponding HPLC run.

3.3.5. Characterisation of NDI crown ether model compounds

NDI crown ether compounds **22** and **23** (*figure 70*) were characterised by NMR spectrometry, mass spectrometry and their purity was confirmed by HPLC ESI-MS.
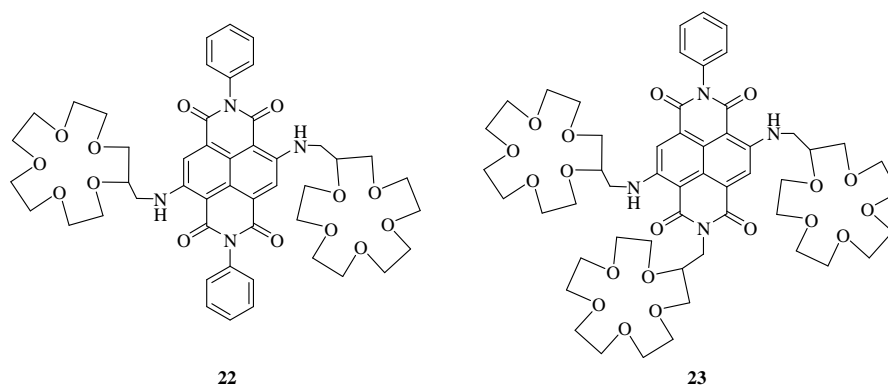
Figure 70: Structure of NDI crown ether compound **22** and **23**.

Figure 71 displays the absorption spectra of the NDI crown ether **22** and the emission spectra upon excitation at 345, 361 and 610 nm respectively. Excitation at 345 and 361 nm reveals no fluorescence bands between 400 and 500 nm but a weak long wavelength emission at 644 nm was detected, resembling the mirror pattern of the highest absorption band. Excitation at 610 nm gave rise to the same expected mirror fluorescence band, which is shifted by 34 nm to 644 nm.
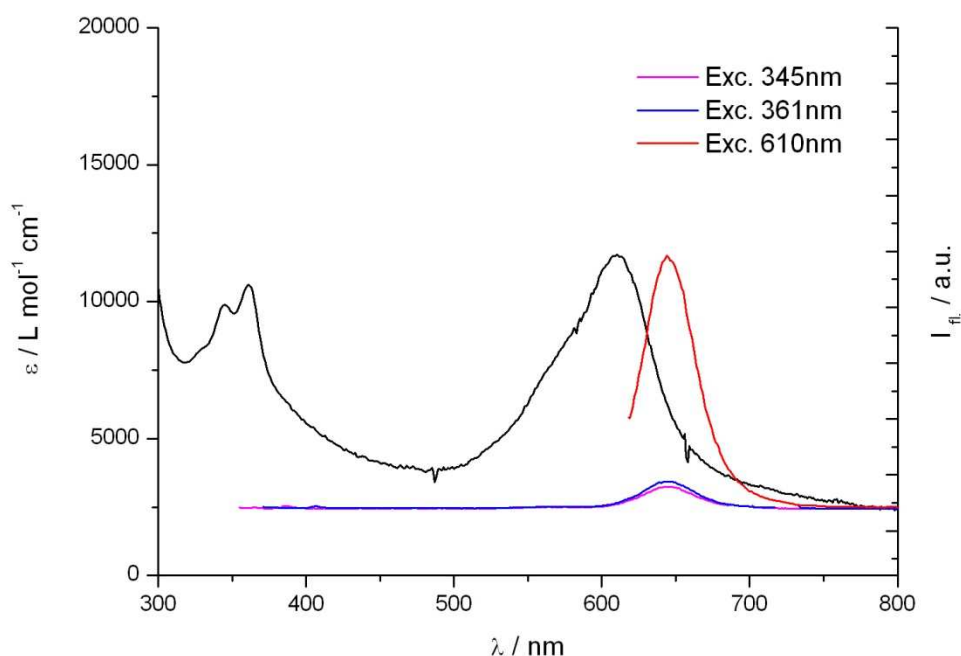

Figure 71: Absorption (black line) and emission spectra (coloured lines: excitation at 345, 361 and 610 nm) of NDI crown ether **22** (17.9 μM in CH_2Cl_2 at room temperature).

3.3.5.1. Complexation studies

Cyclic polyethers are known to form complexes with metal salts.[85] Fascinatingly, depending on the size of the cyclic polyethers, Ba^{2+} and K^+ ions (ion radii: 149 pm and 152 pm)[86] can form sandwich-like complexes, which could even be isolated in crystals (*figure 26* in section 3.1).[87-91]

Lately, Licchelli *et al.*[66] reported binding of a similar NDI with the same 15-crown-5 ethers linked over the imide positions, but with no core substituents (*figure 72* left). Upon titration of the corresponding NDI with barium perchlorate in acetonitrile they observed the appearance of a broad emission band at 440 nm. Licchelli *et al.* concluded from the titration experiments and ESI-MS spectra the formation of a [2+2] adduct with Ba^{2+}, which led to this broad emission band according to self-assembling fluorescence enhancement (red dashed lines in the middle sketch). As an alternative to the reported NDI of Licchelli, we have attached the crown ethers at the core of the NDI and therefore **22** is a blue dye and fluorescent (*figure 72* right).
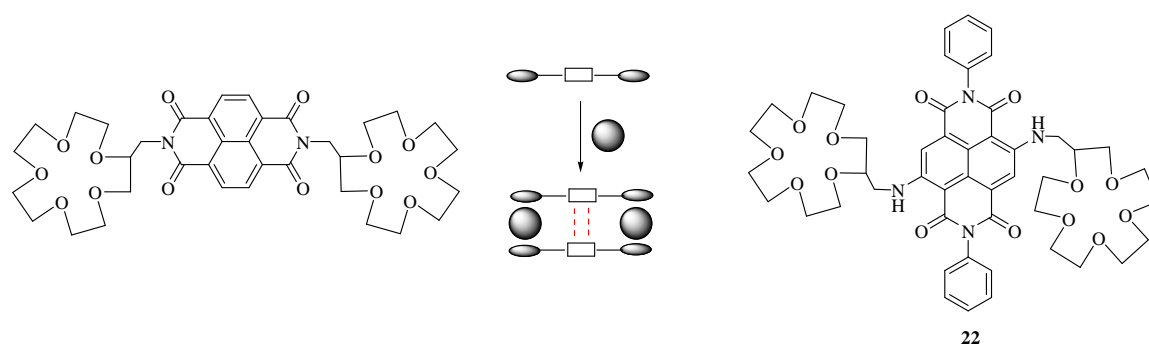

Figure 72: Left: NDI from Licchelli *et al.*[66] and the proposed formation of a [2+2] complex with Ba^{2+} leading to self-assembling fluorescence enhancement (red dashed lines). Right: Fluorescent NDI **22** with 15-crown-5 ethers attached at the core.

On addition of $Ba(ClO_4)_2$ the absorption bands of **22** at 344 nm and 360 nm undergo a decrease in intensity, a red-shift by 5 nm and get generally broader in line with what was reported by Licchelli *et al.* (*figure 73*). On the other hand, the additional absorption band at 606 nm is not shifted, but the decrease in intensity is much more pronounced. In fact, after addition of 1 eq. Ba^{2+} no further change can be observed at the two peaks at 574 nm and 606 nm.
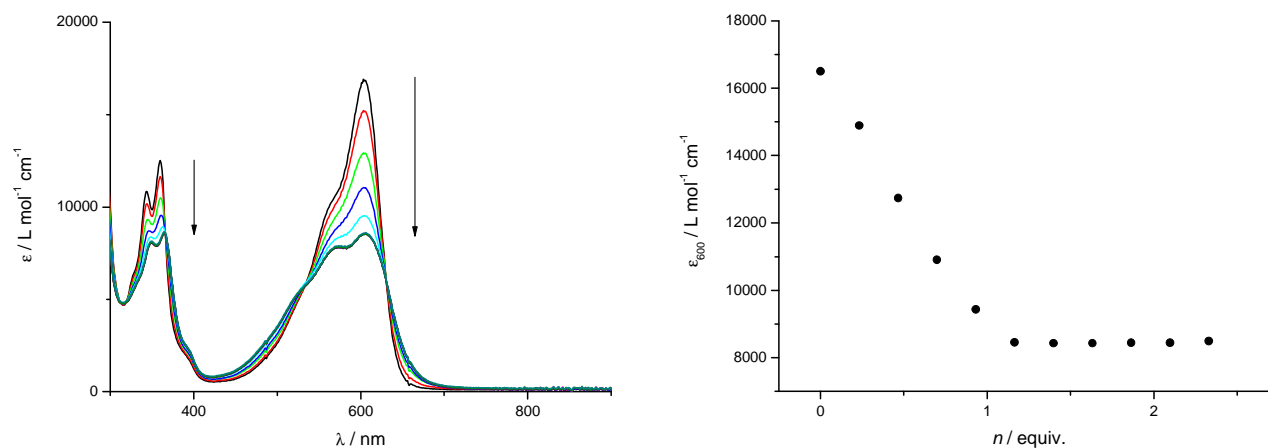

Figure 73: Absorption spectra recorded during the titration of **22** ($1 \cdot 10^{-4}$ M in CH_3CN) with $Ba(ClO_4)_2$ in CH_3CN (left) and titration profile (right).

Whereas a solution of NDI crown ether **22** in acetonitrile ($1 \cdot 10^{-4}$ M) shows a blue-red colour, pointing at the strong emission property of the core substituted NDI, a deeply blue colour was observed in the presence of barium. On contrary to the reported fluorescence enhancement between 400-500 nm we observed a tremendous fluorescence quenching upon the addition of barium (*figure 74*).
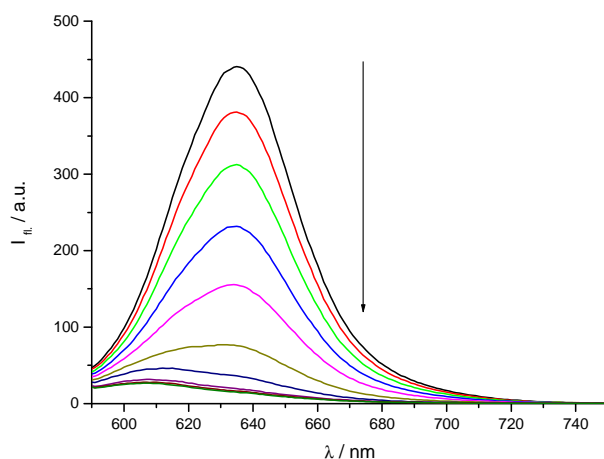
Figure 74: Emission spectra recorded during the titration of **22** ($1 \cdot 10^{-6}$ M in CH_3CN) with $Ba(ClO_4)_2$ in CH_3CN; $\lambda_{exc.} = 580$ nm.

In order to determine the stochiometry of the formed complex a Job plot analysis[101] was carried out, which is also known as the 'method of continuous variation'. In this method, the total molar concentration of metal ion and ligand are held constant, but their mole fractions are varied (see experimental part). Plotting the spectral change of **22** at 606 nm against the mole fractions of these two components a maximum at 0.5 is observed, corresponding to a 1:1 stochiometry of the formed complex (*figure 75*).
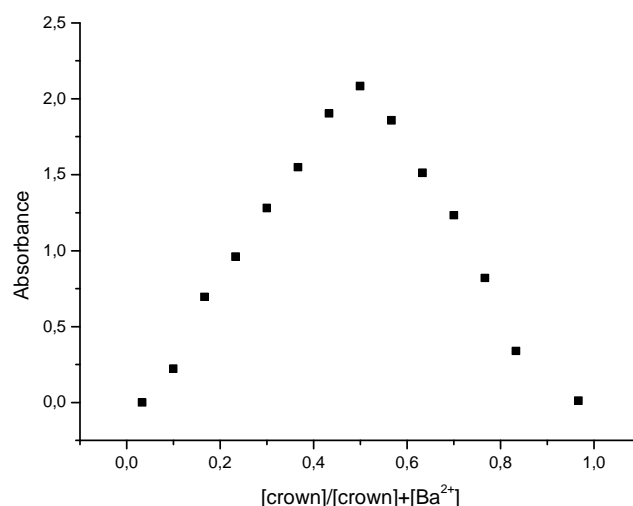
**Figure 75:** Job plot analysis[101] revealed a 1:1 stochiometry

Titration experiments of NDI crown ether **22** with Ba^{2+} in acetonitrile (*figure 71*) and the job plot analysis revealed a 1:1 stochiometry. Further to this, ESI-MS experiments were performed in order to determine the identity of the formed complex in solution by **22** and Ba^{2+}.

Thus, the ESI-MS spectrum of an equimolar solution of $Ba(ClO_4)_2$ and **22** ($1 \cdot 10^{-4}$ M) shows a base peak at m/z 525.0, corresponding to a $[Ba_2(\mathbf{22})_2]^{4+}$ complex, which is in excellent agreement with the calculated spectrum (*figure 76*).
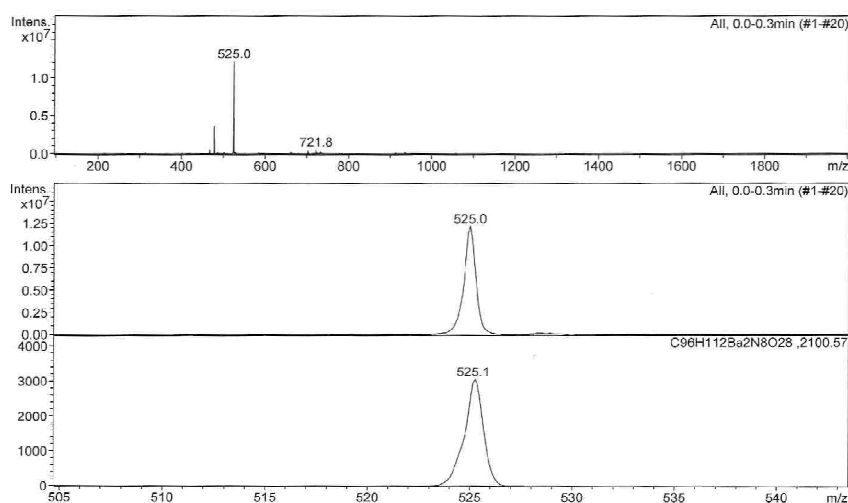

Figure 76: ESI-MS spectrum of the $[Ba_2(\mathbf{22})_2]^{4+}$ complex (top: full range spectrum, middle: enlarged region of the base peak, bottom: calculated spectrum for $[Ba_2(\mathbf{22})_2]^{4+}$).

In the high resolution mode the spacing between the peaks is 0.2 (*figure 77*), confirming the 4+ complex formation corresponding to a [2+2] adduct, in which each Ba^{2+} ion coordinates to two 15-crown-5 units belonging to different molecules of **22** (*figure 78*).
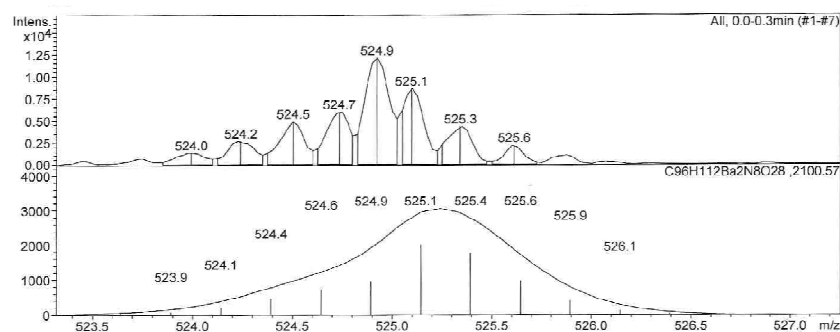

**Figure 77:** ESI-MS spectrum with a higher resolution of the peak at m/z 525.
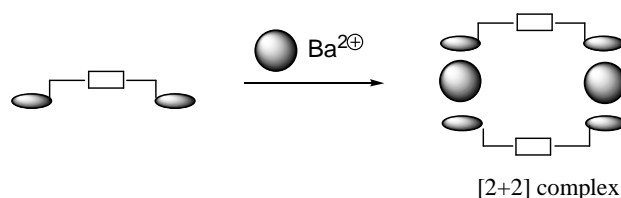
[2+2] complex

Figure 78: [2+2] adduct formation between **22** and Ba^{2+}.

In the following the determination of the binding constant for the [2+2] complex formation (*figure 78*) was tried to figure out. Obviously, the formation of the [2+2] complex consists of several steps. According to *figure 79* the [2+2] complex can be formed by two different pathways with binding constants K_1, K_2 and K_3 or K_1, K_4 and K_5. Since we can not predict which step quenches the fluorescence, a direct measurement of the overall binding constant K was attempted (*figure 79*). The binding constant for a complex with a 1:1 stochiometry, as previously shown by the Job plot analysis (*figure 75*), can be easily determined by a Stern-Volmer plot. In such titration experiments the fluorescence quenching is observed and F_0/F against the concentration is ploted, whereas the slope of the linear fit provides directly the binding constant.
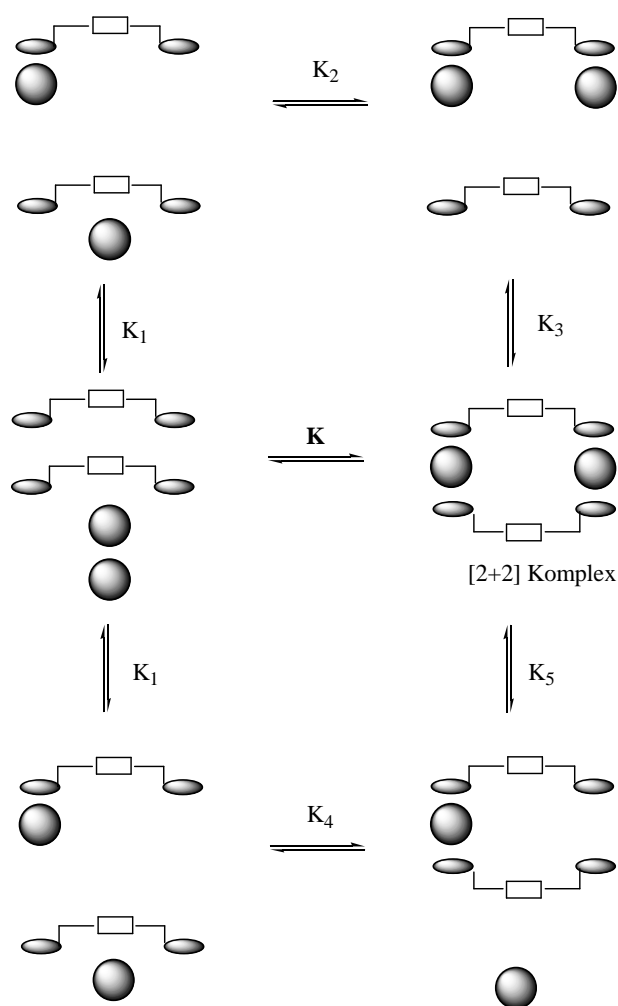
Figure 79: [2+2] complex formation by two different pathways with binding constants K_1, K_2 and K_3 or K_1, K_4 and K_5.

Thus, fluorescence quenching was recorded upon titration with Ba^{2+} as shown in *figure 80*.
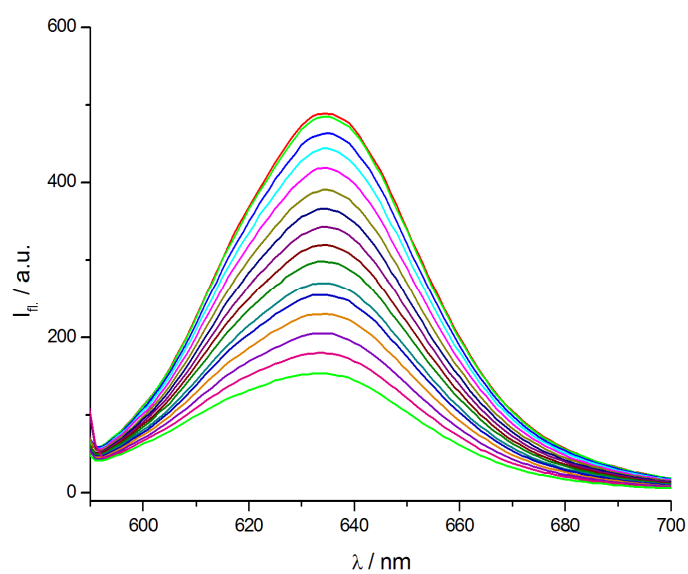
Figure 80: Fluorescence quenching of **22** ($1 \cdot 10^{-4}$ M in CH_3CN) upon titration with Ba^{2+} in CH_3CN; $\lambda_{exc.} = 585$ nm

The Stern-Volmer plot is shown in *figure 81*. Evidently, we do not get a linear plot and thus we can not determine directly the binding constant from these measurements. Furthermore, such a non-linear behaviour can be attributed to combined static and dynamic fluorescence quenching processes.[21] Thus, so far it was not possible to determine the binding constant by fluorescence quenching experiments (see experimental part).

Acctually, we expect a static fluorescence quenching process. But this system is too difficult since we do not know clearly which complex, of the two possible pathways for the formation of the [2+2] complex, is able to quench the fluorescence of NDI **22**. At the moment ESI-MS experiments are under investigation in order to determine the binding constants.
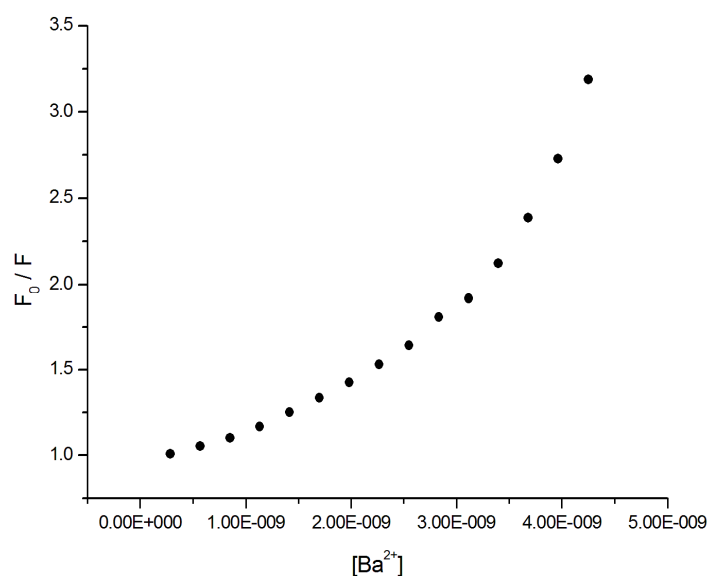

Figure 81: Stern-Volmer plot for the titration of **22** with Ba^{2+} in CH_3CN.

Interestingly, on addition of $K(ClO_4)$ to a solution of **22** in acetonitrile the absorption band at 344 nm undergoes a bathochromic shift of 4 nm, whereas the one at 360 nm remains at the same position (*figure 82*). Additional titration with K^+ results in the formation of a broad unstructured absorbtion peak at 605 nm compared to the titration with Ba^{2+} after addition of 2 eq. This observation points to a probable weaker interaction between the crown ethers and the potassium ion or a different complex formation.
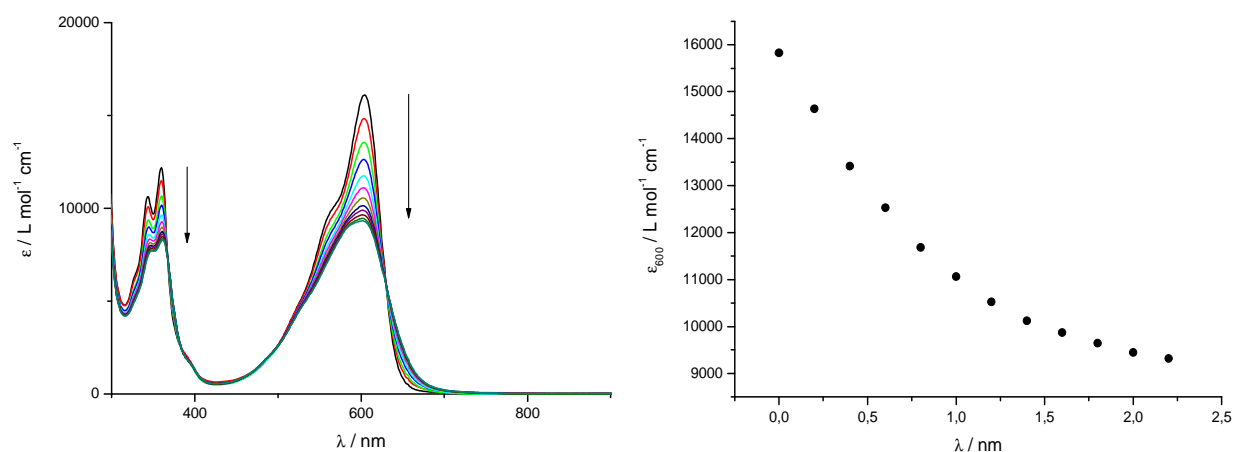

Figure 82: Absorption spectra recorded during the titration of **22** ($1 \cdot 10^{-4}$ M in CH_3CN) with $K(ClO_4)$ in CH_3CN (left) and titration profile (right).

While the emission spectra of a diluted solution of **22** in acetonitrile ($1 \cdot 10^{-6}$ M) recorded during the titration with K^+ remained unchanged, a more concentrated solution of **22** ($1 \cdot 10^{-4}$ M) resulted in fluorescence quenching upon titration with K^+ (*figure 83*). Compared to Ba^{2+}, the complexation with K^+ seems again much weaker due to the higher concentration needed for fluorescence quenching.
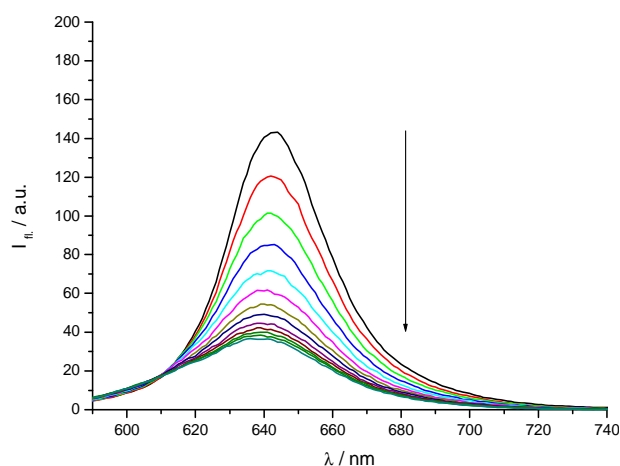

Figure 83: Emission spectra recorded during the titration of **22** ($1 \cdot 10^{-4}$ M in CH_3CN) with $K(ClO_4)$ in CH_3CN; $\lambda_{exc.} = 580$ nm.

In order to determine the stochiometry of the formed complex a Job plot analysis[101] was carried out, resulting in a maximum at around 0.6 (*figure 84*). This observation suggests a different complex formation corresponding to two potassium ions and three **22** crown ether molecules or a multiple thereof. But can this be true? Since potassium and barium have similar ionic radii (152 pm and 149 pm)[86] and the fact of isolated sandwich complexes such an adduct formation seemed unbelievable.
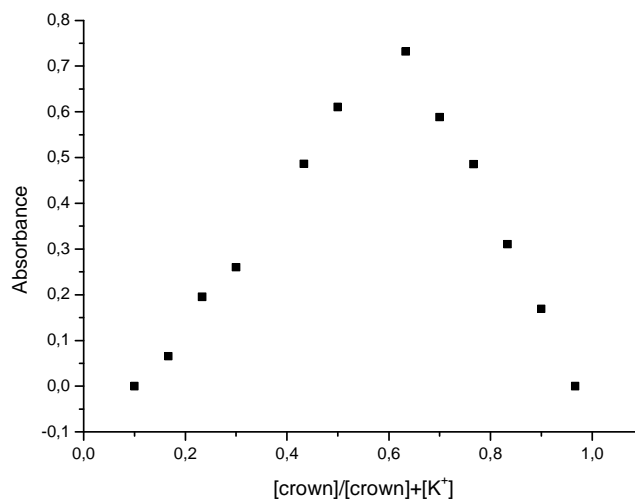

Figure 84: Job plot analysis[101] with a maximum at around 0.6 points to a 2:3 stochiometry (K$^+$:**22**), which indicates an unusual complex formation.

Therefore, ESI-MS experiments were performed in order to clearify the identity of the formed complex in solution by **22** and K^+. The ESI-MS spectrum of an equimolar solution of $K(ClO_4)$ and **22** $(1 \cdot 10^{-4}$ M) shows a base peak at m/z 951.1 and further peaks at 912.0, 935.0 and 943.4 (*figure 85*).
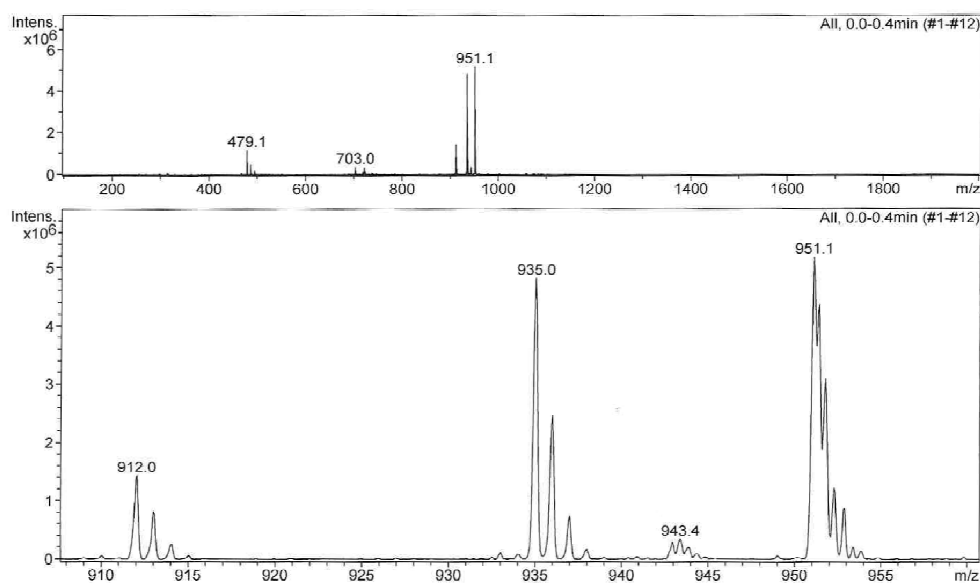
**Figure 85:** ESI-MS spectrum of an equimolar ratio of $K(ClO_4)$ and **22** $(1 \cdot 10^{-4}$ M).

The signals at m/z 912.0 and 935.0 are in fact singly charged, corresponding to the uncomplexed protonated $[22]^+$ and the sodium adduct $[Na(22)]^+$ (*figure 86*). This interesting observation of the sodium adduct is attributed to the prescence of Na^+ cations, probably coming from the glassware used.
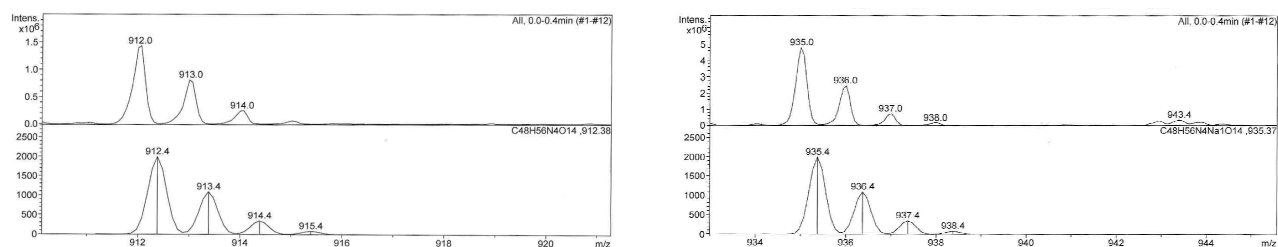
Figure 86: left: ESI-MS spectrum of $[22]^+$ (top) and calculated spectrum (bottom); right: ESI-MS spectrum of $[Na+22]^+$ (top) and calculated spectrum (bottom).

So if the peak at 951.1 corresponds to the $[K_2(22)_2]^{2+}$ complex the intensity compared to the sodium adduct is nearly the same, reflecting in a strong competition between sodium and potassium complex formation with the crown ethers.

72

In the high resolution mode the spacing between the peaks is nearly 0.5, confirming the 2+ complex formation corresponding to a [2+2] adduct, in which each K^+ ion coordinates to two 15-crown-5 units belonging to different molecules of **22** analogous to the Ba^{2+} complex (*figure 87*).
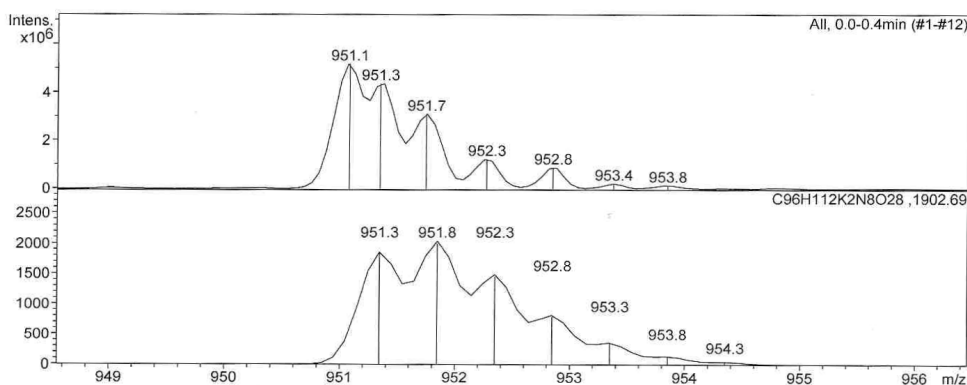
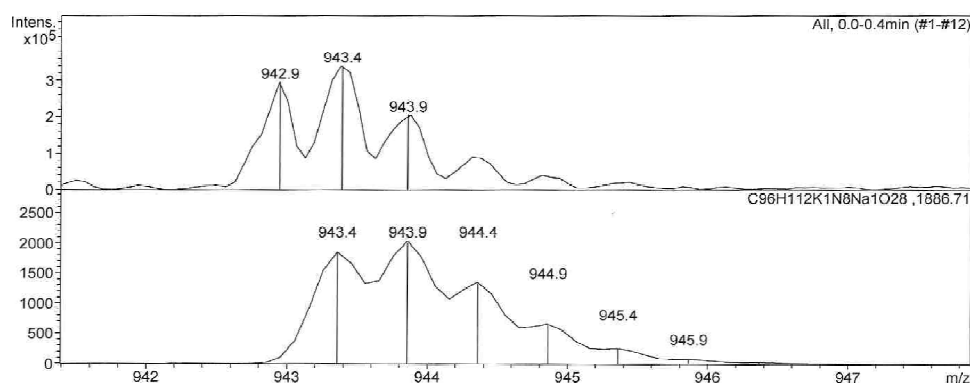**Figure 87:** ESI-MS spectrum of $[K_2(\mathbf{22})_2]^{2+}$ (top) and calculated spectrum (bottom).

Furthermore a possible 1:1 complex formation between **22** and K^+ can be neglected due to comparison with the calculated single charged adduct (*figure 88*).
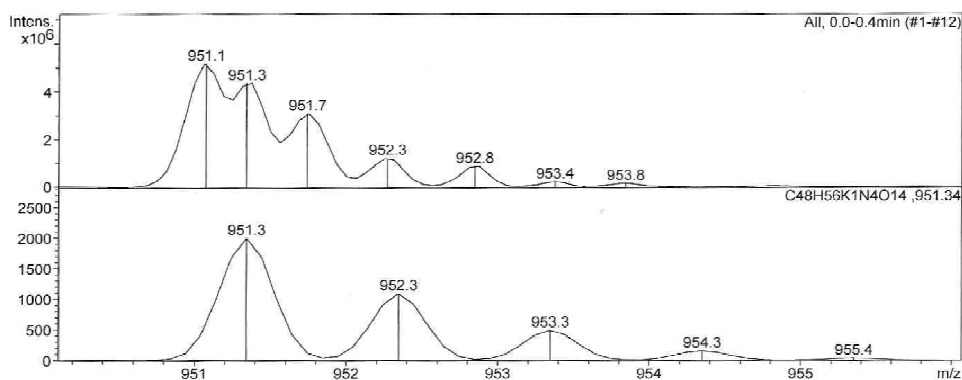

Figure 88: ESI-MS spectrum of $[K_2(\mathbf{22})_2]^{2+}$ (top) and calculated spectrum of a posssible $[K(\mathbf{22})]^+$ complex (bottom).

But what is the small peak at m/z 943.4? In the high resolution mode the spacing between the different peaks is 0.5, meaning that a doubly charged species is present. In fact this peak corresponds to a mixed $[NaK(22)]^{2+}$ complex which is in good agreement with the calculated spectrum (*figure 89*).

Figure 89: ESI-MS spectrum of $[NaK(22)]^{2+}$ (top) and the calculated spectrum (bottom).

So, in conclusion from these complexation studies combined with the ESI-MS spectra we obtain for crown ether **22** with Ba^{2+} a [2+2] adduct. The same [2+2] complex was detected in the ESI-MS spectrum for K^+ with **22**, whereas the binding constant seems to be much weaker from the titration experiments and therefore additional competition with sodium ions into the crown ethers from the glassware can occure (*figure 90*).
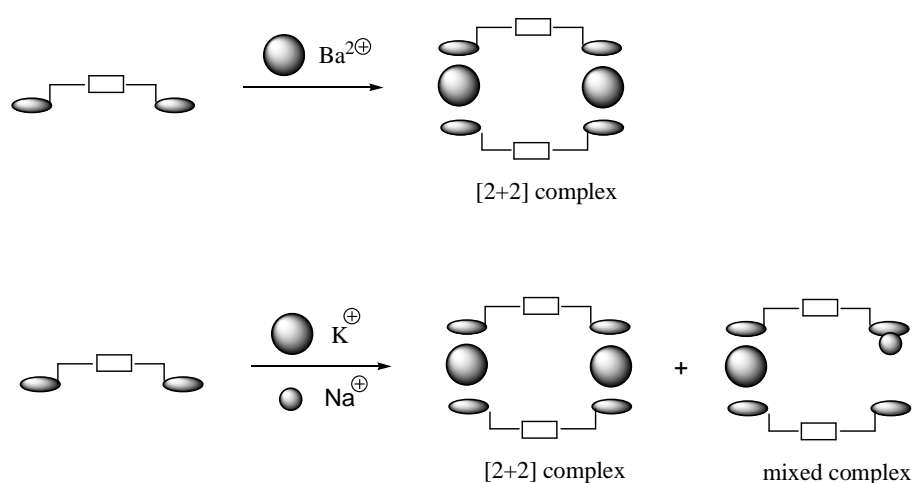
Figure 90: [2+2] complex formation with **22** and Ba^{2+} or K^+.

This competition between potassium and sodium can in fact also be observed in the job plot analysis which shifts the maximum to 0.6 (*figure 84*).

Moreover, Licchelli *et al.* also reported from the [2+2] complex formation of potassium with their NDI system at higher concentrations. But whereas they only studied the competition between barium and potassium a possible interaction with sodium from the glassware and the crown ethers could also lead to the missing fluorescence enhancement as in our systems observed by ESI-MS.

3.3.5.2. STM investigations of NDI crown ether model compound 22

First STM investigations on Au(111) under UHV conditions at room temperature revealed clusters of NDI crown ether **22**, demonstrating the deposition of **22** without decomposition (*figure 91*). In most cases a cluster with a triangular shape was found, which probably consists of three intercalated molecules.
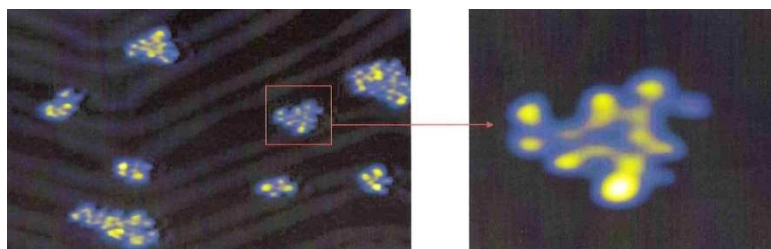

Figure 91: STM image of clusters of molecules (**22**) after deposition on the Au(111) surface at room temperature (left). Enlarged region of a specific cluster - probably it consists of three intercalated molecules (right).

On the contrary, in low temperature UHV STM images at 5 K mainly single molecules are identified on the Au(111) surface (*figure 92* left). Actually, two different conformations on the surface can be recognized by having a closer look at the single molecules. In one case the crown ether moieties have a "trans" arrangement to each other while by rotation around the CH_2-NH bond (red arrow in *figure 92*) they appear in the "cis" form (*figure 92* right).
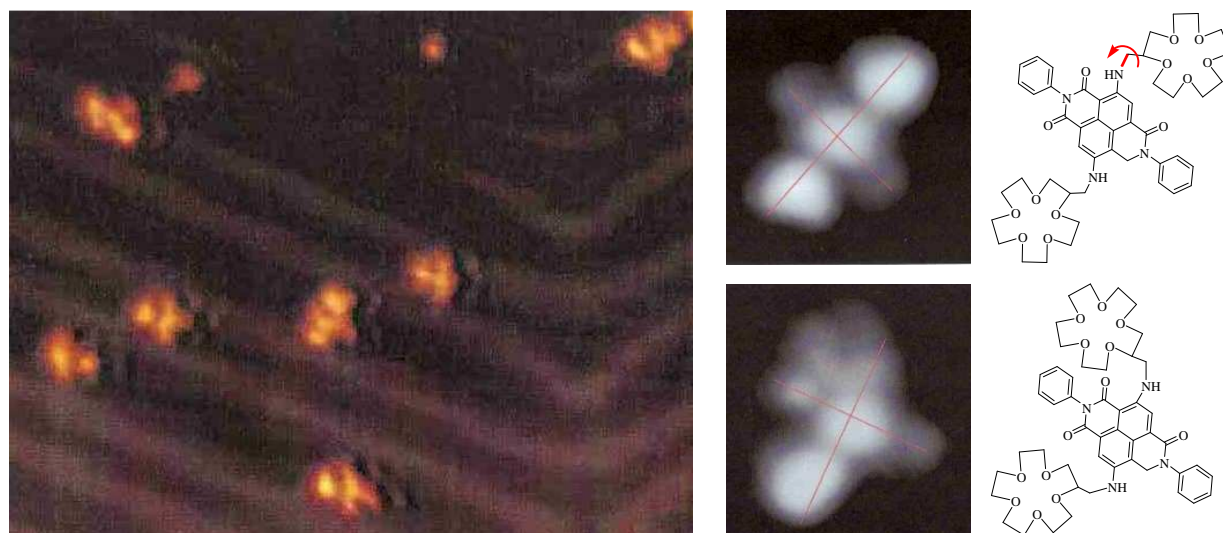

Figure 92: left: STM image of individual molecules (**22**) after the deposition on a Au(111) surface investigated at 5 K; right: two different conformations of single molecules on Au(111) "trans" form (top) and "cis" form (bottom).

3.4. Concept and design of a linear NDI system for FRET studies

For studying the orientation factor κ according to Förster resonance energy transfer mechanism (FRET) we designed a linear rigid NDI molecule (*figure 93*). As mentioned previously the bright color for core substituted NDIs arises from a isolated long wavelength absorption band, whose position can be adjusted over a large range of the visible spectrum by substitution at the 2-, 6-positions. Moreover, the fluorescence properties of the chromophore can be dictated by the chemical nature of the substituents.

For our purpose we considered a 2,6-di-*n*-hexyloxy core substituted NDI as donor and a 2,6-di-*n*-hexylsulphanyl core substituted NDI as acceptor for FRET. Whereas these two chromophores should be separated by a short rigid phenyl linker, which can be varied, we proposed to attach phenyl units at the ends with additional *tert*-butyl groups in order to provide solubility[102,103] during the first steps of the planned synthesis.
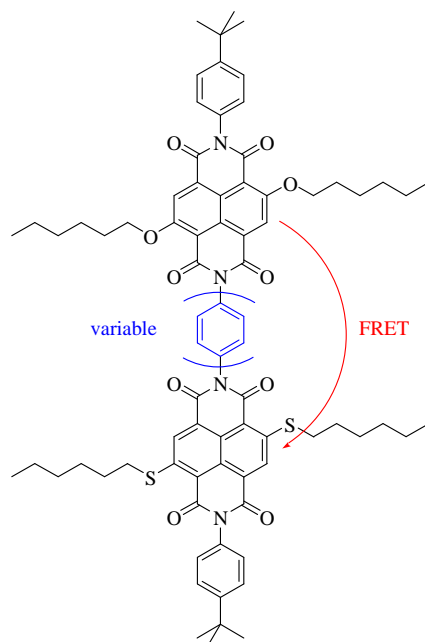
Figure 93: Design of a linear NDI system for studying the orientation factor in FRET.

3.4.1. Synthesis of a linear NDI model compound for FRET studies

3.4.1.1. The linear S_2O_2-NDI model compound

In principle asymmetric *N,N'*-NDIs can be built up either by a direct[78,104-106] or a stepwise[107-113] condensation with the appropriate amines. Our S_2O_2-NDI model compound (**33**) consists of two different core substituted NDIs, which are connected over the imide groups by a short linker. In order to vary the bridging unit we proposed a combination of both procedures for building up **33**, where each core substituted NDI is built up separately. While **29** should result from a direct condensation, **32** contains a saponification step as presented in the retrosynthesis in *scheme 6*.
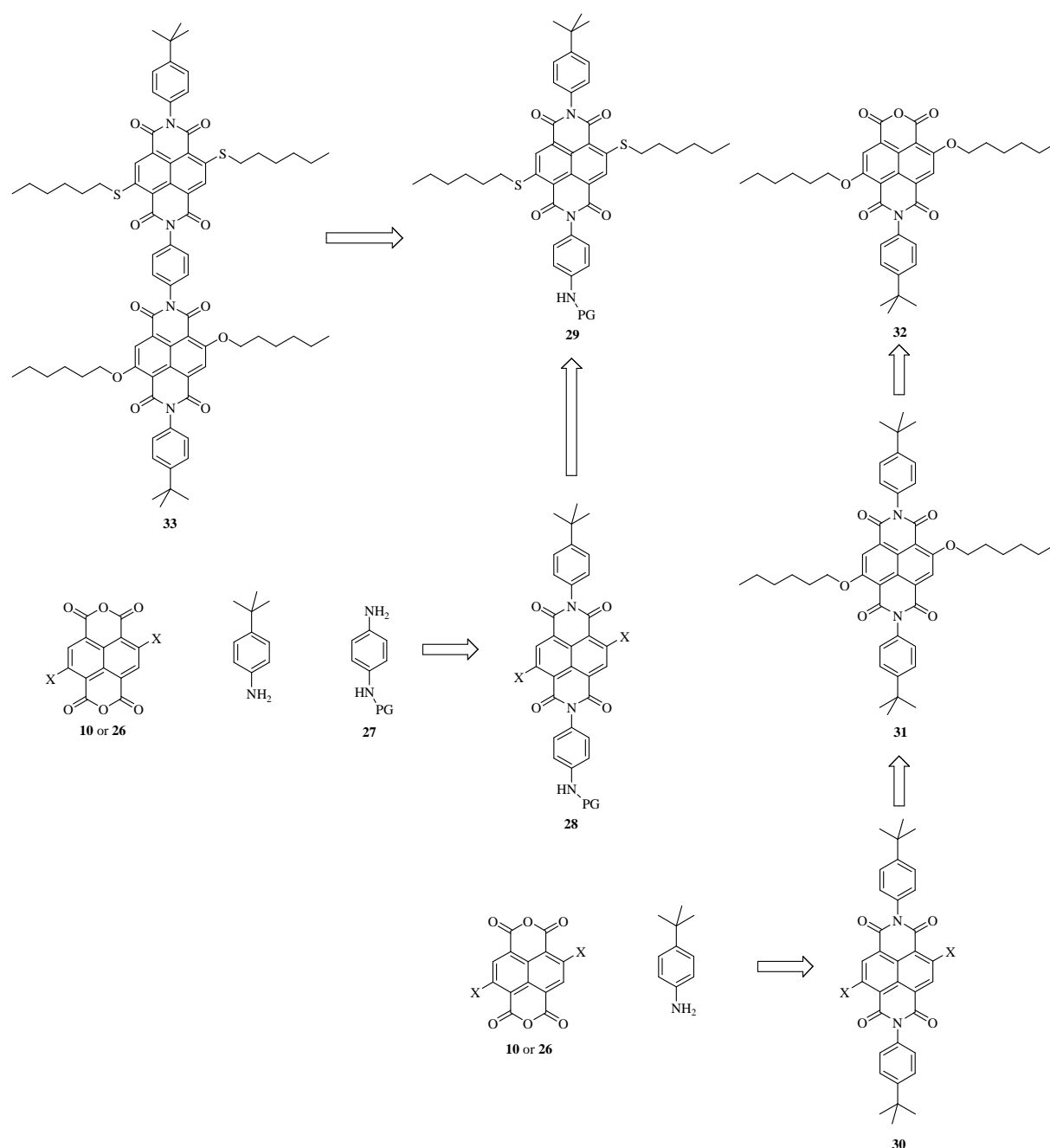
Scheme 6: Retrosynthesis of S_2O_2-NDI **33**; X = Cl or Br; PG = protection group.

The protected asymmetric S_2-NDI **29** was proposed to be built up from a 1:1:1 mixture of either 2,6-dichloro- or 2,6-dibromo-1,4,5,8-naphthalenetetracarboxylic acid dianhydride (**10** or **26**) with 4-*tert*-butylaniline and monoprotected **27**, followed by a nucleophilic aromatic substitution reaction with hexanethiol. On the other hand, condensation of commercially available 4-*tert*-butylaniline with **10** or **26** should yield NDI **30**. Following nucleophilic aromatic substitution with hexanol and subsequent saponification of only one imide function would provide the oxygen core substituted monoanhydride **32**. Final deprotection of **29** and subsequent condensation with monoanhydride **32** should afford the desired target structure S_2O_2-NDI **33**.

2,6-core substituted NDIs can easily be achieved from the corresponding dichloro or dibromo naphthalenetetracarboxylic acid dianhydride (**10** or **26**). Vollmann[114] reported in 1937 the multistep synthesis to **10**, which can be obtained from pyrene by chlorination, HCl elimination and oxidation. This procedure was further modified by the Würthner group,[74] where it was possible to separate the 2,6- from the 2,7-dichloro isomer on the quinone stage as presented in *scheme 7*.
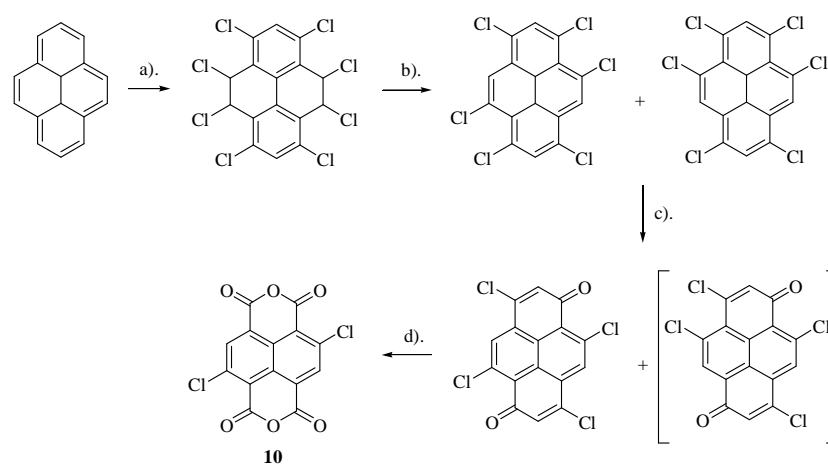
Scheme 7: Synthetic route to 2,6-dichloro-1,4,5,8-naphthalenetetracarboxylic acid dianhydride; a) Cl_2 (g), I_2 (in catalytic amounts), 1,2,4-trichlorobenzene, 25-110 °C, 36-38 %; b) KOH, EtOH, 80 °C, 96-97 %; c) fuming HNO_3, 0-5 °C, 32-45 %; d) fuming HNO_3, conc. H_2SO_4, 100 °C, 45-49 %.

Recently two independent groups developed a one step synthesis to 2,6-dibromo-1,4,5,8-naphthalenetetracarboxylic acid dianhydride **26** from commercially available **3** (*scheme 8*).[74,108] In fact by this pathway it is possible to obtain 2,6-core substituted NDIs in only three steps from commercial available **3**, compared to the multistep synthesis of **10** using noxious chlorine gas. Interestingly, depending on the amount of brominating agent, this approach can also be used to synthesize 2,3,6-tribromo or even 2,3,6,7-tetrabromo NDI derivatives via the corresponding dianhydrides.[75,76,106,115]
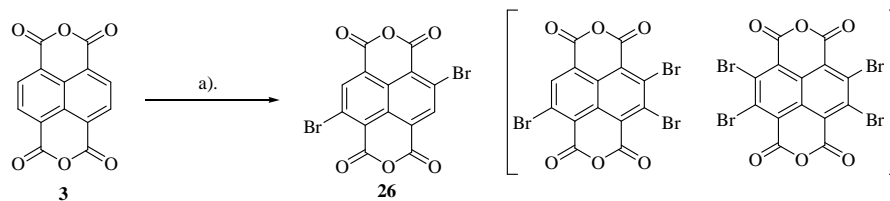
Scheme 8: Synthesis of **26** applying a) DBI (see experimental part), H$_2$SO$_4$, 140 °C, 20 h, 48 %.

Hence, a solution of **3** in sulphuric acid was slowly added to a solution of dibromoisocyanuric acid (DBI)[116,117] in oleum. After recrystallization a pale yellow solid was obtained in 48 % yield, but at this stage it was not possible to separate the formed 2,6-dibromo-1,4,5,8-naphthalenetetracarboxylic acid dianhydride **26** from other brominated side products.

As a linking unit between the two different NDIs mono protected *p*-phenylenediamine derivatives **27** were needed. Whereas *N*-Boc-*p*-phenylenediamine **27a** was obtained from Fluka the other two monoprotected linkers were obtained from *p*-phenylenediamine as shown in *scheme 9*.
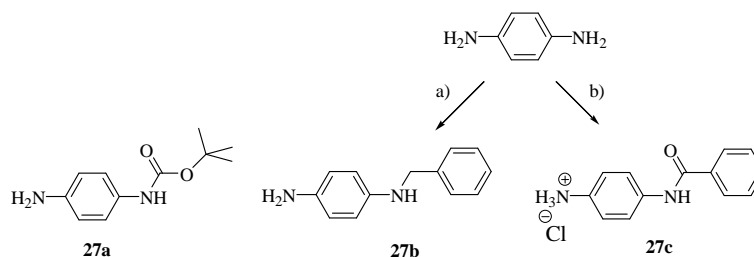
Scheme 9: a) benzylbromide, CH$_2$Cl$_2$, rt 20 min, 21 %; b) sodium dodecyl sulphate, benzoic anhydride, H$_2$O/CH$_3$CN, rt, 5 min, 59 %.[118]

According to the literature several *N, N'*-NDIs, have been built up either by a stepwise[107-113] or a direct condensation[78,104-106] with the appropriate amines as previously mentioned. Our attempt for building up **28** by a 1:1:1 mixture of **10**, 4-*tert*-butylaniline and **27b** or **27c** has so far failed (*scheme 10*). Actually most promising among these protection groups seemed *N*-Boc-*p*-phenylenediamine **27a**, due to the easy removal of the protection group later on (compared to *N*-Bn and *N*-Bz)[119] and because of the previously reported synthesis of asymmetric NDI cyclophanes using a Boc protection strategy. However, investigations to build up **28** under basic (*iso*-propanol/Et$_3$N or DMF/Et$_3$N) or acidic (acetic acid) conditions by 1:1:1 mixtures of **10**, **27a** and 4-*tert*-butylaniline remained unsuccessful (*scheme 10*).
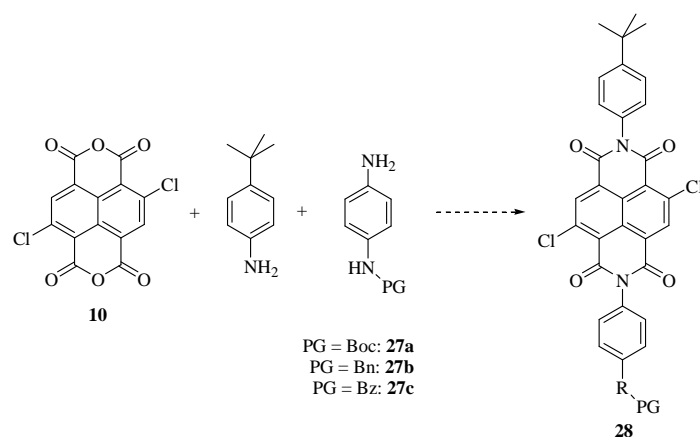
Scheme 10: Attempts for building up *N, N'*-NDI **28**.

Despite the numerous examples in the literature of *N, N'*-NDIs, built up with **3**, and the disappointing results so far, a different strategy over the monoanhydride form, as suggested for the oxygen core substituted NDI part, was recommended. Therefore diimide formation, followed by nucleophilic aromatic substitution with hexanethiol and saponification of just one imide part was proposed to provide the corresponding monoanhydride form (*scheme 6* retrosynthetic approach to **32**). Final condensation of the appropriate core substituted monoanhydride form with the protected linker **27** should lead to **29**.

Scheme 11 displays the synthesis to the desired monoprotected *N, N'*-S_2-NDI **29a**. Thus, condensation of **10** or **26** with 4-*tert*-butylaniline provided the corresponding Cl_2-NDI **30a** or Br_2-NDI **30b** in low 33 and 7 % yield. Astonishingly, one already detected mono core substituted by-product formation for the condensation step of **26** with 4-*tert*-butylaniline, showing the high reactivity of the first halogen exchange. So far, the difficulties in the synthesis and isolation of Cl_2-NDI **30a** and Br_2-NDI **30b** appeared not only from the poor solubility of the starting materials but also from the separation of side-products, which were formed under the harsh reaction conditions. Nevertheless, following nucleophilic aromatic substitution of **30a** or **30b** with hexanethiol provided S_2-NDI **34** in reasonable 42 and 80 % yield after purification.
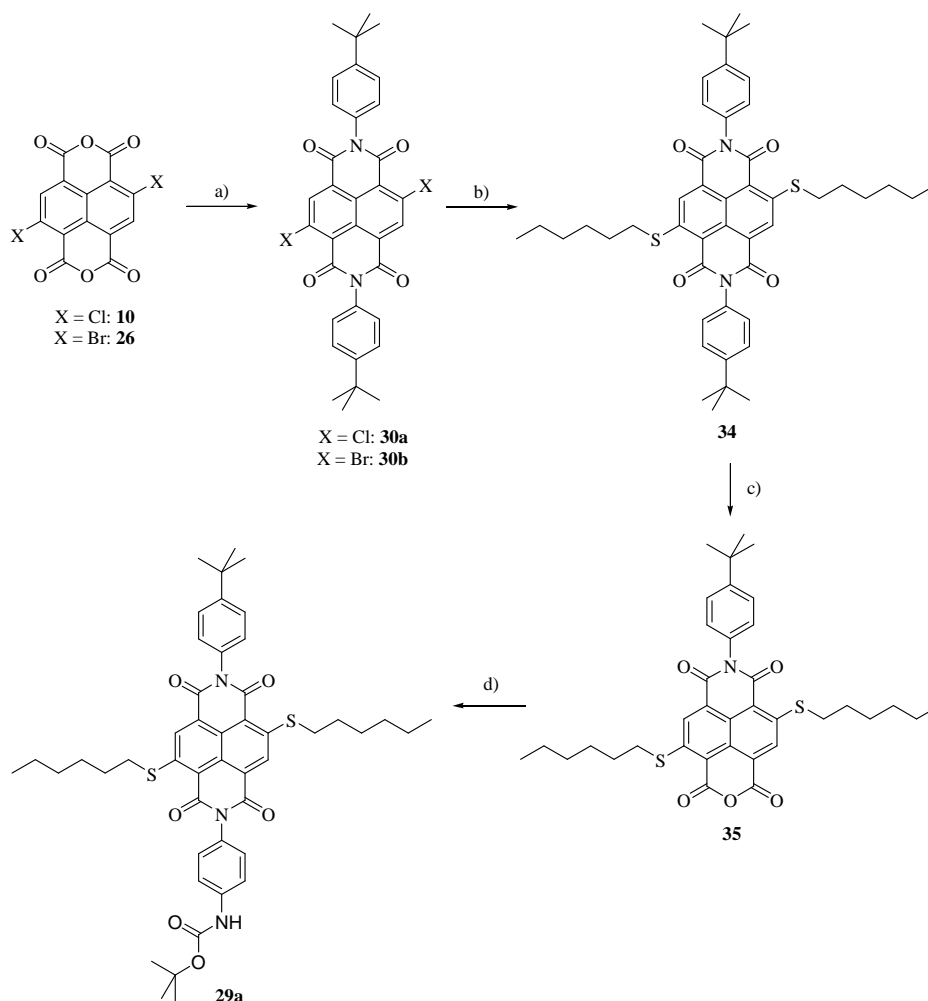
Scheme 11: a) **10**, 4-*tert*-butylaniline, CH₃COOH, reflux, 15 min, 33 %; **26**, 4-*tert*-butylaniline, CH₃COOH, reflux, 10 min, 7 %; b) **30a**, DMF, K₂CO₃, hexane-1-thiol, 65 °C, 2 h, 42 % or **30b**, CH₃CN, K₂CO₃, hexane-1-thiol, rt, 3 d, 80 %; c) KOH/*tert*-butanol, reflux, 30 min, 35 %; d) **27a**, *iso*-propanol/Et₃N, reflux, 1 d.

Saponification of only one imide function of **34** provided after column chromatography monoanhydride **35** as an orange-pink solid in 35 % yield. Final condensation with *N*-Boc-*p*-phenylenediamine (**27a**) indicated after workup product formation by HPLC-ESI-MS. But the isolated red solid still contained the monoanhydride **35** and two other side products. This synthetic pathway, with the low yields obtained, clearly demonstrates the challenge of formation and separation of the products from the generated side-products. On the other hand, we managed the first time to saponify just one imide part of a 2,6- core substituted NDI. It is noteworthy, that saponification of the structurally related perylene diimides is well known,[120-123] whereas for the smaller NDIs no example can be found in the literature. Instead, under different reaction conditions for saponification to the corresponding anhydrides, the used NDIs underwent transformations to their corresponding lactam imides.[71,74]

Building up the desired oxygen core substituted monoanhdride **32** seemed to be even more challenging. Here, the trouble for the synthesis of O_2-NDI **31** arises from the poor nucleophilicity of hexanol (*scheme 6* retrosynthetic approach to **32**). For this reason hexanol was first deprotonated with sodium and then added to Cl_2-NDI **30a**. But all attempts to isolate O_2-NDI **31** in reasonable amounts failed so far, even though product formation was indicated by the green fluorescence on the TLC plate and the correct mass in Maldi (see experimental part). It is suspected that the generated strong nucleophile not only substitutes the halogen atoms at the core, but also opens already the imide functional groups.

Lately, Matile *et al.*[78] reported from a different synthetic route to obtain especially 2,6-alkoxy substituted NDIs over a tetraester naphthalene derivative. This approach was also envisaged for the synthesis of O_2-NDI **31**. Thus, tetraester **36** could be isolated as a yellow oil in excellent 94 % yield after purification (*scheme 12*).
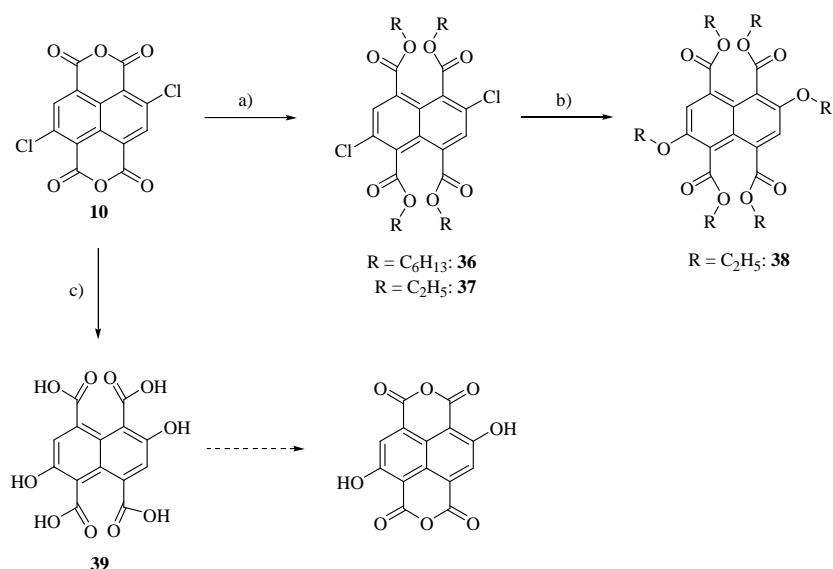
Scheme 12: a) hexanol, 1-bromohexane, K_2CO_3, reflux, 3 h, 94 % for **36** and ethanol, ethylbromide, K_2CO_3, reflux, 6 h, 3 % for **37**; b) DMF, NaOEt, 60 °C, 7 h, 30 %; c) NaOH, H_2O, reflux, 15 h, 76 %.

Unfortunately, further nucleophilic substitution of **36** with a mixture of previously dissolved sodium hydride in hexanol, resulted in gel formation and after workup no product could be isolated. Despite the high yield for tetraester **36**, difficulties in the isolation and purification for the following nucleophilic aromatic substitution step seemed hopeless (see experimental part). However, tetraester formation with hexanol to **36** was much more efficient than for the shorter ethyl-derivative **37**, for which it was possible to obtain single crystals suitable for x-ray analysis (see in the experimental part). On the other hand further nucleophilic substitution of tetraester **37** with sodium ethoxide was achieved according to the described procedure.
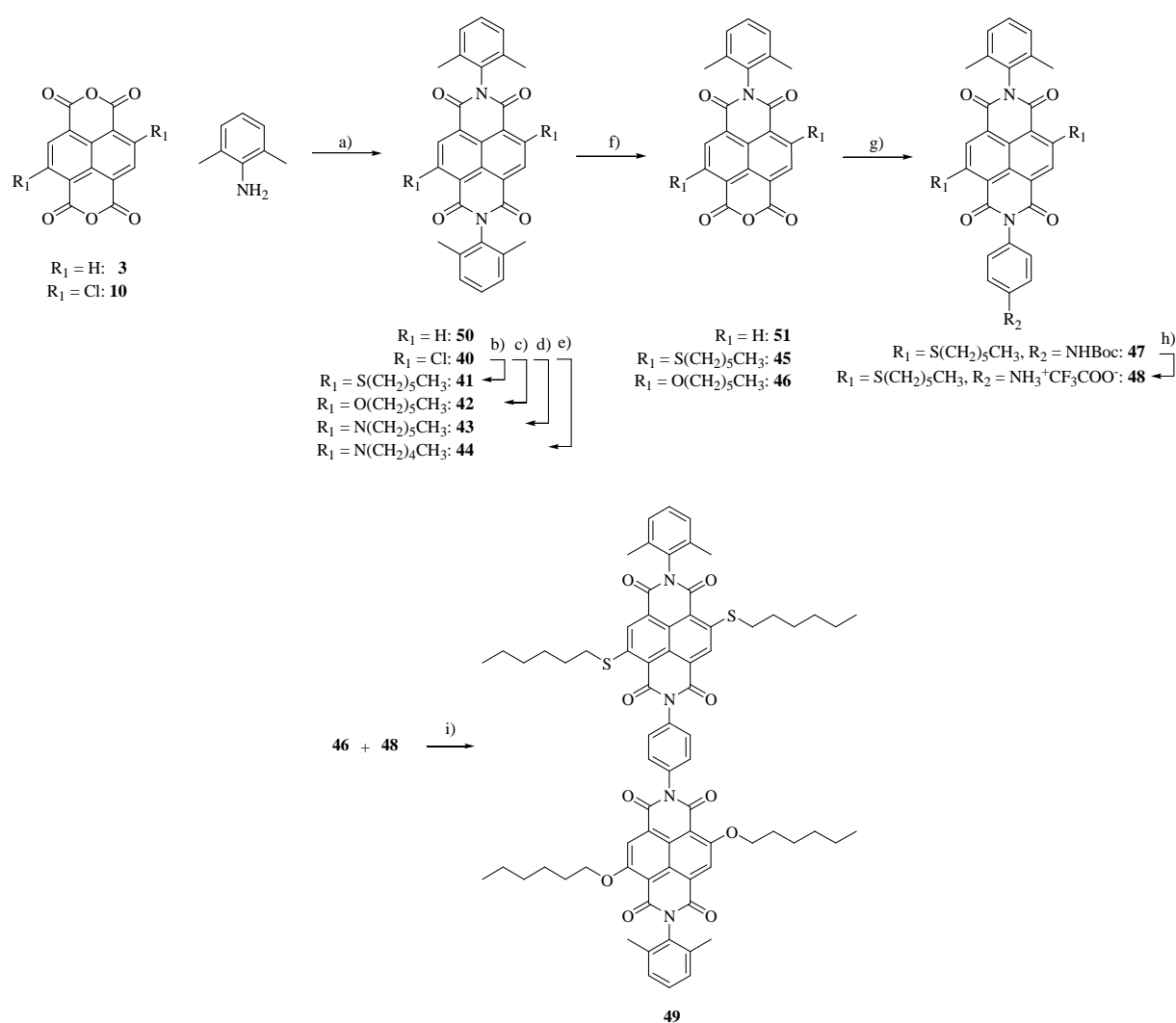
Another pathway towards oxygen core substituted NDIs was proposed by complete saponification and nucleophilic aromatic substitution in one step to the 2,6-dihydroxy-1,4,5,8-naphthalenetetracarboxylic acid **39**, followed by closing of the teracarboxylic acid to the corresponding dianhydride (*scheme 12*). **39** was successfully synthesized from **10** and isolated as a fine white powder. Disappointingly, closing of the tetracarboxylic acid to the consequent dianhydride could not be achieved under various reaction conditions.

According to the low yields for the synthesis of the central building blocks (**30a**, **30b)** and especially the unsatisfactory achievements for the development of an oxygen core substituted NDI, pointed towards a strategy where the imide positions are more shielded.

From carbene chemistry it is known that introduction of sterically demanding substituents at the adjacent nitrogen atoms (e.g. adamantyl or 2,6-diisopropylphenyl) helps to prevent dimerization and even makes them isolatable.[124-126] NDIs bearing bulky 2,6-diisopropylphenyl units at the imide parts were reported to increase the solubility and to prevent dye aggregation, whereas saponification of them provided only the corresponding lactam imides.[74]

As a result we choose especially 2,6-dimethylaniline. Due to the introduced methyl groups at the 2- and 6- position of the phenyl units next to the imide parts, we expected an increased solubility and also prevention of dye aggregation. Moreover, the methyl substituents are supposed to protect the imide parts enough during nucleophilic core substitution of the NDI, whereas the previously achieved saponification of NDIs, applying harsher reaction conditions, should be preserved compared to the reported 2,6-diisopropylphenyl NDIs.

Scheme 13 displays the synthesis of different NDIs and the final target structure S$_2$O$_2$-NDI **49**.

R$_1$ = H: **3**
R$_1$ = Cl: **10**

R$_1$ = H: **50**
R$_1$ = Cl: **40**
R$_1$ = S(CH$_2$)$_5$CH$_3$: **41**
R$_1$ = O(CH$_2$)$_5$CH$_3$: **42**
R$_1$ = N(CH$_2$)$_5$CH$_3$: **43**
R$_1$ = N(CH$_2$)$_4$CH$_3$: **44**

R$_1$ = H: **51**
R$_1$ = S(CH$_2$)$_5$CH$_3$: **45**
R$_1$ = O(CH$_2$)$_5$CH$_3$: **46**

R$_1$ = S(CH$_2$)$_5$CH$_3$, R$_2$ = NHBoc: **47**
R$_1$ = S(CH$_2$)$_5$CH$_3$, R$_2$ = NH$_3^+$CF$_3$COO$^-$: **48**

46 + **48** $\xrightarrow{\text{i)}}$

49

Scheme 13: a) R$_1$ = H: 2,6-dimethylaniline, CH$_3$COOH, reflux, 1 h, 89 %; R$_1$ = Cl: 2,6-dimethylaniline, CH$_3$COOH, reflux, 30 min, 86 %; b) hexanethiol, K$_2$CO$_3$, CH$_3$CN, rt, 2 h, 97 %; c) NaH, hexanol, rt, 2-3 h, 95 %; d) pentylamine, K$_2$CO$_3$, CH$_3$CN, 50 °C, 1 d, 75 %; e) hexylamine, K$_2$CO$_3$, CH$_3$CN, 50 °C, 1 d, 40 %; f) R$_1$ = H: *iso*-propanol/19 M NaOH, 90 °C, 5 min, 8 % or **3**, 2,6-dimethylaniline, pH≈6.0-6.2, reflux, 1 d, 90 %; R$_1$ = S(CH$_2$)$_5$CH$_3$: NaOH/H$_2$O/*tert*-butanol, reflux, 5 min, 67 %; R$_1$ = O(CH$_2$)$_5$CH$_3$: NaOH/H$_2$O/*tert*-butanol, reflux, 5 min, 30 %; g) **45**, *N*-Boc-*p*-phenylenediamine (**27a**), *iso*-propanol/Et$_3$N, reflux, 4 d, 91 %; h) CH$_2$Cl$_2$/CF$_3$COOH, rt, 7 h, quant.; i) **46**, **48**, *iso*-propanol/Et$_3$N, reflux, 4 d, 13 %.

Thus, condensation of 2,6-dichloro-1,4,5,8-naphthalenetetracarboxylic acid dianhydride **10** with 2,6-dimethylaniline provided the central building block Cl$_2$-NDI (**40**) in excellent 86 % yield, compared to the previously obtained yields of 33 % and 7 % for NDIs **30a** and **30b**. Following nucleophilic aromatic substitution of **40** with hexanethiol, hexanol and hexylamine afforded the intense red (**41**), yellow (**42**) and blue (**43**) coloured dyes.

This time both, S_2-NDI **41** and O_2-NDI **42**, were isolated in high yields of 97 % and 95 % respectively under mild reaction conditions, in contrast to the earlier reported S_2-NDI **34** and particularly the mentioned difficulties for the synthesis of an O_2-NDI analogue.

Substitution with an excess of hexylamine (32 eq.) provided N_2-NDI **43** in moderate 40 % yield, which is in good agreement with the literature for 2,6-nitrogen core substituted NDIs.[73,74,78] Interestingly, applying the same reaction conditions as for N_2-NDI **43**, but adding by mistake pentylamine (6eq.) to a suspension of **40** and K_2CO_3 in CH_3CN, the corresponding N_2-NDI **44** was isolated after purification in 75 % yield. Obviously, this example demonstrates that the described procedure in the literature so far for 2,6-aminoalkyl core substituted NDIs, applying high temperatures and using an excess of the amine or even as solvent, is much too harsh. Thus, the presented synthesis of N_2-NDI **44** shows that the yield can be increased by applying a lower temperature and using a smaller excess of the corresponding amine.

Following saponification of only one imide function of S_2-NDI **41** or O_2-NDI **42** to the corresponding monoanhydrides **45** or **46** was achieved by using a mixture of sodium hydroxide, water and *iso*-propanol. After purification by semi-preparative reversed phase HPLC S_2- and O_2-monoanhydride (**45** and **46**) were isolated as red and orange solids in moderate yields of 67 % and 30 % respectively.

Condensation of **45** with *N*-Boc-*p*-phenylenediamine (**27a**) and subsequent deprotection with trifluoro acetic acid afforded **48** as a red salt in 91 % yield over the two steps. Final condensation of the red dye **48** with the yellow monoanhydride dye **46** under basic conditions provided the target structure S_2O_2-NDI **49** as an orange solid in 13 % yield after purification by column chromatography.

Furthermore, NDI **50** was synthesized from **3** and 2,6-dimethylaniline by condensation under acidic conditions and isolated as a white solid in 89 % yield. Following saponification of only one imide unit of **50** to the corresponding monoanhydride **51** was afforded in only 8 % yield. Whereas for the synthesis of core unsubstituted *N, N'*-NDIs another pathway, namely the stepwise introduction of the corresponding amines was envisaged. Therefore careful control of the pH was required for the differentiation in reactivity between anhydride and dicarboxylic acids. Thus, monoanhydride **51** was obtained as white-grey solid in excellent 90 % yield after workup.

3.4.2. Characterisation of linear NDIs

All NDIs and monoanhydride derivatives **40**-**51** have been fully characterized by ^{1}H- and ^{13}C-NMR spectroscopy, mass spectrometry and their purity was analysed by HPLC. Furthermore, it was possible to obtain single crystals suitable for x-ray analysis for NDIs **41** and **42** as well as the monoanhydride **45** (*figure 94*). In all cases the 2,6-dimethylphenyl unit stands perpendicular to the planar naphthalene core, resulting in no observation of an intermolecular π-π stacking, where the hexyl chains are disordered.
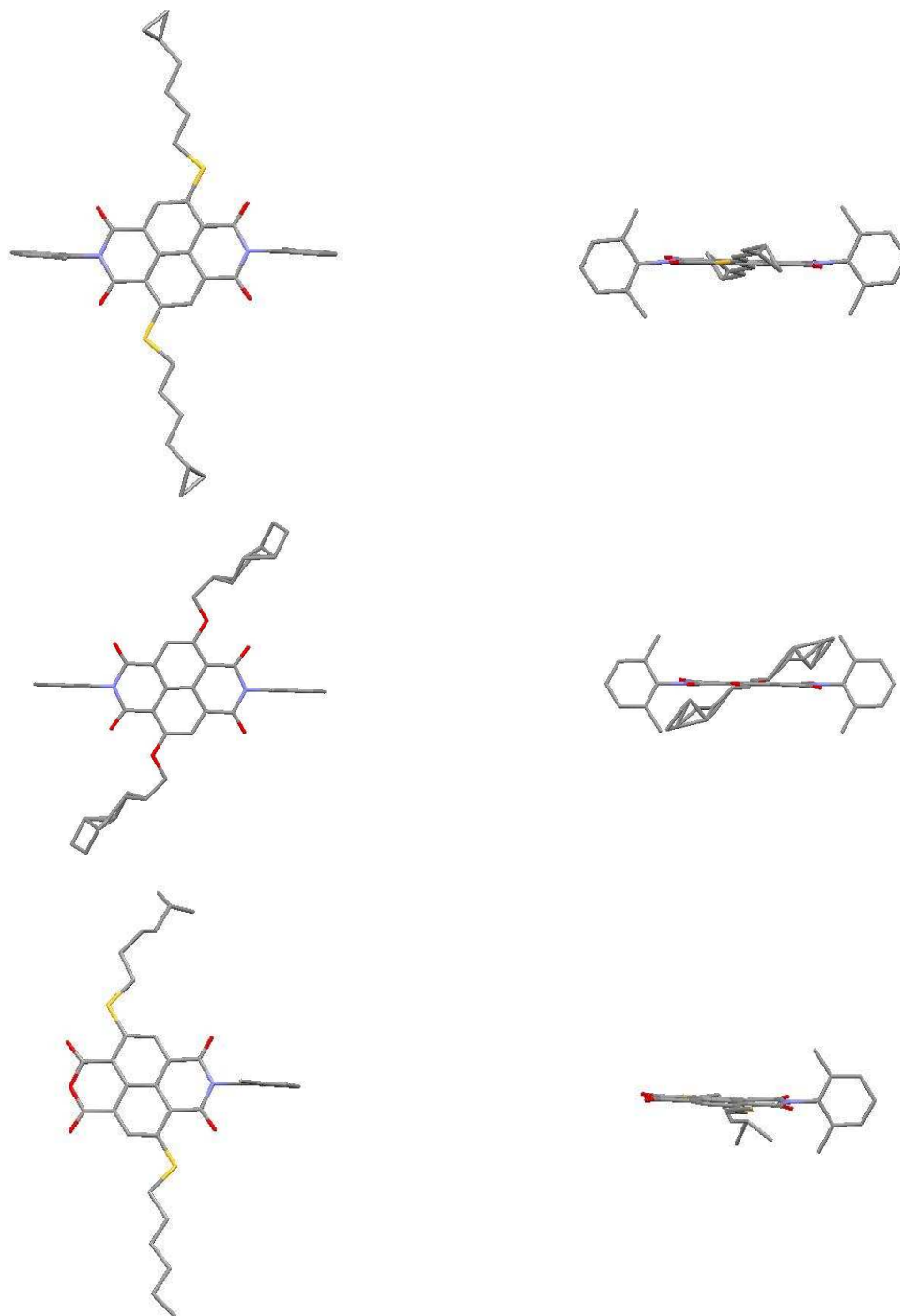

Figure 94: Solid state structures of **41**, **42** and **45**. Left column: top view; Right column: side view.

As previously mentioned the O_2-NDI (**42**), S_2-NDI (**41**) and N_2-NDI (**43**) were isolated as solids with yellow, red and blue colour. The UV/Vis spectra of these three NDIs in dichloromethane are displayed in *figure 95*.

The typical absorption bands between 320 and 400 nm for NDIs as a common subunit are present in all three spectra. The two absorption bands at 353 nm and 369 nm of S_2-NDI **41** are bathochromic shifted and reduced in intensity in comparison to the bands at 344 nm and 360 nm for O_2-NDI **42** and N_2-NDI **43**. Furthermore, all three spectra display additional bands at longer wavelength arising from the 2,6-disubstituted NDI chromophore, indicating a strong electronic interaction between the different substituents and the naphthalene core. The absorption maxima are located at 444 and 470 nm for the yellow O_2-NDI dye, at 533 nm with a pronounced shoulder at about 503 nm for the red S_2-NDI dye and at 615 nm with a shoulder at 575 nm for the blue N_2-NDI dye (*table 2*).

An important colouristic effect for these high brilliance dyes arises from the fact that only this narrow single absorption band is shifted, depending on the core substituent. Moreover, the bathochromic shifted band-shape remains almost the same, while the absorption bands under 400 nm remain unchanged.
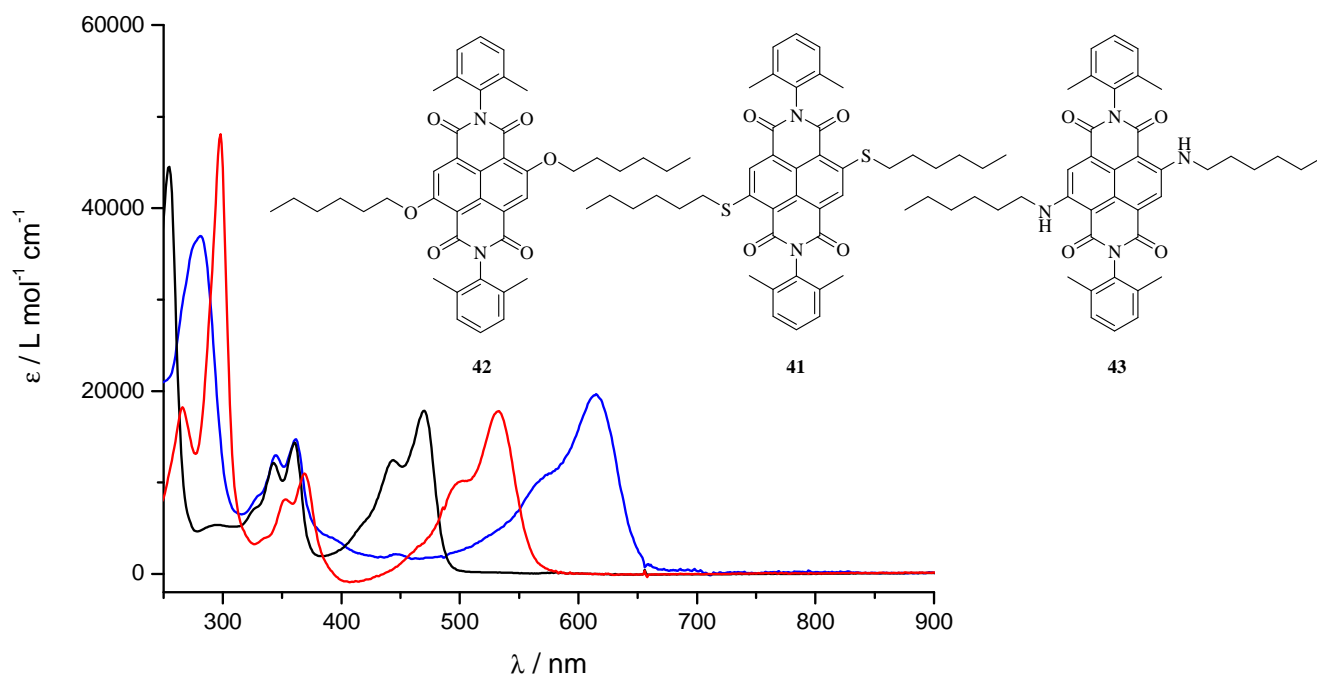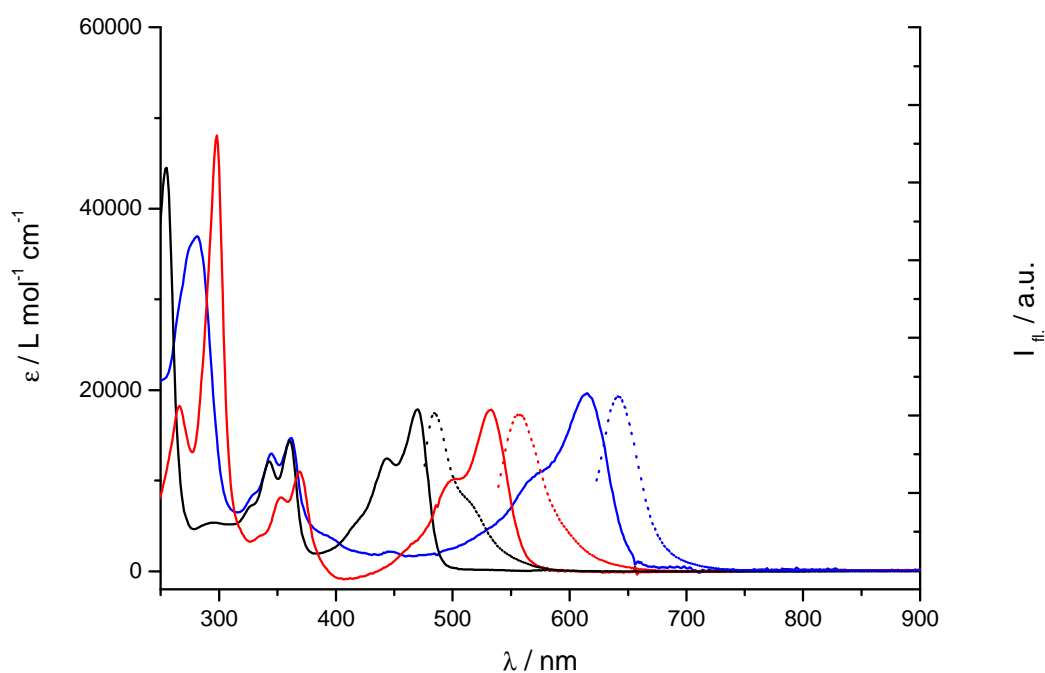

Figure 95: UV/Vis absorption spectra of NDIs **41**, **42** and **43** (sulphur, oxygen and nitrogen substituted; 10 μM) in CH_2Cl_2 at room temperature (**42**: black line, **41**: red line, **43**: blue line).

|	Colour (solid)	λ_{abs} [nm]	ε_{max} [L mol^{-1} cm^{-1}]	λ_{em} [nm]	Stoke shift
NDI **41**	red	503	10 197		
		533	17 814	556	23 nm
NDI **42**	yellow	444	12 429		
		470	17 844	485	15 nm
NDI **43**	blue	575	10 977		
		615	19 640	641	26 nm

Table 2: Optical properties of NDIs **41**, **42** and **43** in dichloromethane.

Figure 96 displays the UV/Vis absorption spectra together with the emission spectra of NDIs **41**, **42** and **43**, according to the previously mentioned photoluminescence properties of heteroalkyl core substituted NDIs. Excitations of these different NDIs revealed the expected mirror images with stoke shifts of 15, 23 and 26 nm, exhibiting photoluminescence of green, orange and red light (*table 2*).

Figure 96: UV/Vis absorption spectra (solid lines) together with the emission spectra (dotted lines) of NDIs **41**, **42** and **43** in CH$_2$Cl$_2$ at room temperature ($\lambda_{exc.}$ = 466 nm for **42**; 525 nm for **41**; 615 nm for **43**).

Thus, a solution of the bichromophoric S_2O_2-NDI (**49**) in dichloromethane displayed exactly the expected mixed absorption band spectra of the corresponding S_2-NDI (**41**) and O_2-NDI (**42**) as shown in *figure 97*. From the structural properties of the introduced 2,6-dimethylphenyl units at the imide positions (*figure 94*) and the excellent matching of the absorption bands we can exclude a possible intermolecular dye aggregation.
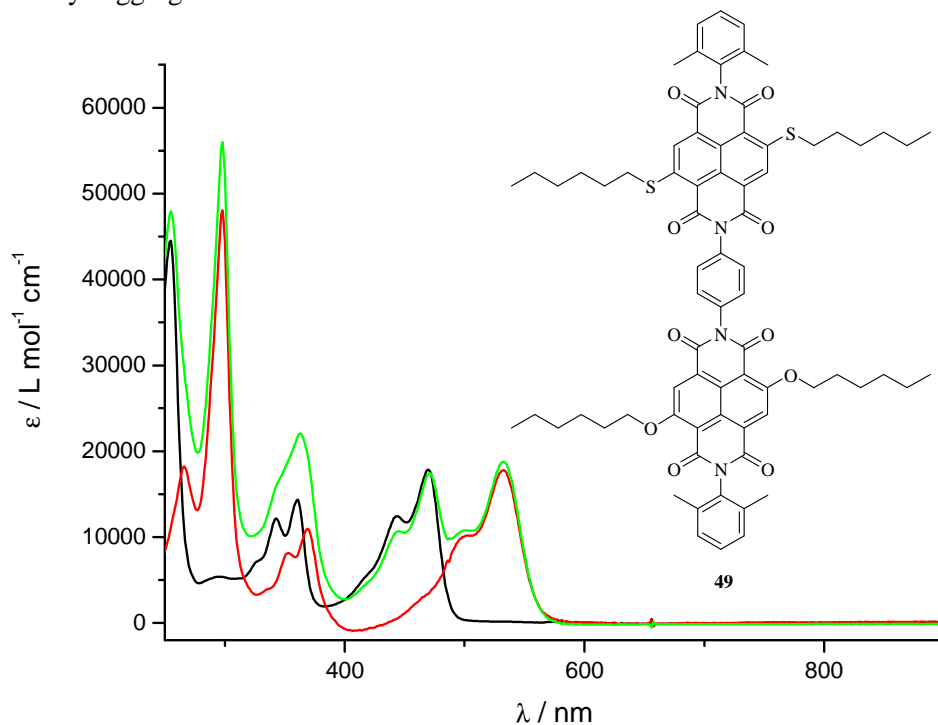
Figure 97: UV/Vis absorption spectra of bichromophoric S_2O_2-NDI **49** (green line; 10 μM) together with the UV/Vis absorption spectra of NDIs **41**, **42** (black and red line; 10 μM)in CH_2Cl_2 at room temperature.

Further, a crucial condition for FRET is the spectral overlap of the emission band of the "donor" with the absorption band of the "acceptor". In the case for the bichromophoric S_2O_2-NDI **49** a spectral overlap of the emission band from the oxygen core substituted NDI ("donor") and the absorption band of the sulphur core substituted NDI ("acceptor") is evident (*figure 96* and *97*).

In fact there is an emission band at 560 nm, as well as one at 487 nm observed upon excitation of a S_2O_2-NDI solution at 445 nm (*figure 98*). Since the detected emission bands were only slightly shifted to higher wavelength for a more concentrated solution (489 nm and 566 nm; 100 μM) and no change was noticed for a more diluted one (1 μM), we exclude a possible intermolecular FRET process under the applied concentrations. Further support for an energy transfer mechanism is given by the excitation spectra, which demonstrates that both absorption bands can be used to detect light emission at 560 nm. The reduced intensity of the excitation spectrum between 320-500 nm, compared to the absorption spectrum, is in agreement with the observed light emission from the oxygen core substituted NDI.
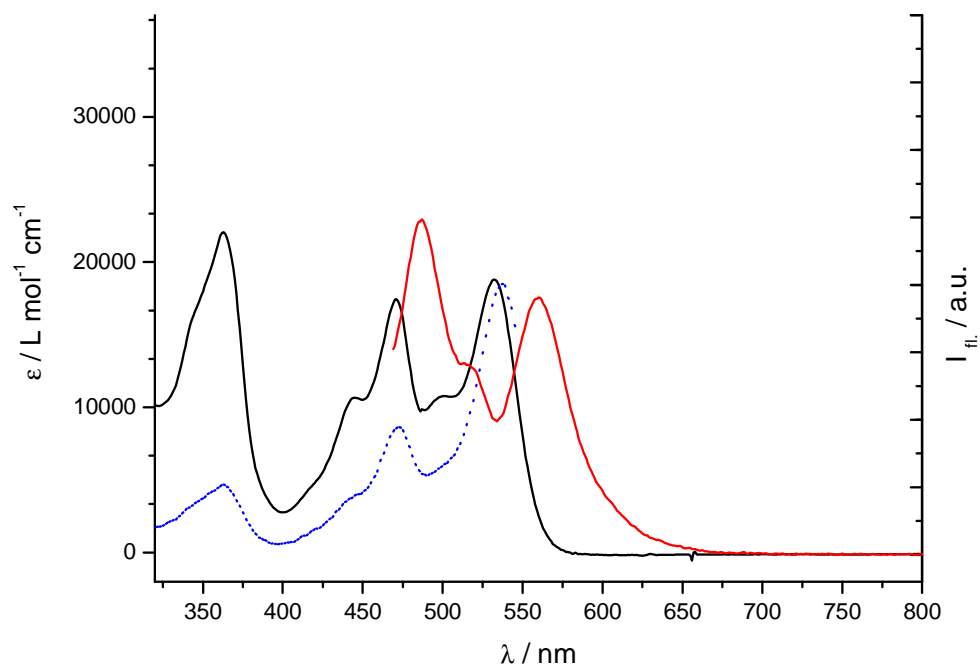
Figure 98: Absorption (straight black line, 10 μM), excitation (dotted blue line; 1 μM; fluorescence detection at 560 nm) and fluorescence (straight red line; 10 μM; $\lambda_{exc.}$ = 445 nm) spectra for dye **49** in CH_2Cl_2.

Several NDIs have been used extensively as electron acceptor units in molecular systems with electron transfer due to their low reduction potential.[50,73,77,79,80,108,109,111,127-130]

Moreover different substituents at the 2- and 6-position of the naphthalene core show enormous effects on the electronic properties, as presented previously, and therefore further analysis of the described NDIs by cyclic voltammetry was envisaged. The cyclic voltammograms of S_2-NDI (**41**), O_2-NDI (**42**) and N_2-NDI (**43**) are presented in *figure 99*. All three compounds displayed two reversible or quasi-reversible reduction waves, corresponding to the formation of radical anions and dianions. Interestingly a continuous shift of the reduction potentials to more negative values from S_2-NDI (-0.488, -0.928) over O_2-NDI (-0.553, -0.992) to N_2-NDI (-0.728, -0.803) was observed (*table 3*). Irreversible oxidation waves were monitored; except the first oxidation peak of the N_2-NDI seemed to be quasi-reversible. Only one was recorded for S_2-NDI and O_2-NDI respectively, while for N_2-NDI clearly two oxidation peaks were observed (*figure 99* and *table 3*).
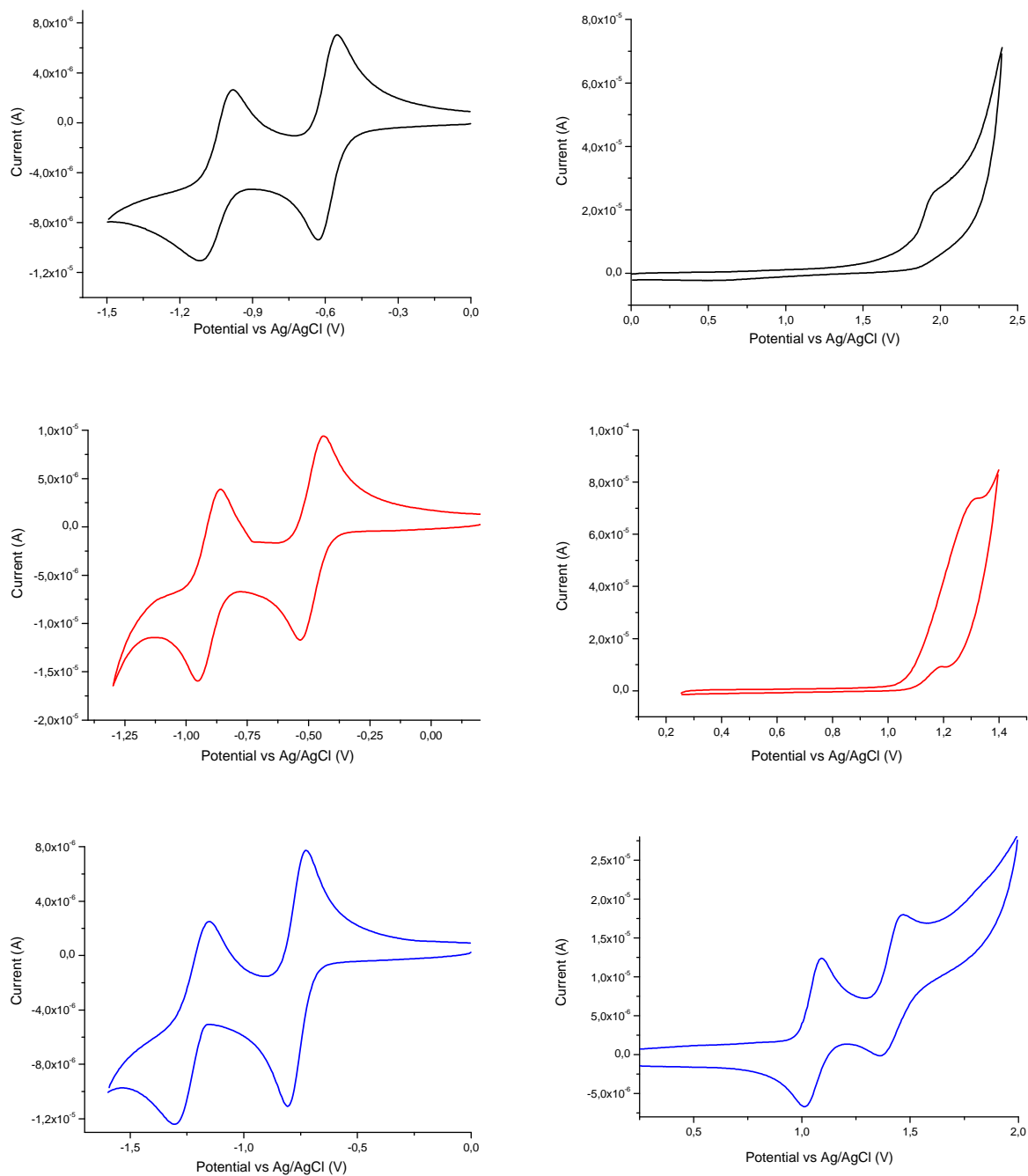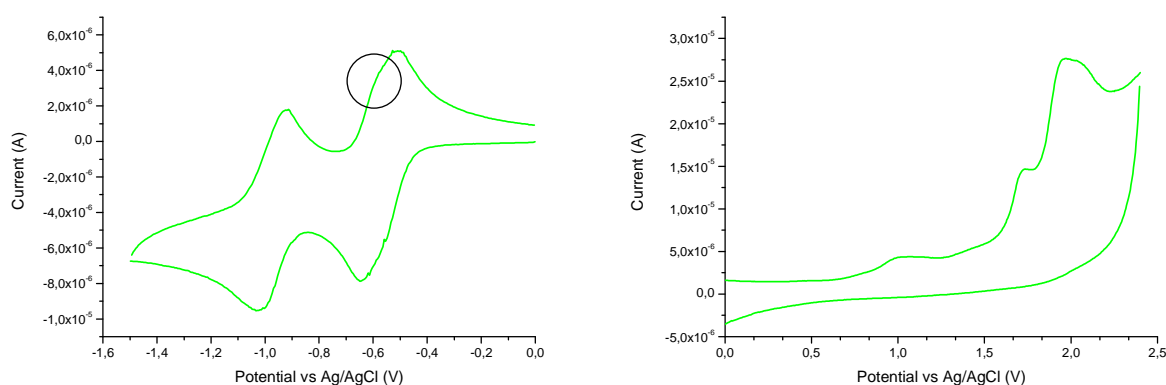
Figure 99: Cyclic voltammograms (left: reduction wave right: oxidation wave) of O_2-NDI (top, black lines), S_2-NDI (middle, red lines) and N_2-NDI (bottom, blue lines).

Also for S_2O_2-NDI **49** a reversible reduction wave was obtained (*figure 100*). Whereas the first reduction peak seems to have a small shoulder, corresponding to the monomer O_2NDI and S_2NDI, the second reduction peak is matching perfectly to the reduction of the sulphur core substituted naphthalene unit. On the other hand, two peaks were recorded for the irreversible oxidation wave according to each core substituted chromophore (*table 3*).

	E_{peak} (V vs Ag/AgCl)			
	X^-/X^{2-}	X/X^-	X/X^+	X^+/X^{2+}
O_2-NDI **42**	-0.992 / -1.283	-0.553 / -0.743	1.942	-
S_2-NDI **41**	-0,928 / -1.017	-0.488 / -0.547	1.717	-
N_2-NDI **43**	-1.158 / -1.298	-0.728 / -0.803	1.011 / 1.090	1.356 / 1.470
S_2O_2-NDI **49**	-0.924 / -1.047	-0.514 / -0.632	1.735 / 1.945	-

Table 3: Redox properties of S_2-NDI (**41**), O_2-NDI (**42**) N_2-NDI (**43**) and S_2O_2-NDI (**49**).

Figure 100: Cyclic voltammograms of S_2O_2-NDI (green lines). The shoulder in the reduction wave corresponds to the O_2-NDI part (indicated by a circle on the left).
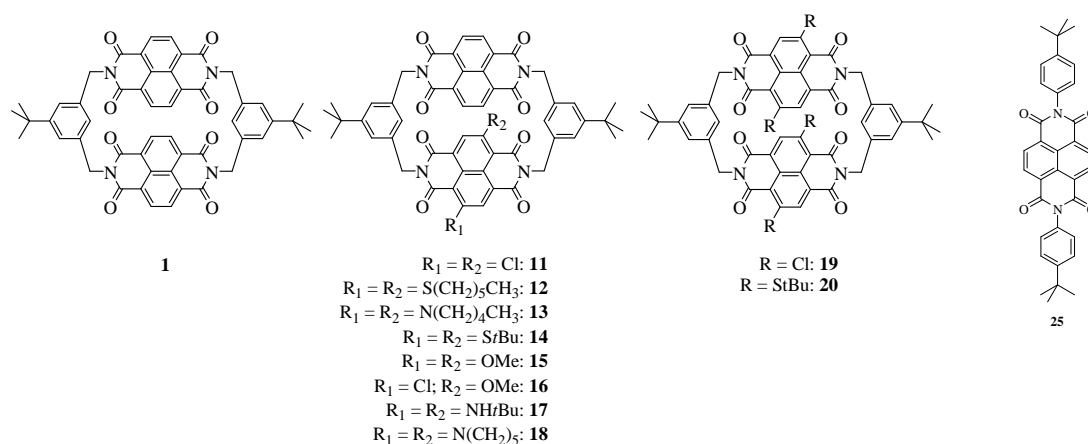
The cyclic voltammogram obtained for S_2O_2-NDI (**49**) is the sum of the cyclic voltammograms of S_2-NDI (**41**) and O_2-NDI (**42**) (the shoulder stemming from O_2-NDI in the reduction wave is indicated by a circle in *figure 100*). This simple addition of the cyclic voltammograms of the individual subunits points towards two electronically decoupled chromophores. As previously discussed, FRET occurs in this linear model compound.

To enlarge the series of model compounds, we are considering various angles between the main axis of both chromophores e.g. by using *meta* or even *ortho* diamino benzene linkers (see chapter 4).

4. Summary and Outlook

In the first project, new rigid symmetric and asymmetric NDI cyclophanes (**1**, **11-20**) were synthesized and fully characterized (*figure 101*).

R₁ = R₂ = Cl: **11**
R₁ = R₂ = S(CH₂)₅CH₃: **12**
R₁ = R₂ = N(CH₂)₄CH₃: **13**
R₁ = R₂ = S*t*Bu: **14**
R₁ = R₂ = OMe: **15**
R₁ = Cl; R₂ = OMe: **16**
R₁ = R₂ = NH*t*Bu: **17**
R₁ = R₂ = N(CH₂)₅: **18**

R = Cl: **19**
R = StBu: **20**

Figure 101: Symmetric and asymmetric NDI cyclophanes (**1**, **11-20**) and linear NDI model compound **25**.

Symmetric NDI cyclophane **1** was designed for STM induced light emission experiments with a compact shape required for the sublimation procedure. By comparison with the monolayers obtained for the model compound **25**, it was demonstrated that NDI cyclophane **1** formed a regular lateral pattern on Au(111) driven by self-assembling without degradation. Furthermore, we showed with STM images that the molecules adopt a staged configuration on the surface with one chromophore over the other, analogous to the solid state structure of **1**. The lateral packing of the chromophore is controlled by the lower chromophore, which forms hydrogen bonds to the neighbour providing long chains of self-assembled cyclophanes.

In order to tune the interaction between the two chromophores, the optical properties of one chromophore were systematically varied by core substituents in the 2- and 6-position of the NDI. The resulting optical coupling of both chromophores was investigated.

The tuneability of the intramolecular FRET process from the unsubstituted to the heteroalkyl core substituted NDI was demonstrated with the chiral planar asymmetric NDI cyclophanes **14**, **15** and **18**. While intramolecular FRET was observed for the yellow methoxysubstituted cyclophane **15**, FRET was increasingly suppressed, due to the bathochromic shift of the absorption band of the core substituted NDI, from the red *tert*-butylsulfanyl cyclophane **14** to the blue piperidinyl substituted cyclophane **18**. X-Ray structure analysis of cyclophane **14** displayed the formation of pillars consisting of alternating enantiomers. A periodic alternation between electron-poor unsubstituted and electron-rich core substituted NDI chromophores pointed at considerable intra- and intermolecular π-π stacking interactions within these pillars. Furthermore, the enrichment of both enantiomers of the *tert*-butylsulfanyl cyclophane **14** was achieved by preparative HPLC and their CD spectra were recorded. X-Ray structure analysis of cyclophane **15** showed no alternation between electron-poor and

93

electron-rich NDIs but contains, as in the solid state structure observed for cyclophane **1**, a solvent molecule in the open cavity.

Comparison of the obtained STM images of asymmetric NDI cyclophanes **11** and **14** with those of cyclophane **1** revealed not only the observation of the different enantiomers on the Au(111) surface, but also lead to the assumption that the core substituted NDI chromophore lies on the gold surface, whereas the unsubstituted one remains spatially separated from the metallic substrate. In addition, the electronic structures of **1**, **11** and **25** were discussed and compared according to molecular modelling, UV/Vis spectroscopy and STS investigations.

NDI model compound **22** comprising two peripheral crown ethers as potential "anchor" groups for the salt layers was successfully synthesized and characterized. In addition a side product (**23**), bearing three crown ether moieties, was isolated (*figure 102*).
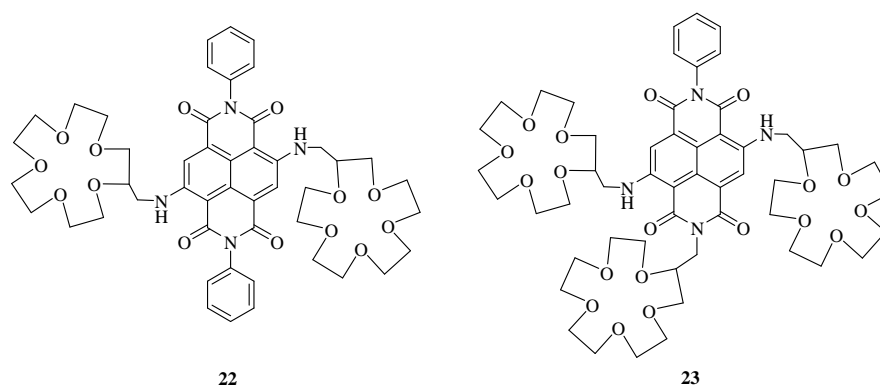

Figure 102: NDI crown ether model compound **22** and the side product **23**.

First STM investigations at room temperature of **22** on Au(111) showed the immobilization without degradation of the crown ether units. While at room temperature **22** tended to form clusters. Single molecules were observed at low temperature STM images, adopting two different conformations. Moreover, complexation studies proved the formation of sandwich complexes with barium and potassium, therefore expecting a higher affinity to the thin insulating salt layer compared to the bare gold surface.

Light emission from the model compounds on the Au(111) surface has not been observed so far. Nevertheless, one possibility in future to determine which chromophore in the cyclophane structures lies on the surface could be achieved by comparison of the STM pictures of cyclophanes **19** and **20** with those already obtained. STM induced light emission measurements of NDI crown ether **22** on thin salt layers are currently under investigations.

In the second project the synthesis of a linear bichromophoric NDI system (S_2O_2-NDI **49**) was realised (*figure 103*).
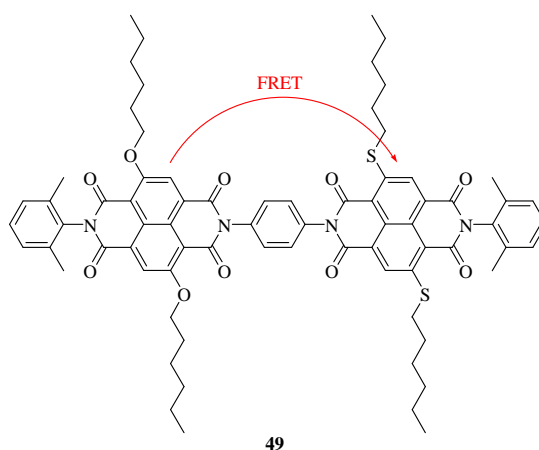

Figure 103: Linear bichromophoric NDI model compound (S_2O_2-NDI **49**) for studies of the orientation factor in a FRET system.

A crucial step in the synthesis of this bichromophoric NDI model compound (S_2O_2-NDI **49**) was the introduction of two methyl units at the 2- and 6-position of the phenyl units at the imide parts, compared to the suggested 4-*tert*-butyl units. The two methyl groups at the imide positions blocked sufficiently the imide structures from nucleophilic attack during core substitution providing improved yields. On the other hand, it was still possible to open one imide in order to form the mono-anhydride by saponification, a procedure not yet reported in the literature.

S_2O_2-NDI **49** was fully characterized by ^{1}H- and ^{13}C-NMR spectroscopy, mass spectrometry and the purity was analysed by HPLC. Fluorescence spectroscopy investigations revealed a FRET from the O_2-NDI to the S_2-NDI chromophore (*figure 103*), while the emission from the oxygen core substituted NDI was still observable. Cyclic voltammetry of S_2O_2-NDI **49** revealed two electrochemically separated chromophores.

Starting from S_2O_2-NDI **49** further bichromophoric FRET systems can be envisaged. For example a S_2N_2-NDI system, which is supposed to be easier to handle during its synthesis due to less reactive nitrogen substituents instead of oxygen core substituents (*figure 104* top left). An analogue to the cyclophane **14** is suggested for comparison of the possible FRET observed in the cyclophane structure (*figure 104* top right). Furthermore, different angles between the two chromophores could be easily achieved by changing the substitution pattern of the bridging diamine benzene linker (*figure 104* bottom). These bichromophoric systems with different angles are particular interesting for studying the κ in the FRET processes.
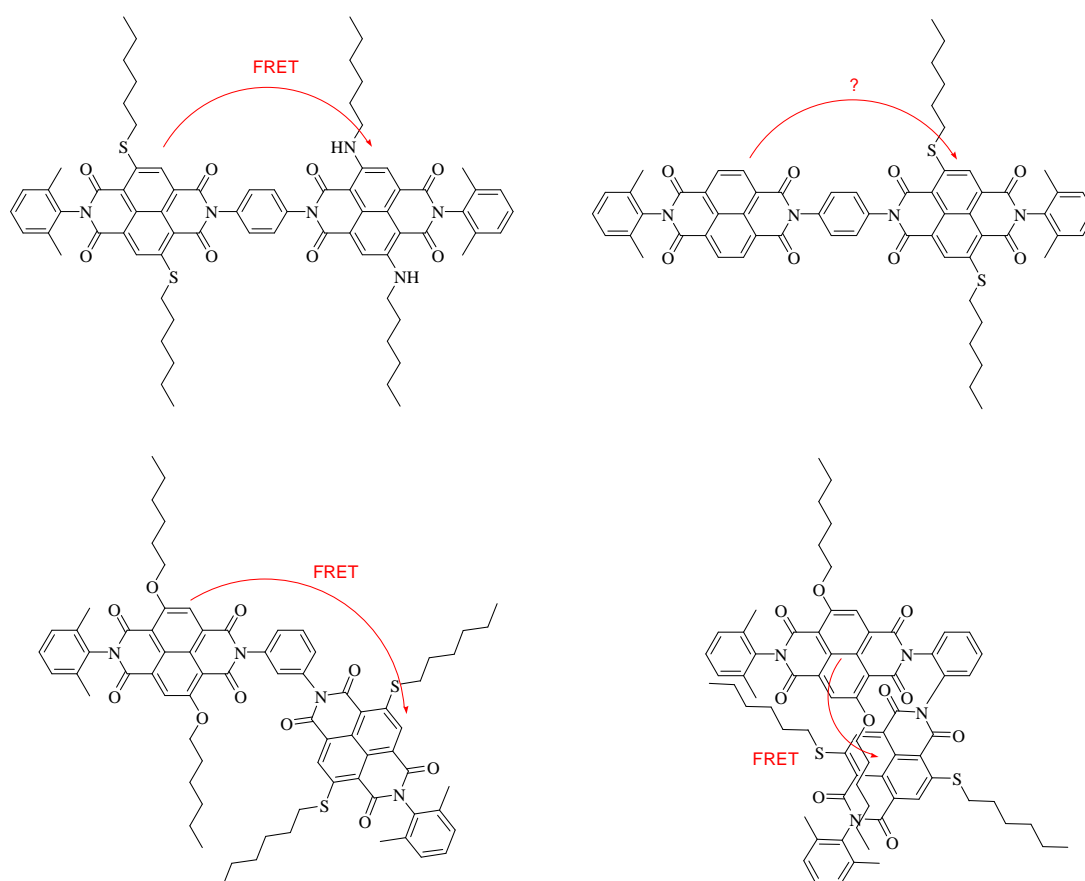
Figure 104: Future bichromophoric FRET systems

Experimental Part

5. Experimental Part

5.1. General Remarks

5.1.1. Solvents and Reagents

Reagents were used as received from *Fluka AG* (Buchs, Switzerland), *Acros AG* (Basel, Switzerland), *Merck* (Darmstadt, Germany) and *Aldrich* (Buchs, Switzerland) unless otherwise stated. Chemicals of the quality *purum*, *purum p.a.* or >98 % were used without further purification. Solvents for chromatography and extractions were distilled prior to use. Further solvents used for reactions corresponded to the quality *puriss p. a., abs., over Molecular Sieves* from *Fluka AG*. HPLC-grade solvents were purchased and used for semi-preparative and analytical HPLC. For an inert atmosphere *Argon 5.6* from *PanGas AG* (Dagmersellen, Switzerland) was used.

5.1.2. Materials and Instruments

Solvents were removed with a *Büchi* (Switzerland) rotary evaporator. For weighing compounds and reagents *Mettler Toledo* (Switzerland) balances PB3002-L (> 1 g), AB265-S/FACT (< 1 g) and AX205 (< 100 mg) were used. A high-vacuum pump from *Edwards* (Sussex, England) was used for drying compounds. For all non-aqueous reactions glassware was flame dried under vacuum and the atmosphere was exchanged by three cycles of evacuating and flushing with argon. For centrifugation an IEC CENTRA-7R refrigerated centrifuge from *Zaffiro AG* (Basel, Switzerland) was used (5000 RPM; 10 °C; 30-40 min.). Microwave reactions were performed in a 50 ml screw-sealed thick-walled glass tube (APCU-GL25; max. 15 bar) equipped with a magnetic stirrer. The reaction tube was placed in a MLS-ETHOS plus Microwave Synthesis System from *MLS GmbH* (Leutkirch, Germany), operated at 170 °C (measured by an ATC-FO fibre optic sensor) for 15 min with a 3 min ramp time; power 400 W for 15 min. The pH was determined with a 691 pH Meter from *Metrohm*. The pH Meter was previous calibrated with a pH = 4 and a pH = 7 solution from *Merck*. **Melting points (mp)** were determined on a SMP3 from *Stuart* in °C.

5.1.3. Chromatographic Methods

Analytical thin layer chromatography (TLC) was performed on 0.25 mm precoated glass plates (5x10 cm, silica gel 60 F_{254}, *Merck AG*, Darmstadt, Germany), on 0.25 mm precoated glass plates (5x10 cm, aluminium oxide 60 F_{254}, *Merck AG*, Darmstadt, Germany) or on 0.25 mm precoated glass plates (5x10 cm, RP-18 F_{254s}, *Merck AG*, Darmstadt, Germany). Compounds were detected at 254 nm (UV) or at 366 nm (fluorescence). <u>Description:</u> TLC (solvent): R_f.

Preparative thin layer chromatography was performed on 2 mm precoated glass plates (20x20 cm, silica gel 60 F_{254}, *Merck AG*, Darmstadt, Germany).

For **normal phase column chromatography** silica gel 60 from *Fluka* (0.043-0.06 mm) or basic aluminium oxide from *Fluka* (Brockmann activity I, 0.05-0.15 mm) were used. For **reversed phase column chromatography** silica gel 100 C_{18} (fully endcapped) from *Fluka* (0.015-0.035 mm) was used.

Analytical and semi-preparative reversed phase HPLC (RP-HPLC) was performed on LiChrospher 100 C 18 from *Merck* (5 μm particle size, 250x4 mm), Reprosil 100 C18 from *Morvay Analytik GmbH* (3 μm particle size, 125x3 mm) and Reprosil 100 C18 from *Morvay Analytik GmbH* (5 μm particle size, 125x20 mm). **Analytical gel permeation chromatography (GPC)** was performed on OligoPore from *Ercatech AG* (Polystyrene/divinylbenzene co-polymer, 6 μm particle size, 300x7.5 mm) with HPLC-grade solvents. Polymer standards of polystyrene were obtained from *Polymer Laboratories*. **Analytical chiral phase HPLC** was performed on CHIRALPAK IA from *Daicel Chemical Industries, LTD* (amylose tris (3,5-dimethylphenylcarbamate) immobilized on 5 μm silica-gel, 4.6x250 mm) with HPLC-grade solvents. **Analytical HPLC-system:** *Agilent* 1100 series 1100 HPLC system with solvent degasser G1379A, bin pump G1312A, auto sampler G1313A, thermostatic column housing G1316A and diode array UV detector G1315B. All samples were filtered prior to use. **Semi-preparative HPLC-system:** *NovaPrep* 200 HPLC system with an UV detector L-7400 and an x/y plotter.

Gas chromatography (GC/MS) was performed on a *Hewlett Packard* 5890 series II using a 25 m 5 % phenyl-methylsilicone column coupled with a *Hewlett Packard* 5970 A (EI) series mass selective detector. Starting with a temperature of 80 °C or 100 °C followed by a gradient of 10 °C/min until 270 °C.

5.1.4. Spectroscopic Methods

Ultra Violet–Visible absorption spectra (UV/Vis) were recorded on an *Agilent* 8453 diode array spectrophotometer using optical 114-QS *Hellma* cuvettes (10 mm light path). Description: UV/Vis (solvent): wavelength of maxima (λ_{max}) in nm (relative extinction coefficient in %).

Fluorescence spectra were measured on a *Shimadzu* RF-5301 PC spectrofluorophotometer using optical 115F-QS *Hellma* cuvettes (10 mm light path) in the presence of air.

Infrared spectra (IR) were measured on a FTIR-1600 Series from *Perkin Elmer*. Description: IR (medium): wave numbers of transmission maxima in cm^{-1}, intensity (s = strong, m = middle, w = weak, br = broad).

Circular dichroism was measured on a Chirascan from *Applied Photophysics* (25 °C, bandwidth: 1 nm, time per point: 1 s) using optical 114-QS *Hellma* cuvettes (10 mm light path).

^{1}H-Nuclear magnetic resonance spectroscopy (^{1}H-NMR) was performed using a *Bruker* DPX-NMR (400 MHz), *Bruker* DRX-500 (500 MHz) or a *Bruker* DRX-600 (600 MHz) spectrometer. Solvents for NMR were obtained from *Cambridge Isotope Laboratories* (Andover, MA, USA). CDCl$_3$ was filtered through basic alumina prior to use. All spectra were recorded at 298 K. COSY and NOESY were recorded if necessary by *Dr. Daniel Häussinger*. Description: ^{1}H-NMR (frequency, solvent): δ_H in ppm relative to residual solvent peaks (peak multiplicity: *s* = singlet, *d* = doublet, *t* = triplet, *q* = quartet, *quin* = quintet, *m* = multiplet, *br* = broad; coupling constants *J* in Hertz).

^{13}C-Nuclear magnetic resonance spectra (^{13}C-NMR) were ^{1}H-decoupled and recorded on a *Bruker* DPX-NMR (100 MHz), *Bruker* DRX-500 (125 MHz) or *Bruker* DRX-600 (150 MHz) spectrometer. For the assignment of carbons DEPT, HMQC and HMBC experiments were carried out if essential by *Dr. Daniel Häussinger*. Description: ^{13}C-NMR (frequency, solvent): δ_C in ppm relative to residual solvent peaks.

Asymmetric NDI cyclophane numbering for NMR assignement:
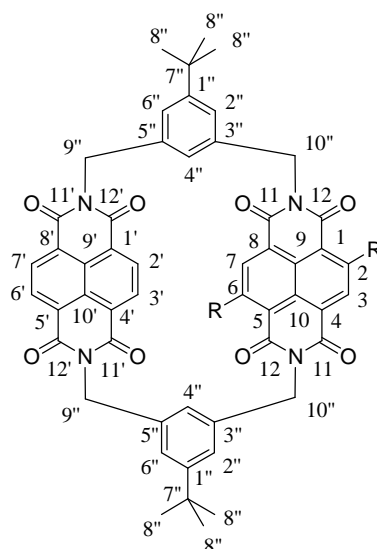
Electron impact mass spectra (EI-MS) and **fast atom bombardment mass spectra (FAB-MS)** were recorded by *Dr. H. Nadig* on a *finnigan* MAT 95Q for EI-MS and on a *finnigan* MAT 8400 for FAB-MS in the mass spectrometry laboratory of the institute. As matrix for FAB-MS m-nitro-benzene alcohol (NBA) or glycine (GLY) was used and if necessary KCl was added. **Electron spray ionisation mass spectra (ESI-MS)** were recorded on a *Bruker Esquire* 3000plus. For HPLC ESI-MS measurements the conditions were set to: nebulizer pressure 40 psi; dry gas flow 9 l/min and drying gas temperature 365 °C. The software ChemStation was used for data acquisition. For **matrix-assisted laser desorption/ionisation mass spectra** in conjunction with **time of flight** mass analysis **(MALDI-TOF-MS)** a *Perseptive Biosystems Vestec Mass Spectrometry Products* Voyager™ Elite Biospectrometry™ Research Station was used. As matrix for MALDI-TOF-MS 1,8,9-anthracenetriol was used. <u>Description</u>: MS (solvent): mass peaks in m/z. Peaks with intensity less than 5 % were not considered.

5.1.5. Elemental Analysis

The elemental analysis **(EA)** was carried out by *H. Kirsch* at the organic department with a *Perkin-Elmer* 240 Analyser. <u>Description</u>: EA (chemical formula, molecular weight): calculated (calc.) abundance of C, H, N in %; found abundance of C, H, N in %.

5.1.6. Electrochemical methods

Electrochemical measurements were carried out in a classical three electrode cell with Pt or glassy carbon as a working electrode, a Pt mesh as counter electrode and an Ag/AgCl electrode in 3 M KCl as reference electrode. Voltammetry experiments were performed with the use of a PGSTAT 12 potentiostat (Autolab) controlled by an HP compact 7600 personal computer using GPES software. All solutions were prepared with dry CH_3CN and $TBABF_4$ 0.1 M as electrochemical salt with 10^{-3} M of the desired organic compound. For spectroelectrochemical experiments a solution of 10^{-4} M of the desired organic compound was used. All these experiments were carried out together with Dr. Yann Leroux.

5.1.7. Scanning tunnelling microscopy methods

The measurements were performed on a room-temperature (RT) and a home built low-temperature (LT) scanning tunnelling microscope (STM). Both machines were equipped with a three chamber ultra high vacuum system (UHV). The pressure was in the range of p $\approx$ $2 \cdot 10^{-11}$ mbar. The LT-STM (*figure 105*) is equipped with a two step cooling system for cooling down to 5.8 K. The Au(111) surfaces were cleaned by Ar^+ ion bombardment followed by annealing (T $\approx$ 400 K). All molecules were sublimed from a home built evaporator. These measurements were done in the group of Richard Berndt by Guillaume Schull, Marco Knutzen, Francesca Matino and Natalia Schneider in Kiel.
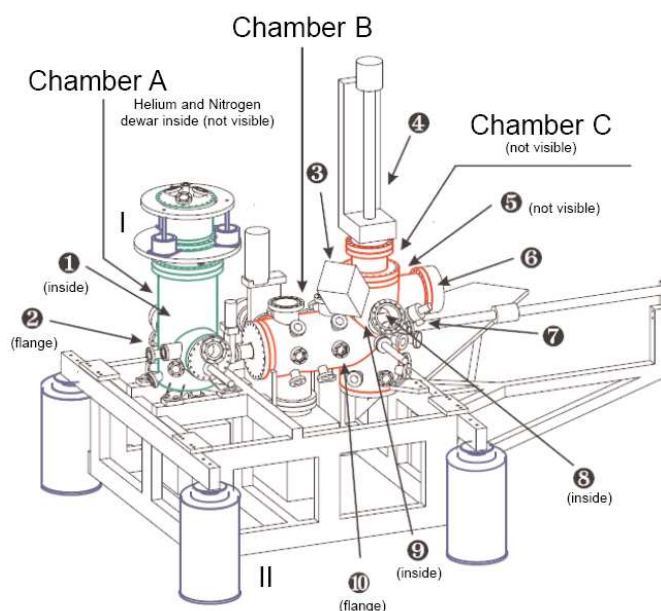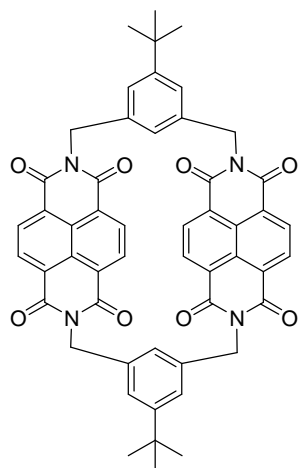

Figure 105: Drawing of the home built LT-STM.

5.2. Synthesis

5.2.1. Synthesis of NDI cyclophanes and reference substance

1,5(1,4,5,8)-Dinaphthalenetetracarboxylic acid diimide-3,7-di(1,3)-5-*tert*-butyl-benzenacycloocta-nodan (1)[84]

a). The yellow suspension of 1,4,5,8-naphthalenetetracarboxylic acid dianhydride (**3**) (0.87 g, 3.2 mmol) and 1,3-bis(aminomethyl)-5-*tert*-butylbenzene (**2**) (0.62 g, 3.2 mmol) in 0.2 ml Et$_3$N and 170 ml *i*-PrOH was refluxed for 3 days. The reaction mixture was cooled to room temperature and filtered. The solvent was evaporated and the residue was purified by column chromatography on silica gel (CH$_2$Cl$_2$/EtOAc 10:1) to provide the symmetric NDI cyclophane **1** as a white solid (32.1 mg, 1.2 %).

b). 1,4,5,8-Naphthalenetetracarboxylic acid dianhydride (**3**) (1.93 g, 7.2 mmol) was solved at 120 °C in 200 ml DMF with 20 ml CH$_3$COOH. Then 50 ml of a solution of 1,3-bis(aminomethyl)-5-*tert*-butylbenzene (**2**) (0.55 g, 2.8 mmol) in 50 ml DMF was dropped in through a dropping funnel over 1 h. This reaction mixture was refluxed for 4 days. Then the reaction mixture was cooled to room temperature and filtered. The solvent was evaporated and the residue was purified by column chromatography on silica gel (CH$_2$Cl$_2$/EtOAc 10:1) to provide the symmetric NDI cyclophane **1** as a white solid (44.5 mg, 3.4 %).

c). The yellow suspension of 1,4,5,8-naphthalenetetracarboxylic acid dianhydride (**3**) (61 mg, 0.23 mmol) and 1,3-bis(aminomethyl)-5-*tert*-butylbenzene (**2**) (149 mg, 0.18 mmol) in 1 ml Et$_3$N and 450 ml *i*-PrOH was refluxed for 3 days. The reaction mixture was cooled to room temperature and filtered. The solvent was evaporated and the residue was purified by column chromatography on silica gel (CH$_2$Cl$_2$/EtOAc 10:1) to provide the symmetric NDI cyclophane **1** as a white solid (59 mg, 40 %).

UHV STM investigations: The experiments were performed with a low-temperature STM operated at 5.7 K in ultrahigh vacuum (below 10^{-10} mbar). The Au(111) samples as well as etched W tips were prepared by argon-ion bombardment and annealing. Cyclophane **1** was deposited from a tantalum crucible maintained at 300 °C and at a rate of approximately 0.2 ML/min as monitored by a quartz microbalance. During deposition a residual gas pressure in the 10-8 mbar range was maintained and the sample was kept at room temperature. The data shown correspond to coverage's of approximately 0.05 monolayers. All images were recorded in a constant-current mode. To demonstrate the deposition of the cyclophane **1** without disruption, the resulting monolayers are compared with the monolayers obtained for the model compound **25** consisting of a single NDI chromophore. LT-STM images of the molecule on Au(111). The conditions were: tunneling voltage V_T = 1700 mV and tunnelling current I_T = 79 pA.

TLC (SiO$_2$; CH$_2$Cl$_2$/EtOAc 10:1): R_f=0.4.

UV/Vis (CH$_3$CN): λ_{max} (ϵ)=232 (50 332), 343 (24 351), 358 (35 057), 379 (30 707 mol^{-1} dm^3 cm^{-1}).

IR (KBr): 3429*br*, 3077*w*, 2961*s*, 1710*s*, 1671*s*, 1581*s*, 1453*s*, 1336*s*, 1244*s*, 1181*m*, 1006*m*, 772*m*.

^{1}H-NMR (400 MHz, CDCl$_3$): δ=8.60 (s, 8H, naphthalene), 7.44 (d, 4H, ^{4}J$_{HH}$=1.5 Hz, 2-H, 6-H), 7.31 (t, 1H, ^{4}J$_{HH}$=1.5 Hz, 4-H), 5.34 (s, 8H, CH$_2$), 1.35 (s, 18H, C(CH$_3$)$_3$).

^{13}C-NMR (400 MHz, CDCl$_3$): δ=162.2, 151.3, 137.5, 130.7, 126.2, 126.1, 125.9, 124.4, 43.4, 34.7, 31.3.

ESI-MS (MeOH): *Positive* ion mode: 2568 ([3xM+Na]$^+$), 1719 ([2xM+Na]$^+$), 871 ([M+Na]$^+$).

FAB-MS (NBA): 849 ([M]$^+$), 793 ([C$_{48}$H$_{31}$N$_4$O$_8$]$^+$).

MALDI-TOF-MS: 870 ([M+Na]$^+$), 893 ([M+2xNa]$^+$), 1717 ([2xM+Na]$^+$), 1740 ([2xM+2xNa]$^+$), ~2567 ([3xM+Na]$^+$).

HPLC-ESI-MS (Reprosil 100 C18, 125x3 mm, pure CH$_3$CN, flow 0.2 ml/min, pressure 30-31 bar, DAD (λ_{det} = 232, 343, 358 and 379 nm, T = 25 °C)): R$_t$ = 6.5 min; m/z 867 ([M+H$_2$O+H]$^+$), 871 ([M+Na]$^+$), 887 ([M+K]$^+$).

EA calc. for C$_{52}$H$_{40}$N$_4$O$_8$ + CH$_2$Cl$_2$ (848.91 + 84.93): C, 68.17; H, 4.53; N, 6.00; found: C, 68.59; H, 4.96; N, 5.59.

mp: >349 °C.

GPC (OligoPore, 6 µm particle size, 300x7.5 mm, pure THF, flow 0.5 ml/min, DAD (λ_{det} = 215, 241, 360 and 381 nm, T = 25 °C)): R$_t$ = 17.1 min.
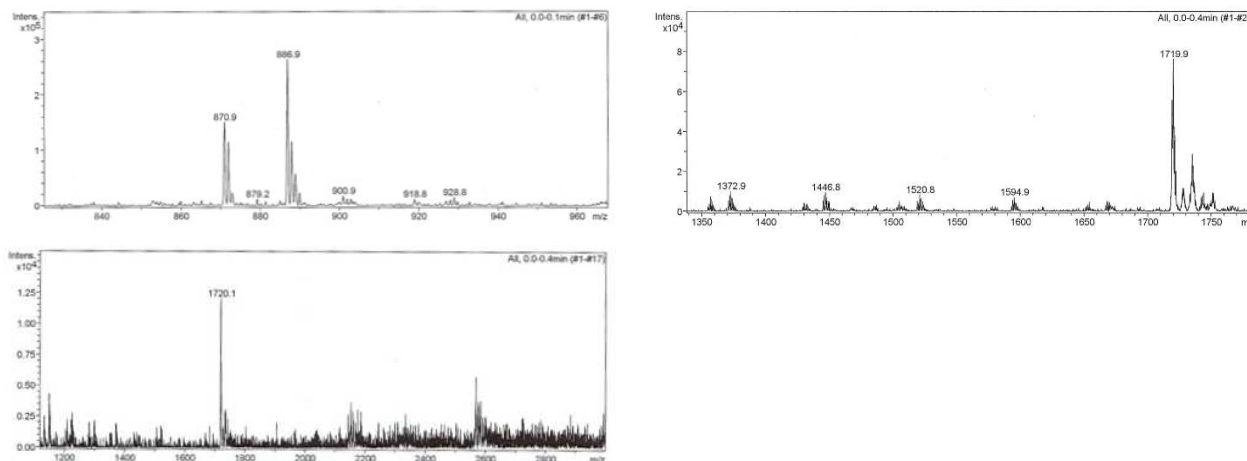

**Figure 106:** ESI-MS spectra obtained in the positive mode by tuning on 871, 1719 and 2567.
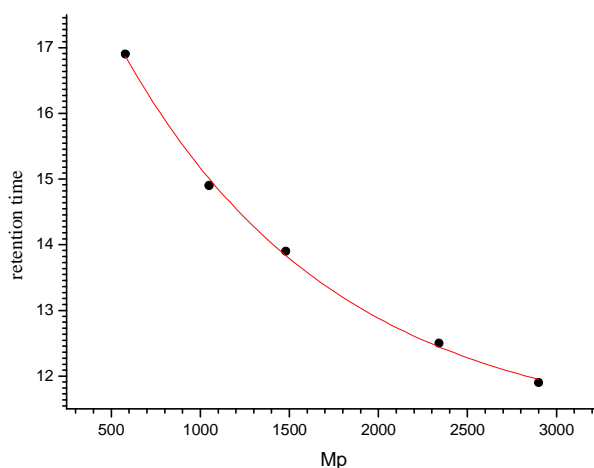
Figure 107: Polymer standards with the corresponding retention time (black dots), with polynomial fit (red curve).

Complexation studies with 1,5-dimethoxynaphthalene (24):

For titration experiments 3 ml of a $1 \cdot 10^{-6}$ M solution of **24** in CH_3CN was transferred into a cuvette for fluorescence spectroscopy. Then cyclophane **1** was once added in portions (10 µl (0.5 eq.) of a stock solution of $0.14 \cdot 10^{-3}$M in CH_3CN) and once linear NDI **25** (10 µl (0.5 eq.) of a stock solution $0.14 \cdot 10^{-3}$M in CH_3CN) to this solution. The fluorescence of **24** was recorded ($\lambda_{Exc.}$ = 295 nm) and the titration were performed until 5 eq. The binding constants (81.18 M^{-1} and 106.17 M^{-1}) were determined by Stern-Volmer plots assuming a 1:1 complex formation as shown in *figure 108*.
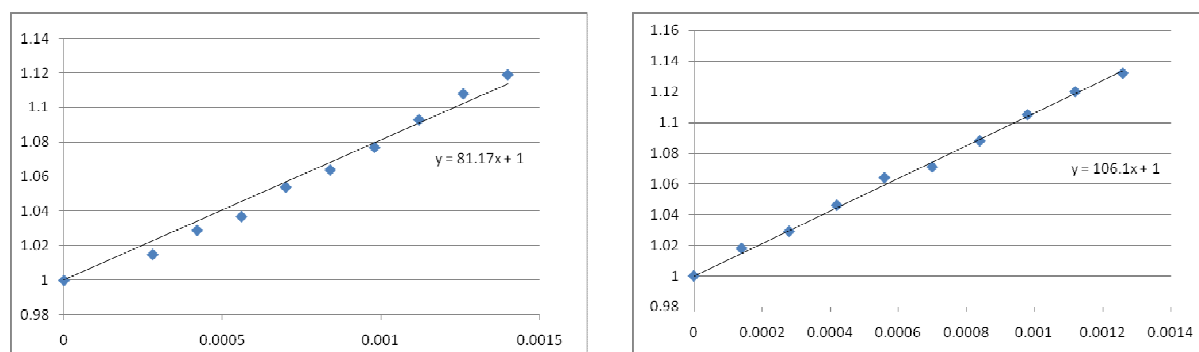
Figure 108: Left: Stern-Volmer plot (F_0/F at 330 nm against [M]) of titration of **24** with cyclophane **1** (81.18 M^{-1}); Right: Stern-Volmer plot (F_0/F at 330 nm against [M]) of titration of **24** with linear NDI **25** (106.17 M^{-1}).

1,3-Bis(aminomethyl)-5-*tert*-butylbenzene (2)[84,126]
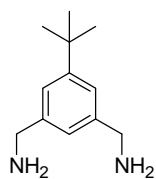
Hydrazine monohydrate (31 ml, 638 mmol) was slowly added to a suspension of 5-*tert*-butyl-1,3-bis(phthalimidomethyl) benzene (6) (11.1 g, 25 mmol) in 300 ml MeOH. The resulting solution was refluxed for 2 h. After cooling to room temperature the reaction mixture was quenched with 200 ml 5 M NaOH solution and extracted with CH_2Cl_2 (4x100 ml). The solvent was evaporated and the remaining yellow oil was distilled under reduced pressure (1 mbar) to afford 1,3-bis(aminomethyl)-5-*tert*-butylbenzene (2) as an air-sensitive colorless oil, which was stored under argon (3.88 g, 82 %).

IR (NaCl): 3350*w*, 3300*w*, 3130*w*, 2966*s*, 2854*w*,1601*m*, 1478*m*, 1365*m*, 908*s*, 733*s*.

^{1}H-NMR (400 MHz, CDCl$_3$): δ=7.20 (d, 2H, $^4J_{HH}$=1.5 Hz, 4-H, 6-H), 7.10 (t, 1H, $^4J_{HH}$=1.5 Hz, 2-H), 3.85 (s, 4H, CH$_2$), 1.32 (s, 9H, C(CH$_3$)$_3$).

^{13}C-NMR (100 MHz, CDCl$_3$): δ=151.7, 143.2, 122.9, 122.6, 46.7, 34.6, 31.3.

ESI-MS (MeOH): *Positive* ion mode: 385 ([2xM]$^+$), 215 ([M+Na]$^+$), 193 ([M]$^+$).

EI-MS (70 eV): 191 ([M]$^+$), 162 ([C$_{11}$H$_{16}$N]$^+$), 135 ([C$_8$H$_{11}$N$_2$]$^+$), 57 ([C$_4$H$_9$]$^+$).

GC-MS: R$_t$ = 18.1 min; 191 ([M]$^+$), 162 ([C$_{11}$H$_{16}$N]$^+$), 57 ([C$_4$H$_9$]$^+$).

EA calc. for C$_{12}$H$_{20}$N$_2$ (192.30): C, 74.95; H, 10.48; N, 14.57; found: C, 71.81; H, 10.33; N, 13.15.
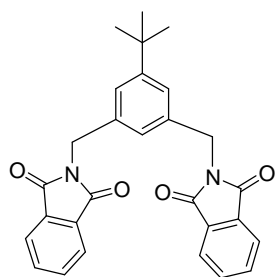
5-*tert*-Butyl-1,3-bis(bromomethyl)benzene (5)[84,125]
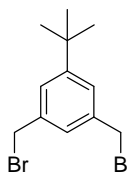
A suspension of 5-*tert*-butyl-1,3-xylene (4) (32.45 g, 200 mmol), NBS (80.45 g, 452 mmol) and AIBN (0.2 g, 1.2 mmol) in 400 ml methyl formate was irradiated with a 500-W bulb for 3 h. The solvent was evaporated and the residue was dissolved in 300 ml CH_2Cl_2. The organic phase was washed twice with concentrated NaHCO$_3$ solution and water, then dried over Na$_2$SO$_4$ and concentrated under reduced pressure. Recrystallization of the solid residue from hexane gave the desired 5-*tert*-butyl-1,3-bis(bromomethyl)benzene (5) as colorless crystals (30.77 g, 48 %).

TLC (SiO$_2$; Hex/EtOAc 3:1): R_f=0.66.

^{1}H-NMR (400 MHz, CDCl$_3$): δ=7.33 (d, 2H, $^4J_{HH}$=1.5 Hz, 4-H, 6-H), 7.25 (t, 1H, $^4J_{HH}$=1.5 Hz, 2-H), 4.48 (s, 4H, CH$_2$), 1.32 (s, 9H, C(CH$_3$)$_3$).

^{13}C-NMR (100 MHz, CDCl$_3$): δ=152.5, 137.9, 126.8, 126.2, 34.7, 33.4, 31.2.

mp: 113 °C.

5-*tert*-Butyl-1,3-bis(phthalimidomethyl)benzene (6)[84]

A mixture of 5-*tert*-butyl-1,3-bis(bromomethyl)benzene (**5**) (8.47 g, 27 mmol), potassium phthalimide (10.78 g, 58 mmol) and K_2CO_3 (21.95 g, 159 mmol) in 200 ml of anhydrous CH_3CN was heated under reflux for 5 h. The reaction mixture was cooled to room temperature and quenched with 200 ml water. After extraction with EtOAc, the combined organic phases were washed with brine, dried over Na_2SO_4 and concentrated under reduced pressure. The residue was purified by column chromatography on silica gel (Hex/EtOAc 3:1 to 1:3) to provide 5-*tert*-butyl-1,3-bis(phthalimidomethyl)benzene (**6**) as a white solid (10.31 g, 86 %).

Once, a stepwise reaction pathway was performed over the mono phthalimide as intermediate. Therefore 5-*tert*-butyl-1,3-bis(bromomethyl)benzene (**5**) (234.4 mg, 0.73 mmol, 1 eq.), potassium phthalimide (149.2 mg, 0.81 mmol, 1.1 eq.) and K_2CO_3 (303.7 mg, 2.2 mmol, 3 eq.) in 30 ml of anhydrous CH_3CN was heated under reflux for 2 h. The reaction mixture was quenched with water and extracted with EtOAc. The combined organic phases were washed against saturated NaCl solution and dried over Na_2SO_4. Then the solvent was evaporated under reduced pressure and after purification by column chromatography on silica gel (Hex/EtOAc 3:2) the mono phthalimide was isolated as white solid (131 mg, 46 %). Due to the low yield of the mono phthalimide formation this reaction pathway was not further considered for the synthesis of 5-*tert*-butyl-1,3-bis(phthalimidomethyl)benzene (**6**).

TLC (SiO$_2$; Hex/EtOAc 2:3): R_f=0.62.

IR (KBr): 3462*br*, 3056*w*, 2955*s*, 2854*w*, 1769*s*, 1714*s*, 1605*s*, 1467*m*, 1430*m*, 1392*s*, 1340*m*, 1092*s*, 952*s*, 733*s*, 711*s*.

^{1}H-NMR (400 MHz, CDCl$_3$): δ=7.84-7.82, 7.71-7.68 (8H, A$_2$B$_2$ spinsystem higher order, Phe), 7.38 (d, 2H, $^4J_{HH}$=1.5 Hz, 4-H, 6-H), 7.32 (t, 1H, $^4J_{HH}$=1.5 Hz, 2-H), 4.80 (s, 4H, CH$_2$), 1.27 (s, 9H, C(CH$_3$)$_3$).

^{13}C-NMR (100 MHz, CDCl$_3$): δ=168.0, 152.2, 136.4, 133.9, 132.1, 126.1, 125.4, 123.3, 41.7, 34.6, 31.2.

ESI-MS (MeOH): *Positive* ion mode: 475 ([M+Na]$^+$), 507([M+MeOH+Na]$^+$).

EI-MS (70 eV): 452 ([M]$^+$), 437 ([C$_{28}$H$_{25}$N$_2$O$_3$]$^+$), 395 ([C$_{24}$H$_{15}$N$_2$O$_4$]$^+$), 305 ([C$_{20}$H$_{19}$NO$_2$]$^+$), 290 ([C$_{20}$H$_{20}$NO]$^+$), 160 ([C$_{12}$H$_{16}$]$^+$).

EA calc. for C$_{28}$H$_{24}$N$_2$O$_4$ (452.51): C, 74.32; H, 5.35; N, 6.19; found: C, 74.17; H, 5.42; N, 6.05.

mp: 183-184 °C.

Monophthalimide:

TLC (SiO$_2$; Hex/EtOAc 2:3): R_f=0.72.

^{1}H-NMR (400 MHz, CDCl$_3$): δ=7.85-7.83, 7.71-7.69 (4H, A$_2$B$_2$ spinsystem higher order, phthalimide), 7.43 (m, 1H, Phe), 7.32 (m, 1H, Phe), 7.28 (m, 1H, Phe), 4.82 (s, 2H, CH$_2$), 4.46 (s, 2H, CH$_2$), 1.30 (s, 9H, C(CH$_3$)$_3$).

^{13}C-NMR (100 MHz, CDCl$_3$): δ=167.9, 152.3, 137.8, 136.5, 133.9, 132.0, 126.4, 126.3, 125.7, 123.3, 41.6, 34.7, 33.7, 31.2.

EI-MS (70 eV): 386 ([M]$^+$), 306 ([C$_{20}$H$_{20}$NO$_2$]$^+$).

EA calc. for C$_{20}$H$_{20}$NO$_2$Br (386.29): C, 62.19; H, 5.22; N, 3.63; found: C, 61.74; H, 5.11; N, 3.70.

1-*tert*-Butoxycarbonyl-1,3-bis(aminomethyl)-5-*tert*-butylbenzene (7)[84]
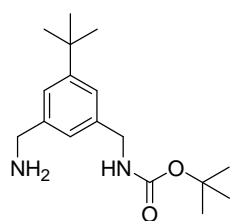
A solution of di-*tert*-butyl-dicarbonate (1.1 g, 5 mmol) in 80 ml dry dioxane was added dropwise to a stirred solution of 1,3-bis(aminomethyl)-5-*tert*-butylbenzene (**2**) (2.4 g, 12.5 mmol) in 500 ml dry dioxane at 0 °C over 1 h. This reaction mixture was then warmed up to room temperature and quenched with water. After extraction with CH$_2$Cl$_2$, evaporation of the solvent and drying one isolated 1-*tert*-butoxycarbonyl-1,3-bis(aminomethyl)-5-*tert*-butylbenzene (**7**) as a yellow oil (0.7 g, 47 %). Further purification by extraction gave colorless oil (22 %).

IR (NaCl): 3344*br*, 2956*s*, 2867*w*, 1694*s*, 1517*m*, 1372*m*, 1261*m*, 1167*s*, 906*s*, 728*s*.

^{1}H-NMR (400 MHz, CDCl$_3$): δ=7.23 (m, 1H, 6-H), 7.18 (m, 1H, 4-H), 7.06 (m, 1H, 2-H), 4.30 (d, 2H, ^{3}J$_{HH}$=5.6 Hz, NHBoc-CH$_2$-Phe), 3.85 (s, 2H, NH$_2$-CH$_2$-Phe), 1.47 (s, 9H, Boc C(CH$_3$)$_3$), 1.31 (s, 9H, C(CH$_3$)$_3$).

^{13}C-NMR (100 MHz, CDCl$_3$): δ=155.9, 152.0, 138.8, 123.5, 123.3, 123.2, 110.0, 46.5, 44.9, 34.7, 31.4, 28.4.

ESI-MS (MeOH): *Positive* ion mode: 585 ([2xM]$^+$), 293 ([M]$^+$).

FAB-MS (NBA): 293 ([M]$^+$), 220 ([C$_{13}$H$_{20}$N$_2$O]$^+$), 176 ([C$_{12}$H$_{19}$N]$^+$), 57 ([C$_4$H$_9$]$^+$).

EA calc. for C$_{17}$H$_{28}$N$_2$O$_2$ (292.42): C, 69.83; H, 9.65; N, 9.58; found: C, 67.32; H, 9.32; N, 8.35.

N, N'-Di-(1'-*tert*-butoxycarbonyl-1',3'-bis(aminomethyl)-5'-*tert*-butylphenyl)-1,4,5,8-naphthalenetetracarboxylic acid diimide (8)[84]
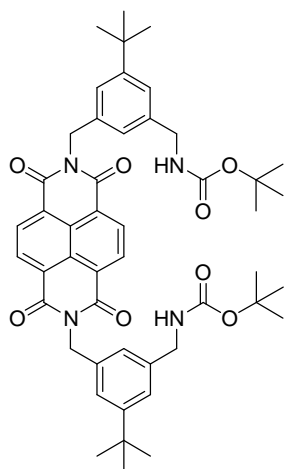
A suspension of 1-*tert*-butoxycarbonyl-1,3-bis(aminomethyl)-5-*tert*-butylbenzene (**7**) (353 mg, 1.2 mmol), 1,4,5,8-naphthalene-tetracarboxylic acid dianhydride (**3**) (162 mg, 0.6 mmol) and 1 ml Et$_3$N in 70 ml *i*-PrOH was refluxed under an argon atmosphere for 3 days. After cooling to room temperature the solvent was evaporated and the residue was purified by column chromatography on silica gel (Hex/EtOAc 2:1) to provide the protected NDI semicircle **8** as a yellow solid (217 mg, 44 %).

TLC (SiO$_2$; EtOAc/Hex 1:2): R_f=0.3.

IR (KBr): 3397*s*, 2966*s*, 1705*s*, 1667*s*, 1505*s*, 1453*s*, 1367*s*, 1326*s*, 1245*s*, 1172*s*, 910*s*, 734*s*.

UV/Vis (CH$_3$CN): λ_{max} (ϵ)=235 (65 453), 342 (26 023), 359 (43 156), 379 (52 026 mol^{-1} dm^3 cm^{-1}).

^{1}H-NMR (400 MHz, CDCl$_3$): δ=8.66 (s, 4H, naphthalene), 7.53, 7.26, 7.24 (s, 6H, 2-H, 4-H, 6-H), 5.35 (s, 4H, NDI-CH$_2$-Phe), 4.27 (d, 4H, ^{3}J$_{HH}$=5.6 Hz, NHBoc-CH$_2$-Phe), 1.43 (s, 18H, Boc C(CH$_3$)$_3$), 1.31 (s, 18H, C(CH$_3$)$_3$).

^{13}C-NMR (100 MHz, CDCl$_3$): δ=162.4, 155.9, 151.9, 138.9, 136.4, 130.9, 126.3, 126.2, 125.8, 125.6, 124.4, 79.3, 44.8, 44.0, 34.7, 31.3, 28.3.
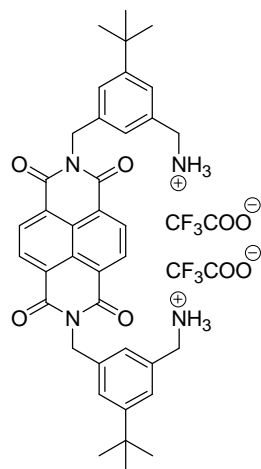
ESI-MS (MeOH): *Positive* ion mode: 855 ([M+K]$^+$), 839 ([M+Na]$^+$).

FAB-MS (NBA): 817 ([M]$^+$), 661 ([C$_{39}$H$_{41}$N$_4$O$_6$]$^+$), 601 ([C$_{35}$H$_{29}$N$_4$O$_6$]$^+$), 57 ([C$_4$H$_9$]$^+$).

MALDI-TOF-MS: 661 ([C$_{39}$H$_{41}$N$_4$O$_6$]$^+$), 601 ([C$_{35}$H$_{29}$N$_4$O$_6$]$^+$).

EA calc. for C$_{48}$H$_{56}$N$_4$O$_8$ (816.99): C, 70.57; H, 6.91; N, 6.86; found: C, 70.03; H, 7.01; N, 6.50.

***N, N'*-Di-(1',3'-bis(aminomethyl)-5'-*tert*-butylphenyl)-1,4,5,8-naphthalenetetracarboxylic acid diimide (9)**[84]

The protected NDI semicircle **8** (217 mg, 0.26 mmol) was solved in CH_2Cl_2 and 5 ml trifluoroacetic acid was dropped to the stirred solution at room temperature. This reaction mixture was stirred for 3 h under an argon atmosphere. After evaporation of the solvent one isolated the deprotected NDI semicircle **9** as a yellow salt in quantitative yield.

IR (KBr): 3179*br*, 2968*m*, 1706*s*, 1666*s*, 1456*m*, 1373*m*, 1330*s*, 1178*br*, 771*w*, 712*s*.

¹H-NMR (400 MHz, DMSO): δ=8.73 (s, 4H, naphthalene), 8.19 (br s, 6H, NH_3^+), 7.51, 7.43, 7.21 (s, 6H, 2-H, 4-H, 6-H), 5.30 (s, 4H, NDI-CH₂-Phe), 3.96 (br s, 4H, NH₂-CH₂-Phe), 1.29 (s, 18H, C(CH₃)₃).

**¹³C-NMR** (100 MHz, DMSO): δ=162.7, 151.3, 137.1, 134.0, 130.8, 126.3, 124.8, 124.8, 124.3, 43.5, 42.3, 34.5, 31.0.

ESI-MS (MeOH): *Positive* ion mode: 617 ([M]⁺), 639 ([M+Na]⁺), 1234 ([2xM]⁺), 1850 ([3xM]⁺).

FAB-MS (NBA): 617 ([M]⁺), 600 ([$C_{35}H_{29}N_4O_6$]⁺⁾).

MALDI-TOF-MS: 767 ([M+2xH₂O]⁺), 601 ([$C_{35}H_{29}N_4O_6$]⁺).

EA calc. for $C_{48}H_{45}F_{15}N_4O_{14}$ + 3CF₃COOH (844.80 + 342.07): C, 48.57; H, 3.82; N, 4.72; found: C, 48.71; H, 4.09; N, 4.71.

1(1,4,5,8)-2,6-Dichloronaphthalenetetracarboxylic acid diimide-5(1,4,5,8)-naphthalenetetra-carboxylic acid diimide-3,7-di(1,3)-5-*tert*-butyl-benzenacycloocta-nodan (11)[99]
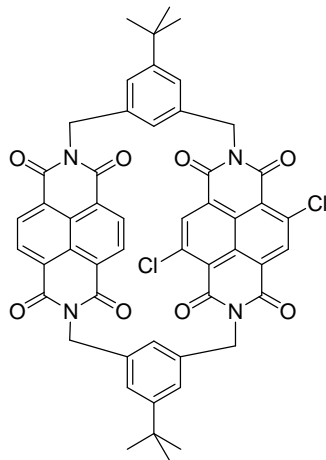
a). *N, N'*-Di-(1',3'-bis(aminomethyl)-5'-*tert*-butylbenzene)-1,4,5,8-naphthalenetetracarboxylic acid diimide trifluoroacetic acid salt **9** (228 mg, 0.27 mmol, 1 eq.) was solved in 20 ml *i*-PrOH and 2 ml Et$_3$N. To this solution 2,6-dichloro-1,4,5,8-naphthalenetetracarboxylic acid dianhydride (108 mg, 0.32 mmol, 1.2 eq.) was added. Then the reaction mixture was refluxed for 5 days. The solvents were evaporated under reduced pressure and the residue was purified by column chromatography on silica gel (CH$_2$Cl$_2$/EtOAc 10:1) to provide the asymmetric Cl$_2$-NDI cyclophane **11** as a white solid (27.8 mg, 11 %).

b). *N, N'*-Di-(1',3'-bis(aminomethyl)-5'-*tert*-butylbenzene)-1,4,5,8-naphthalenetetracarboxylic acid diimide trifluoroacetic acid salt **9** (122 mg, 0.14 mmol, 1 eq.) and 2,6-dichloro-1,4,5,8-naphthalenetetracarboxylic acid dianhydride (74 mg, 0.22 mmol, 1.6 eq.) were refluxed in 300 ml acetic acid for 2 days. Then the reaction mixture was extracted with CH$_2$Cl$_2$. The solvent was evaporated under reduced pressure and the residue was purified by column chromatography on silica gel (CH$_2$Cl$_2$/EtOAc 10:1) to yield the asymmetric Cl$_2$-NDI cyclophane **11** as a white solid (15.4 mg, 12 %).

c). *N, N'*-Di-(1',3'-bis(aminomethyl)-5'-*tert*-butylbenzene)-1,4,5,8-naphthalenetetracarboxylic acid diimide trifluoroacetic acid salt **9** (130.4 mg, 0.154 mmol, 1 eq.), 2,6-dichloro-1,4,5,8-naphthalene-tetracarboxylic acid dianhydride (51.7 mg, 0.153 mmol, 1 eq.) and 30 ml acetic acid were added into a pressure vessel suitable for microwave reactions. The reaction mixture was irradiated for 15 min (400 W, 170 °C) with a 3 min ramp time. After stopping the heating and allowing the reaction mixture to cool to room temperature, the vessel was removed. The solvent was evaporated and the residue purified by column chromatography on silica gel (CH$_2$Cl$_2$/EtOAc 10:1) to provide the asymmetric Cl$_2$-NDI cyclophane **11** as a white solid (39.3 mg, 28 %).

TLC (SiO$_2$; CH$_2$Cl$_2$/EtOAc 10:1): R_f=0.4.

UV/Vis (CH$_3$CN): λ_{max} (ε)=358 (32 237), 380 (29 716), 400 (7684 mol^{-1} dm^3 cm^{-1}).

^{1}H-NMR (400 MHz, CDCl$_3$): δ=8.75, 8.62 (4H, A$_2$B$_2$ spinsystem higher order, 2', 3', 6', 7'), 8.63 (s, 2H, 3, 7), 7.45 (m, 4H, 2'', 6''), 7.31 (m, 2H, 4''), 5.24 (m, 4H, 9''), 5.18 (m, 4H, 10''), 1.35 (s, 18H, 8'').

^{13}C-NMR (100 MHz, CDCl$_3$): δ=162.22 (11', 12'), 160.33 (11), 159.79 (12), 151.37 (1''), 139.83 (2, 6), 137.68, 137.14 (3'', 5''), 135.75 (3, 7), 130.84, 130.65 (2', 3', 6', 7'), 126.46 (2'', 6''), 126.40, 126.30, 126.27, 125.60, 125.98 (4, 8, 9, 10, 1', 4', 5', 8', 9', 10'), 124.60 (4''), 121.89 (1, 5), 43.70 (10''), 43.39 (9''), 34.73 (7''), 31.31 (8'').

HPLC-ESI-MS (Reprosil 100 C18, 125x3 mm, pure CH_3CN, flow 0.2 ml/min, pressure 30-31 bar, DAD (λ_{det} = 196, 239, 360, 380 and 400 nm, T = 25 °C)): R_t = 7.5 min; m/z 935 ($[M+H_2O+H]^+$), 939 ($[M+Na]^+$), 955 ($[M+K]^+$).

HPLC (CHIRALPAK IA, 4.6x250 mm, 50:50 CH_3CN:EtOH, flow 0.3 ml/min, pressure 13-14 bar, DAD (λ_{det} = 196, 239, 360, 380 and 400 nm, T = 25 °C)): R_t = 24.6, 28.4 min.
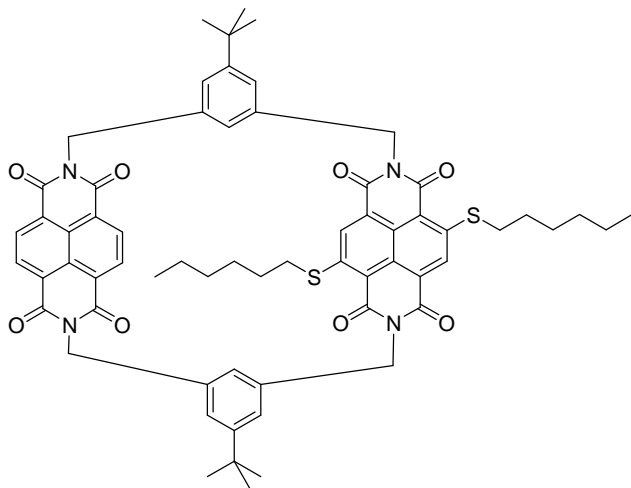
FAB-MS (NBA): 954 ($[M+K]^+$), 918 ($[M]^+$), 861 ($[C_{48}H_{30}Cl_2N_4O_8]^+$).

MALDI-TOF-MS: 922 ($[M]^+$), 1839 ($[2xM]^+$).

EA calc. for $C_{52}H_{38}Cl_2N_4O_8$ + 2x$C_4H_8O_2$ (917.80 + 176.21): C, 65.87; H, 4.98; N, 5.12; found: C, 65.98; H, 4.72; N, 5.12.

mp: >349 °C.

1(1,4,5,8)-2,6-Di(*n*-hexylsulfanyl)naphthalenetetracarboxylic acid diimide-5(1,4,5,8)-naphthalenetetracarboxylic acid diimide-3,7-di(1,3)-5-*tert*-butyl-benzenacycloocta-nodan (12)

To a stirred solution of asymmetric Cl_2-NDI cyclophane **11** (2.6 mg, 0.003 mmol, 1 eq.) in 7 ml HPLC *i*-PrOH, 3.3 mg K_2CO_3 and an excess of hexane-1-thiol (5 µl, 0.035 mmol, 12 eq.) were added. This reaction mixture was refluxed for 2 h under an argon atmosphere. The colour changed from pink to violet. The solvent was evaporated and the residue purified by column chromatography on silica gel (CH_2Cl_2/EtOAc 10:1) to yield asymmetric S_2-NDI cyclophane **12** as a violet solid (1.04 mg, 34 %).

TLC (SiO$_2$; CH_2Cl_2/EtOAc 10:1): R_f=0.75.

UV/Vis (CH_3CN): λ_{max} (ε)=295 (48 800), 359 (27 659), 379 (22 606), 525 (15 991 mol^{-1} dm^3 cm^{-1}).

^{1}H-NMR (500 MHz, CDCl$_3$): δ=8.65, 8.50 (4H, A_2B_2 spinsystem higher order, 2', 3', 6', 7'), 8.48 (s, 2H, 3,7), 7.44, 7.41 (br s, 4H, 2'', 6''), 7.13 (br s, 2H, 4''), 5.40 (d, 2H, $^2J_{HH}$=13.9 Hz, 10''), 5.34 (s, 4H, 9''), 5.30 (d, 2H, $^2J_{HH}$=13.9 Hz, 10''), 3.31-2.92 (m, CH$_2$), 1.93-1.71 (m, CH$_2$), 1.46-1.26 (m, CH$_2$), 1.36 (s, "18H", 8''), 0.90 (m, "6H", CH$_3$).

^{13}C-NMR (150 MHz, CDCl$_3$): δ=162.62, 162.31, 162.18, 161.76, 151.26, 148.59, 137.44, 137.33, 130.82, 130.35, 128.03, 126.09, 125.85, 125.62, 124.04, 123.49, 123.17, 118.50, "52.68-13.91".

HPLC (LiChrospher 100 C18, 250x4 mm, pure CH_3CN, flow 0.5 ml/min, DAD (λ_{det} = 295, 359, 379, 510 and 525 nm, T = 25 °C)): R_t = 23.7 min.

HPLC-ESI-MS (Reprosil 100 C18, 125x3 mm, pure CH_3CN, flow 0.2 ml/min, pressure 30-31 bar, DAD (λ_{det} = 298, 350, 370, 490 and 520 nm, T = 25 °C)): R_t = 30.5 min; m/z 1119 ([M+K]$^+$), 1103 ([M+Na]$^+$), 1098 ([M+H2O]$^+$), 1081 ([M]$^+$).

HPLC (CHIRALPAK IA, 4.6x250 mm, 50:50 CH_3CN:EtOH, flow 0.3 ml/min, pressure 13-14 bar, DAD (λ_{det} = 298, 350, 370, 490 and 520 nm, T = 25 °C)): R_t = 21.8, 23.2 min.

MALDI-TOF-MS: "1085" ([M]$^+$).

1(1,4,5,8)-2,6-Di(*n*-pentylamino)naphthalenetetracarboxylic acid diimide-5(1,4,5,8)-naphthalene-tetracarboxylicacid diimide-3,7-di(1,3)-5-*tert*-butyl-benzenacycloocta-nodan (13)
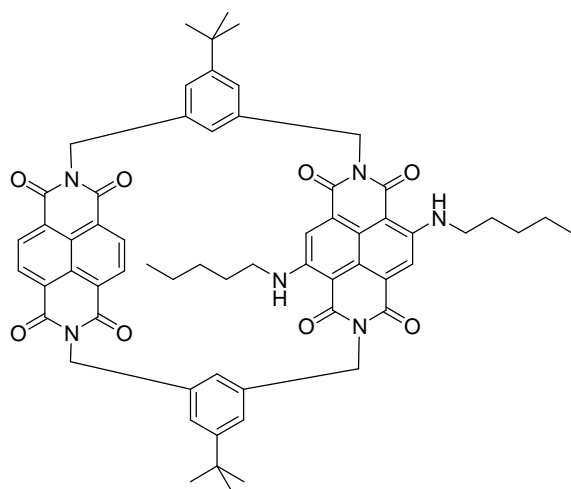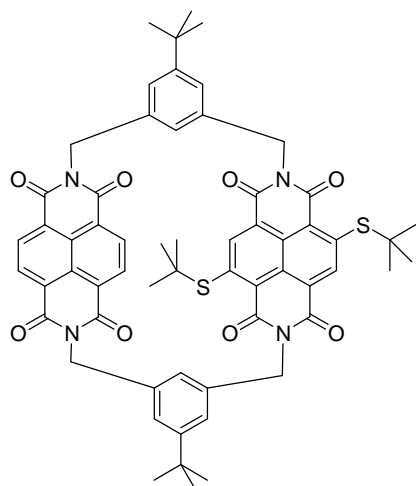

103 mg K_2CO_3 and an excess of pentylamine (1 ml, 8.627 mmol) were added to a stirred suspension of asymmetric Cl_2-NDI cyclophane **11** (39.3 mg, 0.043 mmol, 1 eq.) in 20 ml anhydrous CH_3CN. This reaction mixture was stirred at 70 °C under an argon atmosphere for two days. Then the solvent was evaporated under reduced pressure. The residue was solved in CH_2Cl_2 and washed against H_2O. Afterwards the solvent was evaporated and the residue purified by column chromatography on silica gel (CH_2Cl_2/EtOAc 10:1) to yield ($CH_3(CH_2)_4N)_2$-NDI cyclophane (**13**) as a blue solid (19.63 mg, 45 %).

UV/Vis (HPLC run): λ_{max}=280, 345, 359, 380, 576, 617.

HPLC-ESI-MS (Reprosil 100 C18, 125x3 mm, pure CH_3CN, flow 0.2 ml/min, pressure 30-31 bar, DAD (λ_{det} = 280, 345, 365, 570 and 615 nm, T = 25 °C)): ($CH_3(CH_2)_4N)_2$-NDI cyclophane R_t = 31.6 min; m/z 1020 ([M]$^+$), 1042 ([M+Na]$^+$).

1(1,4,5,8)-2,6-Di(*tert*-butylsulfanyl)naphthalenetetracarboxylic acid diimide-5(1,4,5,8)-naphthalenetetracarboxylicacid diimide-3,7-di(1,3)-5-*tert*-butyl-benzenacycloocta-nodan (14)[99]

112 mg K_2CO_3 and an excess of 2-methyl-propane-2-thiol (1 ml, 8.88 mmol, 8.9 eq.) were added to a stirred suspension of asymmetric Cl_2-NDI cyclophane **11** (117 mg, 0.127 mmol, 1 eq.) in 20 ml anhydrous CH_3CN. This reaction mixture was stirred at room temperature under an argon atmosphere for one day. The colour changed from a white over an orange to a red suspension. The solvent was evaporated and the residue purified by column chromatography on silica gel (CH_2Cl_2/Hex/CH_3COOH 250:250: 8) to yield asymmetric (^{t}BuS)$_2$-NDI cyclophane **14** as a red solid (125.6 mg, 96 %).

TLC (SiO_2; CH_2Cl_2/EtOAc 10:1): R_f=0.87.

UV/Vis (CH_2Cl_2): λ_{max} (ε)=361 (28 872), 381 (24 306), 530 (16 078 mol^{-1} dm^3 cm^{-1}).

^{1}H-NMR (400 MHz, $CDCl_3$): δ=8.92 (s, 2H, 3, 7), 8.72, 8.53 (4H, A_2B_2 spinsystem higher order, 2', 3', 6', 7'), 7.44, 7.41 (br s, 4H, 2'', 6''), 7.19 (br s, 2H, 4''), 5.39-5.29 (m, 8H, 9'', 10''), 1.78 (s, 18H, $SC(CH_3)_3$), 1.36 (s, 18H, 8'').

^{13}C-NMR (100 MHz, $CDCl_3$): δ=162.39, 162.37 (11', 12'), 162.26 (11), 161.91 (12), 151.21 (1''), 148.80 (2, 6), 137.40, 137.29 (3'', 5''), 130.79, 130.57, 130.29 (3, 7, 2', 3', 6', 7'), 126.19, 126.07, 125.50, 123.72, 122.56 (4, 8, 9, 10, 1', 4', 5', 8', 9', 10'), 125.82 (2'', 6''), 124. 41 (4''), 119.83 (1, 5), 48.07 (S$\underline{C}$(CH_3)$_3$), 43.58 (10''), 43.37 (9''), 34.71 (7''), 31.39 (SC($\underline{C}H_3$)$_3$), 31.33 (8'').

HPLC-ESI-MS (Reprosil 100 C18, 125x3 mm, pure CH_3CN, flow 0.2 ml/min, pressure 30-31 bar, DAD (λ_{det} = 196, 239, 360, 380 and 400 nm, T = 25 °C)): R_t = 11 min; m/z 1025 ([M]$^+$), 1047 ([M+Na]$^+$), 1063 ([M+K]$^+$).

HPLC (CHIRALPAK IA, 4.6x250 mm, 50:50 CH_3CN:EtOH, flow 0.3 ml/min, pressure 13-14 bar, DAD (λ_{det} = 298, 350, 370, 490 and 520 nm, T = 25 °C)): R_t = 15.2, 16.0 min.

FAB-MS (NBA): m/z 1025 ([M]$^+$), 913 ([$C_{52}H_{40}N_4O_8S_2$]$^+$).

MALDI-TOF-MS: 1050 ([M+Na]$^+$), "1026" ([M]$^+$) 915 ([$C_{52}H_{40}N_4O_8S_2$]$^+$).

EA calc. for $C_{60}H_{56}N_4O_8S_2$ + $C_2H_4O_2$ (1025.24 + 60.05): C, 68.61; H, 5.57; N, 5.16; found: C, 68.57; H, 6.05; N, 4.50.

1(1,4,5,8)-2,6-Dimethoxynaphthalenetetracarboxylic acid diimide-5(1,4,5,8)-naphthalene-tetracarboxylic acid diimide-3,7-di(1,3)-5-*tert*-butyl-benzenacycloocta-nodan (15)[99]

Asymmetric Cl_2-NDI cyclophane **11** (34.47 mg, 0.038 mmol, 1 eq.) and an excess of sodium methoxide (40 mg, 0.74 mmol, 19.6 eq.) were put in a round flask and suspended in 10 ml dry MeOH. This reaction mixture was stirred at 50 °C under an argon atmosphere for 20 h. The solvent was evaporated under reduced pressure and the residue solved in CH_2Cl_2 and extracted once with H_2O. After purification by column chromatography on silica gel (CH_2Cl_2/EtOAc 10:1) one could isolate 22.64 mg educt, 4 mg mono-substituted Cl-MeO-NDI cyclophane **16** (12 %) and 5 mg of the desired asymmetric $(MeO)_2$-NDI cyclophane **15** (14 %) as a yellow solid.
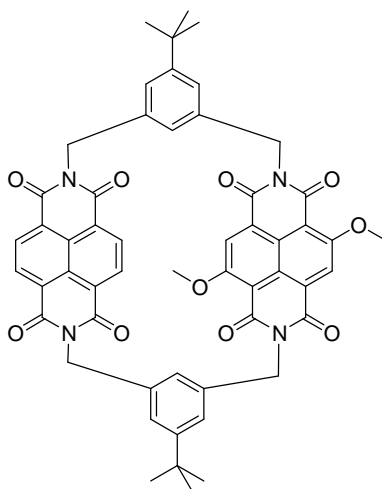
TLC (SiO_2; CH_2Cl_2/EtOAc 10:1): R_f=0.11.

UV/Vis (CH_2Cl_2): λ_{max} (ε)=346 (12 216), 361 (14 957), 383 (11 454), 441 (3 993),

466 (6 590 mol^{-1} dm^3 cm^{-1}).

^{1}H-NMR (400 MHz, $CDCl_3$): δ=8.57, 8.54 (4H, A_2B_2 spinsystem higher order, 2', 3', 6', 7'), 8.35 (s, 2H, 3, 7), 7.43, 7.41 (br s, 4H, 2'', 6''), 7.14 (br s, 2H, 4''), 5.35-5.30 (m, 8H, 9'', 10''), 4.29 (s, 6H, OCH_3), 1.37 (s, 18H, 8'').

^{13}C-NMR (100 MHz, $CDCl_3$): δ=162.26, 162.15 (11', 12'), 161.77 (2, 6), 160.38 (11), 160.19 (12), 151.23 (1''), 137.74, 137.34 (3'', 5''), 130.50, 130.40 (2', 3', 6', 7'), 126.90 (4''), 126.31, 126.16 (2'', 6''), 125.86, 125.72, 125.44, 123.30, 122.83 (4, 8, 9, 10, 1', 4', 5', 8', 9', 10'), 118.79 (1, 5), 110.33 (3, 7), 57.40 (OCH_3), 43.49 (10''), 43.35 (9''), 34.75 (7''), 31.38 (8'').

HPLC-ESI-MS (Reprosil 100 C18, 125x3 mm, pure CH_3CN, flow 0.2 ml/min, pressure 30-31 bar, DAD (λ_{det} = 250, 340, 360, 450 and 460 nm, T = 25 °C)): R_t = 5.9 min; m/z 910 ($[M]^+$), 932 ($[M+Na]^+$), 948 ($[M+K]^+$).

HPLC (CHIRALPAK IA, 4.6x250 mm, 50:50 CH_3CN:EtOH, flow 0.3 ml/min, pressure 13-14 bar, DAD (λ_{det} = 250, 340, 360, 450 and 460 nm, T = 25 °C)): R_t = 17.9, 19.8 min.

MALDI-TOF-MS: "912" ($[M]^+$).
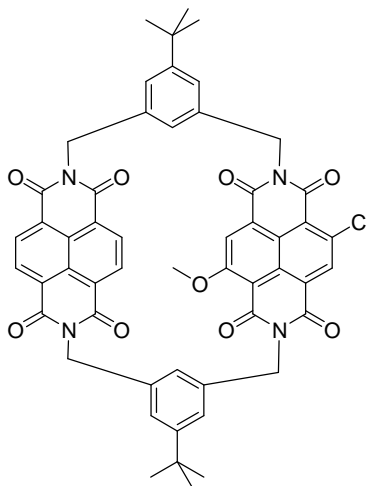
TLC (SiO$_2$; CH$_2$Cl$_2$/EtOAc 10:1): R_f=0.42.

UV/Vis (CH$_3$CN from HPLC run): λ_{max}=343, 359, 380, 415, 436.

^{1}H-NMR (400 MHz, CDCl$_3$): δ=8.86, 8.73, 8.47, 8.47 (4H, A$_2$B$_2$ spinsystem higher order, 2', 3', 6', 7'), 8.70, 8.28 (s, 2H, 3, 7); 7.44 (br m, 4H, 2'', 6''), 7.23 (br m, 2H, 4''), 5.57-5.45, 5.21-5.13 (m, 8H, 9'', 10''); 4.17 (s, 3H, OCH$_3$), 1.37, 1.36 (s, 18H, 8'').

HPLC-ESI-MS (Reprosil 100 C18, 125x3 mm, pure CH$_3$CN, flow 0.2 ml/min, pressure 30-31 bar, DAD (λ_{det} = 250, 340, 360, 450 and 460 nm, T = 25 °C)): R$_t$ = 6.4 min; m/z 931 ([M+H$_2$O]$^+$), 936 ([M+Na]$^+$), 951 ([M+K]$^+$).

MALDI-TOF-MS: "916" ([M]$^+$), "937" ([M+Na]$^+$).

1(1,4,5,8)-2,6-Di(*tert*-butylamino)naphthalenetetracarboxylic acid diimide-5(1,4,5,8)-naphthalenetetracarboxylic acid diimide-3,7-di(1,3)-5-*tert*-butyl-benzenacycloocta-nodan (17)
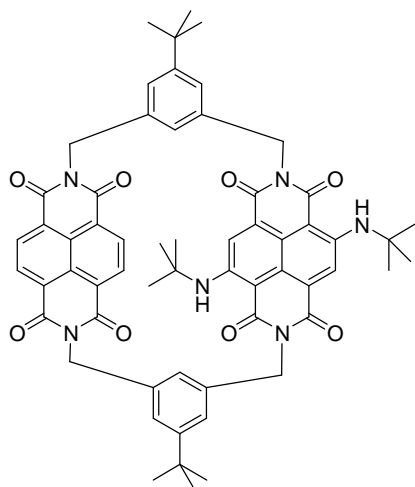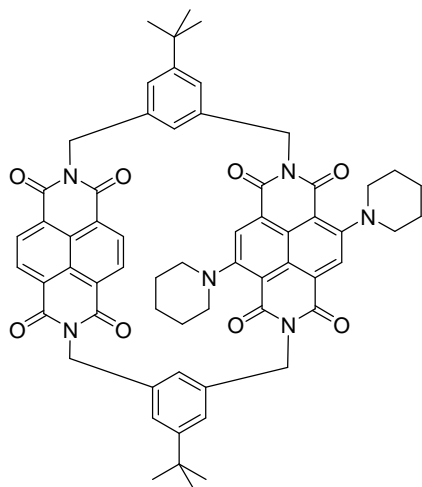
197 mg K$_2$CO$_3$ and an excess of *tert*-butylamine (6 ml, 56.85 mmol) were added to a stirred suspension of asymmetric Cl$_2$-NDI cyclophane **11** (33.1 mg, 0.036 mmol, 1 eq.) in 20 ml anhydrous CH$_3$CN. This reaction mixture was stirred at 70 °C under an argon atmosphere for one day. The colour changed from orange to a red suspension. Then another 10 ml of *tert*-butylamine was added and the reaction mixture was refluxed for another day. The colour changed to violet-blue. Then the solvent was evaporated under reduced pressure. The residue was solved in CH$_2$Cl$_2$ and washed against 3 M HCl, H$_2$O and saturated Na$_2$CO$_3$ solution. Afterwards the solvent was evaporated and the residue purified by column chromatography on silica gel (CH$_2$Cl$_2$/EtOAc 5:1) to afford a mixture of mono- and disubstituted product (HPLC). Further purification by reversed phase column chromatography on silica gel (100 C$_{18}$, fully endcapped, CH$_3$CN) provided (^{t}BuN)$_2$-NDI cyclophane (**17**) as a blue solid (1.77 mg, 5 %).

HPLC-ESI-MS (Reprosil 100 C18, 125x3 mm, pure CH$_3$CN, flow 0.2 ml/min, pressure 30-31 bar, DAD (λ_{det} = 280, 345, 365, 570 and 615 nm, T = 25 °C)): Cl-^{t}BuN-NDI cyclophane R$_t$ = 10.5 min; m/z 973 ([M+H$_2$O]$^+$), 977 ([M+Na]$^+$), 993 ([M+K]$^+$); (^{t}BuN)$_2$-NDI cyclophane R$_t$ = 15.7 min; m/z 992 ([M]$^+$), 1014 ([M+Na]$^+$), 1030 ([M+K]$^+$).

1(1,4,5,8)-2,6-Dipiperidinylnaphthalenetetracarboxylic acid diimide-5(1,4,5,8)-naphthalene-tetracarboxylic acid diimide-3,7-di(1,3)-5-*tert*-butyl-benzenacycloocta-nodan (18)[99]

To a stirred suspension of asymmetric Cl_2-NDI cyclophane **11** (38.7 mg, 0.042 mmol, 1 eq.) in 20 ml anhydrous CH_3CN, 166 mg K_2CO_3 and an excess of piperidine (0.5 ml, 5.06 mmol, 120 eq.) were added. This reaction mixture was stirred at 70 °C under an argon atmosphere for one day. The colour changed immediately to red and over night to blue. The solvent was evaporated under reduced pressure and the residue solved in CH_2Cl_2 and extracted once with H_2O. Purification by column chromatography on silica gel (CH_2Cl_2/EtOAc 25:1) provided asymmetric $((CH_2)_5N)_2$-NDI cyclophane **18** as a blue solid (30.3 mg, 71 %).

TLC (SiO_2; CH_2Cl_2/EtOAc 10:1): R_f=0.87.

UV/Vis (CH_2Cl_2): λ_{max} (ϵ)=310 (30 879), 359 (27 385), 377 (23 294), 615 (11 104 mol^{-1} dm^3 cm^{-1}).

^{1}H-NMR (400 MHz, $CDCl_3$): δ=8.48, 8.40 (4H, A_2B_2 spinsystem higher order, 2', 3', 6', 7'), 8.15 (s, 2H, 3, 7), 7.42, 7.36 (br s, 4H, 2'', 6''), 6.85 (br s, 2H, 4''), 5.36, 5.34, 5.27, 5.22 (d, 8H, $^2J_{HH}$=14.4, 14.2, 14.4, 14.2 Hz, 9'', 10''), 3.19 (m, 4H, piperidine CH_2), 3.14 (m, 4H, piperidine CH_2), 1.78, 1.71 (m, 12H, piperidine CH_2).

^{13}C-NMR (100 MHz, $CDCl_3$): δ=162.36, 162.07 (11'', 12''), 162.02 (11), 160.97 (12), 151.54 (1''), 151.27 (2, 6), 137.90, 136.62 (3'', 5''), 130.44, 130.39 (2', 3', 6', 7'), 125.97, 125.93 (2'', 6''), 125.80, 125.07, 124.82, 124.72, 124.34 (4, 8, 9, 10, 1', 4', 5', 8', 9', 10'), 123.32 (1, 5), 121.11 (4''), 108.30 (3, 7), 53.6 (piperidine CH_2), 43.57 (10''), 43.50 (9''), 34.70 (7''), 31.38 (8''), 26.2, 23.9 (piperidine CH_2).

HPLC-ESI-MS (Reprosil 100 C18, 125x3 mm, pure CH_3CN, flow 0.2 ml/min, pressure 30-31 bar, DAD (λ_{det} = 280, 345, 365, 570 and 615 nm, T = 25 °C)): R_t = 14.3 min; m/z 1016 ([M]$^+$), 1038 ([M+Na]$^+$).

HPLC (CHIRALPAK IA, 4.6x250 mm, 50:50 CH_3CN:EtOH, flow 0.3 ml/min, pressure 13-14 bar, DAD (λ_{det} = 310, 358, 375, 560 and 607 nm, T = 25 °C)): R_t = 17.6, 18.8 min.

MALDI-TOF-MS: "1016" ([M]$^+$).

1,5(1,4,5,8)-2,6-Dichloronaphthalenetetracarboxylic acid diimide-3,7-di(1,3)-5-*tert*-butyl-benzena cycloocta-nodan (19)
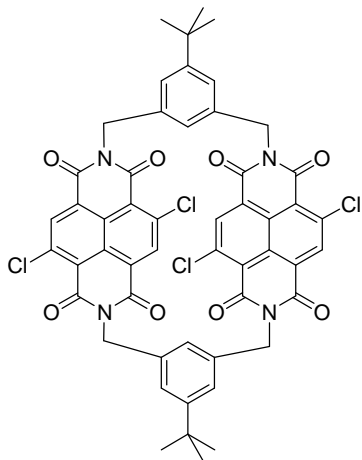
2,6-Dichloro-1,4,5,8-naphthalenetetracarboxylic acid dianhydride (**3**) (499 mg, 1.48 mmol, 1 eq.) was solved in 300 ml acetic acid at 120 °C. 1,3-bis(aminomethyl)-5-*tert*-butylbenzene (**2**) (334 mg, 1.74 mmol, 1.2 eq.) solved in 80 ml acetic acid was dropped into this yellow solution over 1 h. This reaction mixture was further refluxed for 2 days. Then it was cooled to room temperature and the solvent evaporated under reduced pressure. The residue was suspended in dichloromethane and filtered in order to remove the insoluble parts. Further purification of the filtrate by column chromatography on silica gel (CH$_2$Cl$_2$/EtOAc 10:1) provided racemic Cl$_4$-NDI cyclophane **19** as a white solid (38.9 mg, 2.7 %).

TLC (SiO$_2$; CH$_2$Cl$_2$/EtOAc 10:1): R_f=0.88.

UV/Vis (CH$_3$CN from HPLC run): λ_{max}=249, 358, 380, 400.

^{1}H-NMR (difficult to measure due to solubility reasons, 400 MHz, CDCl$_3$): δ=8.70 (br, 4H, naphthalene), 7.47 (br, 4H, Phe), 7.30 (br, "2H", Phe), 5.36 (br, 8H, CH$_2$), 1.35 (br, "18H", C(CH$_3$)$_3$).
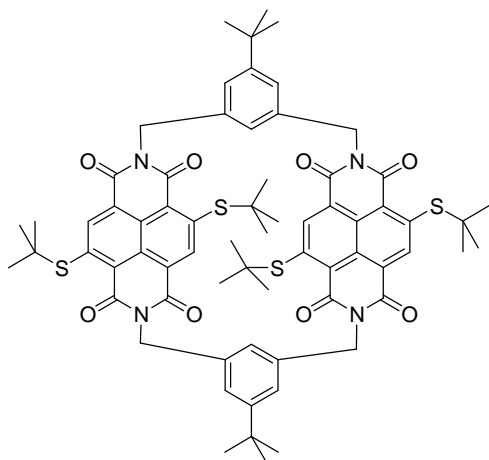
HPLC (Reprosil 100 C18, 125x3 mm, pure CH$_3$CN, flow 0.2 ml/min, pressure 30-31 bar, DAD (λ_{det} = 200, 235, 358, 380 and 400 nm, T = 25 °C)): R_t = 8.4 min.

HPLC (CHIRALPAK IA, 4.6x250 mm, 50:50 CH$_3$CN:EtOH, flow 0.4 ml/min, pressure 18-19 bar, DAD (λ_{det} = 200, 235, 358, 380 and 400 nm, T = 25 °C)): R_t = 18.2, 20.0 min.

FAB-MS (NBA): 987 ([M]$^+$), 931 ([C$_{48}$H$_{28}$Cl$_4$N$_4$O$_8$]$^+$).

MALDI-TOF-MS: 989 ([M]$^+$).

1,5(1,4,5,8)-2,6-Di(*tert*-butylsulfanyl)naphthalenetetracarboxylic acid diimide-3,7-di(1,3)-5-*tert*-butyl-benzenacycloocta-nodan (20)

48 mg K_2CO_3 and an excess of 2-methyl-propane-2-thiol (0.5 ml, 4.44 mmol, 450 eq) were added to a stirred suspension of racemic Cl_4-NDI cyclophane **19** (9.86 mg, 0.01 mmol, 1 eq.) in 5 ml HPLC CH_3CN. This reaction mixture was stirred at room temperature under an argon atmosphere for 2 days. Then the solvent was evaporated under reduced pressure and the residue solved in dichloromethane and washed once against H_2O. Further purification by reversed phase column chromatography on silica gel (100 C_{18}, fully endcapped, CH_3CN to CH_2Cl_2) provided S_4-NDI cyclophane (**20**) as a red solid (5.04 mg, 42 %).

TLC (SiO_2; CH_2Cl_2): R_f=0.46.

UV/Vis (HPLC run): λ_{max}=267, 297, 356, 372, 489, 520.

¹H-NMR (500 MHz, $CDCl_3$): δ=8.90 (s, 4H, naphthalene), 7.38 (s, 4H, phe), 6.87 (s, 2H, phe), 5.37 (d, 4H, $^2J_{HH}$=14.3 Hz, CH_2), 5.29 (d, 4H, $^2J_{HH}$=14.3 Hz, CH_2), 1.65 (s, 36H, $SC(CH_3)_3$), 1.37 (s, 18H, $C(CH_3)_3$).

¹³C-NMR (150 MHz, $CDCl_3$): δ=162.37, 161.82, 151.19, 148.00, 137.08, 131.82, 124.88, 124.65, 122.44, 121.69, 121.11, 48.62, 43.79, 34.73, 31.71, 31.42.

HPLC-ESI-MS (Reprosil 100 C18, 125x3 mm, pure CH_3CN, flow 0.2 ml/min, pressure 30-31 bar, DAD (λ_{det} = 297, 356, 371, 490 and 521 nm, T = 25 °C)): R_t = 16.1 min; m/z 1239 ([M+K]$^+$), 1223 ([M+Na]$^+$).

HPLC (CHIRALPAK IA, 4.6x250 mm, 50:50 CH_3CN:EtOH, flow 0.4 ml/min, pressure 18-19 bar, DAD (λ_{det} = 298, 350, 370, 490 and 520 nm, T = 25 °C)): R_t = 11.9, 12.3, 12.8 min.

5.2.2. Synthesis of NDI crown ethers

**_N,N'_-Diphenyl-2,6-dichloro-1,4,5,8-naphthalenetetracarboxylic acid diimide (21)**
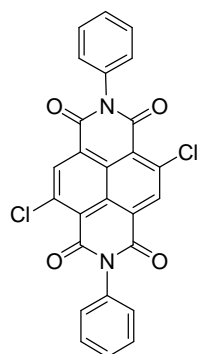
2,6-Dichloro-1,4,5,8-naphthalenetetracarboxylic acid dianhydride (980 mg, 2.91 mmol, 1 eq.) was suspended in 40 ml acetic acid. This suspension was heated to reflux and then one added over the refluxing condenser aniline (1.3 ml, 14.25 mmol, 4.9 eq.) all at once. The colour changed immediately from yellow to dark red. The reaction mixture was refluxed for another 20 min and then cooled to room temperature. The solvent was evaporated under reduced pressure and the residue was suspended in acetic acid. After centrifugation the solvent was decanted off. This step was repeated two times. Then dichloromethane was added to the tube and after centrifugation the solvent was decanted off. This step was repeated three times until the red colour was nearly disappeared and _N,N'_-diphenyl-2,6-dichloro-1,4,5,8-naphthalenetetracarboxylic acid diimide (**21**) was isolated as a violet solid (901 mg, 64 %).

¹H-NMR and **¹³C-NMR** were not possible to measure due to solubility problems.

EI-MS (70 eV): 543 (mono aniline substituted product), 486 ([M]⁺).

N,N'-Diphenyl-2,6-di(2'-aminomethyl-15'-crown-5')-1,4,5,8-naphthalenetetracarboxylic acid diimide (22)

2-Aminomethyl-15-crown-5 (500 mg, 2 mmol, 4.7 eq.) was added to a suspension of *N,N'*-di-phenyl-2,6-dichloro-1,4,5,8-naphthalenetetracarboxylic acid diimide (**21**) (210 mg, 0.43 mmol, 1 eq.) in 20 ml toluene and 2 ml Et$_3$N. This reaction mixture was refluxed for 3 days. The solvent was evaporated and the residue was purified by column chromatography on silica gel (CH$_2$Cl$_2$/Hex/Et$_3$N 10:3:0.5). The blue solid was solved in CH$_2$Cl$_2$ and washed once with 1 M HCl and once with saturated NaHCO$_3$ solution. After evaporation of the solvent *N,N'*-diphenyl-2,6-di(2'-aminomethyl-15'-crown-5')-1,4,5,8-naphthalenetetracarboxylic acid diimide (**22**) was isolated as a blue solid (83.3 mg, 21 %). In addition a side product bearing three 15-crown-5 units could be isolated (30.33 mg, 7 %).
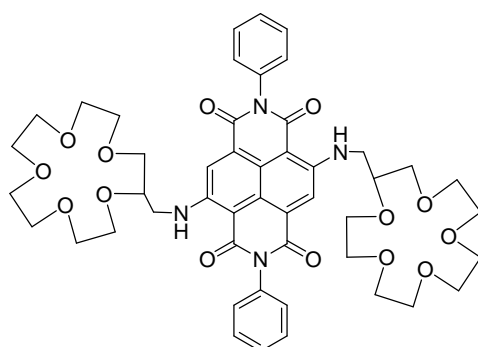
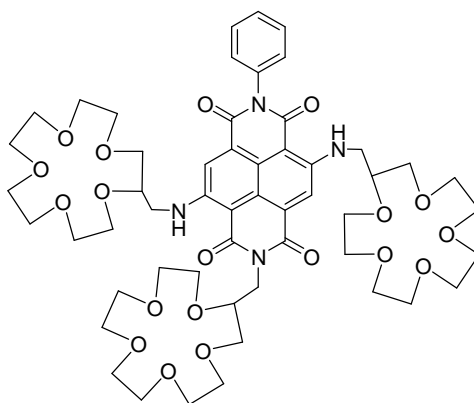**TLC** (SiO$_2$; CH$_2$Cl$_2$/Tol/Et$_3$N 5:5:0.5): R_f=0.27.

UV/Vis (MeOH): λ_{max} (ε)=281 (22 469), 345 (9 899), 361 (10 609), 610 (11 704 mol^{-1} dm^3 cm^{-1}).

^{1}H-NMR (400 MHz, CDCl$_3$): δ=9.48 (t, 2H, $^3J_{HH}$=5.7 Hz, NH), 8.33 (s, 2H, naphthalene), 7.58 (t, 4H, $^3J_{HH}$=7.4 Hz, Phe), 7.51 (t, 2H, $^3J_{HH}$=7.4 Hz, Phe), 7.31 (d, 4H, $^3J_{HH}$=7.4 Hz, Phe), 3.87-3.62 (m, 42H, crown ether).

^{13}C-NMR (100 MHz, CDCl$_3$): δ=166.32, 163.25, 149.80, 135.40, 129.42, 128.75, 128.66, 126.22, 121.77, 119.25, 102.27, 78.28, 71.32, 71.02, 70.97, 70.73, 70.57, 70.55, 70.47, 70.38, 44.55.

HPLC-ESI-MS (Reprosil 100 C18, 125x3 mm, CH$_3$CN:H$_2$O/TFA(0.1%)/CH$_3$CN(1%) 50:50, flow 0.4 ml/min, pressure 140 bar, DAD (λ_{det} = 220, 280, 340, 360 and 600 nm, T = 25 °C)): R$_t$ = 16.3 min; m/z 913 ([M]$^+$), 935 ([M+Na]$^+$).

FAB-MS (NBA): 913 ([M]$^+$), 693 ([C$_{38}$H$_{37}$N$_4$O$_9$]$^+$).

TLC (SiO$_2$; CH$_2$Cl$_2$/Tol/Et$_3$N 5:5:0.5): R_f=0.08.

UV/Vis (HPLC run): λ_{max}=282, 346, 364, 612.

^{1}H-NMR (400 MHz, CDCl$_3$): δ=9.61 (t, 1H, $^3J_{HH}$=5.4 Hz, NH), 9.45 (t, 1H, $^3J_{HH}$=5.4 Hz, NH), 8.28, 8.26 (s, 2H, naphthalene), 7.57 (t, 2H, $^3J_{HH}$=7.4 Hz, Phe), 7.50 (t, 1H, $^3J_{HH}$=7.4 Hz, Phe), 7.32 (d, 2H, $^3J_{HH}$=7.1 Hz, Phe), 4.34-3.64 (m, 63H, crown ether).

HPLC-ESI-MS (Reprosil 100 C18, 125x3 mm, CH$_3$CN:H$_2$O/TFA(0.1%)/CH$_3$CN(1%) 50:50, flow 0.4 ml/min, pressure 140 bar, DAD (λ_{det} = 210, 250, 300, 400 and 600 nm, T = 25 °C)): R_t = 6.7 min; m/z 1069 ([M]$^+$), 1091 ([M+Na]$^+$).

FAB-MS (NBA): 1069 ([M]$^+$), 894 ([C$_{43}$H$_{53}$N$_4$O$_{14}$]$^+$).

**Complexation studies of NDI crown ether 22 with BaCl$_2$O$_8$ and KClO$_4$:**

For Job plot analysis stock solutions of NDI crown ether **22**, BaCl$_2$O$_8$ and KClO$_4$ were made (1·10^{-4}M). Then 14 different solutions with different concentrations were measured by UV&Vis (table 3) and Job plot analysis showed maxima at 0.5 for Ba^{2+} and 0.6 for K$^+$.

| NDI crown ether **22**	BaCl$_2$O$_8$ or KClO$_4$
2.9 ml (9.666·10^{-5} M)	0.1 ml (1·10^{-5} M)
....	…….
0.3 ml (1·10^{-5} M)	2.9 ml (9.666·10^{-5} M)

As discussed in section 3.3.5.1 a 1:1 complex is formed according to ESI-MS measurements, whereas the shift for K$^+$ is explained by a weaker binding constant and competition with sodium ions from the glass ware.

As discussed in section 3.3.5.1 the binding constant according to a system with three complex constants was analysed. The Stern-Volmer plot showed not a linear behaviour as expected for a 1:1 complex formation. The observed curve can come from a combined dynamic and static quenching process.[21] Thus, ploting $(F_0/F-1)/[Q]$ against $[Q]$ results in a linear function (*figure 109*) from which $K_{dynamic}$ and K_{static} can be determined by solving the quadratic equation: $K_S^2 - K_S I + S = 0$, whereas I is the intercept and S the slope. For our case $I = 4 \cdot 10^6$ and $S = 3 \cdot 10^{13}$ this quadratic equation is not possible to solve. We propose that for our system only a static quenching process is responsible, but the system is complicated because we do not know which complex already quenches the fluorescence.
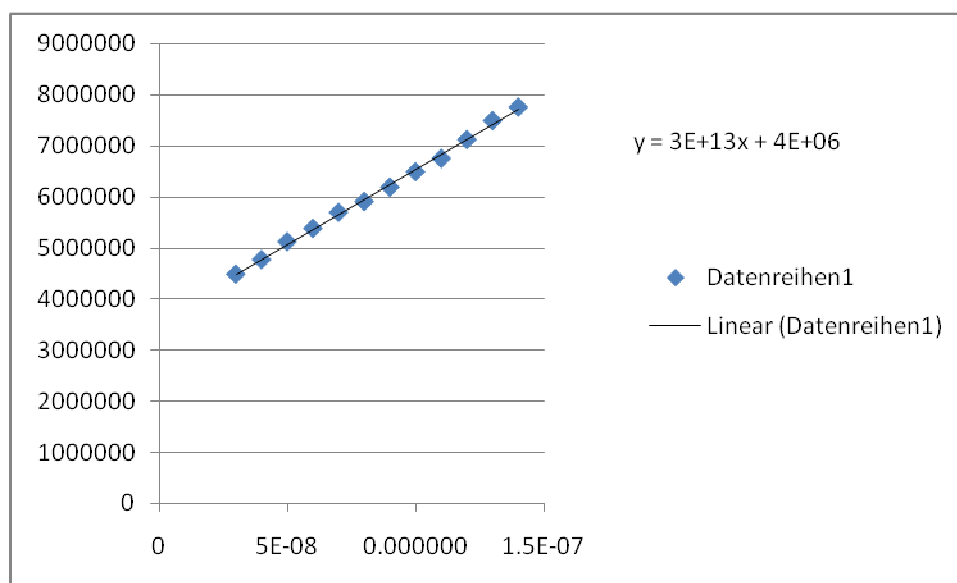
Figure 109: Linear function for a combined dynamic and static quenching process, which is in our case not possible to solve.

1,5-Dimethoxy-naphthalene (24)[84]
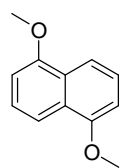
1,5-Dihydroxy-naphthalene (1.57 g, 9.8 mmol, 1 eq.), 1.63 g K_2CO_3 and 300 ml dry acetone were added into a two necked round flask. Then iodomethane (2 ml, 21.7 mmol, 2 eq.) was added and the reaction mixture was refluxed for 1 day. Then the solvent was evaporated under reduced pressure and the residue purified by column chromatography on silica gel (CH_2Cl_2) to afford 1,5-dimethoxy-naphthalene (24) (1.01 g, 55 %).

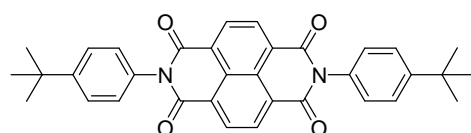**UV/Vis** ($CHCl_3$): λ_{max}=231, 296, 312, 330.

^{1}H-NMR (400 MHz, $CDCl_3$): δ=7.86 (d, 2H, $^3J_{HH}$=8.0 Hz), 7.40 (t, 2H, $^3J_{HH}$=8.0 Hz), 6.86 (d, 2H, $^3J_{HH}$=7.7 Hz), 4.00 (s, 6H, CH_3).

EI-MS (70 eV): 188 ([M]$^+$), 173 ([$C_{11}H_9O_2$]$^+$).

EA calc. for $C_{12}H_{12}O_2$ (188.22): C, 76.57; H, 6.43; found: C, 75.54; H, 6.51.

mp: 180-181 °C.

N, N'-Di-(4'-*tert*-butylphenyl)-1,4,5,8-naphthalenetetracarboxylic acid diimide (25)[71,84]

1,4,5,8-Naphthalenetetracarboxylic acid dianhydride (3) (118 mg, 0.44 mmol), 4-*tert*-butylaniline (0.18 ml, 1.12 mmol) and 5 ml acetic acid were refluxed for 24 h. After cooling to room temperature the reaction mixture was quenched with water, extracted with CH_2Cl_2 and dried over Na_2SO_4. The solvent was evaporated and the residue was purified by column chromatography on silica gel (CH_2Cl_2) to provide the linear NDI model compound 25 as a yellow solid (86 mg, 37 %).

STM investigations: RT-STM images of the molecule on Au (111). The conditions were: coverage $\Theta \approx 0.5$ monolayers (ML), bias voltage $V_B = 2431$ mV and tunnelling current $I_T = 186$ pA.

TLC (SiO_2; CH_2Cl_2): R_f=0.4.

UV/Vis (CH_3CN): λ_{max} (ε)=235 (45 732), 341 (17 066), 357 (27 428), 377 (31 016 mol^{-1} dm^3 cm^{-1}).

IR (KBr): 3500*br*, 3069*m*, 2956*s*, 2856*w*, 1706*s*, 1672*s*, 1578*s*, 1511*s*, 1444*s*, 1350*s*, 1250*s*, 1194*s*, 1111*m*, 978*s*, 839*s*, 761*s*, 711*m*, 556*s*.

^{1}H-NMR (400 MHz, $CDCl_3$): δ=8.84 (s, 4H, naphthalene), 7.60 (4H, A_2B_2 spinsystem higher order, Phe), 7.27 (4H, A_2B_2 spinsystem higher order, Phe), 1.40 (s, 18H, 6CH_3).

^{13}C-NMR (100 MHz, $CDCl_3$): δ=163.0, 152.0, 131.7, 131.4, 127.7, 127.1, 127.0, 126.6, 34.8, 31.3.

ESI-MS (MeOH): *Positive* ion mode: 531 ([M]$^+$), 553 ([M+Na]$^+$), 585 ([M+MeOH+Na]$^+$).

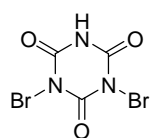**EI-MS** (70 eV): 530 ([M]$^+$), 515 ([$C_{33}H_{27}N_2O_4$]$^+$).

HPLC-ESI-MS (Reprosil 100 C18, 125x3 mm, pure CH_3CN, flow 0.2 ml/min, pressure 30-31 bar, DAD (λ_{det} = 191, 235, 340, 357 and 375 nm, T = 25 °C)): R_t = 4.5 min.

EA calc. for $C_{34}H_{30}N_2O_4$ (530.62): C, 76.96; H, 5.70; N, 5.28; found: C, 76.93; H, 5.74; N, 5.10.

mp: >349 °C.

5.2.3. Synthesis of linear NDI's
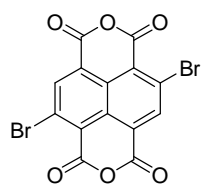
Dibromoisocyanuric acid (DBI)[116,117]

To a solution of cyanuric acid (12.9 g, 99.95 mmol, 1 eq.) and LiOH·H$_2$O (4.84 g, 115.35 mmol, 1.2 eq.) in 1 l of H$_2$O one added at 25 °C Br$_2$ (20 ml, 389.19 mmol, 3.9 eq.). This reaction mixture was stirred for 2 h and then cooled with an ice bath for 15 min. The precipitate was filtered off and washed with H$_2$O. After drying at the high vacuum dibromoisocyanuric acid (**DBI**) was isolated as a white solid (10.9 g, 38 %) and used without further purification.

EI-MS (70 eV): 362.7 ([C$_3$Br$_3$N$_3$O$_3$]$^+$), 284.8 ([C$_3$HBr$_2$N$_3$O$_3$]$^+$), 206.9 ([C$_3$H$_2$BrN$_3$O$_3$]$^+$), 229.0 ([C$_3$H$_3$N$_3$O$_3$]$^+$).

EA calc. for C$_3$HBr$_2$N$_3$O$_3$ (286.87): C, 12.56; H, 0.35; N, 14.65; found: C, 15.30; H, 0.89; N, 18.00.

### 2,6-Dibromo-1,4,5,8-naphthalenetetracarboxylic acid dianhydride (26)

A solution of 1,4,5,8-naphthalenetetracarboxylic acid dianhydride (1 g, 3.73 mmol, 1 eq.) in 32 ml H$_2$SO$_4$ was slowly added to a solution of dibromoisocyanuric acid (**DBI**) (2.1 g, 7.32 mmol, 2 eq.) in 22 ml H$_2$SO$_4$ and the resulting mixture was stirred at 140 °C for 20 h. The reaction mixture was then poured on ice and the precipitate was filtered off and dried at the high vacuum. The yellow solid was recrystallized in H$_2$SO$_4$ and 2,6-dibromo-1,4,5,8-naphthalenetetracarboxylic acid dianhydride (**26**) was isolated as a pale yellow solid (756 mg, 48 %).

^{1}H-NMR and **^{13}C-NMR** were not possible to measure due to solubility problems.

EI-MS (NBA): 423 ([M]$^+$), 382 ([C$_{13}$H$_4$Br$_2$O$_4$]$^+$), 345 ([C$_{14}$H$_3$BrO$_6$]$^+$), 229.0 ([C$_3$H$_3$N$_3$O$_3$]$^+$).

N-Benzyl-benzene-1,4-diamine (27b)
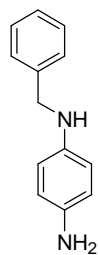
p-Phenylenediamine (3.17 g, 29.3 mmol, 1 eq.) was solved in 70 ml CH_2Cl_2. To this solution benzylbromide (1 ml, 8.4 mmol, 0.3 eq.) was added at once. The reaction mixture was further stirred at room temperature for 20 min. Then 1 M HCl was added until pH≈1 and washed once with CH_2Cl_2. Further 5 M NaOH solution was added until pH≈10 and extracted three times with CH_2Cl_2. The combined organic phases were dried over Na_2SO_4 and the solvent was evaporated under reduced pressure. The slightly brown residue was purified by column chromatography on silica gel (EtOAc) to provide *N*-benzyl-benzene-1,4-diamine (**27b**) as yellow oil (0.35 g, 21 %).

TLC (SiO$_2$; EtOAc): R_f=0.5.

^{1}H-NMR (400 MHz, CDCl$_3$): δ=7.34-7.27 (m, 4H, Bz), 7.25-7.20 (m, 1H, Bz), 6.55-6.52 (2H, A$_2$B$_2$ spinsystem higher order, Phe), 6.49-6.47 (2H, A$_2$B$_2$ spinsystem higher order, Phe), 4.20 (s, 2H, CH$_2$), 3.34 (br s, 3H, NH, NH$_2$).

^{13}C-NMR (100 MHz, CDCl$_3$): δ=141.2, 139.8, 137.7, 128.3, 127.4, 126.9, 116.7, 114.3, 49.2.

ESI-MS (MeOH): *Positive* ion mode: 199 ([M]$^+$).

### *N*-(4-Amino-phenyl)benzamide (27c)[127]
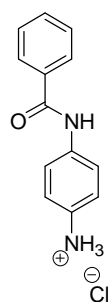
Sodium dodecyl sulfate (42.02 mg, 0.146 mmol, 0.02 eq.) was added to a solution of *p*-phenylenediamine (1.04 g, 9.62 mmol, 1 eq.) in 25 ml H$_2$O. To this mixture a solution of benzoic anhydride (2.12 g, 9.34 mmol, 1 eq.) in 20 ml dry CH$_3$CN was added all at once. The colour changed immediately to grey and a white solid precipitated. The reaction mixture was stirred at room temperature for further 5 min. The solvent was evaporated under reduced pressure and the residue purified by column chromatography on basic alox (EtOAc) to provide a yellow oil. It was solved in EtOH and acidified with 1 M HCl until a solid precipitated. This white solid was filtered and dried to yield *N*-(4-Amino-phenyl)benzamide (**27c**) (1.42 g, 59 %).

^{1}H-NMR (400 MHz, DMSO): δ=10.44 (s, 1H, NH), 10.04 (br s, 3H, NH$_3^+$), 7.98-7.96 (2H, spinsystem higher order), 7.89-7.86 (2H, spinsystem higher order), 7.62-7.58 (1H, spinsystem higher order), 7.56-7.52 (2H, spinsystem higher order), 7.35-7.33 (2H, spinsystem higher order).

^{13}C-NMR (100 MHz, DMSO): δ=165.6, 138.6, 134.5, 131.6, 128.3, 127.6, 127.2, 123.2, 121.2.

ESI-MS (MeOH): *Positive* ion mode: 447 ([2xM-HCl+Na]$^+$), 235 ([M-HCl+Na]$^+$) 213 ([M-HCl]$^+$).

N-(4'-*tert*-butylphenyl)-*N*'-(*N*-Boc-*p*-phenyl)-2,6-dichloro-1,4,5,8-naphthalenetetracarboxylic acid diimide (28)
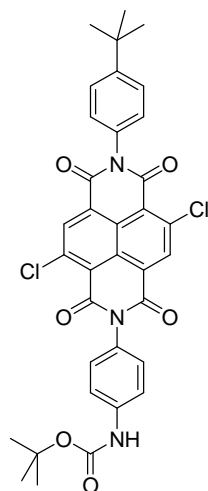
a). 2,6-Dichloro-1,4,5,8-naphthalenetetracarboxylic acid dianhydride (69.68 mg, 0.21 mmol, 1 eq.) was suspended in 90 ml *i*-PrOH and 1 ml Et$_3$N. *N*-Boc-*p*-phenylenediamine (42.84 mg, 0.21 mmol, 1 eq.) and 4-*tert*-butylaniline (0.03 ml, 0.19 mmol, 1 eq.) were added and the reaction mixture was refluxed under an argon atmosphere for 21 h. After 5 min the solution turned black. The solvent was evaporated and the residue purified by column chromatography on silica gel (CH$_2$Cl$_2$/MeOH 5:1 to 5:2). Unfortunately no product formation could be detected by NMR or ESI-MS.

b). A solution of *N*-Boc-*p*-phenylenediamine (119.4 mg, 0.57 mmol, 1 eq.) and 4-*tert*-butylaniline (0.1 ml, 0.62 mmol, 1 eq.) in 30 ml dry DMF and 1 ml Et$_3$N was slowly dropped into an orange solution of 2,6-Dichloro-1,4,5,8-naphthalenetetracarboxylic acid dianhydride (193.1 mg, 0.57 mmol, 1 eq.) in 40 ml dry DMF at room temperature over 3 h. This reaction mixture was further heated at 40 °C for 17 h. Then the solvent was removed at the high vacuum at 40 °C and a black solid was isolated. Unfortunately no product formation could be detected by NMR or ESI-MS.

c). 2,6-Dichloro-1,4,5,8-naphthalenetetracarboxylic acid dianhydride (69.91 mg, 0.21 mmol, 1 eq.) was suspended in 90 ml acetic acid. *N*-Boc-*p*-phenylenediamine (49.79 mg, 0.24 mmol, 1 eq.) and 4-*tert*-butylaniline (0.04 ml, 0.25 mmol, 1 eq.) were added and the reaction mixture was refluxed for 18 h. After 5 min the solution turned black. To the cooled reaction mixture 100 ml H$_2$O was added and further extracted with dichloromethane. The combined organic phases were once washed against saturated Na$_2$CO$_3$. Then the solvent was evaporated under reduced pressure and a violet solid was isolated. Without further purification the crude solid was solved in 20 ml CH$_2$Cl$_2$. 46.16 mg K$_2$CO$_3$ and an excess hexane-1-thiol (0.5 ml, 3.55 mmol, 17 eq.) were added. This reaction mixture was refluxed under an argon atmosphere for 3 h. The solvent was removed and the residue purified by column chromatography on silica gel (CH$_2$Cl$_2$). An orange solid was isolated (15.37 mg, 10 %) which turned to be *N,N'*-di-(4'-*tert*-butylphenyl)-2,6-di-(*n*-hexylsulfanyl)-1,4,5,8-naphthalenetetracarboxylic acid diimide (**30a**).

N-(4'-*tert*-butylphenyl)-*N'*-(*N*-Boc-*p*-phenyl)-2,6-di-(*n*-hexylsulfanyl)-1,4,5,8-naphthalene-tetracarboxylic acid diimide (29a)
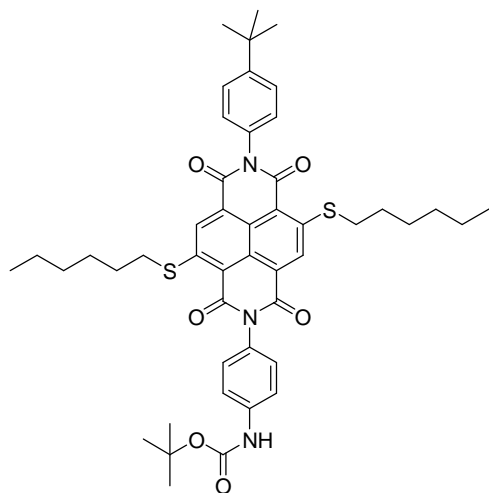
S$_2$ monoimide (**35**) (7.29 mg, 0.012 mmol, 1 eq.) and *N*-Boc-*p*-phenylenediamine (5.71 mg, 0.027 mmol, 2.3 eq.) were suspended in 20 ml *i*-PrOH and 0.1 ml Et$_3$N. The red reaction mixture was refluxed for one day. Then the cooled solution was washed against saturated Na$_2$CO$_3$ solution and the solvent was removed under reduced pressure. The residue was purified by column chromatography on silica gel (CH$_2$Cl$_2$ to CH$_2$Cl$_2$/MeOH 10:2) and 7.77 mg of a red solid could be isolated. The isolated red solid still contains S$_2$ monoimide **29a** (R$_t$ = 9.2 min) and two other side products (R$_t$ = 19.0, 21.7 min).

HPLC-ESI-MS (LiChrospher 100 C18, 250x4 mm, pure CH$_3$CN, flow 0.2 ml/min, DAD (λ_{det} = 263, 295, 367, 487 and 522 nm, T = 25 °C)): R$_t$ = 10.8 min, m/z 1682 ([2xM+K]$^+$), 1662 ([2xM+Na]$^+$), 1553 ([2xC$_{43}$H$_{47}$N$_3$O$_6$S$_2$+Na]$^+$), 1532 ([2xC$_{43}$H$_{47}$N$_3$O$_6$S$_2$]$^+$).

N,N'-Di-(4'-*tert*-butylphenyl)-2,6-dichloro-1,4,5,8-naphthalenetetracarboxylic acid diimide (30a)
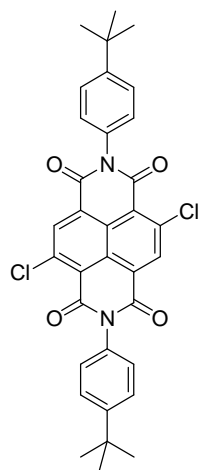
2,6-Dichloro-1,4,5,8-naphthalenetetracarboxylic acid dianhydride (**10**) (232.5 mg, 0.69 mmol, 1 eq.) was solved under reflux in 30 ml acetic acid. To this solution 4-*tert*-butylaniline (0.3 ml, 1.87 mmol, 2.7 eq.) was added at once and the orange solution turned immediately black. This reaction mixture was further refluxed for 15 min. After cooling to room temperature the grey precipitate was filtered off and washed with H$_2$O. Drying at the high vacuum provided *N,N'*-di-(4'-*tert*-butylphenyl)-2,6-dichloro-1,4,5,8-naphthalenetetracarboxylic acid diimide (**30a**) as a fine grey powder (134 mg, 33 %).

IR (KBr): 3063*s*, 2964*s*, 2871*w*, 1718*s*, 1676*s*, 1566*m*, 1511*m*, 1421*s*, 1358*w*, 1319*s*, 1222*s*, 913*m*, 824*m*, 759*m*, 716*m*, 564*m*.

^{1}H-NMR (400 MHz, CDCl$_3$): δ=8.85 (s, 2H, naphthalene), 7.60, 7.25 (8H, A$_2$B$_2$ spinsystem higher order, Phe), 1.40 (s, 18H, C(CH$_3$)$_3$).

^{13}C-NMR not enough soluble.

FAB-MS (NBA): "599" ([M]$^+$).

EA calc. for C$_{34}$H$_{28}$Cl$_2$N$_2$O$_4$ (599.51): C, 68.12; H, 4.71; N, 4.67; found: C, 66.51; H, 4.45; N, 4.30.

N,N'-Di-(4'-*tert*-butylphenyl)-2,6-dibromo-1,4,5,8-naphthalenetetracarboxylic acid diimide (30b)
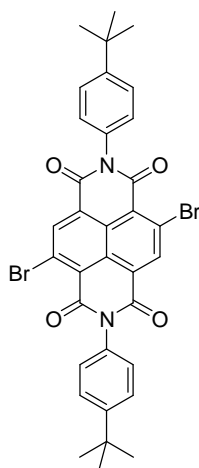
2,6-Dibromo-1,4,5,8-naphthalenetetracarboxylic acid dianhydride (**26**) (716 mg, 1.68 mmol, 1 eq.) was solved under reflux in 40 ml acetic acid. To this solution 4-*tert*-butylaniline (0.7 ml, 4.36 mmol, 2.6 eq.) was added at once and the yellow solution turned immediately red. This reaction mixture was further refluxed for 10 min. After cooling to room temperature the violet precipitate was filtered off and washed with H_2O. Further purification by column chromatography on silica (CH_2Cl_2) provided *N,N'*-di-(4'-*tert*-butylphenyl)-2,6-dibromo-1,4,5,8-naphthalene-tetracarboxylic acid diimide (**30b**) as a yellow solid (82.7 mg, 7 %). The mono substituted by product could also be isolated in 10.38 mg as a violet solid. Another fraction was isolated after column chromatography, but it was not clear by ^{1}H-NMR what the compound could be (purple solid 52.2 mg).
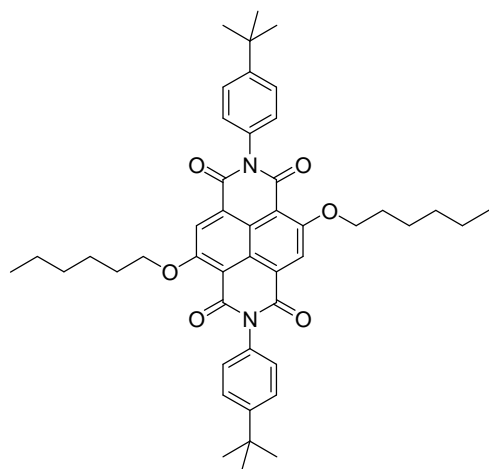
^{1}H-NMR (400 MHz, CDCl$_3$): δ=9.06 (s, 2H, naphthalene), 7.60, 7.25 (8H, A_2B_2 spinsystem higher order, Phe), 1.40 (s, 18H, C(CH$_3$)$_3$).

^{13}C-NMR not enough soluble.

EI-MS (300 °C): 686 ([M]$^+$), 671 ([C$_{33}$H$_{25}$Br$_2$N$_2$O$_4$]$^+$), 593 ([C$_{33}$H$_{25}$BrN$_2$O$_4$]$^+$).

FAB-MS (NBA): 686 ([M]$^+$).

EA calc. for C$_{34}$H$_{28}$Br$_2$N$_2$O$_4$ (688.41): C, 59.32; H, 4.10; N, 4.07; found: C, 58.77; H, 4.09; N, 3.78.

N,N'-Di-(4'-*tert*-butylphenyl)-2,6-di-(*n*-hexyloxy)-1,4,5,8-naphthalenetetracarboxylic acid diimide (31)

a). 1.92 g Na was solved in 70 ml hexane-1-ol. 35 ml of this solution was added to *N,N'*-di-(4'-*tert*-butylphenyl)-2,6-dichloro-1,4,5,8-naphthalenetetracarboxylic acid diimide (**30a**) (230.6 mg, 0.39 mmol, 1 eq.). This reaction mixture was further stirred at room temperature for 2 days under an argon atmosphere. Then the mixture was quenched with 150 ml 1 M HCl and extracted with CH_2Cl_2. The combined organic phases were washed against saturated Na_2CO_3 and dried over Na_2SO_4 solution. The solvent was evaporated under reduced pressure and the yellow residue was purified by column chromatography on silica (CH_2Cl_2). Unfortunately no product formation was observed by NMR or ESI-MS.
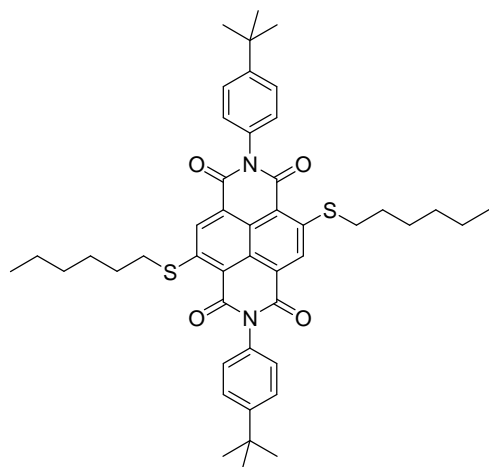
b). 1.4 g Na was solved in 25 ml hexane-1-ol. 15 ml of this solution was added to a suspension of *N,N'*-di-(4'-*tert*-butylphenyl)-2,6-dichloro-1,4,5,8-naphthalenetetracarboxylic acid diimide (**30a**) (124 mg, 0.21 mmol, 1 eq.) in 20 ml dry toluene. This reaction mixture was further stirred at room temperature for 3 h under an argon atmosphere (yellow solution). Then 70 ml acetic acid was added and stirred at 120 °C for 0.5 h. After cooling to room temperature the mixture was diluted with CH_2Cl_2 and washed with H_2O and saturated Na_2CO_3 solution. After drying over Na_2SO_4 the solvent was evaporated. The yellow residue was further purified by column chromatography on silica (CH_2Cl_2). Product formation (**31**) was only detected by TLC (green fluorescent compound) and Maldi-MS.

TLC (SiO_2; CH_2Cl_2): R_f=0.5.
MALDI-TOF-MS: 733 ([M]$^+$)

N,N'-Di-(4'-*tert*-butylphenyl)-2,6-di-(*n*-hexylsulfanyl)-1,4,5,8-naphthalenetetracarboxylic acid diimide (34)

a). *N,N'*-Di-(4'-*tert*-butylphenyl)-2,6-dichloro-1,4,5,8-naphthalenetetracarboxylic acid diimide (**30a**) (94.7 mg, 0.16 mmol, 1 eq.) was solved in 8 ml dry DMF. To this solution one added 110 mg K_2CO_3 and hexane-1-thiol (0.1 ml, 0.71 mmol, 4.4 eq.). This reaction mixture was further stirred at 65 °C for 2 h under an argon atmosphere. Then the mixture was quenched with ice water and extracted with CH_2Cl_2. Further the solvent was evaporated under reduced pressure and the residue purified by column chromatography on silica gel (CH_2Cl_2/Hex 2:1). After evaporation of the solvent *N,N'*-di-(4'-*tert*-butylphenyl)-2,6-di-(*n*-hexylsulfanyl)-1,4,5,8-naphthalene tetracarboxylic acid diimide (**34**) was isolated as a orange solid (50.5 mg, 42 %).

b). *N,N'*-Di-(4'-*tert*-butylphenyl)-2,6-dibromo-1,4,5,8-naphthalenetetracarboxylic acid diimide (**30b**) (73.0 mg, 0.11 mmol, 1 eq.) and 143 mg K_2CO_3 were suspended in 18 ml CH_3CN. To this suspension an excess of hexane-1-thiol (5 ml, 35.5 mmol) was added and the reaction mixture stirred at room temperature for 3 days. After removal of the solvent, the orange residue was purified by column chromatography on silica gel (CH_2Cl_2). After evaporation of the solvent under reduced pressure *N,N'*-di-(4'-*tert*-butylphenyl)-2,6-di-(*n*-hexylsulfanyl)-1,4,5,8-naphthalenetetracarboxylic acid diimide (**34**) was isolated as a orange solid (65 mg, 80 %).

TLC (SiO_2; CH_2Cl_2/Hex 2:1): R_f=0.4.

UV/Vis ($CHCl_3$): λ_{max} (ε)=298 (55 036), 353 (13 257), 370 (16 036), 534 (20 813 mol^{-1} dm^3 cm^{-1}).

^{1}H-NMR (400 MHz, $CDCl_3$): δ=8.77 (s, 2H, naphthalene), 7.59, 7.27 (8H, A_2B_2 spinsystem higher order, Phe), 3.16 (t, 4H, $^3J_{HH}$=7.4 Hz, CH_2), 1.82 (quin, 4H, $^3J_{HH}$=7.5 Hz, CH_2), 1.52 (m, 4H, CH_2), 1.39 (s, 18H, $C(CH_3)_3$), 1.31 (m, 8H, CH_2), 0.89 (t, 6H, $^3J_{HH}$=7.0 Hz, CH_3).

^{13}C-NMR (100 MHz, $CDCl_3$): δ=163.6, 162.8, 151.9, 149.5, 131.8, 128.7, 127.9, 126.5, 125.5, 124.1, 119.4, 34.8, 32.3, 31.4, 30.9, 28.8, 27.9, 22.5, 14.0.

**HPLC-ESI-MS** (LiChrospher 100 C18, 250x4 mm, pure CH_3CN, flow 0.2 ml/min, DAD (λ_{det} = 263, 295, 367, 487 and 522 nm, T = 25 °C)): R_t = 15.5 min; m/z 804 ([M+CH_3CN]$^+$), 1546 ([2xM+H_2O]$^+$), 1549 ([2xM+Na]$^+$).

EI-MS (70 eV): 762 ([M]$^+$).

FAB-MS (NBA): "763" ([M]$^+$).

EA calc. for $C_{46}H_{54}N_2O_4S_2$ (763.06): C, 72.41; H, 7.13; N, 3.67; found: C, 71.50; H, 6.98; N, 3.43.

N-(4'-*tert*-butylphenyl)-2,6-di-(*n*-hexylsulfanyl)-1,8-naphthalenedicarboxylic acid imide-4,5-naphthalenedicarboxylic acid anhydride (35)
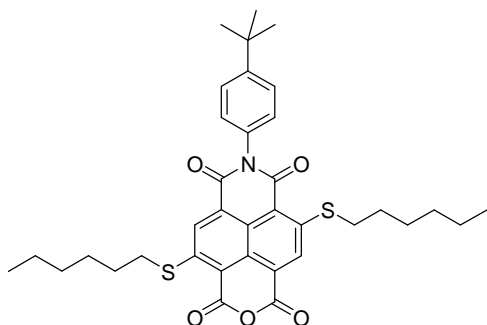
To a solution of *N,N'*-di-(4'-*tert*-butylphenyl)-2,6-di-(*n*-hexylsulfanyl)-1,4,5,8-naphthalenetetracarboxylic acid diimide (**34**) (21.9 mg, 0.03 mmol, 1 eq.) in 10 ml *tert*-butanol one added a KOH/*tert*-butanol solution (0.3 ml, 0.21 mmol, 7 eq. KOH). This reaction mixture was refluxed for 30 min. Then the cooled solution was quenched with H_2O and acetic acid. After extraction with CH_2Cl_2 the solvent was evaporated under reduced pressure and the residue purified by column chromatography on silica gel (CH_2Cl_2/Hex/CH_3COOH 8:4:0.2). The S_2 monoimide (**35**) was isolated as orange-pink solid (6.33 mg, 35 %).

TLC (SiO_2; CH_2Cl_2/Hex/CH_3COOH 8:4:0.2): R_f=0.3.

UV/Vis (HPLC run): λ_{max} = 266, 296, 346, 362, 490, 520; side product ($C_{45}H_{54}N_2O_3S_2$) λ_{max} = 222, 256, 300, 424*br*, 496*br*.

^{1}H-NMR (400 MHz, $CDCl_3$): δ=8.76 (s, 1H, naphthalene), 8.70 (s, 1H, naphthalene), 7.58 (2H, A_2B_2 spinsystem higher order, Phe), 7.24 (2H, A_2B_2 spinsystem higher order, Phe), 3.22 (t, 2H, $^3J_{HH}$=7.2 Hz, CH_2), 3.19 (t, 2H, $^3J_{HH}$=7.2 Hz, CH_2), 1.87 (quin, 2H, $^3J_{HH}$=7.1 Hz, CH_2), 1.83 (quin, 2H, $^3J_{HH}$=7.1 Hz, CH_2), "1.55 (m, 4H, CH_2)", 1.38 (s, 9H, $C(CH_3)_3$), 1.35 (m, 8H, CH_2), 0.91 (t, 3H, $^3J_{HH}$=6.8 Hz, CH_3), 0.90 (t, 3H, $^3J_{HH}$=6.8 Hz, CH_3).

^{13}C-NMR (100 MHz, $CDCl_3$): δ=163.2, 162.3, 152.1, 151.2, 150.0, 131.5, 130.3, 128.6, 127.7, 127.5, 126.6, 124.9, 120.1, 115.3, 34.8, 32.4, 32.2, 31.3, 28.7, 28.7, 28.0, 27.7, 22.5, 14.0.

HPLC-ESI-MS (LiChrospher 100 C18, 250x4 mm, pure CH_3CN, flow 0.2 ml/min, DAD (λ_{det} = 263, 295, 367, 487 and 522 nm, T = 25 °C)): R_t = 9.1 min; m/z 1287 ([2xM+Na]$^+$), side product ($C_{45}H_{54}N_2O_3S_2$) R_t = 22.2 min, m/z 1489 ([2xM+H_2O]$^+$), 1493 ([2xM+Na]$^+$).

FAB-MS (NBA): 734 ([$C_{45}H_{54}N_2O_3S_2$]$^+$), 632 ([M]$^+$).

2,6-Dichloro-1,4,5,8-naphthalenetetracarboxylic acid tetrahexyl ester (36)
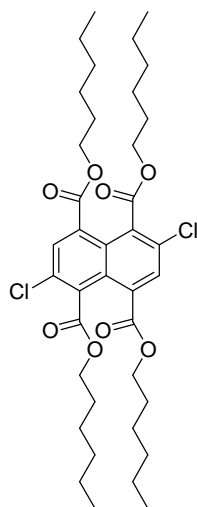
2,6-Dichloro-1,4,5,8-naphthalenetetracarboxylic acid dianhydride (**10**) (608.1 mg, 1.8 mmol, 1 eq.) was suspended in 15 ml hexanol and 13 ml 1-bromohexane. To this suspension K_2CO_3 (1.1 g, 7.9 mmol, 4.4 eq.) was added and the mixture refluxed for 3 h, while the yellow suspension turned brown. The reaction mixture was cooled to room temperature, evaporated to dryness, redissolved in CH_2Cl_2 and washed with H_2O. The combined organic phases were further dried over Na_2SO_4 and the solvent was evaporated under reduced pressure. Purification by column chromatography on silica (CH_2Cl_2/Hex 3:1) and bulb distillation provided 2,6-dichloro-1,4,5,8-naphthalenetetracarboxylic acid tetrahexyl ester (**36**) as a yellow oil (1.208 g, 94 %).
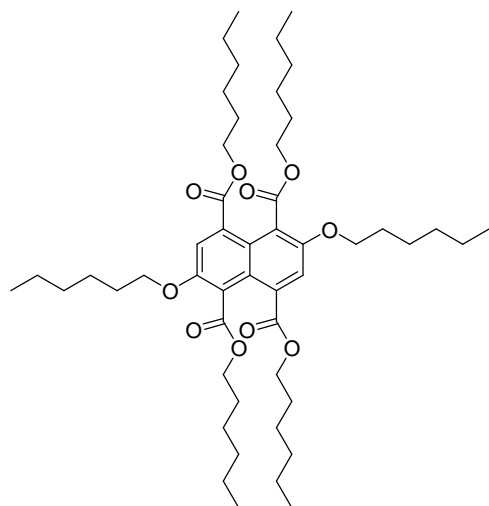
^{1}H-NMR (400 MHz, CDCl$_3$): δ=7.92 (s, 2H, naphthalene), 4.34-4.30(m, 10H, CH$_2$), 1.83-1.75 (m, 10H, CH$_2$), 1.45-1.44 (m, 10H, CH$_2$), 1.36-1.32 (m, 20H, CH$_2$), 0.93-0.88 (m, 12H, CH$_3$).

^{13}C-NMR (100 MHz, CDCl$_3$): δ=166.4, 165.7, 133.0, 132.1, 132.0, 131.7, 128.1, 66.4, 66.3, 31.4, 31.3, 28.3, 28.2, 25.6, 25.5, 22.5, 13.9.

ESI-MS (MeOH): *Positive* ion mode: 1440 ([2xM+Na]$^+$), "751" ([M+K]$^+$), "734" ([M+Na]$^+$).

MALDI-TOF-MS: 746 ([M+K]$^+$), 730 ([M+Na]$^+$).

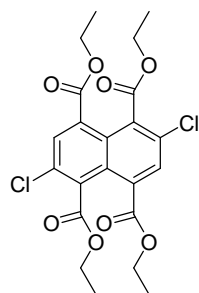**2,6-Dihexoxy-1,4,5,8-naphthalenetetracarboxylic acid tetrahexyl ester**

a). 2,6-Dichloro-1,4,5,8-naphthalenetetracarboxylic acid dianhydride (**10**) (557 mg, 1.7 mmol, 1 eq.) was suspended in 70 ml hexanol. To this suspension K_2CO_3 (2.1 g, 15.5 mmol, 9.4 eq.) was added and the mixture refluxed for one day. The slurry brown reaction mixture was cooled to room temperature, dissolved in CH_2Cl_2 and washed with H_2O. The combined organic phases were further dried over Na_2SO_4 and the solvent was evaporated under reduced pressure. Purification by column chromatography on silica (EtOAc/Hex 1:2) and bulb distillation provided a yellow oil. Unfortunately no product formation was detected by ESI-MS or ^{1}H-NMR.

b). 1.2 g NaH was solved in 10 ml hexanol. To this solution 2,6-dichloro-1,4,5,8-naphthalene-tetracarboxylic acid tetrahexyl ester (**36**) (1.056 g, 1.5 mmol, 1 eq.) in 5 ml dry DMF was added at once. Suddenly a gel formation was observed. This gel was heated to 140 °C in order to get a solution

again. This reaction mixture was further heated for 2 h. Then the reaction mixture was cooled to room temperature and the solvent evaporated at the high vacuum. The residue was diluted with CH_2Cl_2 and washed against H_2O. Purification by column chromatography on silica (EtOAc/Hex 1:2) gave yellow oil (482 mg). Unfortunately no product formation was detected by ESI-MS or ^{1}H-NMR.

2,6-Dichloro-1,4,5,8-naphthalenetetracarboxylic acid tetraethyl ester (37)
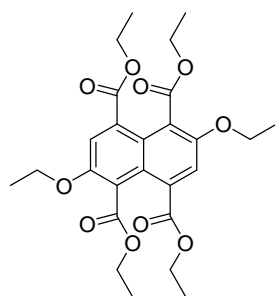
2,6-Dichloro-1,4,5,8-naphthalenetetracarboxylic acid dianhydride (**10**) (515.8 mg, 1.5 mmol, 1 eq.) was suspended in 5 ml ethanol and 5 ml ethyl bromide (68.2 mmol). To this suspension K_2CO_3 (1.01 g, 7.3 mmol, 4.9 eq.) was added and the mixture refluxed for 6 h, while the yellow suspension turned brown. The reaction mixture was cooled to room temperature, evaporated to dryness, redissolved in CH_2Cl_2 and washed with H_2O (H_2O phase remained orange). Then the solvent was evaporated under reduced pressure and subsequent purification by column chromatography on silica (CH_2Cl_2) provided 2,6-dichloro-1,4,5,8-naphthalenetetracarboxylic acid tetraethyl ester (**37**) as a colorless solid (22.47 mg, 3 %).

Despite the fact, that the way of Matile for synthesising 2,6-alkoxy substituted NDIs over a tetraester naphthalene derivative didn't work with hexanol it was possible to obtain single crystals upon slow evaporation from a diluted solution of **37** in CH_2Cl_2 suitable for x-ray analysis (*figure 110*). So, tetraester **37** crystallizes with an inversion center, whereas the ester moieties are rotated by 50-58° out of the naphthalene plane.
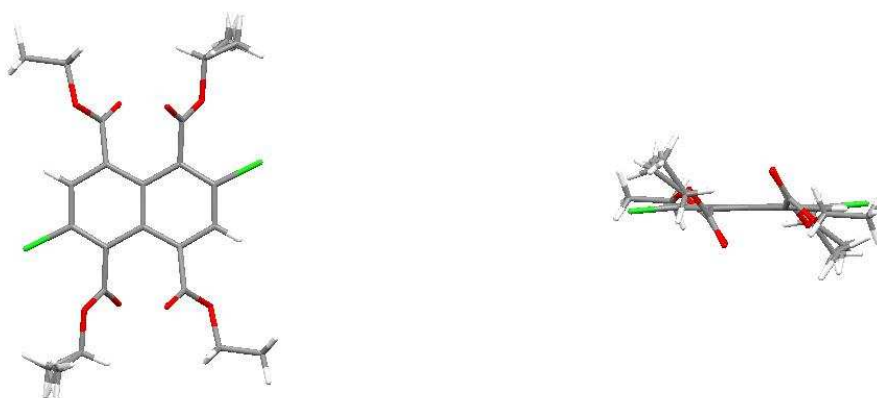

Figure 110: Solid state structure of **37**; top view (left) and front view (right).

2,6-Diethoxy-1,4,5,8-naphthalenetetracarboxylic acid tetraethyl ester (38)

2,6-Dichloro-1,4,5,8-naphthalenetetracarboxylic acid tetraethyl ester (37) (22.47 mg, 0.05 mmol, 1 eq.) was solved in 3 ml DMF. To this solution NaOEt (11 mg, 0.16 mmol, 3.2 eq.) was added and the mixture heated at 60 °C for 7 h. Then the reaction mixture was quenched with H_2O and extracted with CH_2Cl_2. The solvent was evaporated under reduced pressure and further purification by column chromatography on silica (EtOAc/Hex 2:8) provided 2,6-diethoxy-1,4,5,8-naphthalenetetracarboxylic acid tetraethyl ester (38) as a yellow solid (7.6 mg, 30 %).

^{1}H-NMR (400 MHz, CDCl$_3$): δ=7.94 (s, 2H, naphthalene), 4.43-4.38(m, 12H, CH$_2$), 1.43 (t, $^3J_{HH}$=7.2 Hz, 19H, CH$_3$).

2,6-Dihydroxy-1,4,5,8-naphthalenetetracarboxylic acid (39)
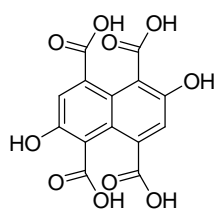
2,6-Dichloro-1,4,5,8-naphthalenetetracarboxylic acid dianhydride (10) (193.5 mg, 0.57 mmol, 1 eq.) and NaOH (196.5 mg, 4.91 mmol, 8.5 eq.) were solved in 40 ml H_2O at reflux. This reaction mixture was further heated for 15 h. After cooling to room temperature H_2O and 10 ml 1 M HCl were added. The white precipitate was separated by centrifugation (1000 RPM; 15 °C; 15 min.). After drying at the high vacuum 2,6-dihydroxy-1,4,5,8-naphthalenetetracarboxylic acid (39) was isolated as a white solid (146 mg, 76 %). Several attempts to get the dianhydride failed (e.g. boiling in CH$_3$COOH, xylene or closing with acetic acid anhydride).

^{1}H-NMR (400 MHz, DMSO): δ=13.97-13.78 (br, 4H, COOH), 7.99 (s, 2H, naphthalene).
^{13}C-NMR (100 MHz, DMSO): δ=167.0, 165.9, 134.1, 132.8, 130.6, 130.3, 127.2.
EI-MS (70 eV): 336 ([M]$^+$), 292 ([C$_{13}$H$_7$O$_8$]$^+$).

N,N'-Di-(2',6'-dimethylphenyl)-2,6-dichloro-1,4,5,8-naphthalenetetracarboxylic acid diimide (40)
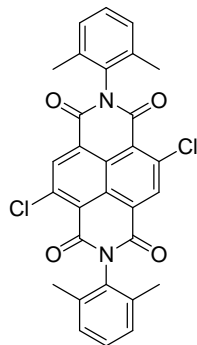
2,6-Dichloro-1,4,5,8-naphthalenetetracarboxylic acid dianhydride (**10**) (1.316 g, 3.90 mmol, 1 eq.) was suspended in 50 ml acetic acid. This suspension was heated to reflux and then 2,6-dimethylaniline (1.2 ml, 9.69 mmol, 2.5 eq.) was added through the reflux condenser at once. This reaction mixture was further refluxed for 30 min. After cooling to room temperature the reaction mixture was centrifuged (5000 RPM; 10 °C; 30 min.). After decantation of the solvent the solid residue was suspended in H_2O and centrifuged again. Final drying at the high vacuum provided N,N'-di-(2',6'-dimethylphenyl)-2,6-dichloro-1,4,5,8-naphthalenetetracarboxylic acid diimide (**40**) as an orange solid (1.825 g, 86 %).

IR (KBr): 3380*br*, 2918*w*, 1718*s*, 1677*s*, 1563*m*, 1474*m*, 1415*s*, 1358*m*, 1310*s*, 1228*s*, 912*s*, 835*m*, 768*s*, 708*m*, 530*m*, 440*m*.

^{1}H-NMR (400 MHz, CDCl$_3$): δ=8.91 (s, 2H, naphthalene), 7.34 (2H, A part of the AB$_2$ spinsystem higher order, Phe), 7.26 (4H, B part of the AB$_2$ spinsystem higher order, Phe), 2.15 (s, 12H, CH$_3$).

^{13}C-NMR (100 MHz, CDCl$_3$): δ=160.18, 159.79, 140.86, 136.46, 135.18, 132.77, 129.45, 128.80, 127.99, 126.25, 122.61, 17.86.

EI-MS (70 eV): 542 ([M]$^+$), 693 ([C$_{29}$H$_{17}$Cl$_2$N$_2$O$_4$]$^+$).

EA calc. for C$_{30}$H$_{20}$Cl$_2$N$_2$O$_4$ (543.40): C, 66.31; H, 3.71; N, 5.16; found: C, 65.71; H, 3.69; N, 5.12.

N,N'-Di-(2',6'-dimethylphenyl)-2,6-di-(*n*-hexylsulfanyl)-1,4,5,8-naphthalenetetracarboxylic acid diimide (41)
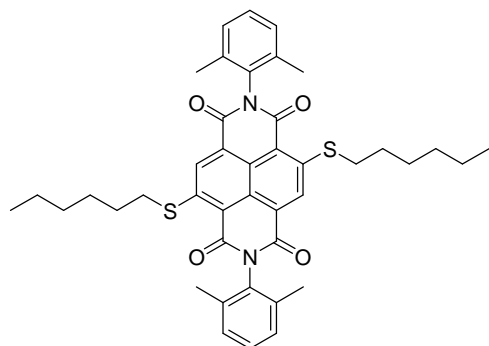
N,N'-Di-(2',6'-dimethylphenyl)-2,6-dichloro-1,4,5,8-naphthalenetetracarboxylic acid diimide (**40**) (1.073 g, 1.97 mmol, 1 eq.) and K_2CO_3 (512 mg, 3.70 mmol, 2 eq.) were suspended in 30 ml dry CH_3CN. Then hexane-1-thiol (1 ml, 7.10 mmol, 3.6 eq.) was added and the reaction mixture stirred for 2 h under an argon atmosphere at room temperature. To the orange suspension CH_2Cl_2 was added and washed once with H_2O. The solvent was evaporated under reduced pressure and the residue purified by column chromatography on silica gel (CH_2Cl_2/Hex/CH_3COOH 10:1:0.2) to yield *N,N'*-di-(2',6'-dimethylphenyl)-2,6-di-(*n*-hexylsulfanyl)-1,4,5,8-naphthalenetetracarboxylic acid diimide (**41**) as a red solid (1.357 g, 97 %).

TLC (SiO_2; CH_2Cl_2/Hex/CH_3COOH 10:1:0.2): R_f=0.8.

UV/Vis (CH_2Cl_2): λ_{max} (ε)=298 (48 068), 353 (8 156), 369 (10 985), 533 (17 814 mol^{-1} dm^3 cm^{-1}).

IR (KBr): 3449*br*, 2925*s*, 2856*m*, 1702*s*, 1661*s*, 1547*s*, 1431*s*, 1362*w*, 1320*s*, 1231*s*, 1162*w*, 917*m*, 838*m*, 767*s*, 711*m*, 583*w*, 531*m*.

^{1}H-NMR (400 MHz, $CDCl_3$): δ=8.83 (s, 2H, naphthalene), 7.31 (2H, A part of the AB$_2$ spinsystem higher order, Phe), 7.24 (4H, B part of the AB$_2$ spinsystem higher order, Phe), 3.21 (t, 4H, $^3J_{HH}$=7.4 Hz, CH$_2$), 2.15 (s, 12H, PheCH$_3$), 1.85 (quin, 4H, $^3J_{HH}$=7.5 Hz, CH$_2$), 1.55 (m, 4H, CH$_2$), 1.33 (m, 8H, CH$_2$), 0.89 (t, 6H, $^3J_{HH}$=7.0 Hz, CH$_3$).

^{13}C-NMR (100 MHz, $CDCl_3$): δ=162.7, 161.8, 149.7, 135.3, 133.2, 129.1, 128.8, 128.6, 125.9, 124.0, 119.2, 32.2, 31.3, 28.7, 27.8, 22.4, 17.9, 14.0.

FAB-MS (NBA): 707 ([M]$^+$), 623 ([$C_{36}H_{34}N_2O_4S_2$]$^+$), 539 ([$C_{30}H_{22}N_2O_4S_2$]$^+$).

MALDI-TOF-MS: 707 ([M]$^+$).

HPLC-ESI-MS (Reprosil 100 C18, 125x3 mm, pure CH_3CN, flow 0.2 ml/min, pressure 30-31 bar, DAD (λ_{det} = 298, 353, 370, 500 and 534 nm, T = 25 °C)): R_t = 15.0 min; m/z 707 ([M]$^+$).

EA calc. for $C_{42}H_{46}N_2O_4S_2$ (706.96): C, 71.36; H, 6.56; N, 3.96; found: C, 71.05; H, 6.60; N, 3.86.

N,N'-Di-(2',6'-dimethylphenyl)-2,6-di-(n-hexyloxy)-1,4,5,8-naphthalenetetracarboxylic acid diimide (42)
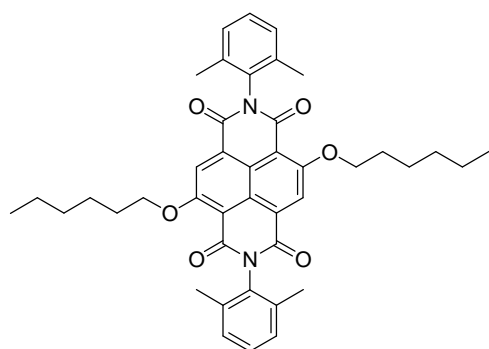
a). NaH (33.6 mg, 1.4 mmol, 6 eq.) was solved in 21 ml hexane-1-ol and diluted with another 20 ml hexane-1-ol. This solution was slowly dropped into an orange-red suspension of N,N'-di-(2',6'-dimethylphenyl)-2,6-dichloro-1,4,5,8-naphthalenetetracarboxylic acid diimide (40) (129.6 mg, 0.24 mmol, 1 eq.) in 30 ml hexane-1-ol at room temperature over 42 min. The reaction mixture was further stirred for 1.5 h at room temperature. Then transferred to a separation funnel with CH_2Cl_2 and washed with H_2O. The solvents were evaporated under reduced pressure and following purification by column chromatography on silica gel (CH_2Cl_2/Hex/CH_3COOH 20:1:0.2) provided N,N'-di-(2',6'-dimethylphenyl)-2,6-di-(n-hexyloxy)-1,4,5,8-naphthalenetetra-carboxylic acid diimide (42) as a bright orange solid (153.2 mg, 95%).

b). NaH (629 mg, 26.21 mmol, 7.8 eq.) was solved in 50 ml hexane-1-ol and diluted with another 30 ml hexane-1-ol. This solution was slowly dropped into an orange-red suspension of N,N'-di-(2',6'-dimethylphenyl)-2,6-dichloro-1,4,5,8-naphthalenetetracarboxylic acid diimide (40) (1.825 g, 3.36 mmol, 1 eq.) in 150 ml hexane-1-ol at room temperature over 2 h. The reaction mixture was further stirred for 1 h at room temperature and 10 min at 50 °C. Then the solvent was evaporated under reduced pressure and after purification by column chromatography on silica gel (CH_2Cl_2/Hex/ CH_3COOH 20:1:0.2) N,N'-di-(2',6'-dimethylphenyl)-2,6-di-(n-hexyloxy)-1,4,5,8-naphthalene-tetracarboxylic acid diimide (42) was isolated as a bright orange solid (1.266 g, 56%).

TLC (SiO$_2$; CH_2Cl_2/Hex/CH_3COOH 10:1:0.2): R_f=0.5.

UV/Vis (CH_2Cl_2): λ_{max} (ε)=255 (44 507), 343 (12 156), 361 (14 358), 444 (12 429), 470 (17 844 mol^{-1} dm^3 cm^{-1}).

IR (KBr): 3430br, 2926s, 2857m, 1709s, 1672s, 1575s, 1441s, 1364m, 1329m, 1296m, 1217s, 1000m, 906m, 857m, 765s, 702w, 531w.

^{1}H-NMR (400MHz, CDCl$_3$): δ=8.58 (s, 2H, naphthalene), 7.30 (2H, A part of the AB$_2$ spinsystem higher order, Phe), 7.23 (4H, B part of the AB$_2$ spinsystem higher order, Phe), 4.42 (t, 4H, $^3J_{HH}$=6.8 Hz, CH$_2$), 2.15 (s, 12H, PheCH$_3$), 1.97 (quin, 4H, $^3J_{HH}$=7.1 Hz, CH$_2$), 1.51 (m, 4H, CH$_2$), 1.33 (m, 8H, CH$_2$), 0.87 (m, 6H, CH$_3$).

^{13}C-NMR (100MHz, CDCl$_3$): δ=161.8, 160.6, 160.2, 135.4, 133.6, 128.9, 128.5, 127.4, 124.5, 120.2, 111.2, 70.8, 31.3, 28.9, 25.4, 22.5, 17.9, 13.9.

**FAB-MS** (NBA): 675 ([M]$^+$), 591 ([C$_{36}$H$_{34}$N$_2$O$_6$]$^+$), 507 ([C$_{30}$H$_{22}$N$_2$O$_6$]$^+$).

MALDI-TOF-MS: 675 ([M]$^+$).

HPLC-ESI-MS (Reprosil 100 C18, 125x3 mm, pure CH_3CN, flow 0.2 ml/min, pressure 30-31 bar, DAD (λ_{det} = 250, 340, 360, 450 and 460 nm, T = 25 °C)): R_t = 9.7 min; m/z 1387 ([2xM+K]$^+$), 1371 ([2xM+Na]$^+$), 675 ([M]$^+$).

EA calc. for $C_{42}H_{46}N_2O_6$ (674.83): C, 74.75; H, 6.87; N, 4.15; found: C, 74.64; H, 6.92; N, 4.09.

N,N'-Di-(2',6'-dimethylphenyl)-2,6-di-(*n*-hexylamino)-1,4,5,8-naphthalenetetracarboxylic acid diimide (43)
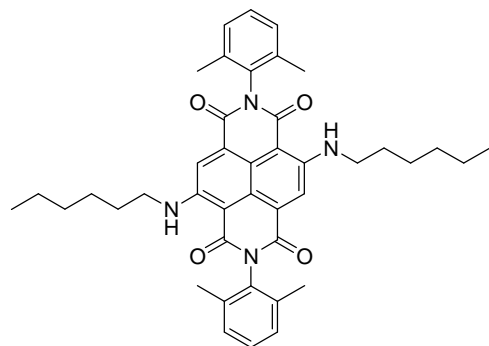
N,N'-Di-(2',6'-dimethylphenyl)-2,6-dichloro-1,4,5,8-naphthalenetetracarboxylic acid diimide (**40**) (128.1 mg, 0.236 mmol, 1 eq.) and K_2CO_3 (82.9 mg, 0.56 mmol, 2 eq.) were suspended in 20 ml HPLC CH_3CN. Then hexylamine (1 ml, 7.56 mmol, 32 eq.) was added, whereas the colour changed immediately from orange to red. The reaction mixture was further stirred for one day under an argon atmosphere at 50 °C. The solvent was evaporated under reduced pressure and the residue purified by reversed phase column chromatography on silica gel 100 C_{18} (CH_3CN to CH_2Cl_2) to yield *N,N'*-di-(2',6'-dimethylphenyl)-2,6-di-(*n*-hexylamino)-1,4,5,8-naphthalenetetracarboxylic acid diimide (**43**) as a blue solid (63.67 mg, 40%).

TLC (SiO_2; CH_2Cl_2): R_f=0.6.

UV/Vis (HPLC run): λ_{max}=281, 344, 362, 570, 614.

^{1}H-NMR (400MHz, $CDCl_3$): δ=9.31 (t, 2H, $^3J_{HH}$=5.1 Hz, NH), 8.27 (s, 2H, naphthalene), 7.32 (2H, A part of the AB_2 spinsystem higher order, Phe), 7.25 (4H, B part of the AB_2 spinsystem higher order, Phe), 3.48 (q, 4H, $^3J_{HH}$=7.1 Hz, CH_2), 2.15 (s, 12H, PheCH_3), 1.75 (quin, 2H, $^3J_{HH}$=7.3 Hz, CH_2), 1.44 (m, 4H, CH_2), 1.31 (m, 8H, CH_2), 0.88 (t, 6H, $^3J_{HH}$=7.0 Hz, CH_3).

^{13}C-NMR (100MHz, $CDCl_3$): δ=165.7, 162.4, 149.6, 135.4, 133.8, 129.0, 128.6, 126.2, 122.0, 119.0, 101.8, 43.3, 31.4, 29.2, 26.7, 22.5, 17.8, 14.0.

FAB-MS (NBA): 673 ([M]$^+$).

HPLC-ESI-MS (Reprosil 100 C18, 125x3 mm, pure CH_3CN, flow 0.2 ml/min, pressure 30-31 bar, DAD (λ_{det} = 280, 345, 365, 570 and 615 nm, T = 25 °C)): R_t = 21.2 min; m/z 695 ([M+Na]$^+$), 673 ([M]$^+$).

EA calc. for $C_{42}H_{48}N_4O_4$ (672.87): C, 74.97; H, 7.19; N, 8.33; found: C, 72.13; H, 7.09; N, 7.50.

N,N'-Di-(2',6'-dimethylphenyl)-2,6-di-(*n*-pentylamino)-1,4,5,8-naphthalenetetracarboxylic acid diimide (44)
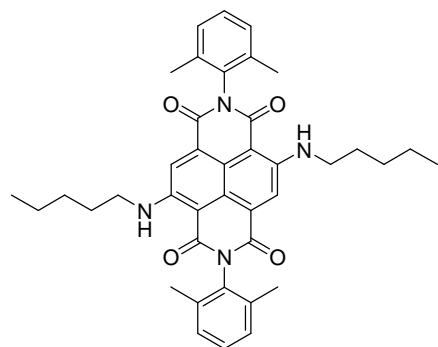
N,N'-Di-(2',6'-dimethylphenyl)-2,6-dichloro-1,4,5,8-naphthalenetetracarboxylic acid diimide (**40**) (74.02 mg, 0.136 mmol, 1 eq.) and 102 mg K_2CO_3 were suspended in 2 ml HPLC CH_3CN. Then pentylamine (0.1 ml, 0.863 mmol, 6 eq.) was added, whereas the colour changed immediately from orange to red. The reaction mixture was stirred for one day under an argon atmosphere at 50 °C, whereas the colour changed to deeply blue. The solvent was evaporated under reduced pressure and the residue purified by reversed phase column chromatography on silica gel 100 C_{18} (CH_3CN to CH_2Cl_2) to yield *N,N'*-di-(2',6'-dimethylphenyl)-2,6-di-(*n*-pentylamino)-1,4,5,8-naphthalenetetracarboxylic acid diimide (**44**) as a blue solid (65.4 mg, 75%).

TLC (SiO_2; CH_2Cl_2): R_f=0.5.

UV/Vis (CH_3CN): λ_{max} (ε)=281 (36 967), 345 (12 972), 362 (14 715), 615 (19 640 $mol^{-1} dm^3 cm^{-1}$).

^{1}H-NMR (400MHz, $CDCl_3$): δ=9.31 (t, 2H, $^3J_{HH}$=5.1 Hz, NH), 8.26 (s, 2H, naphthalene), 7.32 (2H, A part of the AB_2 spinsystem higher order, Phe), 7.25 (4H, B part of the AB_2 spinsystem higher order, Phe), 3.48 (q, 4H, $^3J_{HH}$=7.1 Hz, CH_2), 2.15 (s, 12H, $PheCH_3$), 1.75 (quin, 4H, $^3J_{HH}$=7.2 Hz, CH_2), 1.44-1.33 (m, 8H, CH_2), 0.90 (t, 6H, $^3J_{HH}$=7.1 Hz, CH_3).

^{13}C-NMR (100MHz, $CDCl_3$): δ=165.7, 162.4, 149.6, 135.5, 133.8, 129.0, 128.6, 126.2, 122.1, 119.0, 101.8, 43.3, 29.2, 29.0, 22.3, 17.8, 13.9.

HPLC-ESI-MS (Reprosil 100 C18, 125x3 mm, pure CH_3CN, flow 0.2 ml/min, pressure 30-31 bar, DAD (λ_{det} = 280, 345, 365, 570 and 615 nm, T = 25 °C)): R_t = 15.1 min; m/z 668 ([M+Na]$^+$), 646 ([M]$^+$).

N-(2',6'-dimethylphenyl)-2,6-di-(*n*-hexylsulfanyl)-1,8-naphthalenedicarboxylic acid imide-4,5-naphthalenedicarboxylic acid anhydride (45)
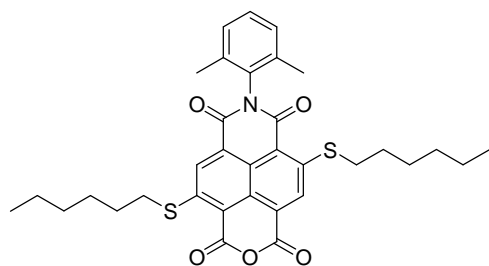
208.32 mg NaOH was solved in a mixture of 10 ml H_2O and 10 ml *tert.*-butanol. Then 0.8 ml of this NaOH solution (0.208 mmol, 0.8 eq.) was added in one lot to a refluxing solution of *N,N'*-di-(2',6'-dimethylphenyl)-2,6-di-(*n*-hexylsulfanyl)-1,4,5,8-naphthalenetetracarboxylic acid diimide (**41**) (153.43 mg, 0.217 mmol, 1 eq.) in 20 ml *tert.*-butanol.

The colour changed immediately from red to dark red. The reaction mixture was further refluxed for 5 min. After cooling to room temperature the solvents were removed under reduced pressure. Then the residue was solved in CH_2Cl_2 and washed with CH_3COOH. The solvents were evaporated and further purification by semi-preparative reversed phase HPLC (Reprosil 100 C18 from, 5 μm particle size, 125x20 mm, CH_3CN) provided S_2 monoimide (**45**) as a dark red solid (87.33 mg, 67%).

TLC (SiO_2; CH_2Cl_2/Hex/CH_3COOH 10:1:0.2): R_f=0.7.

UV/Vis (HPLC run): λ_{max}=294, 344, 362, 495, 524.

^{1}H-NMR (400MHz, $CDCl_3$): δ=8.77 (s, 1H, naphthalene), 8.71 (s, 1H, naphthalene), 7.31 (1H, A part of the AB_2 spinsystem higher order, Phe), 7.24 (2H, B part of the AB_2 spinsystem higher order, Phe), 3.25 (t, 2H, $^3J_{HH}$=7.5 Hz, CH_2), 3.19 (t, 2H, $^3J_{HH}$=7.3 Hz, CH_2), 2.13 (s, 6H, PheCH$_3$), 1.88 (quin, 2H, $^3J_{HH}$=7.3 Hz, CH_2), 1.84 (quin, 2H, $^3J_{HH}$=7.3 Hz, CH_2), "1.59 (m, 4H, CH_2)", 1.36 (m, 8H, CH_2), 0.91 (t, 3H, $^3J_{HH}$=6.8 Hz, CH_3), 0.90 (t, 3H, $^3J_{HH}$=6.9 Hz, CH_3).

^{13}C-NMR (100MHz, $CDCl_3$): δ=162.3, 161.3, 159.3, 158.2, 151.3, 150.1, 135.3, 132.9, 130.3, 129.2, 128.7, 128.7, 127.5, 125.6, 124.6, 120.2, 120.0, 32.4, 32.2, 31.3, 31.3, 28.7, 28.7, 28.0, 27.6, 22.5, 17.9, 14.0, 14.0.

FAB-MS (NBA): 604 ([M]$^+$), 520 ([$C_{28}H_{25}NO_5S_2$]$^+$), 436 ([$C_{22}H_{13}NO_5S_2$]$^+$).

MALDI-TOF-MS: 605 ([M]$^+$).

HPLC-ESI-MS (Reprosil 100 C18, 125x3 mm, pure CH_3CN, flow 0.2 ml/min, pressure 30-31 bar, DAD (λ_{det} = 298, 353, 370, 500 and 534 nm, T = 25 °C)): R_t = 8.1 min; m/z 642 ([M+K]$^+$), 604 ([M]$^+$).

EA calc. for $C_{34}H_{37}NO_5S_2$ (603.79): C, 67.64; H, 6.18; N, 2.32; found: C, 67.06; H, 6.06; N, 2.31.

N-(2',6'-dimethylphenyl)-2,6-di-(*n*-hexyloxy)-1,8-naphthalenedicarboxylic acid imide-4,5-naphthalenedicarboxylic acid anhydride (46)
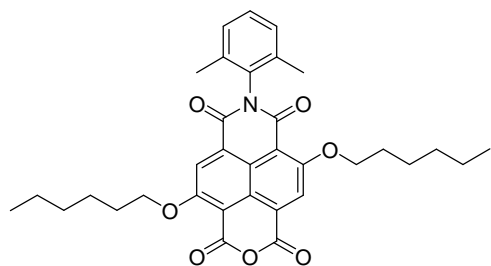
208.32 mg NaOH was solved in a mixture of 10 ml H_2O and 10 ml *tert*.-butanol. Then 0.8 ml of this NaOH solution (0.208 mmol, 0.9 eq.) was added in one lot to a refluxing solution of *N,N'*-di-(2',6'-dimethylphenyl)-2,6-di-(*n*-hexyloxy)-1,4,5,8-naphthalenetetracarboxylic acid diimide (42) (153.22 mg, 0.227 mmol, 1 eq.) in 20 ml *tert*.-butanol. The colour changed immediately from yellow to red. The reaction mixture was further refluxed for 5 min. After cooling to room temperature the solvents were removed under reduced pressure. Then the residue was solved in CH_2Cl_2 and washed with CH_3COOH. The solvents were evaporated and purification by column chromatography on silica gel (CH_2Cl_2/Hex/CH_3COOH 8:4:0.2) gave a yellow-orange solid. Further purification by semi-preparative reversed phase HPLC (Reprosil 100 C18 from, 5 µm particle size, 125x20 mm, CH_3CN) provided O_2 monoimide (46) as an orange solid (38.41 mg, 30%).

TLC (SiO_2; CH_2Cl_2/Hex/CH_3COOH 10:1:0.2): R_f=0.4.

UV/Vis (HPLC run): λ_{max}=245, 338, 354, 440, 464.

^{1}H-NMR (500MHz, $CDCl_3$): δ=8.55 (s, 1H, naphthalene), 8.50 (s, 1H, naphthalene), 7.30 (1H, A part of the AB_2 spinsystem higher order, Phe), 7.23 (2H, B part of the AB_2 spinsystem higher order, Phe), 4.47 (t, 2H, $^3J_{HH}$=6.4 Hz, CH_2), 4.40 (t, 2H, $^3J_{HH}$=6.6 Hz, CH_2), 2.13 (s, 6H, PheCH_3), 1.99 (m, 4H, CH_2), 1.61 (m, 2H, CH_2), 1.52 (m, 2H, CH_2), 1.39 (m, 4H, CH_2), 1.33 (m, 4H, CH_2), 0.92 (m, 3H, CH_3), 0.88 (m, 3H, CH_3).

^{13}C-NMR (125MHz, $CDCl_3$): δ=161.4, 161.4, 160.5, 159.9, 159.7, 155.2, 135.3, 133.4, 129.1, 128.6, 128.5, 125.9, 124.2, 123.5, 121.6, 120.0, 112.1, 107.0, 71.1, 71.0, 31.3, 31.3, 28.9, 25.4, 22.5, 17.9, 14.0, 14.0.

MALDI-TOF-MS: 595 ($[M+Na]^+$), 571 ($[M]^+$).

HPLC-ESI-MS (Reprosil 100 C18, 125x3 mm, pure CH_3CN, flow 0.2 ml/min, pressure 30-31 bar, DAD (λ_{det} = 250, 340, 360, 450 and 460 nm, T = 25 °C)): R_t = 7.0 min; m/z 572 ($[M]^+$).

N-(2',6'-dimethylphenyl)-N'-(N-Boc-p-phenyl)-2,6-di-(n-hexylsulfanyl)-1,4,5,8-naphthalenetetracarboxylic acid diimide (47)
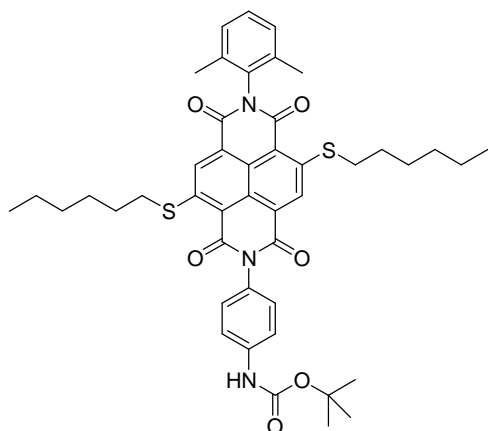
S_2 monoimide (**45**) (87.33 mg, 0.145 mmol, 1 eq.) and *N*-Boc-*p*-phenylenediamine (30.98 mg, 0.149 mmol, 1 eq.) were solved in 17 ml *i*-PrOH and 1 ml Et$_3$N. This reaction mixture was refluxed under an argon atmosphere for 4 days. Then the solvent was removed under reduced pressure and the residue was purified by column chromatography on silica gel (CH$_2$Cl$_2$/Hex 8:4 to 8:1 to CH$_2$Cl$_2$/MeOH 100:1) to afford BocS$_2$ NDI (**47**) as a red solid (104.5 mg, 91%).

TLC (SiO$_2$; CH$_2$Cl$_2$): R_f=0.7.

UV/Vis (HPLC run): λ_{max}=262, 294, 350, 366, 490, 520.

^{1}H-NMR (400MHz, CDCl$_3$): δ=8.80 (s, 1H, naphthalene), 8.78 (s, 1H, naphthalene), 7.57 (2H, A$_2$B$_2$ spinsystem higher order, Phe), 7.31 (1H, A part of the AB$_2$ spinsystem higher order, Phe), 7.24 (2H, B part of the AB$_2$ spinsystem higher order, Phe), 7.24 (2H, A$_2$B$_2$ spinsystem higher order, Phe), 6.67 (s, 1H, NH), 3.19 (t, 2H, $^3J_{HH}$=7.8 Hz, CH$_2$), 3.17 (t, 2H, $^3J_{HH}$=7.8 Hz, CH$_2$), 2.15 (s, 6H, PheCH$_3$), 1.83 (quin, 4H, $^3J_{HH}$=7.5 Hz, CH$_2$), 1.55 (m, 13H, BOC CH$_3$ + CH$_2$), 1.33 (m, 8H, CH$_2$), 0.88 (t, 6H, $^3J_{HH}$=6.8 Hz, CH$_3$).

^{13}C-NMR (100MHz, CDCl$_3$): δ=163.7, 162.8, 162.7, 161.8, 152.4, 149.7, 149.6, 139.1, 135.4, 133.2, 129.1, 129.1, 128.7, 128.6, 125.8, 124.2, 123.9, 119.4, 119.0, 32.2, 31.3, 29.7, 28.8, 28.8, 28.3, 27.8, 22.5, 17.9, 14.0.

FAB-MS (NBA): 794 ([M]$^+$), 739 ([C$_{41}$H$_{43}$N$_3$O$_6$S$_2$]$^+$), 654 ([C$_{35}$H$_{31}$N$_3$O$_6$S$_2$]$^+$).

HPLC-ESI-MS (Reprosil 100 C18, 125x3 mm, pure CH$_3$CN, flow 0.2 ml/min, pressure 30-31 bar, DAD (λ_{det} = 298, 353, 370, 500 and 534 nm, T = 25 °C)): R$_t$ = 9.8 min; m/z 852 ([M+CH$_3$CN+H$_2$O]$^+$), 832 ([M+K]$^+$), 816 ([M+Na]$^+$), 794 ([M]$^+$), 739 ([C$_{41}$H$_{43}$N$_3$O$_6$S$_2$]$^+$).

EA calc. for C$_{45}$H$_{51}$N$_3$O$_6$S$_2$ (794.03): C, 68.07; H, 6.47; N, 5.29; found: C, 68.00; H, 6.42; N, 5.23.

N-(2',6'-dimethylphenyl)-*N*'-(4'-aminophenyl)-2,6-di-(*n*-hexylsulfanyl)-1,4,5,8-naphthalenetetracarboxylic acid diimide (48)
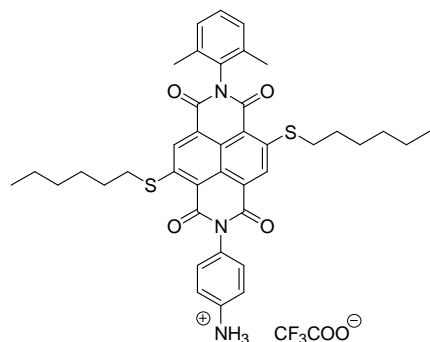
BocS$_2$ NDI (**47**) (104.5 mg, 0.132 mmol, 1eq.) was solved in 5 ml dry CH$_2$Cl$_2$. Then 2 ml CF$_3$COOH was added to the solution and stirred for 7 h at room temperature under an argon atmosphere. The colour changed from pink to dark violet. Then the solvent was evaporated and S$_2$NH$_2$ was isolated as a dark red solid (quantitative).

UV/Vis (HPLC run): λ_{max}=296, 350, 366, 490, 518.

A sample for NMR analysis was solved in CH$_2$Cl$_2$ and run over a short basic alox column in order to obtain the amine.

^{1}H-NMR (400MHz, CDCl$_3$): δ=9.15 (br, 2H, NH$_2$) 8.50 (s, 1H, naphthalene), 8.46 (s, 1H, naphthalene), 7.50 (4H, A$_2$B$_2$ spinsystem higher order, Phe), 7.31 (1H, A part of the AB$_2$ spinsystem higher order, Phe), 7.21 (2H, B part of the AB$_2$ spinsystem higher order, Phe), 2.83 (t, 2H, ^{3}J$_{HH}$=6.7 Hz, CH$_2$), 2.77 (t, 2H, ^{3}J$_{HH}$=6.7 Hz, CH$_2$), 2.12 (s, 6H, PheCH$_3$), 1.72 (quin, 2H, ^{3}J$_{HH}$=6.7 Hz, CH$_2$), 1.63 (quin, 2H, ^{3}J$_{HH}$=6.7 Hz, CH$_2$), 1.45 (m, 4H, CH$_2$), 1.29 (m, 8H, CH$_2$), 0.86 (m, 6H, CH$_3$).

^{13}C-NMR (100MHz, CDCl$_3$): δ=163.3, 162.5, 162.4, 161.5, 149.7, 149.6, 135.5, 134.8, 132.9, 130.8, 129.2, 128.6, 128.4, 128.0, 125.6, 125.5, 124.1, 123.9, 123.7, 119.2, 118.8, 32.2, 31.4, 31.3, 28.9, 28.8, 27.7, 27.6, 22.4, 18.0, 13.9.

FAB-MS (NBA): 827 ([M+CF$_3$COOH+H$_2$O]$^+$), 694 ([M]$^+$).

HPLC-ESI-MS (Reprosil 100 C18, 125x3 mm, pure CH$_3$CN, flow 0.2 ml/min, pressure 30-31 bar, DAD (λ_{det} = 298, 353, 370, 500 and 534 nm, T = 25 °C)): R$_t$ = 7.3 min; m/z 754 ([M+CH$_3$CN+H$_2$O]$^+$), 695 ([M]$^+$).

S$_2$O$_2$-NDI (49)
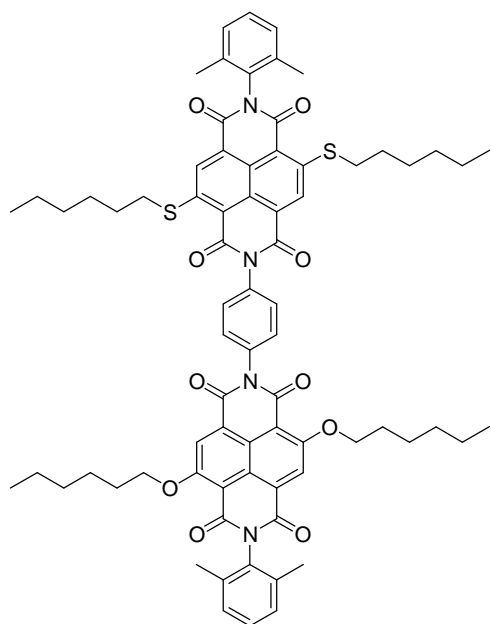
In order to obtain the amine, S$_2$-NDI **48** was flushed with EtOAc over a short basic aluminiumoxide column. S$_2$-NDI amine (88.21 mg, 0.127 mmol, 1.8 eq.) was solved in a mixture of *i*-PrOH/Et$_3$N (20 ml: 1 ml) and then added to O$_2$ monoimide (**46**) (41.25 mg, 0.072 mmol, 1eq.). This reaction mixture was refluxed under an argon atmosphere for 4 days. Then the solvent was removed under reduced pressure. The orange-red residue was solved in CH$_2$Cl$_2$ and washed with CH$_3$COOH and H$_2$O. Further purification by basic aluminium oxide column chromatography on silica (EtOAc) and reversed phase column chromatography on silica gel 100 C$_{18}$ (CH$_3$CN to CH$_3$CN:MeOH (1:1) to CH$_2$Cl$_2$) provided S$_2$O$_2$ NDI (**49**) as an orange solid (11.28 mg, 13%).

UV/Vis (CH$_2$Cl$_2$): λ_{max} (ε)=298 (55 977), 363 (22 056), 445 (10 659), 471 (17 449), 501 (10 775), 532 (18 792 mol^{-1} dm^3 cm^{-1}).

^{1}H-NMR (500MHz, CDCl$_3$): δ=8.83 (s, 2H, S$_2$ naphthalene), 8.60, 8.58 (s, 2H, O$_2$ naphthalene), 7.54 (4H, A$_2$B$_2$ spinsystem higher order, Phe), 7.31 (2H, A part of the AB$_2$ spinsystem higher order, Phe), 7.24 (4H, B part of the AB$_2$ spinsystem higher order, Phe), 4.45-4.42 (m, 4H, O$_2$ CH$_2$), 3.25-3.20 (m, 4H, S$_2$ CH$_2$), 2.17 (s, 12H, PheCH$_3$), 2.00 (m, 4H, O$_2$ CH$_2$), 1.86 (m, 4H, S$_2$ CH$_2$), 1.59 (m, CH$_2$), 1.34 (m, CH$_2$), 0.89 (m, CH$_3$).

^{13}C-NMR (150MHz, CDCl$_3$): δ=163.3, 162.7, 162.5, 162.5, 161.8, 161.8, 160.9, 160.6, 160.6, 160.2, 149.8, 149.7, 135.5, 135.4, 135.4, 134.7, 133.6, 130.0, 129.7, 129.2, 129.0, 128.9, 128.6, 128.6, 127.6, 127.5, 125.9, 125.6, 124.4, 124.2, 124.1, 124.0, 120.3, 120.1, 119.3, 119.3, 111.2, 111.2, 70.9, 70.8, 32.3, 31.9, 31.5, 31.4, 31.3, 29.4, 29.1, 29.0, 28.8, 28.8, 27.8, 25.5, 25.5, 22.7, 22.5, 22.5, 17.9, 14.1, 14.1, 14.0.

MALDI-TOF-MS: 1272 ([M+Na]$^+$), 1250 ([M]$^+$).

HPLC-ESI-MS (Reprosil 100 C18, 125x3 mm, CH$_3$CN:EtOH (50:50), flow 0.3 ml/min, pressure 61-62 bar, DAD (λ_{det} = 250, 340, 360, 450 and 460 nm, T = 25 °C)): R$_t$ = 3.7 min; m/z 1269 ([M+Na]$^+$), 1247 ([M]$^+$).

N,N'-Di-(2',6'-dimethylphenyl)-1,4,5,8-naphthalenetetracarboxylic acid diimide (50)
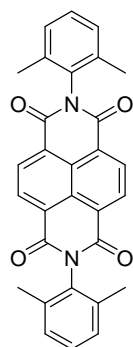
1,4,5,8-Naphthalenetetracarboxylic acid dianhydride (1.8 g, 6.7 mmol, 1 eq.) was suspended in 50 ml acetic acid. Then 2,6-dimethylaniline (2.5 ml, 20.2 mmol, 3 eq.) was added in one lot through the condenser. This reaction mixture was further refluxed for 1 h. After cooling to room temperature the white precipitate was separated by centrifugation (5000 RPM; 10 °C; 30 min.). After drying at the high vacuum *N,N'*-Di-(2',6'-dimethylphenyl)-1,4,5,8-naphthalenetetracarboxylic acid diimide (**50**) was isolated as a white solid (2.8 g, 89 %).

UV/Vis (HPLC run): λ_{max}=235, 340, 358, 378.

^{1}H-NMR (400 MHz, CDCl$_3$): δ=8.89 (s, 4H, naphthalene), 7.34 (2H, A part of the AB$_2$ spinsystem higher order, Phe), 7.26 (4H, B part of the AB$_2$ spinsystem higher order, Phe), 2.16 (s, 12H, CH$_3$).

^{13}C-NMR (100 MHz, CDCl$_3$): δ=162.12, 135.34, 131.50, 129.32, 128.73, 126.93, 17.85.
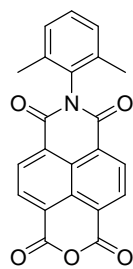
HPLC (Reprosil 100 C18, 125x3 mm, pure CH$_3$CN, flow 0.2 ml/min, pressure 30-31 bar, DAD (λ_{det} = 232, 343, 358, and 379 nm, T = 25 °C)): R_t = 4.1 min.

EI-MS (70 eV): 474 ([M]$^+$), 459 ([C$_{29}$H$_{19}$N$_2$O$_4$]$^+$).

EA calc. for C$_{30}$H$_{22}$N$_2$O$_4$ (474.51): C, 75.94; H, 4.67; N, 5.90; found: C, 73.77; H, 4.53; N, 5.26.

N-(2',6'-dimethylphenyl)-1,8-naphthalenedicarboxylic acid imide-4,5-naphthalenedicarboxylic acid anhydride (51)

a). *N,N'*-Di-(2',6'-dimethylphenyl)-1,4,5,8-naphthalenetetracarboxylic acid diimide (**50**) (283.2 mg, 0.597 mmol, 1 eq.) was heated at 90 °C in 10 ml *tert*-butanol and 0.2 ml 4 M NaOH solution for 5 min. No colour change was observed and no product formation due to TLC and HPLC (R_t = 3.4 min) was observed.

b). *N,N'*-Di-(2',6'-dimethylphenyl)-1,4,5,8-naphthalenetetracarboxylic acid diimide (**50**) (283.2 mg, 0.597 mmol, 1 eq.) was heated at 90 °C in 10 ml *tert*-butanol and 0.3 ml 19 M NaOH solution for 5 min. The colour changed to yellow. To the cooled reaction mixture CH$_3$COOH was added until pH≈5 and it was extracted with CH$_2$Cl$_2$. Product formation was observed by HPLC R_t = 3.4 min.

c). *N,N'*-Di-(2',6'-dimethylphenyl)-1,4,5,8-naphthalenetetracarboxylic acid diimide (**50**) (283.2 mg, 0.597 mmol, 1 eq.) was heated at 90 °C in 10 ml *i*-PrOH and 1 ml 19 M NaOH solution for 5 min. The colour changed to yellow and then to red. To the cooled reaction mixture CH$_3$COOH was added until pH≈5 and it was extracted with CH$_2$Cl$_2$. After evaporation of the solvent under reduced pressure the residue was purified by reversed phase column chromatography on silica gel 100 C$_{18}$ (CH$_3$CN) and monoimide **51** was isolated as a white-grey solid (17.5 mg, 8 %).

d). 1,4,5,8-Naphthalenetetracarboxylic acid dianhydride (**3**) (4.8 g, 17.9 mmol, 1 eq.) and 6.9 g KOH were solved in 1 l H$_2$O and stirred for 3 h at room temperature. Then H$_3$PO$_4$ was added until pH≈6.0-6.2 followed by addition of 2,6-dimethylaniline (2 ml, 16.2 mmol, 0.9 eq.). This reaction mixture was then refluxed for 1 day. After cooling to room temperature CH$_3$COOH was added until a white solid precipitated. After filtration and drying at the high vacuum monoimide **51** was isolated as a white-grey solid (5.99 g, 90 %).

UV/Vis (HPLC run): λ$_{max}$=234, 332, 347.

^{1}H-NMR (400 MHz, CDCl$_3$): δ=8.56 (2H, A$_2$B$_2$ spinsystem higher order, naphthalene), 8.19 (2H, A$_2$B$_2$ spinsystem higher order, naphthalene), 6.78 (2H, B part of the AB$_2$ spinsystem higher order, Phe), 6.39 (1H, A part of the AB$_2$ spinsystem higher order, Phe), 2.06 (s, 6H, CH$_3$).

^{13}C-NMR (100 MHz, CDCl$_3$): δ=168.25, 160.07, 144.05, 137.85, 131.55, 130.67, 129.13, 127.67, 125.38, 121.64, 120.46, 115.71, 17.75.

HPLC-ESI-MS (Reprosil 100 C18, 125x3 mm, pure CH$_3$CN, flow 0.2 ml/min, pressure 30-31 bar, DAD (λ$_{det}$ = 232, 343, 358, 379 and 520 nm, T = 25 °C)): R_t = 3.3 min; m/z 372 ([M]$^+$).

EI-MS (70 eV): 371 ([M]$^+$), 356 ([C$_{21}$H$_{10}$NO$_5$]$^+$).

EA calc. for C$_{22}$H$_{13}$NO$_5$ (371.35): C, 71.16; H, 3.53; N, 3.77; found: C, 56.26; H, 3.38; N, 2.15.

5.3. Solid state structures

Solid state structures were determined by Dr. Markus Neuburger and Dr. Silvia Schaffner in the chemical crystallography laboratory of the inorganic department.
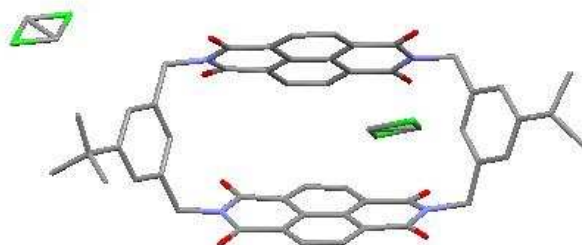
Crystal data for **1**: formula $C_{53}H_{42}Cl_2N_4O_8$, M = 933.84, F(000) = 972, colorless plate, size $0.09 \cdot 0.14 \cdot 0.30$ mm^3, triclinic, space group P -1 , Z = 2, a = 11.2478(2) Å, b = 13.9007(2) Å, c = 14.9298(3) Å, α = 90.3583(11)°, β = 110.9346(11)°, γ = 90.1421(12)°, V = 2180.15(7) Å^3, $D_{calc.}$ = 1.422 Mg $\cdot$ m^{-3}. The crystal was measured on a Nonius KappaCCD diffractometer at 173K using graphite-monochromated Mo K_α-radiation with λ = 0.71073 Å, Θ_{max} = 27.871°. Minimal/maximal transmission 0.97/0.98, μ = 0.214 mm^{-1}. The COLLECT suite has been used for datacollection and integration. From a total of 20283 reflections, 10386 were independent (merging r = 0.041). From these, 6267 were considered as observed (I>1.0σ(I)) and were used to refine 622 parameters. The structure was solved by direct methods using the program SIR92. Least-squares refinement against F was carried out on all non-hydrogen atoms using the program CRYSTALS. R = 0.0662 (observed data), wR = 0.1089 (all data), GOF = 1.1417. Minimal/maximal residual electron density = -1.09/0.43 e Å^{-3}. Chebychev polynomial weights were used to complete the refinement.
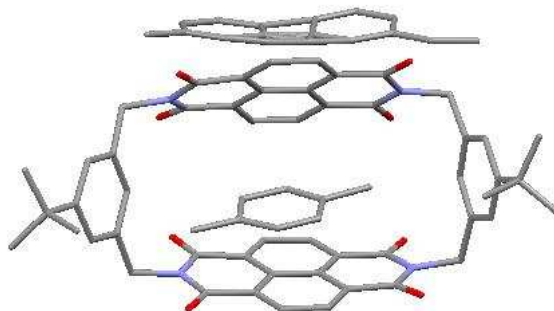
Crystal data for **1**: formula $C_{68.60}H_{61.20}N_4O_8$, M = 1069.66, F(000) = 2259.200, colorless block, size 0.32 · 0.34 · 0.44 mm^3, monoclinic, space group P 2_1/c, Z = 4, a = 17.7349(2) Å, b = 16.9022(2) Å, c = 19.1495(2) Å, α = 90°, β = 92.6081(6)°, γ = 90°, V = 5734.29(11) $Å^3$, $D_{calc.}$ = 1.239 Mg · m^{-3}. The crystal was measured on a Nonius KappaCCD diffractometer at 173K using graphite-monochromated Mo K_α-radiation with λ = 0.71073 Å, Θ_{max} = 27.858°. Minimal/maximal transmission 0.97/0.97, μ = 0.081 mm^{-1}. The COLLECT suite has been used for datacollection and integration. From a total of 50388 reflections, 13631 were independent (merging r = 0.033). From these, 9239 were considered as observed (I>3.0σ(I)) and were used to refine 802 parameters. The structure was solved by direct methods using the program SIR92. Least-squares refinement against F was carried out on all non-hydrogen atoms using the program CRYSTALS. R = 0.0839 (observed data), wR = 0.0867 (all data), GOF = 1.0531. Minimal/maximal residual electron density = -0.46/1.12 e $Å^{-3}$. Chebychev polynomial weights were used to complete the refinement.
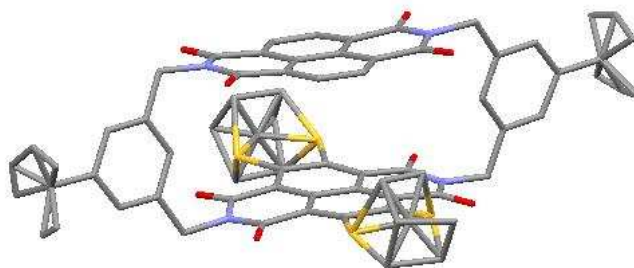
Crystal data for **14**: formula $C_{64}H_{64}N_4O_{10}S_2$, M = 1113.37, F(000) = 4704, red plate, size 0.05 · 0.14 · 0.23 mm^3, orthorhombic, space group P b c a , Z = 8, a = 15.4787(5) Å, b = 23.2471(6) Å, c = 31.7802(9) Å, α = 90°, β = 90°, γ = 90°, V = 11435.6(6) Å^3, $D_{calc.}$ = 1.293 Mg · m^{-3}. The crystal was measured on a Area diffractometer at 123K using graphite-monochromated Mo K_α-radiation with λ = 0.71073 Å, Θ_{max} = 26.438°. Minimal/maximal transmission 0.98/0.99, μ = 0.157 mm^{-1}. The COLLECT suite has been used for datacollection and integration. From a total of 106563 reflections, 11720 were independent (merging r = 0.061). From these, 9267 were considered as observed (I>2.0σ(I)) and were used to refine 901 parameters. The structure was solved by direct methods using the program SIR92. Least-squares refinement against F was carried out on all non-hydrogen atoms using the program CRYSTALS. R = 0.0749 (observed data), wR = 0.1278 (all data), GOF = 1.0525. Minimal/maximal residual electron density = -0.40/0.44 e Å^{-3}. Chebychev polynomial weights were used to complete the refinement.
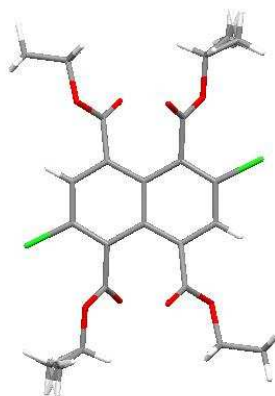
Crystal data for **37**: formula $C_{22}H_{22}Cl_2O_8$, M = 485.32, F(000) = 504, colourless plate, size 0.03 · 0.16 · 0.29 mm^3, monoclinic, space group P 2_1/n , Z = 2, a = 6.17610(10) Å, b = 13.4935(3) Å, c = 13.7276(3) Å, α = 90°, β = 100.8260(10)°, γ = 90°, V = 1123.66(4) Å^3, $D_{calc.}$ = 1.434 Mg · m^{-3}. The crystal was measured on a Area diffractometer at 123K using graphite-monochromated Mo K_α-radiation with λ = 0.71073 Å, Θ_{max} = 36.280°. Minimal/maximal transmission 0.95/0.99, μ = 0.335 mm^{-1}. The Apex2 suite has been used for datacollection and integration. From a total of 45316 reflections, 5428 were independent (merging r = 0.021). From these, 4414 were considered as observed (I>2.0σ(I)) and were used to refine 154 parameters. The structure was solved by direct methods using the program SIR92. Least-squares refinement against F was carried out on all non-hydrogen atoms using the program CRYSTALS. R = 0.0325 (observed data), wR = 0.0507 (all data), GOF = 1.0343. Minimal/maximal residual electron density = -0.35/0.56 e Å^{-3}. Chebychev polynomial weights were used to complete the refinement.
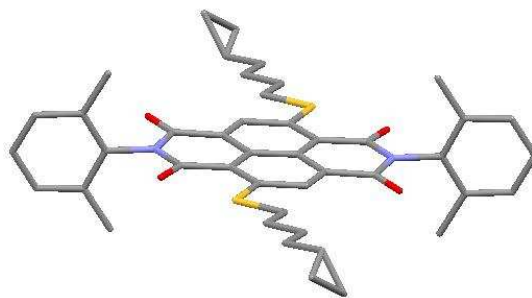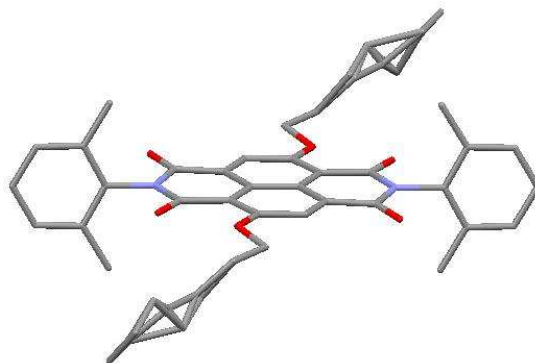
Crystal data for **41**: formula $C_{42}H_{46}N_2O_4S_2$, M = 706.97, F(000) = 752, red block, size 0.06 · 0.11 · 0.23 mm^3, triclinic, space group P -1 , Z = 2, a = 12.290(3) Å, b = 13.380(3) Å, c = 13.710(3) Å, α = 61.45(3)°, β = 73.60(3)°, γ = 88.67(3)°, V = 1883.0(10) Å^3, $D_{calc.}$ = 1.247 Mg · m^{-3}. The crystal was measured on a Nonius KappaCCD diffractometer at 173K using graphite-monochromated Mo K_α-radiation with λ = 0.71073 Å, Θ_{max} = 29.594°. Minimal/maximal transmission 0.98/0.99, μ = 0.185 mm^{-1}. The COLLECT suite has been used for datacollection and integration. From a total of 64099 reflections, 10326 were independent (merging r = 0.060). From these, 5540 were considered as observed (I>3.0σ(I)) and were used to refine 523 parameters. The structure was solved by direct methods using the program SIR92. Least-squares refinement against F was carried out on all non-hydrogen atoms using the program CRYSTALS. R = 0.0493 (observed data), wR = 0.0508 (all data), GOF = 1.1119. Minimal/maximal residual electron density = -0.66/0.63 e Å^{-3}. Chebychev polynomial weights were used to complete the refinement.

Crystal data for **42**: formula $C_{42}H_{46}N_2O_6$, M = 674.84, F(000) = 1440, orange block, size 0.08 · 0.09 · 0.23 mm^3, orthorhombic, space group P c c n , Z = 4, a = 14.8769(7) Å, b = 29.2672(15) Å, c = 8.1590(5) Å, α = 90°, β = 90°, γ = 90°, V = 3552.5(3) Å^3, $D_{calc.}$ = 1.262 Mg · m^{-3}. The crystal was measured on a Nonius KappaCCD diffractometer at 123K using graphite-monochromated Mo K_α-radiation with λ = 0.71073 Å, Θ_{max} = 27.552°. Minimal/maximal transmission 0.99/0.99, μ = 0.084 mm^{-1}. The COLLECT suite has been used for datacollection and integration. From a total of 39321 reflections, 4098 were independent (merging r = 0.070). From these, 2621 were considered as observed (I>1.2σ(I)) and were used to refine 262 parameters. The structure was solved by direct methods using the program SIR92. Least-squares refinement against F was carried out on all non-hydrogen atoms using the program CRYSTALS. R = 0.0543 (observed data), wR = 0.0585 (all data), GOF = 1.0644. Minimal/maximal residual electron density = -0.26/0.25 e Å^{-3}. Chebychev polynomial weights were used to complete the refinement.

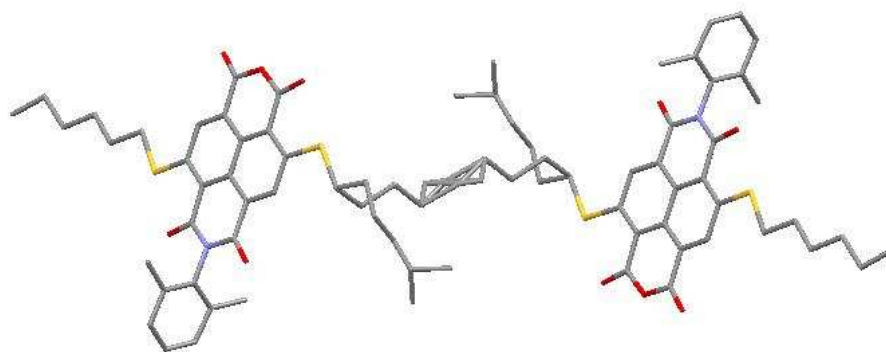Crystal data for **45**: formula $C_{34}H_{37}N_1O_5S_2$, M = 603.80, F(000) = 1280, red block, size 0.08 · 0.12 · 0.14 mm^3, monoclinic, space group P 2_1/n , Z = 4, a = 19.4044(12) Å, b = 9.7138(6) Å, c = 19.7887(14) Å, α = 90°, β = 115.080(3)°, γ = 90°, V = 3378.3(4) Å^3, $D_{calc.}$ = 1.187 Mg · m^{-3}. The crystal was measured on a Nonius KappaCCD diffractometer at 293K using graphite-monochromated Mo K_α-radiation with λ = 0.71073 Å, Θ_{max} = 26.092°. Minimal/maximal transmission 0.98/0.98, μ = 0.197 mm^{-1}. The COLLECT suite has been used for datacollection and integration. From a total of 39408 reflections, 6467 were independent (merging r = 0.044). From these, 6445 were considered as observed (I>2.0σ(I)) and were used to refine 433 parameters. The structure was solved by direct methods using the program SIR92. Least-squares refinement against Fsqd was carried out on all non-hydrogen atoms using the program CRYSTALS. R = 0.0785 (observed data), wR = 0.3110 (all data), GOF = 0.9614. Minimal/maximal residual electron density = -0.43/0.75 e Å^{-3}. Chebychev polynomial weights were used to complete the refinement.

Appendix

Appendix

Abbreviations

A	acceptor
Å	angstrom
AIBN	azobisisobutyronitrile
Alox	aluminium oxide
Bn	benzyl
BOC	*tert*.-Butyloxycarbonyl
Br_2	bromine
Bz	benzoyl
°C	Celsius
CD	circular dichroism
$CDCl_3$	deuterated chloroform
CF_3COOH	trifluoroacetic acid
CH_2Cl_2	dichloromethane
CH_3Cl	chloroform
CH_3CN	acetonitrile
CH_3COOH	acetic acid
CV	cyclic voltametry
D	donor
DAD	diode array detector
DMF	dimethylformamide
DMSO	dimethylsulfoxide
EA	elemental analysis
E_F	Fermi level
e.g.	for example (exempli gratia)
EI	electron impact
ESI	electron spray ionisation
Et_3N	triethylamine
EtOAc	ethyl acetate
EtOH	ethanol
eq.	equivalents
eV	electron volts
exc.	Excitation
FAB	fast atom bombardement
FRET	Förster resonance energy transfer

FT	fourier transformation
g	grams
GC	gas chromatography
GPC	gel permeation chromatography
h	hours
HCl	hydrochloric acid
Hex	hexane
HOMO	highest occupied molecular orbital
HPLC	high performance liquid chromatography
H_2SO_4	sulfuric acid
I	tunnelling current
i-PrOH	*iso*-propanol
IR	infrared
IUPAC	International Union of Pure and Applied Chemistry
K	kelvin
KBr	potassium bromide
K_2CO_3	potassium carbonate
KOH	potassium hydroxide
LiOH	lithium hydroxide
LT	low temperature
LUMO	lowest unoccupied molecular orbital
M	molar
MALDI	matrix-assisted laser desorption ionisation
mbar	millibar
MeOH	methanol
mg	milligrams
MHz	megahertz
min	minutes
ml	milliliters
mp	melting point
mV	millivolt
MS	mass spectrometry
NaCl	sodium chloride
NaH	sodium hydride
$NaHCO_3$	sodium bicarbonate
Na_2CO_3	sodium carbonate
NaOH	sodium hydroxide

Na$_2$SO$_4$	sodium sulphate
NBA	*m*-nitro-benzene alcohol
NBS	*N*-bromosuccinimide
NDI	naphthalenediimide
nm	nanometer
NMR	nuclear magnetic resonance
PG	protection group
Phe	phenyl
ppm	parts per million
RPM	round per minute
rt	room temperature
s	seconds
S$_0$, S$_1$	ground and first singlet state
SiO$_2$	silica gel
STM	scanning tunnelling microscopy
STS	scanning tunnelling spectroscopy
T$_1$	first triplet state
TLC	thin layer chromatography
TOF	time of flight
UHV	ultra high vacuum
UV/Vis	ultra violet – visible light absorption
V	bias voltage
W	watt

References

1). F.Vögtle, *Cyclophane-Chemistry*, Teubner, Stuttgart, 1990.

2). *Modern Cyclophane Chemistry*, ed. R. Gleiter and H. Hopf, Wiley-VCH, Weinheim, 2004.

3). N. Néel, J. Kröger, L. Limot, T. Frederiksen, M. Brandbyge, R. Berndt, *Phys. Rev. Lett.*, 2007, **98**, 065502-1.

4). D. J. Cram, H. Steinberg, *J. Am. Chem. Soc.*, 1951, **73**, 5691.

5). W. M. Schubert, W. A. Sweeney, H. K. Latourette, *J. Am. Chem. Soc.*, 1954, **76**, 5462.

6). B. H. Smith, *Bridged Aromatic Compounds*, Academic Press, New York, 1964.

7). M. M. Pellegrin, *Recl. Trav. Chim. Pays-Bas*, 1899, **18**, 457.

8). C. J. Brown, A. C. Farthing, *Nature*, 1949, **164**, 915.

9). Y. Sekine, M. Brown, V. Boekelheide, *J. Am. Chem. Soc.*, 1979, **101**, 3126.

10). M. Haenel and H. A. Staab, *Chem. Ber.*, 1973, **106**, 2203.

11). T. Umemoto, S. Satani, Y. Sakata and S. Misumi, *Tetrahedron Lett.*, 1975, **16**, 3159.

12). H. Irngartinger, R. G. H. Kirrstetter, C. Krieger, H. Rodewald and H. A. Staab, *Tetrahedron Lett.*, 1977, **18**, 1425.

13). R. H. Mitchell, R. J. Carruthers and J. C. M. Zwinkels, *Tetrahedron Lett.*, 1976, **17**, 2585.

14). Z. Pechlivanidis, H. Hopf and L. Ernst, *Eur. J. Org. Chem.*, 2009, 223.

15). Z. Pechlivanidis, H. Hopf, J. Grunenberg and L. Ernst, *Eur. J. Org.Chem.*, 2009, 238.

16). A. J. Blacker, J. Jazwinski, J.-M. Lehn, M. Cesario, J. Guilhem, C. Pascard, *Tetrahedron Lett.*, 1987, **28**, 6057.

17). T. Iijima, S. A. Vignon, H. R. Tseng, T. Jarrosson, J. K. M. Sanders, F. Marchioni, M. Venturi, E. Apostoli, V. Balzani, J. F. Stoddart, *Chem.–Eur. J.*, 2004, **10**, 6375.

18). G. D. Fallon, M. A.-P. Lee, S. J. Langford and P. J. Nichols, *Org. Lett.*, 2004, **6**, 655.

19). N. Lozac'h, A. L. Goodson, W. H. Powell, *Angew. Chem.*, 1979, **91**, 951; *Angew. Chem. Int. Ed.*, 1979, **18**, 887.

20). N. Lozac'h, A. L. Goodson, *Angew. Chem.*, 1984, **96**, 1; *Angew. Chem. Int. Ed.*, 1984, **23**, 33.

21). *Principles of Fluorescence Spectroscopy*, ed. J. R. Lakowicz, Springer, New York, 2006, ch. 13, p. 443.

22). G. J. Kavarnos, N. J. Turro, *Chem. Rev.*, 1986, **86**, 401.

23). T. Förster, *Naturwissenschaften*, 1946, **6**, 166.

24). T. Förster, *Ann. Phys.*, 1948, **2**, 55.

25). S. E. Braslavsky, E. Fron, H. B. Rodriguez, E. S. Roman, G. D. Scholes, G. Schweitzer, B. Valeur, J. Wirz, *Photochem. Photobiol. Sci.*, 2008, **7**, 1444.

26). G. Binnig, H. Rohrer, *Helv. Phys. Acta*, 1982, **55**, 726.

27). G. Binnig, H. Rohrer, C. Gerber, E. Weibel, *Phys. Rev. Lett.*, 1982, **49**, 57.

28). G. Binnig, H. Rohrer, *Rev. Mod. Phys.*, 1987, **59**, 615.

29). http://www.ieap.uni-kiel.de/surface/ag-berndt/

30). Diploma Thesis of Marco Knutzen: Electronic structure of functionalized organic molecules adsorbed on Au(111).

31). S. W. Wu, G. V. Nazin, W. Ho, *Phys. Rev. B*, 2008, **77**, 205430.

32). J. Repp, G. Meyer, *Phys. Rev. Lett.*, 2005, **94**, 026803.

33). R. Berndt, R. Gaisch, J. K. Gimzewski, B. Reihl, R. R. Schlittler, W. D. Schneider, M. Tschudy, *Science*, 1993, **262**, 1425.

34). G. Hoffmann, L. Libioulle, R. Berndt, *Phys. Rev. B*, 2002, **65**, 212107.

35). R. Berndt, R. Gaisch, W. D. Schneider, J. K. Gimzewski, B. Reihl, R. R. Schlittler, M. Tschudy, *Surface Science*, 1994, **307**, 1033.

36). X. H. Qiu, G. V. Nazin, W. Ho, *Science*, 2003, **299**, 542.

37). Z.-C. Dong, X.-L. Guo, A. S. Trifonov, P. S. Dorozhkin, K. Miki, K. Kimura, S. Yokoyama, S. Mashiko, *Phys. Rev. Lett.*, 2004, **92**, 086801.

38). E. Ćavar, M.-C. Blüm, M. Pivetta, F. Patthey, M. Chergui, W.-D. Schneider, *Phys. Rev. Lett.*, 2005, **95**, 196102.

39). D. Ino, T. Yamada, M. Kawai, *J. Chem. Phys.*, 2008, **129**, 014701.

40). *Scanning Probe Microscopy*, ed. R. Wiesendanger, Springer, Berlin Heidelberg, 1998, ch. 5, p. 97.

41). J. V. Barth, *Annu. Rev. Phys. Chem.*, 2007, **58**, 375.

42). R. Strohmaier, J. Petersen, B. Gompf, W. Eisenmenger, *Surface Science*, 1998, **418**, 91.

43). F. Jäckel, M. D. Watson, K. Müllen, J. P. Rabe, *Phys. Rev. B*, 2006, **73**, 045423 1-6.

44). M. D. Watson, F. Jäckel, N. Severin, J. P. Rabe, K. Müllen, *J. Am. Chem. Soc.*, 2004, **126**, 1402.

45). R. E. Palmer, Q. Guo, *Phys. Chem. Chem. Phys.*, 2002, **4**, 4275.

46). H. A. Staab, D.-Q. Zhang, C. Krieger, *Liebigs Ann./Recueil*, 1997, 1551.

47). K. D. Johnstone, K. Yamaguchi, M. G. Gunter, *Org. Biomol. Chem.*, 2005, **3**, 3008.

48). K. D. Johnstone, N. Bampos, J. K. M. Sanders, M. J. Gunter, *Chem. Commun.*, 2003, **12**, 1396.

49). G. D. Fallon, M. A.-P. Lee, S. J. Langford, P. J. Nichols, *Org. Lett.*, 2004, **6**, 655.

50). S. V. Bhosale, C. H. Jani, S. J. Langford, *Chem. Soc. Rev.*, 2008, **37**, 331.

51). T. Iijima, S.A. Vigogn, H.–R. Tseng, T. Jarrosson, J. K. M. Sanders, F. Marchioni, M. Venturi, E. Apostoli, V. Balzani, J. F. Stoddart, *Chem. Eur. J.*, 2004, **10**, 6375.

52). K. D. Johnstone, N. Bampos, J. K. M. Sanders, M. J. Gunter, *New J. Chem.*, 2006, **30**, 861.

53). S. I. Pascu, C. Naumann, G. Kaiser, A. D. Bond, J. K. M. Sanders, T. Jarrosson, *Dalton Trans.*, 2007, **35**, 3874.

54). D. G. Hamilton, J. E. Davies, L. Prodi, J. K. M. Sanders, *Chem. Eur. J.*, 1998, **4**, 608.

55). D. G. Hamilton, N. Feeder, S. J. Teat, J. K. M. Sanders, *New J. Chem.*, 1998, **22**, 1019.

56). Q. Zhang, D. G. Hamilton, N. Feeder, S. J. Teat, J. M. Goodman, J. K. M. Sanders, *New J. Chem.*, 1999, **23**, 897.

57). J. G. Hansen, N. Feeder, D. G. Hamilton, M. J. Gunter, J. Becher, J. K. M. Sanders, *Org. Lett.*, 2000, **2**, 449.

58). D. G. Hamilton, M. Montalti, L. Prodi, M. Fontani, P. Zanello, J. K. M. Sanders, *Chem. Eur. J.*, 2000, **6**, 608.

59). A. C. Try, M. M. Harding, D. G. Hamilton, J. K. M. Sanders, *Chem. Commun.*, 1998, **6**, 723.

60). G. Kaiser, T. Jarrosson, S. Otto, Y.-F. Ng, A. D. Bond, J. K. M: Sanders, *Angew. Chem. Int. Ed.*, 2004, **43**, 1959.

61). S. A. Vignon, T. Jarrosson, T. Iijima, H.-R. Tseng, J. K. M. Sanders, J. F. Stoddart, *J. Am. Chem. Soc.*, 2004, **126**, 9884.

62). M. J. Gunter, S. M. Farquhar, *Org. Biomol. Chem.*, 2003, **1**, 3450.

63). G. D. Pantos, P. Pengo, J. K. M. Sanders, *Angew. Chem. Int. Ed.*, 2007, **46**, 194.

64). G. D. Pantos, J.-L. Wietor, J. K. M. Sanders, *Angew. Chem. Int. Ed.*, 2007, **46**, 2238.

65). A. Bilyk, M. M. Harding, *J. Chem. Soc., Chem. Commun.*, 1995, **16**, 1697.

66). M. Licchelli, A. O. Biroli, A. Poggi, *Org. Lett.*, 2006, **8**, 915.

67). M. Licchelli, L. Linati, A. O. Biroli, E. Perani, A. Poggi, D. Sacchi, *Chem. Eur. J.*, 2002, **8**, 5161.

68). Y. S. Chong, M. D. Smith, K. D. Shimizu, *J. Am. Chem. Soc.*, 2001, **123**, 7463.

69). J. M. Lavin, K. D. Shimizu, *Organic Letters*, 2006, **8**, 2389.

70). H. N. Lee, Z. Xu, S. K. Kim, K. M. K. Swamy, Y. Kim, S.-J. Kim, J. Yoon, *J. Am. Chem. Soc.*, 2007, **129**, 3828.

71). H. Langhals, H. Jaschke, *Chem. Eur. J.*, 2006, **12**, 2815.

72). A. Blaszczyk, M. Fischer, C. von Hänisch, M. Mayor, *Helv. Chim. Acta*, 2006, **89**, 1986.

73). F. Würthner, S. Ahmed, C. Thalacker, T. Debaerdemaeker, *Chem. Eur. J.*, 2002, **8**, 4742.

74). C. Thalacker, C. Röger, F. Würthner, *J. Org. Chem.*, 2006, **71**, 8098.

75). C. Röger, S. Ahmed, F. Würthner, *Synthesis*, 2007, **12**, 1872.

76). C. Röger, F. Würthner, *J. Org. Chem.*, 2007, **72**, 8070.

77). A. L. Sisson, N. Sakai, N. Banerji, A. Fürstenberg, E. Vauthey, S. Matile, *Angew. Chem. Int. Ed.*, 2008, **47**, 3727.

78). R. S. K. Kishore, V. Ravikumar, G. Bernardinelli, N. Sakai, S. Matile, *J. Org. Chem.*, 2008, **73**, 738.

79). Z. Chen, Y. Zheng, H. Yan, A. Facchetti, *J. Am. Chem. Soc.*, 2009, **131**, 8.

80). H. Yan, Z. Chen, Y. Zheng, C. Newman, J. R. Quinn, F. Dötz, M. Kastler, A. Facchetti, *Nature*, 2009, **457**, 679.

81). V. Gorteau, G. Bollot, J. Mareda, S. Matile, *Org. Biomol. Chem.*, 2007, **5**, 3000.

82). J. Mareda, S. Matile, *Chem. Eur. J.*, 2009, **15**, 28.

83). S. Bhosale, A. L. Sisson, P. Talukdar, A. Fürstenberg, N. Banerji, E. Vauthey, G. Bollot, J. Mareda, C. Röger, F. Würthner, N. Sakai, S. Matile, *Science*, 2006, **313**, 84.

84). S. Gabutti, M. Knutzen, M. Neuburger, G. Schull, R. Berndt, M. Mayor, *Chem. Commun.*, 2008, **20**, 2370.

85). C. J. Pedersen, *J. Am. Chem. Soc.*, 1967, **89**, 7017.

86). A. F. Holleman, N. Wiberg, *Lehrbuch der Anorganischen Chemie*, Walter de Gruyter, Berlin, 1995.

87). C. J. Pederson, *J. Am. Chem. Soc.*, 1970, **92**, 386.

88). D. Wang, X. Sun, H. Hu, Y. Liu, B. Chen, Z. Zhou, K. Yu, *Polyhedron*, 1989, **8**, 2051.

89). P. R. Mallinson, M. R. Truter, *J. Chem. Soc.*, *Perkin Trans. 2*, 1972, 1818.

90). N. S. Poonia, *J. Am. Chem. Soc.*, 1974, **96**, 1012.

91). J. E. Ellis, D. W. Blackburn, P. Yuen, M. Jang, *J. Am. Chem. Soc.*, 1993, **115**, 11616.

92). F. Vonau, D. Aubel, L. Bouteiller, G. Reiter and L. Simon, *Phys. Rev. Lett.*, 2007, **99**, 086103.

93). E. I. Altman, R. J. Colton, *Surf. Sci.*, 1992, **279**, 49.

94). B. Jancy, S. K. Asha, *Journal of Polymer Science, Part A: Polymer Chemistry*, 2009, **47**, 1224.

95). D. Veldman, S. M. A. Chopin, S. C. J. Meskers, M. M. Groeneveld, R. M. Williams, R. A. J. Janssen, *J. Phys. Chem. A*, 2008, **112**, 5846.

96). R. O. Marcon, S. Brochsztain, *J. Phys. Chem. A*, 2009, **113**, 1747.

97). S. Wang, G. C. Bazan, S. Tretiak, S. Mukamel, *J. Am. Chem. Soc.*, 2000, **122**, 1289.

98). W. Wang, J. Xu, Y.-H. Lai, *Org. Lett.*, 2003, **5**, 2765.

99). S. Gabutti, S. Schaffner, M. Neuburger, M. Fischer, G. Schäfer, M. Mayor, *Org. Biomol. Chem.*, 2009, **7**, 3222.

100). M Adachi, Y. Murata, S. Nakamura, *J. Phys. Chem.*, 1995, **99**, 14240.

101). P. Job, *Ann. Chim.*, 1928, **9**, 113.

102). S. Demming, H. Langhals, *Chem. Ber.*, 1988, **121**, 225.

103). S. Erten, Y. Posokhov, S. Alp, S. Icil, *Dyes and Pigments*, 2005, **64**, 171.

104). C. T. Miller, R. Weragoda, E. Izbicka, B. L. Iverson, *Biooorg. Med. Chem.*, 2001, **9**, 2015.

105). Shionogi & Co., Ltd., European Pat. EP 1340755A1, 2003.

106). BASF AG, German Pat. DE 102005061997A1, 2007.

107). P. Pengo, G. D. Pantos, S. Otto, J. K. M. Sanders, *J. Org. Chem.*, 2006, **71**, 7063.

108). F. Chaignon, M. Falkenström, S. Karlsson, E. Blart, F. Odobel, L. Hammarström, *Chem. Commun.*, 2007, **42**, 64

109). M. Borgström, N. Shaikh, O. Johansson, M. F. Anderlund, S. Styring, B. Akermark, A. Magnuson, L. Hammarström, *J. Am. Chem. Soc.*, 2005, **127**, 17504.

110). W. Sum, V. Kwan, J. F: Penneau, L. L. Miller, *J. Electroanal. Chem.*, 1990, **291**, 295.

111). L. Flamigni, E. Baranoff, J.-P. Collin, J.-P. Sauvage, *Chem. Eur. J.*, 2006, **12**, 6592.

112). P. Ganesan, X. Yang, J. Loos, T. J. Savenije, R. D. Abellon, H. Zuilhof, E. J. R. Sudhölter, *J. Am. Chem. Soc.*, 2005, **127**, 14530.

113). W. S. Horne, N. Ashkenasy, M. Reza Ghadiri, *Chem. Eur. J.*, 2005, **11**, 1137.

114). H. Vollmann, H. Becker, M. Corell, H. Streeck, *Liebigs Ann.*, 1937, **531**, 1-159.

115). X. Gao, W. Qiu, X. Yang, Y. Liu, Y. Wang, H. Zhang, T. Qi, Y. Liu, K. Lu, C. Du, Z. Shuai, G. Yu, D. Zhu, *Org. Lett.*, 2007, **9**, 3917.

116). W. Gottardi, *Monatsh. Chem.*, 1968, **99**, 815.

117). W. Gottardi, *Monatsh. Chem.*, 1977, **108**, 1067.

118). S. Naik, G. Bhattacharjya, B. Talukdar, B. K. Patel, *Eur. J. Org. Chem.*, 2004, 1254.

119). *Protective Groups in Organic Synthesis, Third Edition,* ed. T. W. Greene, P. G. M. Wuts, John Wiley & Sons, Inc., New York, 1999.

120). F. Würthner, V. Stepanenko, Z. Chen, C. R. Saha-Möller, N. Kocher, D. Stalke, *J. Org. Chem.*, 2004, **69**, 7933.

121). F. Würthner, *Chem. Commun.*, 2004, **14**, 1564.

122). Y. Zhao, M. R. Wasielewski, *Tetrahedron Lett.*, 1999, **40**, 7047.

123). M. R. Wasielewski, *J. Org. Chem.*, 2006, **71**, 5051.

124). A. J. Arduengo, R. L. Harlow, M. Kline, *J. Am. Chem. Soc.*, 1991, **113**, 361.

125). A. J. Arduengo, J. R. Goerlich, W. J. Marshall, *Liebigs Ann.*, 1997, 365.

126). A. J. Arduengo, R. Krafczyk, R. Schnutzler, *Tetrahedron*, 1999, **55**, 14523.

127). A. Mayr, M. Srisailas, Q. Zhao, Y. Gao, H. Hsieh, M. Hoshmand-Kochi, N. St. Fleur, *Tetrahedron*, 2007, **63**, 8206.

128). B. A. Jones, A. Facchetti, M. R. Wasielewski, T. J. Marks, *J. Am. Chem. Soc.*, 2007, **129**, 15259.

129).   B. A. Jones, A. Facchetti, T. J. Marks, M. R. Wasielewski, *Chem. Mater.*, 2007, **19**, 2703.

130).   C. Röger, Y. Miloslavina, D. Brunner, A. R. Holzwart, F. Würthner, *J. Am. Chem. Soc.*, 2008, **130**, 5929.

125).   E. Weber, H.-P. Josel, H. Puff, S. Franken, *J. Org. Chem.*, 1985, **50**, 3125.

126).   Y. Tobe, S. Sasaki, M. Mizuno, K. Hirose, K. Naemura, *J. Org. Chem.*, 1998, **63**, 7481.

127).   S. Naik, G. Bhattacharjya, B. Talukdar, B. K. Patel, *Eur. J. Org. Chem.*, 2004, 1254.

Curriculum Vitae

Personalien

Name	Sandro Gabutti
Geburtsdatum	8. Oktober 1979
Zivilstand	ledig
Nationalität	Schweizer
Bürgerort	Basel, Manno
Heimatort	Basel

Ausbildung

1986-1991	Primarschule Therwil
1991-1996	Sekundarschule Therwil / Oberwil
1996-2000	Gymnasium Oberwil (Typus C)
2001-2005	Bachelor of Science in Chemistry
2005-2006	Master of Science in Chemistry bei Prof. W.-D. Woggon: „Towards an enzyme mimic of the excentric cleavage of carotinoids – synthesis of ruthenium complexes attached to beta cyclodextrin"
2006-2009	Doktorarbeit in der Forschungsgruppen von Prof. M. Mayor am Departement Chemie der Universität Basel

Weitere Tätigkeiten

2006-2008	Assistenz im organisch-chemischen Praktikum für Studierende der Pharmazie und Biologie

Publications and Presentations

1   "A Rigid Naphthylbisimide Cyclophane", Posterpräsentation im Rahmen Frontiers in Photochemistry, 9-13 Sept. **2007**, Villars / Ollon (CH).

2   "A Rigid Naphthylbisimide Cyclophane", Posterpräsentation im Rahmen des KOPOs (konjugierte Oligomere und Polymere), 24-27 Sept. **2007**, Ulm (DE).

3   S. Gabutti, M. Knutzen, M. Neuburger, G. Schull, R. Berndt, M. Mayor, "A rigid sublimable naphthalenediimide cyclophane as model compound for UHV STM experiments", Chem. Comm., **2008**, 20, 23.

4   S. Gabutti, S. Schaffner, M. Neuburger, M. Fischer, G. Schäfer, M. Mayor, "Planar Chiral asymmetric naphthalenediimide cyclophanes: synthesis, characterization and tunable FRET properties", Org. Biomol. Chem., **2009**, 7, 3222.

5   Front cover, "Planar chiral asymmetric naphthalenediimide cyclophanes: synthesis, characterization and tunable FRET properties", Org. Biomol. Chem., **2009**, 7, 3222.

6   S. Gabutti, M. Mayor, "Rigid NDI cyclophanes", Vortrag im Rahmen des KOPOs (konjugierte Oligomere und Polymere), 13-16 Sept. **2009**, Ulm (DE).